

AD-A065 291

CALIFORNIA UNIV SANTA BARBARA DEPT OF CHEMISTRY  
PHOTOLUMINESCENCE SPECTROSCOPY WITH A CW DYE LASER. A STUDY OF --ETC(U)  
1977 D O HARRIS

F/G 7/2

AFOSR-73-2565

UNCLASSIFIED

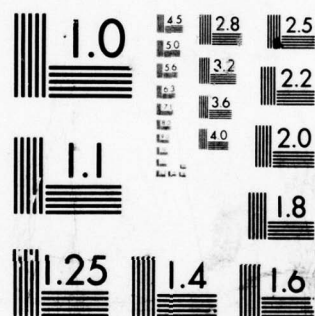
AFOSR-TR-79-0101

NL

1 OF 2

AD  
A065291





MICROCOPY RESOLUTION TEST CHART  
NATIONAL BUREAU OF STANDARDS-1963-A



18

19

11

LEVEL II

AFOSR-TR. 79-0101

FEB 6 REC'D

9

FINAL REPORT,  
June 1973 - December 1977

AD A0 65291

Organization: AFOSR  
Subelement: Physical Chemistry

Project: 9538 Task: 01  
Grant #: AFOSR-73-2565

15 NSF-MPS-72-  
04978

6

PHOTOLUMINESCENCE SPECTROSCOPY WITH A CW DYE LASER.  
A STUDY OF THE DIATOMIC ALKALINE EARTH METAL HALIDES AND OXIDES.

10

D.O. Harris  
Department of Chemistry  
University of California  
Santa Barbara, California

072 475

11 1977

16 2383, 9538

Abstract

17 BY 01

DDC FILE COPY

Increased Air Force capabilities in reconnaissance, communication and several other areas depend on the development of new laser technology. Chemical laser systems possess certain properties such as wavelength, power and efficiency, which make them highly attractive for many applications. To assure development of different and improved chemical laser systems, an understanding of the basic properties and characteristics of potentially useful molecules and reactions is critical. This research involved the study of diatomic systems in various experiments involving observation of photo- and chemiluminescence, and by reanalysis of literature spectroscopic data. Continuous wave (cw) tunable dye lasers were used to excite photoluminescence from several diatomic metal oxides and halides. Experiments included excitation, fluorescence and various forms of double resonance spectroscopy.

12 124 p

Just page

DDC  
RECEIVED  
MAR 6 1979

B

DISTRIBUTION STATEMENT A  
Approved for public release  
Distribution Unlimited

AIR FORCE OFFICE OF SCIENTIFIC RESEARCH (AFSC)  
NOTICE OF TRANSMITTAL TO DDC  
This technical report has been reviewed and is approved for public release IAW AFR 190-12 (7b). Distribution is unlimited.  
A. D. BLOSE  
Technical Information Officer

Approved for public release;  
distribution unlimited.  
072 475

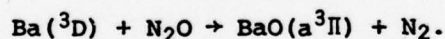
79-02 28 109

# 1) Spectroscopic Studies of the Barium Plus Oxidant Reaction

There has been considerable interest in efficient chemiluminescent reactions between metal atoms and suitable oxidants as candidates for chemically pumped laser systems. This prompted a detailed study of the nature and mechanism of the reaction of Barium with  $N_2O$ ,  $O_2$  and  $NO_2$ . In particular, it has been observed that in the reaction of  $Ba + N_2O \rightarrow BaO$ , fully 20% of all the Ba atoms reacting yield photons originating from the  $A^1\Sigma$  excited state of BaO. In addition, one third of those photons arise from  $v'=1$  of the  $A^1\Sigma$  state. It was therefore of interest to investigate the possibility of there being a population inversion between  $A^1\Sigma(v'=1)$  and vibrational levels of the  $X^1\Sigma$  ground state of BaO under the conditions existing in the  $Ba + N_2O$  flame.

Experiments were carried out in which single vibrational levels  $v'$ , of the  $A^1\Sigma$  state were pumped from adjacent ground state vibrational levels using a tunable cw dye laser. By monitoring the photoluminescence intensity originating from a pumped excited state level,  $v'$ , to a third ground state level it was possible to measure the relative populations of the two adjacent ground state vibrational levels. Repeated application of this technique yielded the relative vibrational population distribution of the ground state manifold as a function of various flame conditions. Using previously available data and our results suggest that a population inversion may exist between  $A^1\Sigma(v'=1)$  and  $X^1\Sigma(v''=7)$ . Our experiments and results are reported in detail in references 1 and 2.

A second area of interest was the details of the mechanism of the  $Ba + N_2O$  reaction which leads to the observed high  $A \rightarrow X$  chemiluminescence efficiency and why such a large proportion of the emitting molecules are in the  $A^1\Sigma(v'=1)$  state. Specifically it had been proposed that metastable  $BaO(a^3\Pi)$  which cannot emit to the ground state serves as a reservoir state for the reaction. Molecules trapped in this state relax vibrationally to the first few vibrational levels of the  $a^3\Pi$  metastable state and are then transferred collisionally to the  $A^1\Sigma$  state from which they emit. This leads to the high chemiluminescence efficiency. It had been further proposed that the  $BaO(a^3\Pi)$  was initially formed via the reaction of  $Ba(^3D)$  excited state atoms ( $\Delta E \sim 1$  e.v.) present in the flame by the reaction



In order to test this hypothesis we carried out a series of experiments in which total  $A^1\Sigma - X^1\Sigma$  chemiluminescent yield as a function of  $Ba(^3D)$  concentration was monitored. As reported in reference 3, it was found that an increase of  $Ba(^3D)$  concentration by a factor of ten to a hundred had no significant effect on chemiluminescent yield. Thus we conclude that  $Ba(^3D)$  is not the key reactant leading to the observed high chemiluminescence efficiency.

ACCESSION for	
NTIS	Write Section <input checked="" type="checkbox"/>
DDC	Dist Section <input type="checkbox"/>
UNCLASSIFIED	<input type="checkbox"/>
JUSTIFICATION	
BY	
DISTRIBUTION/AVAILABILITY CODES	
Dist.	AVAIL. and/or SPECIAL
A	

## 2) The $a^3\Pi$ State of MgO

We recently completed our laser induced fluorescence study of MgO. MgO is produced by the reaction  $\text{Mg} + \text{O}_2$  in an apparatus similar to that used for the study of BaO. Three lines of the  $\text{Ar}^+$  laser have the following chance coincidences with transitions in the MgO  $B^1\Sigma - X^1\Sigma$  system

476.5 nm R(26) 5-4 band  $^{24}\text{MgO}$

R(49) 4-3 band  $^{24}\text{MgO}$

R(70) 3-2 band  $^{24}\text{MgO}$

496.5 nm R(36) 2-2 band  $^{26}\text{MgO}$

514.5 nm P(10) 4-5 band  $^{24}\text{MgO}$

R(25) 3-4 band  $^{26}\text{MgO}$

R(50) 2-3 band  $^{25}\text{MgO}$

R(70) 1-2 band  $^{24}\text{MgO}$

Photoluminescence spectra from  $B^1\Sigma$  to both the  $X^1\Sigma$  ground state and the  $A^1\Pi$  excited state ( $T_e = 3563 \text{ cm}^{-1}$ ) and calculated Franck-Condon factors confirm these assignments. In addition to the B-X and A-X systems, transitions were observed and assigned to the previously unobserved  $a^3\Pi$  state which is isoconfigurational with the  $A^1\Pi$  state. In the case of the 476.5 nm excitation, the 5 GHz linewidth of the  $\text{Ar}^+$  laser produces simultaneous excitation of all three levels listed above. However, when the laser is operated single mode by insertion of an intracavity Fabry Perot etalon the spectrum is greatly simplified by reducing the number of coincidences. The laser can be scanned over its gain profile in 150 MHz steps thus exciting each of the coincidences sequentially with little overlap, and the resulting fluorescence spectrum is particularly simple. As was expected a  $B^1\Sigma \rightarrow X^1\Sigma$  P-R doublet is seen, but in addition transitions to a  $^3\Pi_0$  and a  $^3\Pi_1$  are also observed. These normally unallowed  $B^1\Sigma - a^3\Pi$  "extra" lines are made possible by specific perturbations between levels of the  $X^1\Sigma$  and  $a^3\Pi$  manifolds. Additional fluorescence spectra were obtained as a function of etalon setting. By comparing relative intensities of each line and noting those sets which remain constant relative to each other as the etalon is tuned, transitions originating in the  $v=4$  and 5 of  $B^1\Sigma$  MgO can also be uniquely assigned.

The perturbations are a sensitive probe of the positions of the energy levels of  $a^3\Pi$  relative to those of  $X^1\Sigma$ . For example, the perturbation allowed extra lines of the  $J'=69$  (3,3) transition to appear on either side of the main  $B^1\Sigma - X^1\Sigma$  lines thus indicating that the  $\Pi_0$  and  $\Pi_1$  levels bracket the



corresponding  $\Sigma$  level. Conversely, however, for the  $J'=25$  (5,5) lines the extra lines both appear to the red of the main line.

Analysis of these perturbations using some sixty lines has resulted in an accurate determination of the molecular constants of the  $a^3\Pi$  state.

This work is described in detail in reference 4.

3) Excitation, Microwave Laser Double Resonance and Laser-Laser Double Resonance Spectroscopy of CaCl, CaF and SrF

We have carried out an extensive program on the spectroscopy of the alkali metal halides. Despite the simplicity of these molecules, little prior work has been done due to the complexity of their spectra. The first electronic excited state of these molecules corresponds to the excitation of an ns electron to an empty np orbital on the metal resulting in two nearby molecular electronic states:  $A^2\Pi$  and  $B^2\Sigma$ . Since the excitation involves a non-bonding electron, most of the molecular parameters in the  $A^2\Pi$  and  $B^2\Sigma$  states are only slightly changed relative to the  $X^2\Sigma$  ground state. Consequently, the A-X and B-X spectra occur mainly as  $\Delta V=0$  transitions yielding extremely dense and overlapped spectra. Despite this complexity which prevented their study and analysis using conventional spectroscopic techniques, it has been possible to use tunable lasers to completely characterize several electronic states of several alkaline earth monohalides. Included are (1) a study of the  $B^2\Sigma - X^2\Sigma$  system of CaCl (reference 5) using tunable laser excitation spectroscopy; (2) an accurate determination of the ground state constants of CaCl using laser-microwave optical double resonance (reference 6) and (3) a rotational analysis of the  $E^2\Sigma - B^2\Sigma$  system of CaCl using optical-optical double resonance (reference 7). Similar studies on SrF (references 8 and 9) and on CaF (references 10 and 11) have also been carried out.

### Publications and References

1. "Vibrational Population Distribution of Ground State BaO Formed by the Reaction  $\text{Ba} + \text{O}_2$ ," Michael A. Revelli, Brian G. Wicke and David O. Harris, Chem. Phys. Lett. 39, 454 (1976).
2. "Vibrational Population Distributions of Ground State Barium Oxide Formed in the  $\text{Ba} + \text{O}_2$  and  $\text{Ba} + \text{N}_2\text{O}$  Reactions," Michael A. Revelli, Brian G. Wicke and David O. Harris, J. Chem. Phys. 66, 732 (1977).
3. "On the Importance of  $\text{Ba}(^3\text{D})$  as the Key Reactant Leading to  $\text{BaO}(\text{A-X})$  Chemiluminescence in the  $\text{Ba} + \text{N}_2\text{O}$  Reaction," Brian G. Wicke, Michael A. Revelli and David O. Harris, J. Chem. Phys. 63, 3120 (1975).
4. "Argon Ion and Dye Laser Induced  $\text{MgO } \text{B}^1\Sigma^+ - \text{X}^1\Sigma^+$  and  $\text{B}^1\Sigma^+ - \text{A}^1\Pi$  Photoluminescence Spectra (Analysis of  $\text{a}^3\Pi_1 - \text{X}^1\Sigma^+$  Perturbations)," Tatsuya Ikeda, Ning Bew Wong and David O. Harris, J. Mol. Spectr. 68, 452 (1977).
5. "High-Resolution Laser Excitation Spectroscopy (Analysis of the  $\text{B}^2\Sigma^+ - \text{X}^2\Sigma^+$  System of  $\text{CaCl}$ )," Peter J. Domaille, Timothy C. Steimle, Ning Bew Wong and David O. Harris, J. Mol. Spectr. 65, 354 (1977).
6. "The Rotational Spectrum of the  $\text{X}^2\Sigma^+$  State of the  $\text{Ca}^{35}\text{Cl}$  Radical Using Laser Microwave Optical Double Resonance," Peter J. Domaille, Timothy C. Steimle and David O. Harris, J. Mol. Spectr. 66, 503 (1977).
7. "Optical-Optical Double Resonance with Two Dye Lasers: Rotational Analysis of the  $\text{E}^2\Sigma - \text{B}^2\Sigma$  System of  $\text{Ca}^{35}\text{Cl}$ ," Peter J. Domaille, Timothy C. Steimle and David O. Harris, J. Chem. Phys. 68, 4977 (1978).
8. "Rotational Analysis of the  $\text{B}^2\Sigma^+ - \text{X}^2\Sigma^+$  System of SrF Using a cw Tunable Dye Laser," Timothy C. Steimle, Peter J. Domaille and David O. Harris, J. Mol. Spectr. 68, 134 (1977).
9. "The Rotational Spectrum of the  $\text{X}^2\Sigma^+$  State of the SrF Radical Using Laser Microwave Optical Double Resonance," Peter J. Domaille, Timothy C. Steimle and David O. Harris, J. Mol. Spectr. 68, 146 (1977).
10. "Continuous Wave Dye Laser Excitation Spectroscopy  $\text{CaF } \text{A}^2\Pi_x - \text{X}^2\Sigma^+1$ ," Robert W. Field, David O. Harris and Takehiko Tanaka, J. Mol. Spectr. 57, 107 (1975).
11. "Microwave Optical Double Resonance and Reanalysis of the  $\text{CaF } \text{A}^2\Pi_x - \text{X}^2\Sigma$  Band System," Jun Nakagawa, Peter J. Domaille, Timothy C. Steimle and David O. Harris, J. Mol. Spectr. 70, 374 (1978).

### Talks

1. "CW Dye Laser Excitation Spectroscopy of Transient Molecules," Spring Conference of the Optical Society of America, Anaheim, California, March 19, 1974.
2. "Studies in Microwave Optical Double Resonance," 30th Southwest Regional American Chemical Society Meeting, Houston, Texas, December 9, 1974.
3. "A Model for Microwave Optical Double Resonance," paper TC11, 30th Symposium on Molecular Spectroscopy and Structure, Ohio State University, Columbus, Ohio, June 16, 1975.
4. "Laser Induced Fluorescence in MgO: Direct Observation of the Lowest  $^3\Pi$  State and the Analysis of Perturbations in the Ground State," paper TE7, 30th Symposium on Molecular Spectroscopy and Structure, Ohio State University, Columbus, Ohio, June 16, 1975.
5. "Optical-Optical Double Resonance in MgO: Observation of Excited  $^1\Pi$  States and the  $E^1\Sigma^+$  State," paper TE8, 30th Symposium on Molecular Spectroscopy and Structure, Ohio State University, Columbus, Ohio, June 16, 1975.
6. "Laser Spectroscopy of Small Molecules," National Bureau of Standards, Washington, D.C., September 20, 1975.
7. "Laser Spectroscopy of Small Molecules," Department of Chemistry, California State University, Northridge, February 20, 1976.
8. "Laser Spectroscopy of Small Molecules," Department of Chemistry, University of California, Davis, March 9, 1976.
9. "Vibrational Population Distribution of the Ground State of Barium Oxide," paper TC9, 31st Ohio State Symposium on Molecular Spectroscopy, Ohio State University, Columbus, Ohio, June 15, 1976.
10. "Two Photon Excitation Spectra and Energy Transfer Processes in CaCl," paper TN5, 31st Ohio State Symposium on Molecular Spectroscopy, Ohio State University, Columbus, Ohio, June 15, 1976.
11. "Microwave Optical Double Resonance of Gas Phase SrF," Winter meeting of the American Physical Society, Stanford, California, December 20-22, 1976.
12. "A Microwave Optical Double Resonance Stark Effect Study of the  $A^1\Sigma^+$  State of BaO," Winter Meeting of the American Physical Society, Stanford, California, December 20-22, 1976.



Talks (continued)

13. "Rotational Analysis of the  $B^2\Sigma-X^2\Sigma$  System of SrF," Winter Meeting of the American Physical Society, Stanford, California, December 20-22, 1976.
14. "Laser Spectroscopic Studies of Small Molecules," Department of Chemistry, University of California, Irvine, May 23, 1977.
15. "Microwave Optical Double Resonance Study and Optical Re-Analysis of CaF  $A^2\Pi-X^2\Sigma$  Band," 32nd Symposium on Molecular Structure, Ohio State University, Columbus, Ohio, June 15, 1977.
16. "Microwave Optical Double Resonance: Study of the  $X^2\Sigma^+$  State of the SrF Radical," 32nd Symposium on Molecular Structure, Ohio State University, Columbus, Ohio, June 15, 1977.
17. "Rotational Analysis of the  $B^2\Sigma-X^2\Sigma$  System of SrF," 32nd Symposium on Molecular Structure, Ohio State University, Columbus, Ohio, June 15, 1977.

# VIBRATIONAL POPULATION DISTRIBUTION OF GROUND STATE BaO FORMED BY THE REACTION $\text{Ba} + \text{O}_2^\dagger$

Michael A. REVELLI, Brian G. WICKE and David O. HARRIS

Department of Chemistry and Quantum Institute, University of California, Santa Barbara, California 93106, USA

Received 11 December 1975

Revised manuscript received 23 January 1976

The vibrational population distribution of  $X^1\Sigma^+(v'' = 0 \text{ through } v'' = 7)$  BaO formed in the reaction  $\text{Ba} + \text{O}_2$  at 0.3 torr has been measured by laser induced photoluminescence intensities. On the basis of the assumed similarity between the  $\text{Ba} + \text{O}_2$  and  $\text{Ba} + \text{N}_2\text{O}$  reactions, these data suggest that a population inversion may exist between  $A^1\Sigma^+(v' = 1)$  and  $X^1\Sigma^+(v'' = 7)$  BaO formed in the latter reaction at  $\approx 16$  torr.

Recent interest in efficient chemiluminescent reactions between metal atoms and suitable oxidants, as candidates for chemically pumped laser systems, has prompted detailed studies of the distribution of product molecules [1-3]. Analysis of the band intensity of chemiluminescence has been used to determine the vibrational population distribution of electronically excited products of a chemical reaction [4]. In contrast, we have used an analysis of the relative intensity of laser induced photoluminescence to characterize the ground state vibrational distribution of product molecules. Reported here is the vibrational distribution of ground state BaO formed by the reaction  $\text{Ba} + \text{O}_2$  at 0.3 torr total pressure. The implications these results may have for the  $\text{Ba} + \text{N}_2\text{O}$  reaction are suggested.

Barium oxide molecules were produced by reacting gas phase barium atoms, entrained in a 0.3 torr argon gas flow, with an excess of  $\text{O}_2$ . The details of the oven design have been described previously [5]. The output of a rhodamine 6G tunable cw dye laser was directed vertically through the flame. As illustrated schematically in fig. 1, when the laser is tuned it is possible to sequentially excite a single vibrational level,  $v'$ , of the  $A^1\Sigma^+$  state from two adjacent levels,

$v_1''$  and  $v_2''$ , of the  $X^1\Sigma^+$  ground state. Photoluminescence originating from this excited upper state level to a third ground state level,  $v_3''$ , is monitored using a monochromator (3 nm resolution) and a photomultiplier tube. The particular  $v_3''$  was chosen so that the laser induced photoluminescence was outside the dye laser tuning range (565-620 nm) to eliminate interference from scattered laser light. Contributions to the band intensity from background chemiluminescence were eliminated by chopping the dye laser at 25 Hz

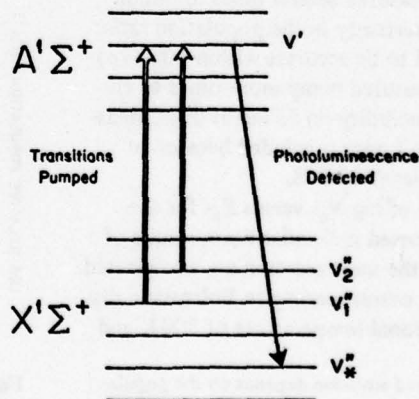


Fig. 1. Schematic energy level diagram for BaO, showing typical dye laser pumped transitions and an observed photoluminescence band.

<sup>†</sup> This research was supported in part by AFOSR Grant No. AFOSR-73-2565, and NSF Grant No. MPS-72-04978.



and phase sensitive detection of the laser induced luminescence.

Because a single photoluminescence band was monitored while sequentially pumping out of two adjacent  $X^1\Sigma(v''_i)$  levels, the ratio of these two  $A^1\Sigma(v') \rightarrow X^1\Sigma(v''_i)$  emission intensities is proportional only to the ground state population,  $N_{v''_i}$ ; the Franck-Condon factor for the  $v' \leftarrow v''_i$  transition,  $q_{v'v''_i}$ ; and the laser power density,  $\rho_{v'v''_i}$ , at the wavelength of the  $v' \leftarrow v''_i$  absorption<sup>†</sup>. The ratio of the populations in the ground state levels  $v''_1$  and  $v''_2$  is given by:

$$N_{v''_1}/N_{v''_2} = (I_{v''_1}/I_{v''_2}) q_{v'v''_2}/q_{v'v''_1} \rho_{v'v''_1}/\rho_{v'v''_2},$$

where  $I_{v''_i}$  is the integrated intensity of the  $v' \rightarrow v''_i$  photoluminescence resulting from the  $v''_i \rightarrow v'$  excitation. The advantage of detecting the same fluorescence band is that it is then unnecessary to correct the observed intensities for the Franck-Condon factors for emission or for the wavelength dependence of the monochromator optics and phototube. Care must be taken, however, to ensure that the laser does not saturate the absorption.

Repeated application of this technique provides a method for measuring successive population ratios,  $N_{v''}/N_{v''+1}$ ,  $N_{v''+1}/N_{v''+2}$ , etc., through the ground state vibrational manifold. Results for the  $Ba + O_2$  reaction at 0.3 torr for  $v'' = 0$  through  $v'' = 7$  are given in table 1. This technique enabled intensity measurements to be made of relative populations which span five orders of magnitude. Each pair of relative emission intensities was measured several times to obtain an estimate of the uncertainty in the population ratio; each ratio is estimated to be accurate within 10% (1 $\sigma$ ). Several ratios were measured many more times to ensure statistical reproducibility on different days. Measurements beyond  $v'' = 7$  were precluded because of vanishing signal from levels  $v''_i \geq 8$ .

Fig. 2 shows a plot of  $\log N_{v''}$  versus  $E_{v''}$  for the data in table 1; the crossed molecular beam results of Schultz et al. [6] for the same reaction are also plotted. For comparison, lines corresponding to Boltzmann distributions with vibrational temperatures of 500 K and

Table 1

Measured intensity ratios and relative populations of the  $v'' = 0$  through  $v'' = 7$  vibrational states of  $BaO X^1\Sigma$  formed in the reaction  $Ba + O_2$  at  $P = 0.3$  torr. Successive ratios are normalized to  $N_0 = 1$  and are accurate to  $\pm 10\%$

$v''$	Measured intensity ratio $I_{v''}/I_{v''+1}$	Relative population $N_{v''}$
0		(1.000)
1	1.40	0.123
2	8.46	0.0187
3	1.52	0.0043
4	0.57	0.00097
5	1.18	0.00028
6	1.60	0.000064
7	1.34	0.000029

2500 K are shown in the figure. Preliminary results of experiments currently in progress indicate the vibrational population distribution approaches slightly lower Boltzmann temperatures for the  $Ba + O_2$  reaction at pressures greater than 0.3 torr.

Preliminary experiments on the  $Ba + N_2O \rightarrow BaO + N_2$  reaction using this same technique suggest a relative steady state vibrational population distribution in the ground electronic state of  $BaO$  similar to that measured for the barium plus oxygen system. On the basis of this assumed similarity, the  $Ba + O_2$  results can be used to obtain an estimate of the possibility of a population inversion existing between  $A^1\Sigma(v' = 1)$

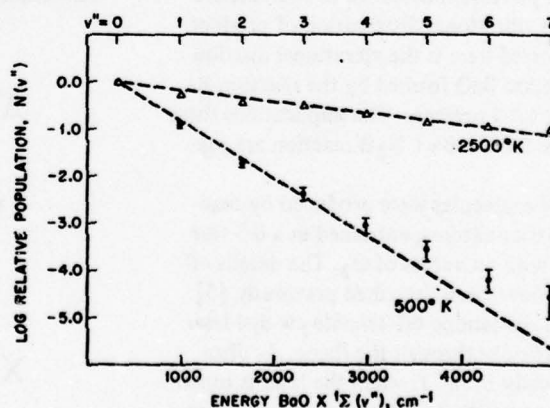


Fig. 2.  $BaO X^1\Sigma$  vibrational population distribution for the reaction  $Ba + O_2$ .  $\blacklozenge$  0.3 torr data (table 1).  $\triangle$  low pressure molecular beam data (ref. [6]). Dashed lines show Boltzmann distributions with vibrational temperatures of 2500 K and 500 K.

<sup>†</sup> The intensity of observed emission depends on the population of the excited state. In turn, this excited state population is proportional to the rate of absorption. This absorption transition rate does not, however, depend explicitly on the frequency  $\nu_{abs}$ .

and  $X^1\Sigma(v''=7)$  in BaO formed from the reaction of  $Ba + N_2O$ .  $A(v'=1)$  and  $X(v''=7)$  are of interest because (a) it has been reported [4] that for the  $Ba + N_2O$  reaction  $\approx 7\%$  of all the barium atoms introduced into the reaction zone lead to photons originating from  $A^1\Sigma(v'=1)$ , and (b) the Franck-Condon factor for the  $A^1\Sigma(v'=1) \rightarrow X^1\Sigma(v''=7)$  is the most favorable of high lying  $v''$ . Under the experimental conditions used in this study, all the barium atoms are consumed by the chemical reaction. If it is assumed that all the barium reacts to give BaO, then the known Ba flow rate and the flame geometry give a total BaO concentration of  $3 \times 10^{13}$  molecules/cm<sup>3</sup>. If it is further assumed that all of the BaO molecules are partitioned into the observed levels  $X(v''=0) - X(v''=7)$  according to the ratios in table 1, then the population in  $v''=7$  is  $\approx 7 \times 10^8$  molecules/cm<sup>3</sup>. This estimate is an upper limit since it is based on the assumption that the steady state density of product molecules in any state other than the first eight vibrational levels of  $X^1\Sigma$  is zero.

In the  $Ba + N_2O$  flame, Jones and Broida report [4] that the population density of  $A^1\Sigma(v'=1)$  peaks at  $\approx 1 \times 10^9$  molecules/cm<sup>3</sup> at approximately 16 torr. This  $A(v'=1)$  population density along with the  $Ba + O_2$  comparison described above strongly suggest that a population inversion between  $A^1\Sigma(v'=1)$  and  $X^1\Sigma(v''=7)$  exists in the  $Ba + N_2O$  flame under the conditions reported by Jones and Broida [4]. The reasons are as follows. First, the increased exothermicity of the  $Ba + N_2O$  reaction will produce more excited state BaO molecules, leaving fewer molecules to be partitioned within the ground state. If there is substantial population density in an unobserved "reservoir state", this effect could be significant [7,8]. Second, for the  $Ba + O_2$  reaction, the relative population of  $X^1\Sigma(v''=7)$  measured at higher total pressures (16 torr compared to 0.3 torr) should be reduced due to collisional relaxation of vibrationally excited molecules within the ground state manifold. (Fig. 2 indicates

that substantial vibrational relaxation has occurred at 0.3 torr.) Our preliminary data suggest that vibrational relaxation of product BaO(X) is similar for the  $Ba + O_2$  and  $Ba + N_2O$  reactions. If these assumptions are correct, the population density of BaO  $X^1\Sigma(v''=7)$  will be less than  $10^8$  molecules/cm<sup>3</sup> at 16 torr. Since the population density of BaO  $A^1\Sigma(v'=1)$  is  $3 \times 10^9$  molecules/cm<sup>3</sup> at 16 torr for the  $Ba + N_2O$  reaction [4], a significant population difference may exist between these two levels, and laser operation may be possible on the  $A^1\Sigma(v'=1) \rightarrow X^1\Sigma(v''=7)$  transition at approximately 791 nm.

Detailed pressure dependence studies of the BaO  $X^1\Sigma(v'')$  population distribution for the  $Ba + O_2$  and  $Ba + N_2O$  reactions are underway in this laboratory.

We gratefully acknowledge the support of NSF and AFOSR and would like to thank R.W. Field, G.A. Capelle and C.R. Jones for their helpful suggestions at the outset of this work.

#### References

- [1] C.D. Jonah, R.N. Zare and Ch. Ottinger, J. Chem. Phys. 56 (1972) 263.
- [2] R.H. Obenauf, C.J. Hsu and H.B. Palmer, J. Chem. Phys. 57 (1972) 5607.
- [3] S.A. Edelstein, D.J. Eckstrom, B.E. Perry and S.W. Benson, J. Chem. Phys. 61 (1974) 4932.
- [4] C.R. Jones and H.P. Broida, J. Chem. Phys. 60 (1974) 4369.
- [5] J.B. West, R.S. Bradford Jr., J.D. Eversole and C.R. Jones, Rev. Sci. Instr. 46 (1975) 164.
- [6] A. Schultz, H.W. Cruse and R.N. Zare, J. Chem. Phys. 57 (1972) 1354; P.J. Dagdigian, H.W. Cruse, A. Schultz and R.N. Zare, J. Chem. Phys. 61 (1974) 4450.
- [7] R.W. Field, C.R. Jones and H.P. Broida, J. Chem. Phys. 60 (1974) 4377.
- [8] C.J. Hsu, W.D. Krugh and H.B. Palmer, J. Chem. Phys. 60 (1974) 5118.



# Vibrational population distributions of ground state barium oxide formed in the $\text{Ba} + \text{O}_2$ and $\text{Ba} + \text{N}_2\text{O}$ reactions\*

Michael A. Revelli,<sup>†</sup> Brian G. Wicke,<sup>‡</sup> and David O. Harris

Department of Chemistry and Quantum Institute, University of California, Santa Barbara, California 93106  
(Received 25 August 1976)

The relative ground state vibrational population distributions of BaO formed in the chemical reactions  $\text{Ba} + \text{O}_2$  and  $\text{Ba} + \text{N}_2\text{O}$  have been measured as a function of total pressure between 0.3 and 10 torr using the technique of dye laser induced photoluminescence. Interpretation of these results together with previously reported excited state vibrational distribution measurements by Jones and Broida for the  $\text{Ba} + \text{N}_2\text{O}$  reaction suggest that a population inversion does exist between  $A^1\Sigma^+(v' = 1)$  and  $X^1\Sigma^+(v'' = 7)$  BaO at  $\approx 16$  torr.

## INTRODUCTION

Previous experiments<sup>1,2</sup> have measured the relative vibrational population distribution of ground state BaO formed by the reaction of  $\text{Ba} + \text{O}_2$  under nearly single collision conditions. Recently, we reported<sup>3</sup> a relative vibrational population distribution for ground state BaO produced in the same reaction at 0.3 torr total pressure. In this paper, we have extended these measurements to include both  $\text{O}_2$  and  $\text{N}_2\text{O}$  as oxidants at total pressures between 0.3 and 10 torr.

Our interest in the  $\text{Ba} + \text{N}_2\text{O}$  reaction stems from the high chemiluminescent efficiency first reported by Jones and Broida<sup>4</sup> and from the dependence of the chemiluminescent efficiency on total pressure.<sup>5-7</sup> At low pressure ( $3 \times 10^{-3}$  torr), the photon yield for the  $\text{Ba} + \text{N}_2\text{O}$  reaction measured by Palmer *et al.* was 0.4%.<sup>5</sup> In contrast, at total pressures near 10 torr, Jones and Broida<sup>7</sup> found that approximately 20% of all Ba atoms consumed in the chemical reaction produce emission in the  $A-X$  system. Using chemiluminescent band intensities they showed that about 1/3 of the  $A-X$  photons originate from the  $A^1\Sigma^+(v' = 1)$  level. Their absolute intensity measurements implied a peak steady state concentration of BaO  $A^1\Sigma^+(v' = 1)$  of  $1 \times 10^9$  molecules/cm<sup>3</sup>. Given this large population density in one vibrational level of an excited electronic state, Jones and Broida suggested that the  $\text{Ba} + \text{N}_2\text{O}$  reaction at a total pressure near 10 torr might be a viable candidate for a chemical laser system. In examining further this possible population inversion, we have measured the BaO  $X^1\Sigma^+$  vibrational population distribution as a function of total pressure under conditions essentially identical to those of Jones and Broida.

## EXPERIMENTAL

Details of the apparatus used to produce metal-vapor oxidant flames have been described previously<sup>8</sup> so only a brief description will be given here. Barium vapor from barium metal in an alumina crucible heated to  $\sim 1100^\circ\text{K}$  was entrained in argon and allowed to react with either  $\text{O}_2$  or  $\text{N}_2\text{O}$  in a separate chamber to produce a flame of 2 or 3 cm<sup>3</sup>. Flow rates indicate an oxidant rich reaction with argon the most abundant species by approximately a factor of 1000. Pressures of 0.3 to 10 torr in the reaction zone were established by varying the pumping speed. Minor adjustments of the oxidant flow preserved the flame geometry.

Relative vibrational populations in the ground state were measured using the technique of laser induced photoluminescence described previously.<sup>3</sup> The output of a Rhodamine 6G cw dye laser was directed vertically through the flame; photoluminescence was monitored with a 1 m monochromator. The laser was 100% amplitude modulated at 25 Hz to eliminate contributions to the signal from chemiluminescence. The laser was tuned to excite a single vibrational level  $v'$  of the  $A^1\Sigma^+$  state from two adjacent levels  $v_1''$  and  $v_2''$  of the ground  $X^1\Sigma^+$  state. Vibrationally resolved (1 nm resolution) photoluminescence from  $A^1\Sigma^+(v')$  to a third ground state level  $v_3''$  was monitored. The particular  $v_3''$  was chosen so that the resultant photoluminescence was outside the dye laser region to eliminate interference from scattered laser light. Frequent experimental checks were made to ensure that the free running dye laser intensity was sufficiently low so that the laser induced fluorescence intensity was linear with laser power.

Because a single emission band was monitored while sequentially pumping from two adjacent  $X^1\Sigma^+(v_i'')$  levels, the ratio of the two  $X^1\Sigma^+(v_i'') \rightarrow A^1\Sigma^+(v') \rightarrow X^1\Sigma^+(v_3'')$  photoluminescence intensities in the linear absorption region is given by

$$\frac{I_1}{I_2} = \frac{I(v_1'' \rightarrow v' \rightarrow v_3'')}{I(v_2'' \rightarrow v' \rightarrow v_3'')} = \frac{\text{Rate of absorption from } v_1''}{\text{Rate of absorption from } v_2''} \quad (1)$$

It should be noted that the rate of absorption from  $v_i''$  is given in molecules/sec and not in energy/sec; as a result, the factor  $h\nu$  appearing in many energy absorption rate expressions<sup>9</sup> is inappropriate here. In this linear absorption limit the rate of absorption from a lower level is given in terms of the Einstein  $B$  coefficient for absorption and the laser power density  $\rho$  by

$$\text{Rate}(v_i'' \rightarrow v') = \rho_{v', v_i''} N_{v_i''} B_{v', v_i''} \quad (2)$$

Although the absolute intensity of a particular photoluminescence band does depend on other molecular and experimental parameters (e.g., the Einstein  $A$  coefficient for the  $v' \rightarrow v_3''$  transition, detector efficiency, etc.), the ratio, given in Eq. (1), is independent of these other factors. Hence, the measurement here of successive intensity ratios obviates the necessity of calibrating the detector system. Substituting Eq. (2) into Eq. (1) gives an expression for the ratio of the populations of the two adjacent ground state levels as

$$\frac{N_{v_1''}}{N_{v_2''}} = \frac{(I_1/\rho_{v_1''})}{(I_2/\rho_{v_2''})} \frac{\langle A(v') | M | X(v_1'') \rangle^2}{\langle A(v') | M | X(v_2'') \rangle^2}, \quad (3)$$

where the ratio of Einstein *B* coefficients has been replaced by the ratio of the square of the electronic transition moment matrix elements.

Previous population distribution analyses on BaO have assumed the square of the electronic transition moment either was constant in the BaO  $A^1\Sigma^+ - X^1\Sigma^+$  electronic system or was expressible as a constant electronic factor times the Franck-Condon factor for the vibronic transition. Indeed, in the absence of detailed information on the behavior of the electronic transition moment on internuclear distance  $r$ , the latter Franck-Condon approximation represents the only real alternative. For the BaO  $A - X$  system, however, Best and Hoffman<sup>10</sup> have carried out a detailed analysis of BaO emission intensities as a function of vibronic band, and have obtained experimentally the variation of the electronic transition moment  $\langle M(R) \rangle$  with internuclear distance. We have used their electronic transition moment function and the RKR-derived potential functions for the  $X^1\Sigma^+$  and the  $A^1\Sigma^+$  states of BaO to calculate the necessary transition moment ratios given in Eq. (3). It is interesting to note the magnitude of the contributions to the required ratios in Eq. (3). The Franck-Condon factors are extremely important, easily leading to an order of magnitude change in the ratio in Eq. (3). The additional correction to our results not adequately accounted for by the Franck-Condon factors leads only to a further 5% variation in this ratio. This contribution is surprisingly small<sup>11</sup> because the electronic transition moment determined by Best and Hoffman is virtually constant over the range of  $r$  centroids sampled by the laser excitation transitions we have used in this work.

Normalized band intensities ( $I/\rho$ ) were recorded in our experiments using a ratio amplifier. The signal voltage  $Z_I$  was supplied from a 1P28 PMT at the exit slit of the monochromator tuned to the  $A^1\Sigma^+(v') - X^1\Sigma^+(v'')$  band. The laser intensity  $\rho$  was monitored using another photomultiplier which sampled a small fraction of the unmodulated dye laser output directly, giving a voltage signal  $Z_\rho$ . The ratio amplifier provided the algebraic ratio  $Z_I/Z_\rho$ , which was later corrected

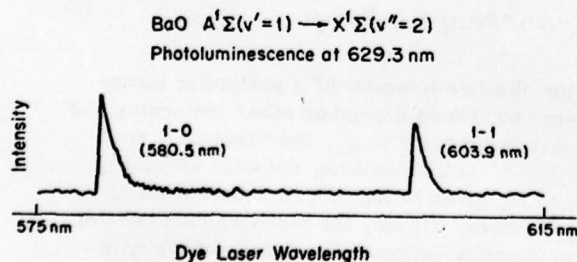


FIG. 1. BaO  $A^1\Sigma^+(v'=1) \rightarrow X^1\Sigma^+(v''=2)$  photoluminescence recorded at 629.3 nm as a function of dye laser excitation wavelength. The band on the left arises from pumping the  $A-X$  (1-0) band; that on the right from the  $A-X$  (1-1) band. The BaO was produced in a Ba + O<sub>2</sub> flame at 0.3 torr.

TABLE I. Relative populations of the vibrational levels in  $X^1\Sigma$  BaO formed by the reaction of Ba with oxidant at pressures of 0.3 to 10 torr. Successive ratios are normalized to  $N_0=1.0$  and are accurate to  $\approx 10\%$ .

	0.3 torr <sup>a</sup>	1 torr	3 torr	5 torr	
Ba + O <sub>2</sub>					
$N_0$	(1.0000)	(1.0000)	(1.0000)	(1.0000)	
$N_1$	0.123	0.108	0.114	0.136	
$N_2$	0.0184	0.0132			
$N_3$	0.0043	0.0018			
$N_4$	0.00098				
$N_5$	0.00029				
$N_6$	0.000065				
$N_7$	0.000030				
	0.3 torr	1 torr	3 torr	5 torr	10 torr
Ba + N <sub>2</sub> O					
$N_0$	(1.0000)	(1.0000)	(1.0000)	(1.0000)	(1.0000)
$N_1$	0.162	0.153	0.117	0.111	0.096
$N_2$	0.0322	0.0209			
$N_3$	0.0108	0.0050			
$N_4$	0.0034	0.0015			

<sup>a</sup>Because the variation in the electronic transition moment has been included these numbers differ slightly from those previously published in Ref. 3.

for the wavelength sensitivity related to  $Z_\rho$ .

Figure 1 shows a typical excitation spectrum; here the monochromator was set to detect rotationally unresolved photoluminescence in the  $A^1\Sigma^+(v'=1) - X^1\Sigma^+(v''=2)$  band at 629.3 nm.<sup>12</sup> As the laser was scanned at 0.5 nm/sec with a 0.05 nm bandwidth across its tuning range, an excitation signal was observed only when the laser pumped molecules into  $A^1\Sigma^+(v'=1)$  from  $X^1\Sigma^+(v'')$  levels. Limited by the tuning range of Rhodamine 6G, Fig. 1 shows two laser induced photoluminescence signals corresponding to emission in the (1-2) band at 629.3 nm as the laser pumps (1-0) at 580.5 nm and (1-1) at 603.9 nm, respectively. Together with the appropriate transition moment ratios, the ratio of these band intensities was then used to obtain the  $N_{v'',0}/N_{v'',1}$  population ratio according to Eq. (3). Repeated application of this technique provided a method for measuring successive population ratios  $N_{v'',0}/N_{v'',1}$ ,  $N_{v'',1}/N_{v'',2}$ , etc., through the ground state vibrational manifold. Data were recorded using a Nicolet signal averager, and intensities were measured by digital integration of the area under each band.

## RESULTS

Successive vibrational band intensity ratios were determined for pressures between 0.3 and 10 torr. Repeated measurements of each pair of vibrational band intensities established a random error of  $\pm 10\%$  for each ratio. Several ratios were measured many more times to ensure statistical reproducibility on different days. Relative populations normalized to  $N_0=1$  were obtained from the measured band intensity ratios and Eq. (3). Results for the Ba + O<sub>2</sub> and Ba + N<sub>2</sub>O reactions are given in Table I.



## DISCUSSION

Population measurements for vibrational levels beyond those given in Table I were not possible because of vanishing signal strength; nevertheless, the Ba + O<sub>2</sub> data at 0.3 torr can be used to establish a sensitivity limit for these experiments. This limit can then in turn be used to examine the possibility of a population inversion between levels of the A<sup>1</sup>Σ<sup>+</sup> state and the ground state for BaO produced in the Ba + N<sub>2</sub>O reaction under the high quantum efficiency conditions reported earlier.<sup>7</sup>

A barium atom flux of 10<sup>17</sup> atoms/sec in an argon gas flow rate of 10<sup>21</sup> atoms/sec, assuming complete reaction, produces a BaO partial pressure of one mtorr or 3 × 10<sup>13</sup> molecules/cm<sup>3</sup>. If it is further assumed that these molecules are partitioned only into the first eight vibrational levels of X<sup>1</sup>Σ<sup>+</sup> according to the Ba + O<sub>2</sub> data at 0.3 torr, then the population density in X<sup>1</sup>Σ<sup>+</sup>(v'' = 7) is ≈ 8 × 10<sup>8</sup> molecules/cm<sup>3</sup>. Because this estimate is based on the assumption that the steady state population density of BaO in any state other than the first eight vibrational levels of the ground state is zero, it places an approximate upper limit on the minimum sensitivity of these experiments.

The possibility of an inversion existing in the BaO distribution formed from the Ba + N<sub>2</sub>O reaction at 10 torr can now be examined. Jones and Broida reported that the number of BaO emitters in the Ba + N<sub>2</sub>O flame is approximately 10<sup>9</sup>/cm<sup>3</sup> in the A<sup>1</sup>Σ<sup>+</sup>(v' = 1) vibrational level. Of the modestly high lying ground state levels, X<sup>1</sup>Σ<sup>+</sup>(v'' = 7) has the most favorable Franck-Condon factor with A<sup>1</sup>Σ<sup>+</sup>(v' = 1). Using the same technique, which detected no more than 8 × 10<sup>8</sup> molecules/cm<sup>3</sup> in X<sup>1</sup>Σ<sup>+</sup>(v'' = 7) for the Ba + O<sub>2</sub> reaction at 0.3 torr, we were unable to detect any population in this state for the Ba + N<sub>2</sub>O reaction at any pressure between 0.3 and 10 torr. This observation might have been anticipated because the increased exothermicity of the Ba + N<sub>2</sub>O reaction relative to oxygen will produce more excited state BaO molecules, leaving fewer to populate the ground state. Previous results using Ar<sup>+</sup> 488.0 nm laser induced photoluminescence revealed that under identical conditions the Ba + O<sub>2</sub> reaction produced approximately five times higher a concentration of BaO X<sup>1</sup>Σ<sup>+</sup>(v'' = 0) than the reaction with N<sub>2</sub>O. Also, if there is substantial population density in an unobserved reservoir state, this effect could be significant.<sup>13</sup> These results along with those of Jones and Broida strongly suggest that a A<sup>1</sup>Σ<sup>+</sup>(v' = 1) - X<sup>1</sup>Σ<sup>+</sup>(v'' = 7) population inversion exists in the Ba + N<sub>2</sub>O flame under the conditions previously reported. If this population difference is significant, laser operation near 791 nm may be possible.

It was disappointing that we were unable to measure directly the relative populations for higher vibrational levels at the higher pressures. This is contrary to what might be expected; from collisional quenching the total ground state population should increase with increasing pressure. Previous results show that the ground state vibrational distribution for BaO formed at 10<sup>-3</sup> torr is thermal (2500 °K).<sup>1,2</sup> Similarly, our data for the Ba

+ O<sub>2</sub> reaction at 0.3 torr indicate ground state vibrational equilibration corresponding to a temperature of 500 °K. Indeed, at still higher pressures, some vibrational relaxation in the excited A<sup>1</sup>Σ<sup>+</sup> state occurs. For example, at 3 torr emission from A<sup>1</sup>Σ<sup>+</sup>(v' = 1) while pumping A<sup>1</sup>Σ<sup>+</sup>(v' = 2) is clearly observed despite an A<sup>1</sup>Σ<sup>+</sup> radiative lifetime of 350 nsec.<sup>14</sup>

The fact that we were unable to measure these higher vibrational population ratios must be ascribed to either higher flame noise or to lower signal strengths. We feel that it is the latter. For example, absolute signal strengths of the (1-2) photoluminescence band were observed to decrease by almost a factor of 20 over the 0.3 to 5 torr pressure range while the noise remained nearly constant. We must attribute this reduction in absolute signal strength at higher pressures to a decrease in the total ground state molecular BaO density. In turn, the lower BaO density could result from one or a combination of the following factors: The first is a lowered Ba atom flux rate. At high argon buffer gas pressures there may be increased conductive cooling of the alumina crucible containing the barium metal thus lowering its vapor pressure. A drop of approximately 125° would account for a factor of 10 decrease in the number of Ba atoms entering the argon stream with a consequent reduction in the number of barium atoms available for reaction. In fact, at the higher pressures, it was necessary to reduce slightly the total O<sub>2</sub> or N<sub>2</sub>O concentration in order to maintain the 2-3 cm<sup>3</sup> flame volume. This maintenance of flame geometry was essential to the valid comparison between the Jones and Broida A<sup>1</sup>Σ<sup>+</sup> population estimates and our ground state data. Secondary reactions which at higher pressures are more effective in removing ground state molecules are a second possibility for the lowered BaO density. We know, for example, that such a mechanism exists because we are not able to observe laser induced photoluminescence of BaO much beyond the flame zone. A third possibility is that a dark reservoir state exists which traps excited state molecules some time after their initial formation. If the population in such a state is significant, it would leave fewer BaO molecules of the total available to be partitioned into the ground state levels. Such a state has been postulated<sup>13</sup> to account for the high A-X photon yield and its pressure dependence.

## CONCLUSION

It should be emphasized that the above considerations do not affect the A<sup>1</sup>Σ<sup>+</sup>(v' = 1) - X<sup>1</sup>Σ<sup>+</sup>(v'' = 7) population comparison made earlier. A valid comparison required that both sets of measurements be made under nearly identical flame conditions. Unfortunately working within this constraint we found that the number of BaO X<sup>1</sup>Σ<sup>+</sup>(v'' > 1) molecules in the high pressure flames to be below the sensitivity limit of the technique as established by the Ba + O<sub>2</sub> data at 0.3 torr, thus precluding a direct measurement of the BaO X<sup>1</sup>Σ<sup>+</sup>(v'' = 7) population at 10 torr.

In addition to the results specific to the Ba + N<sub>2</sub>O and Ba + O<sub>2</sub> reactions reported here, it has been demon-

strated that the laser induced photoluminescence technique is a sensitive and versatile probe of the steady state population distributions of ground state product molecules formed in chemical reactions.

#### ACKNOWLEDGMENTS

We gratefully acknowledge Mr. Jack Waidner for his design and construction of the ratio amplifier used in these experiments.

\*This research was supported in part by AFOSR Grant No. AFOSR-73-2565, and NSF Grant No. MPS-72-04978.

†Present address: Lawrence Livermore Laboratory, L-404, Livermore, CA 94550.

‡Present address: TRW System Group, One Space Park, R1/1196, Redondo Beach, CA 90278.

<sup>1</sup>A. Schultz, H. W. Cruse, and R. N. Zare, *J. Chem. Phys.* **57**, 1354 (1972).

<sup>2</sup>P. J. Dagdigian, H. W. Cruse, A. Schultz, and R. N. Zare, *J. Chem. Phys.* **61**, 4450 (1974).

<sup>3</sup>M. A. Revelli, B. G. Wicke, and D. O. Harris, *Chem.*

*Phys. Lett.* **39**, 454 (1976).

<sup>4</sup>C. R. Jones and H. P. Broida, *J. Chem. Phys.* **59**, 6677 (1973).

<sup>5</sup>C. J. Hsu, W. D. Krugh, and H. B. Palmer, *J. Chem. Phys.* **60**, 5118 (1974).

<sup>6</sup>D. J. Eckstrom, S. A. Edelstein, and S. W. Benson, *J. Chem. Phys.* **60**, 2930 (1974).

<sup>7</sup>C. R. Jones and H. P. Broida, *J. Chem. Phys.* **60**, 4369 (1974).

<sup>8</sup>J. B. West, R. S. Bradford, Jr., J. D. Eversole, and C. R. Jones, *Rev. Sci. Instrum.* **46**, 164 (1975).

<sup>9</sup>G. Herzberg, *Spectra of Diatomic Molecules* (Van Nostrand-Reinhold, New York, 1950).

<sup>10</sup>G. T. Best and H. S. Hoffman, *J. Quant. Spectrosc. Radiat. Transfer* **13**, 69 (1973).

<sup>11</sup>Note that this small variation in the electronic transition moment is inconsistent with the observed BaO A-X band intensities reported by Best and Hoffman (see Ref. 10).

<sup>12</sup>The maximum laser induced photoluminescence signals for the BaO A-X bands occurred at wavelengths slightly red shifted from the reported bandheads.

<sup>13</sup>R. W. Field, C. R. Jones, and H. P. Broida, *J. Chem. Phys.* **60**, 4377 (1974).

<sup>14</sup>S. E. Johnson, *J. Chem. Phys.* **56**, 149 (1972).



# On the importance of $\text{Ba}(^3D)$ as the key reactant leading to $\text{BaO}(A-X)$ chemiluminescence in the $\text{Ba} + \text{N}_2\text{O}$ reaction\*

Brian G. Wicke, Michael A. Revelli, and David O. Harris

Department of Chemistry and Quantum Institute, University of California, Santa Barbara, California 93106  
(Received 8 April 1975)

Experiments have been performed to examine the importance of metastable  $\text{Ba}(^3D)$  as the key reactant leading to  $\text{BaO}(A-X)$  chemiluminescence in the  $\text{Ba} + \text{N}_2\text{O}$  reaction. It has been found that the steady state concentration of  $\text{Ba}(^3D)$  increases substantially in the reaction of Ba with  $\text{N}_2\text{O}$ ; in contrast, the  $\text{Ba}(^3D)$  steady state concentration decreases when  $\text{O}_2$  and  $\text{NO}_2$  are used as oxidants. By simultaneously monitoring the  $\text{BaO}(A-X)$  chemiluminescence and the  $\text{Ba}(^3D)$  steady state concentration, it is shown that with the oxidant unchanged, an order of magnitude increase in  $\text{Ba}(^3D)$  has no major effect ( $\pm 15\%$ ) on the  $\text{BaO}(A-X)$  emission. These results restrict the role played by  $\text{Ba}(^3D)$  in the reaction mechanism leading to  $A \rightarrow X$  chemiluminescence.

## INTRODUCTION

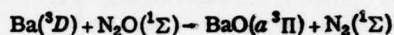
Recently there has been considerable interest in the reaction  $\text{Ba} + \text{N}_2\text{O}$ .<sup>1-6</sup> The primary reason for this interest was the finding of Jones and Broida that under proper conditions the  $\text{BaO}(A-X)$  chemiluminescence from this reaction correspond to a photon yield of over 20%.<sup>3</sup> Even more striking was the finding that one-third of the photons originate from  $\text{BaO } A^1\Sigma^+$  ( $v'=1$ ). Since this observation, the  $\text{Ba} + \text{N}_2\text{O}$  reaction has been the subject of much further experimental study. While there is general agreement concerning the high photon yield, some other features of this reaction are less generally accepted.

The kinetics mechanism leading to the  $A-X$  chemiluminescence appears to be moderately complex and is not well understood. The effects of pressure on the total photon yield and the chemiluminescence spectral distribution have been reported by Jones and Broida.<sup>3</sup> Based on the observed vibrational population of  $A^1\Sigma^+$ , on known perturbations between  $\text{BaO } a^3\Pi$  and  $A^1\Sigma^+$ , and on the pressure dependence of the total photon yield, Field, Jones, and Broida have suggested that  $\text{BaO } a^3\Pi$  is the original  $\text{Ba} + \text{N}_2\text{O}$  reaction product<sup>4</sup>; according to this proposed mechanism, collisionally induced transitions from  $\text{BaO } a^3\Pi$  then lead to  $A^1\Sigma^+$  emission.

Much of the recent discussion of the mechanism for the mechanism for the  $\text{Ba} + \text{N}_2\text{O}$  reaction has centered on how the  $\text{BaO } a^3\Pi$  state can be formed from the reactants.<sup>1,2</sup> Field, Jones, and Broida<sup>2,4</sup> proposed a reaction mechanism based on adiabatic correlation between  $\text{Ba}(^1S)$  and virtually free  $\text{O}(^3P)$  from  $\text{N}_2\text{O}$  to give  $\text{BaO}(a^3\Pi)$ . The adiabatic dissociation products of ground state  $\text{N}_2\text{O}$ , however, are  $\text{O}(^1D)$  and  $\text{N}_2(^1\Sigma)$ . Using both weak spin-orbit and ( $J, J$ ) adiabatic correlations, Husain and Wiesenfeld<sup>1</sup> have shown that  $\text{Ba}(^3D) + \text{N}_2\text{O}(^1\Sigma)$  are adiabatically correlated to the  $a^3\Pi$  state of  $\text{BaO}$ . Hence Husain and Wiesenfeld<sup>1</sup> suggest that  $\text{Ba}(^3D)$  is required to produce  $\text{BaO } a^3\Pi$  via an adiabatic reaction pathway.

The experiments reported here examine the importance of  $\text{Ba}(^3D)$  in producing chemiluminescence in the  $\text{Ba} + \text{N}_2\text{O}$  reaction. It must be emphasized at the beginning that these results have different implications for different reaction mechanisms. Within the framework of Field's proposal<sup>2,4</sup> involving  $\text{BaO}(a^3\Pi)$  and Husain's

adiabatic correlations,<sup>1</sup> these experiments examine the importance of the step



in the reaction leading eventually to  $A-X$  chemiluminescence.

## RESULTS

The experiments reported here utilize atomic spectroscopy to monitor the relative concentrations of excited Ba species under various pressure conditions and in the presence of various oxidizers. In particular, the  $\text{Ba}(^3D)$  population and the  $\text{BaO}(A-X)$  chemiluminescence were monitored under identical experimental conditions, and in some cases simultaneously. The basic apparatus is identical to that used in the  $\text{BaO}$  chemiluminescence studies.<sup>3,7</sup> A ceramic crucible containing barium metal was resistively heated to about 1100 °K by a tungsten wire heater. Vapor phase barium atoms were entrained by argon carrier gas and flowed upward into the burner region, where various oxidants were added to the argon-barium stream. The output from a tunable cw dye laser<sup>8</sup> was directed downward through the burner region, coinciding with part of the barium flow. A 1 m scanning monochromator observed both chemiluminescence and photoluminescence in the burner region through a side window. Most of the work reported here was performed at total pressures of 50–200 mtorr with argon the most abundant species by at least two orders of magnitude.

At modest argon flow, a chamber pressure of 50 mtorr and in the absence of any added oxidant, no atomic or molecular emission between 400 and 600 nm was observed. When the dye laser was tuned to one of the  $^3D-^3P$  absorptions of barium (see Fig. 1), weak photoluminescence emission was visible by eye. This emission was unambiguously assigned to  $\text{Ba } ^3P-^3D$  by observing the photoluminescence through the monochromator. Emission was observed at the laser wavelength and at the wavelengths of the allowed transitions from the laser pumped upper level to other fine structure levels of  $^3D$ . Considerably weaker emission from the fine structure levels of  $^3P$  other than the pumped component were also observed; these other  $^3P$  fine structure levels were populated by collision induced transitions between the

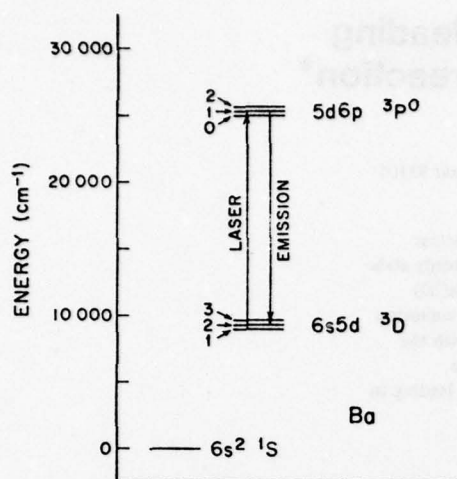


FIG. 1. A partial schematic energy level diagram for atomic barium displaying the levels utilized in our experiments. For clarity, four triplet levels and four singlet levels between  $^3D$  and  $^3P^0$  have been omitted.

fine structure components. Figure 1 shows the appropriate energy level diagram of Ba.

At constant laser power, the intensity of laser induced emission for any particular  $^3P$ - $^3D$  fine structure component is directly proportional to the amount of  $Ba(^3D)$  present; this emission intensity may therefore be used to measure changes in the  $Ba(^3D)$  concentration under differing reaction conditions. To insure that scattered laser light did not interfere, the monochromator was tuned to a  $^3P$ - $^3D$  fine structure component other than that which was pumped by the laser. Care was also taken to ensure that bright chemiluminescence was not confused with the laser induced photoluminescence.

The importance of  $Ba(^3D)$  in the kinetics of  $Ba + N_2O$  must not be dismissed on the basis of the small thermal population of  $Ba(^3D)$  at the oven temperatures used. The excitation energy  $^1S$ - $^3D$  is approximately  $9300 \text{ cm}^{-1}$  (see Fig. 1), implying that on the order of 0.01% of the barium would be present as  $Ba(^3D)$  at thermal equilibrium. Although this thermal population is too small to account for the 20% photon yield,  $Ba(^3D)$  may itself be produced from  $Ba(^1S)$  in the chemical reaction. While monitoring laser induced  $Ba^3P$ - $^3D$  emission, various oxidants were slowly introduced into the burner chamber. With  $N_2O$ , there was a dramatic increase in the laser induced emission from triplet barium; the peak intensity was a factor of 10-50 greater than in the absence of  $N_2O$  with other conditions constant. Additional  $N_2O$  then decreased the  $Ba(^3D)$  concentration, presumably because of consumption of barium in the stream. When the barium flow was increased, more  $N_2O$  was needed to peak the  $Ba(^3D)$  concentration. Under these conditions no barium emission was observed in the absence of laser excitation. In the case of  $N_2O$ , it is clear that  $Ba(^3D)$  is formed in the chemical reaction.

In contrast to the behavior with  $N_2O$ , use of either  $O_2$  or  $NO_2$  as oxidant only decreased the  $Ba(^3D)$  concentration. Although these results do not imply that no  $Ba(^3D)$

formed, it may be concluded that the steady state concentration of  $Ba(^3D)$  does not increase in the reaction of Ba with these two oxidants.

In the presence of  $N_2O$ , the  $Ba(^3D)$  concentration is markedly increased. Although the  $Ba(^3D)$  concentration is still low, it must not be inferred that it is too small to account for the large chemiluminescence photon yield. There are numerous kinetic schemes in which a small steady state concentration of the key reactant can lead to extremely efficient product formation. In order to determine if  $Ba(^3D)$  is such an efficient reactant in producing  $BaO(A-X)$  chemiluminescence, the A-X emission intensity was monitored while changing the  $Ba(^3D)$  concentration. The  $Ba(^3D)$  concentration was changed by making a slight modification in the apparatus. The crucible heater coil was powered by free floating alternating current. For subsequent experiments, a small dc voltage was applied (0-3 V) between the heater filament near the outlet of the crucible and the metal plate separating the oven from the burner region, making the filament slightly negative with respect to the grounded plate.<sup>7</sup> The  $Ba(^3D)$  concentration was monitored with no oxidant in the burner chamber while changing this small auxiliary dc voltage. It was found that for a given heater setting a very large increase in the  $Ba(^3D)$  concentration could be obtained by applying a small voltage. The optimal dc voltage and the resulting  $Ba(^3D)$  increase depended reproducibly on the heater setting. Typically 2 V increased the  $Ba(^3D)$  concentration by a factor of 100. Under these conditions the direct circuit was carrying less than 1 mA of current, and in the absence of laser induced photoluminescence no atomic emission was observed. Increased  $Ba(^3D)$  under these conditions may result from electron impact excitation of  $Ba(^1S)$  by thermionic electrons from the tungsten heater. It was also possible to drive a discharge in the oven region by supplying several volts of dc and drawing 1 A of current in the direct circuit. Under these more extreme conditions, spontaneous emission from excited barium atoms and barium ions ( $Ba^+$ ) could be observed.

With excess  $N_2O$  flowing into the burner region and a total pressure of 200 mtorr, the  $BaO(A-X)$  chemiluminescence emission was measured as a function of  $Ba(^3D)$  concentration. Figure 2 shows successive spectra recorded by sweeping the monochromator through a 7.0 nm region containing the strong  $A^1\Sigma^+(v'=1) - X^1\Sigma^+(v''=1)$  emission band. Figure 2a shows this chemiluminescence emission with dc off. Figure 2b shows the same spectral region under identical conditions *except* that the dc was set to nominally 2 V. The intensity of the A-X emission changes very little (a 10% decrease in Fig. 2b). Figure 2c shows the same spectral region under identical conditions with the dc off and the dye laser tuned to the  $^3D_1$ - $^3P_1$  barium transition at 599.71 nm. The new emission at 606.31 nm is the barium  $^3P_1$ - $^3D_2$  line. Figure 2d shows the same spectral region with the dc set at 2 V and the dye laser tuned to the same Ba transition as in 2c; note the large increase in Ba laser induced emission. As Fig. 2 illustrates, an order of magnitude increase in the steady state concentration of  $Ba(^3D)$  produced only a modest change in the A-X emission.



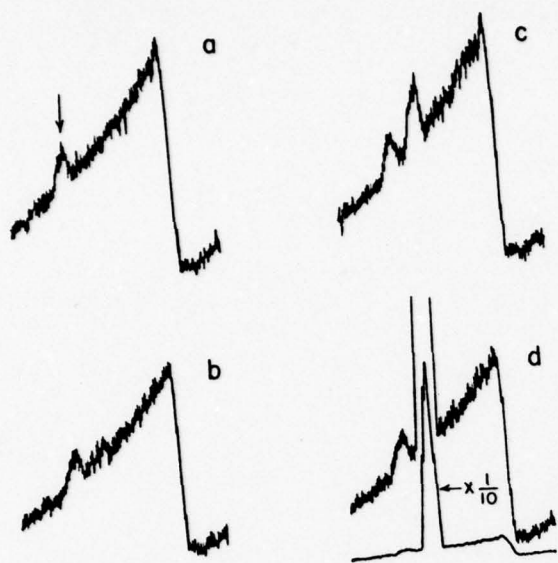


FIG. 2. Effect of Ba( $^3D$ ) on BaO  $A^1\Sigma^+(v'=1) - X^1\Sigma^+(v''=1)$  chemiluminescence for Ba + N<sub>2</sub>O. Experimental conditions and sensitivity are constant except as noted. The weak feature (identified by the arrow in a) at 607 nm is consistent with several  $A \rightarrow X$  and  $A' \rightarrow X$  emissions. (a)  $A(v'=1) - X(v''=1)$  chemiluminescence with auxiliary dc voltage off. (b) Same as a except the auxiliary dc is on. (c) Same as a except the dye laser is tuned to the Ba  $^3D \rightarrow ^3P$  absorption at 599.71 nm; the new feature at 606.31 nm is a Ba  $^3P \rightarrow ^3D$  laser induced emission. (d) Same as c except that the dc is turned on; note the large increase in the Ba laser induced emission with no corresponding change in the  $A \rightarrow X$  chemiluminescence (insert shows 1/10 sensitivity).

The  $A(v'=1)$  level was chosen because  $v'=1$  is reported<sup>4</sup> to be strongly perturbed by BaO  $a^3\Pi$ . If the  $A \rightarrow X$  chemiluminescence were limited by the Ba( $^3D$ ) concentration, this band should have shown a marked increase in intensity as Ba( $^3D$ ) was increased by more than an order of magnitude. This is clearly not the case.

The Ba + N<sub>2</sub>O chemiluminescence spectrum from 350 to 620 nm was also examined as a function of increased Ba( $^3D$ ) steady state concentration; no segment of the chemiluminescence spectrum was modified by more than  $\pm 15\%$  when the small dc voltage was applied. For fixed experimental conditions, the effect of the dc on the intensity of the chemiluminescence was reproducible, and all regions of the spectrum appeared to be affected equivalently. For example, chemiluminescence at all wavelengths might increase by 5% under some conditions, but under modified conditions, a decrease of 10% might be observed. No feature of the chemiluminescence was observed to change by as much as 20% despite the order of magnitude increase in Ba( $^3D$ ). We are examining these small changes for possible further information concerning the reaction kinetics. There is the possibility that under the more extreme conditions of the discharge, the total barium flow characteristics may change.

## CONCLUSIONS

We emphasize that our results do not imply that Ba( $^1S$ ) is the only barium reactant leading to  $A \rightarrow X$  chemiluminescence. Were Ba( $^1S$ ) the only barium reactant, our experiments would be expected to show no large change in the  $A \rightarrow X$  chemiluminescence, as observed. However, if Ba( $^1S$ ) and Ba( $^3D$ ) are both reactants leading to chemiluminescence, the effect on the  $A \rightarrow X$  chemiluminescence of increasing Ba( $^3D$ ) would be critically dependent on the nature of the reaction mechanism and on the cross sections for reaction of Ba( $^1S$ ) and Ba( $^3D$ ); the effect on the chemiluminescence spectral distribution might be small and either positive or negative. The results reported here are consistent with several mechanisms for the Ba + N<sub>2</sub>O reaction. A mechanism in which Ba( $^3D$ ) is not involved in producing the chemiluminescence, or a mechanism in which Ba( $^3D$ ) is one of several important barium reactants, is consistent with these results. Further, a mechanism in which Ba( $^3D$ ) is the *only* important reactant leading to  $A \rightarrow X$  chemiluminescence may be consistent with these results, but the observed lack of dependence of  $A \rightarrow X$  emission on increased Ba( $^3D$ ) places severe restrictions on the overall mechanism in this case.

It is possible to use these experimental results together with other data for this reaction to infer conclusions about specific reaction mechanisms. We refrain from such discussion here, however, to insure that these results are not linked to any one mechanism. Considerable additional work is clearly required to unravel the kinetics of this reaction. We believe that adequate attention has not been paid to the first step of the reaction.

This use of spectroscopy to monitor the possible importance of one reactant or intermediate is another of many examples of the utility of spectroscopy in studying kinetic mechanisms without altering the reaction itself. Additional studies of this type may be helpful in attempting to deduce the kinetic mechanism responsible for other chemiluminescence producing reactions.

## ACKNOWLEDGMENTS

We thank Professor H. P. Broida for his always constructive comments and R. W. Field for his suggestion of how to monitor the relative barium ( $^3D$ ) concentration. We gratefully acknowledge the support of AFOSR.

\*Work supported in part by AFOSR Grant No. AFOSR-73-2565.

<sup>1</sup>D. Husain and J. R. Wiesenfeld, *J. Chem. Phys.* **62**, 2010 (1975).

<sup>2</sup>R. W. Field, C. R. Jones, and H. P. Broida, *J. Chem. Phys.* **62**, 2012 (1975).

<sup>3</sup>C. R. Jones and H. P. Broida, *J. Chem. Phys.* **60**, 4369 (1974).

<sup>4</sup>R. W. Field, C. R. Jones, and H. P. Broida, *J. Chem. Phys.* **60**, 4377 (1974).

<sup>5</sup>D. J. Eckstrom, S. A. Edelstein, and S. W. Benson, *J. Chem. Phys.* **60**, 2930 (1974).

<sup>6</sup>C. J. Hsu, W. D. Krugh, and H. B. Palmer, *J. Chem. Phys.* **60**, 5118 (1974).

<sup>7</sup>J. B. West, R. S. Bradford, Jr., J. D. Eversole, and C. R. Jones, *Rev. Sci. Instrum.* **46**, 164 (1975).

<sup>8</sup>R. W. Field, A. D. English, T. Tanaka, D. O. Harris, and D. A. Jennings, *J. Chem. Phys.* **59**, 2191 (1973).

# Argon Ion and Dye Laser Induced MgO $B^1\Sigma^+-X^1\Sigma^+$ and $B^1\Sigma^+-A^1\Pi$ Photoluminescence Spectra Analysis of $a^3\Pi_i \sim X^1\Sigma^+$ Perturbations<sup>1</sup>

TATSUYA IKEDA,<sup>2</sup> NING BEW WONG, AND DAVID O. HARRISDepartment of Chemistry and Quantum Institute, University of California,  
Santa Barbara, California 93106

AND

ROBERT W. FIELD<sup>3</sup>Department of Chemistry, Massachusetts Institute of Technology,  
Cambridge, Massachusetts 02139

We have experimentally demonstrated that the electronic ground state of MgO is  $X^1\Sigma^+$ . The lowest energy excited state was shown to be  $a^3\Pi_i$ , for which the following constants were determined (1 $\sigma$  uncertainty in parentheses):

$T_e$	2623 (7) $\text{cm}^{-1}$
$\omega_e$	648 (5)
$\omega_e x_e$	3.9 (9)
$B_e$	0.5022 (13)
$\alpha_e$	0.0042 (8) (Pekeris' relation)
$A$	-64 (1)

The  $a^3\Pi_i$  state was observed and characterized from its perturbations of the  $X^1\Sigma^+$  ( $v_X > 2$ ) levels. These perturbations were detected in the photoluminescence from the  $B^1\Sigma^+$  state induced by the 476.5-, 496.5-, and 514.5-nm lines of an argon ion laser. The three laser lines were shown to coincide with a total of eight strong and assignable molecular lines belonging to the  $B^1\Sigma^+-X^1\Sigma^+$  system of the three isotopic species  $^{24}\text{Mg}^{16}\text{O}$ ,  $^{25}\text{Mg}^{16}\text{O}$ , and  $^{26}\text{Mg}^{16}\text{O}$ . The 496.5-nm line excited the less abundant  $^{26}\text{Mg}^{16}\text{O}$  species almost exclusively. Rotationally resolved photoluminescence from eight  $B^1\Sigma^+$  ( $v_B, J_B$ ) levels was observed into vibronic levels  $X^1\Sigma^+$  ( $v_X = 0-7$ ) and  $A^1\Pi$  ( $v_A = 0-8$ ).  $X^1\Sigma^+ \sim a^3\Pi_i$  perturbations appeared as level shifts often accompanied by extra transitions into levels of dominant  $a^3\Pi_i$  character; a total of 20 extra lines were assigned.  $A^1\Pi \sim X^1\Sigma^+$  perturbations were also observed, and six extra lines were assigned. Measurement of the relative intensities of  $B^1\Sigma^+-A^1\Pi$  and  $B^1\Sigma^+-X^1\Sigma^+$  photoluminescence originating simultaneously from a single ( $v_B, J_B$ ) level permitted determination of the transition moment ratio

$$R_{B-X}/R_{B-A} = 1.35 \pm 0.07.$$

The electronically excited  $A^1\Pi$  state was present in our Mg + N<sub>2</sub>O flame in sufficient concentration to record the MgO  $B^1\Sigma^+ \leftarrow A^1\Pi$  excitation spectrum using a cw Rhodamine 6G dye laser. This observation raises the possibility of direct population monitoring of other electronically excited species in flames.

<sup>1</sup> This work was supported by AFSOR Grant 73-2565 and NSF Grants MPS72-04978 and CHE-7505959.

<sup>2</sup> Present address: Foster Grant Company, Inc., Leominster, Mass. 01453.

<sup>3</sup> Alfred P. Sloan Fellow.

## I. INTRODUCTION

In this paper we report on laser induced photoluminescence spectra of MgO. Several important advantages of laser over conventional spectroscopy are illustrated: spectral simplification, ability to detect and assign lines differing in intensity by several orders of magnitude, and high sensitivity. The most significant result reported here is the spectroscopic characterization of the lowest energy electronically excited state of MgO,  $a^3\Pi_i$ , as obtained from analysis of  $X^1\Sigma^+ \sim a^3\Pi_i$  perturbations. It is unlikely that the "extra lines," transitions into levels of dominant  $a^3\Pi_i$  character which were essential in characterizing this state, could have been assigned from an ordinary emission spectrum.

Magnesium monoxide has been the subject of numerous spectroscopic (1-22) and theoretical investigations (23-26). Eight singlet states are known below 40 000  $\text{cm}^{-1}$ :  $X^1\Sigma^+$  (2-4),  $A^1\Pi$  (4, 8, 9 (incorrect)),  $B^1\Sigma^+$  (1-4, 6-8),  $C^1\Sigma^-$  (11, 12, 14),  $D^1\Delta$  (14, 15),  $E^1\Sigma^+$  (16, 19),  $F^1\Pi$  (17, 19), and  $G^1\Pi$  (18, 19). Two triplet states are known,  $a^3\Pi$  and  $d^3\Delta$  (5 (unidentified), 6 (incorrect), 10, 13 (incorrect), 15 (unidentified), 20-22), but no rotationally resolved spectrum, rotational analysis, or direct determination of the energy of triplet states relative to singlets has been reported.

The electronic ground state for all of the alkaline earth monoxides except MgO is known to be  $X^1\Sigma^+$  (27-29). However, in MgO the  $A^1\Pi$  state, and by Hund's rule also the isoconfigurational  $a^3\Pi_i$  state, lie at very low energy,  $T_e(A^1\Pi) = 3563 \text{ cm}^{-1}$  (4). The possibility that MgO  $a^3\Pi_i$  is actually the electronic ground state has been vigorously debated and can now be experimentally eliminated.

The  $a^3\Pi_i$  state has a degeneracy of 6 and is found here to lie at

$$T_e = 2623 \pm 7 \text{ cm}^{-1}$$

above  $X^1\Sigma^+$  and

$$T_e(A^1\Pi) - T_e(a^3\Pi) = 940 \text{ cm}^{-1}$$

below  $A^1\Pi$ . The existence of a very low-lying high-degeneracy, metastable electronic state of MgO has thermochemical (10, 30) and kinetic significance. This situation is unique among the alkaline earth monoxides; the lowest-lying  $a^3\Pi$  state occurs in BeO and CaO near 8000  $\text{cm}^{-1}$  and still higher in SrO and BaO. It is of interest that an SCF calculation (24) accurately predicts the  $A^1\Pi$ - $a^3\Pi_i$  splitting and that all of the other ab initio calculations (some for  $r$  values rather far from  $r_e$  of both states) overestimate this splitting (23-25).

Determination of the energy location of the triplet manifold relative to the singlet is difficult for light diatomic molecules. The singlet-triplet separation is obtained either from analysis of intercombination bands or spin-orbit perturbations. Both occur because the spin-orbit term in the Hamiltonian mixes singlet and triplet wavefunctions. This mixing lends intensity to nominally spin-forbidden transitions. Intercombination bands are often observed in emission because a spin-selective reaction sequence forms metastable molecules in the lowest state of a given multiplicity under conditions such that phosphorescence is not quenched.

Even when such intercombination transitions are observable, low intensity and spectral complexity often combine to make a complete rotational analysis prohibitively difficult. Perturbations, on the other hand, are more generally observable because a smaller spin-orbit interaction energy is required, but they provide fragmentary infor-



mation, perhaps only a perturbation interaction energy and the energies of a few rotational levels. The critical point about fragmentary perturbation information is that the rotational quantum number and parity of the perturbing levels are unambiguously determined by  $\Delta J = 0$  and  $+\leftrightarrow -$  perturbation selection rules. Consequently rotational and vibrational constants of accuracy comparable to those derived from a complete rotational analysis, and, in addition, electronic and vibrational assignments of the perturbing levels are obtainable.

The classic example of the use of perturbations to determine a singlet-triplet separation was the demonstration that the electronic ground state of  $C_2$  is  $^1\Sigma_g^+$  rather than  $^3\Pi_u$  as was previously believed (31). Matching  $b^3\Sigma_g^- \sim X^1\Sigma_g^+$  perturbations were observed in the singlet-singlet Phillips  $A^1\Pi_u-X^1\Sigma_g^+$  (32) and triplet-triplet Ballik-Ramsay  $b^3\Sigma_g^- - a^3\Pi_u$  (33) bands. In addition to those of  $C_2$ , perturbations have been observed for other molecules which are isovalent to MgO, namely, CaO (34, 35), SrO (36, 38), and BaO (39, 40), and have recently been used to locate and characterize the lowest energy  $a^3\Pi$  and  $A^1\Pi$  states of these molecules (27).

All previous investigations of the spectrum of MgO involved conventional absorption and emission spectroscopy. We report here an extension of the  $B^1\Sigma^+-X^1\Sigma^+$  and  $B^1\Sigma^+-A^1\Pi$  systems by laser induced photoluminescence spectroscopy. This work was initiated with the expectation that the relative spectral simplicity and sensitivity to weak features inherent in laser induced photoluminescence spectroscopy would permit observation of  $B^1\Sigma^+-a^3\Pi$  intercombination transitions due either to  $a^3\Pi \sim A^1\Pi$  or  $a^3\Pi \sim X^1\Sigma^+$  perturbations. Eight MgO  $B-X$  transitions coincident with several argon ion laser lines were rovibronically and isotopically assigned. The photoluminescence spectra included transitions involving higher vibrational levels of the  $B^1\Sigma^+$ ,  $A^1\Pi$ , and  $X^1\Sigma^+$  states than those previously studied (3, 4, 8). It was in these higher vibrational levels,  $v = 3-7$ , of the  $X^1\Sigma^+$  state that  $X^1\Sigma^+ \sim a^3\Pi_i$  perturbations were observed.  $A^1\Pi \sim X^1\Sigma^+$  perturbations were also observed. A total of 20 rotation-vibration levels of dominant  $a^3\Pi_i$  character were observed, and spectroscopic constants for the MgO  $a^3\Pi_i$  state were determined. This analysis leaves no doubt that  $a^3\Pi_i$  ( $v = 0$ ) lies above  $X^1\Sigma^+$  ( $v = 0$ ) even though  $a^3\Pi_i$  must dissociate adiabatically to a limit at lower energy than that of  $X^1\Sigma^+$ .

## II. EXPERIMENTAL METHOD

MgO was generated in a dilute Mg +  $N_2O$  flame at 1-5-Torr total pressure in a vacuum flow system similar to one described previously (41). Magnesium metal (99.99%), with its natural isotope abundance ratios  $^{24}\text{Mg}:^{25}\text{Mg}:^{26}\text{Mg} = 7:1:1$ , was vaporized at approximately 1 g/hr from an aluminum oxide crucible supported and heated by a tungsten basket heater (40 A at 3 V). The Mg vapor was entrained in argon and flowed into the flame region where it was reacted with an excess of  $N_2O$ .

Radiation from a Spectra Physics  $\text{Ar}^+$  laser was directed vertically through a Brewster window into the center of the flame region. The strongest photoluminescence was observed with the 476.5-, 496.5-, and 514.5-nm laser lines at typical powers of 2, 2, and 5 W, respectively. As discussed later, the 476.5-nm line was found to excite at least three MgO  $B-X$  transitions and the 514.5-nm line at least four. An intracavity air-spaced etalon was used in some experiments with the 476.5- and 514.5-nm line in order to frequency narrow and tune these lines across their 5-GHz wide gain profile. This etalon



permitted selective excitation of individual MgO transitions and considerably facilitated assignment of the fluorescence spectra. Photoluminescence excited by the other available  $\text{Ar}^+$  lines was too weak to be isotopically and rovibronically assigned.

An image of the photoluminescence was focused on the entrance slit of a 1-m monochromator employing a 1200-groove/mm grating blazed at 500 nm. Spectra were recorded on a strip chart recorder while the monochromator wavelength was scanned. Hg and Ne pen lamp lines were used for wavelength calibration; measurement accuracy was typically  $\pm 0.02$  nm.

In addition to the  $\text{Ar}^+$  laser induced photoluminescence spectra, excitation spectra were recorded in the 570–620-nm region using a cw, tunable dye laser (41). The dye laser was operated in a single longitudinal mode at typically 30 mW. Individual rotational lines in the  $B^1\Sigma^+-A^1\Pi$  (1,0) and (0,0) bands were excited and detected by the resultant shorter wavelength  $B^1\Sigma^+-X^1\Sigma^+$   $\Delta v = 0$  photoluminescence near 499 nm. The intensity of the  $B-A$  (1,0) excitation band was three times that for the (0,0).  $B-X$  fluorescence induced by  $B \leftarrow A$  excitation with a 30-mW single mode dye laser was more than  $10^2$  weaker than that excited by  $B \leftarrow X$  excitation with a 1-W single mode  $\text{Ar}^+$  laser.

### III. RESULTS

#### A. Assignment of $\text{Ar}^+$ Laser Induced Photoluminescence Spectra

Fluorescence progressions in the MgO  $B^1\Sigma^+-X^1\Sigma^+$  and  $B^1\Sigma^+-A^1\Pi$  systems result from  $\text{Ar}^+$  laser excitation into the  $B^1\Sigma^+$  state. The  $B-X$  and  $B-A$  systems are known, respectively, as the green ( $\nu_{00} = 20\,004\text{ cm}^{-1}$ ) and red ( $\nu_{00} = 16\,500\text{ cm}^{-1}$ ) systems (4). Because of the dynamic range of laser photoluminescence spectroscopy, vibrational progressions in both systems were observed extending to larger  $\Delta v$  values than were observable by conventional emission spectroscopy. Lines with relative intensities differing by more than  $10^2$  were readily recorded. For each laser coincidence, longer progressions were observed in  $B-A$  than  $B-X$  fluorescence. As expected for  $^1\Sigma^+-^1\Sigma^+$  and  $^1\Sigma^+-^1\Pi$  transitions,  $B-X$  fluorescence appeared as a progression of  $P, R$  doublets and  $B-A$  as  $P, Q, R$  triplets.

The major problem associated with assigning the specific MgO  $B-X$  lines that coincide with  $\text{Ar}^+$  laser lines arose from high sensitivity to less abundant species. Isotopic molecules  $^{24}\text{Mg}^{16}\text{O}$ ,  $^{25}\text{Mg}^{16}\text{O}$ ,  $^{26}\text{Mg}^{16}\text{O}$  as well as vibrationally excited  $X^1\Sigma^+$  levels up to  $v_X = 5$  were found here to result in assignable fluorescence features. Rotation, vibration, and isotopic assignments were inextricably linked. In addition, perturbations of the  $v > 2$  levels of  $A^1\Pi$  and  $X^1\Sigma^+$  rendered the use of calculated spectra and isotope shifts, based on accepted  $B$ -,  $A$ -, and  $X$ -state constants (4), hazardous.

Assignment of the  $\text{Ar}^+$  laser coincidences with MgO  $B-X$  lines involves determination of  $\Delta v = v'_B - v''_X$ ,  $\Delta J = J'_B - J''_X$ ,  $v'_B$ ,  $J'_B$ , and isotopic species. Assignments were guided and confirmed by the following types of information:

1. Because the vibrational and rotational constants of the  $B$  and  $X$  states are similar, the  $B-X$  band system has compact sequence structure. In emission, the strongest bands originating from a common  $v'_B$  level are  $\Delta v = 0$  and, at least six times weaker,  $\Delta v = \pm 1$ . The three  $\text{Ar}^+$  lines observed to excite strong photoluminescence, 476.5, 496.5, and 514.5 nm, fall, respectively, in the  $\Delta v = +1, 0$ , and  $-1$  regions. The 476.5-nm

line coincides with three  $B-X$  transitions. Each was shown to belong to the  $B-X$   $\Delta v = +1$  sequence by its location approximately  $\omega''_e$  to the blue of the most intense (therefore  $\Delta v = 0$ )  $B-X$   $P, R$  doublet which originated from the common laser-populated ( $v'_B, J'_B$ ) level. The  $\Delta v = 0$  assignment of the single  $MgO$   $B-X$  line excited at 496.5 nm and the  $\Delta v = -1$  assignments of the four lines excited at 514.5 nm were confirmed by the location of the laser excitation line relative to the three strongest  $B-X$   $P, R$  doublets.

2. Fluorescence in the same ( $v'_B, v''_X$ ) band as the laser excitation line determines whether the laser frequency coincides with that of an  $R$ - or  $P$ -branch line. If, as for

TABLE Ia  
Fluorescence lines Due to the Coincidence of the 476.5-nm Laser Line with  $R(26)$   
of the  $B-X$  (5,4) Band of  $^{24}MgO$

B-X System					B-A System				
Band <sup>a</sup>	$\nu_{obs}$ ( $cm^{-1}$ )	$\nu_{calc}$ ( $cm^{-1}$ )	$q^c$	$\Delta\nu^d$ ( $cm^{-1}$ )	Band	$\nu_{obs}$ ( $cm^{-1}$ )	$\nu_{calc}$ ( $cm^{-1}$ )	$q$	
(5,3) R	21719.8	1.2	$0.328 \times 10^{-2}$	2.5	(5,0) R	20545.0	-0.9	$0.104 \times 10^{-1}$	
P	21658.2	0.6		2.0	Q	20518.0	-0.7		
					P	20489.4	-1.3		
(5,4) R	20981.0	2.5	0.105	0.9	(5,1) R	19891.4	-1.1	0.124	
P	20919.9	1.0		0.1	Q	19864.1	-1.5		
					P	19836.5	-1.4		
(5,5) R	20257.8	9.0	0.752	-0.7	(5,2) R	19246.1	-0.8	0.205	
P	20199.2	10.3		-0.8	Q	19220.2	-0.1		
					P	19192.2	-0.6		
(5,6) R	19496.1	-33.3	0.135	-0.6	(5,3) R			$0.577 \times 10^{-3}$	
P	19438.8	-31.3		-0.5	Q				
					P				
(5,7) R	18802.0	-19.4	$0.572 \times 10^{-2}$	-4.0	(5,4) R	17977.4	-1.8	0.114	
P	18743.1	-18.5		-4.3	Q	17951.6	-1.5		
					P	17923.9	-2.2		
Extra Lines <sup>e</sup>					(5,5) R	17354.2	-2.9	$0.385 \times 10^{-1}$	
Band	$\nu_{obs}$ ( $cm^{-1}$ )	$\nu_{calc}$ ( $cm^{-1}$ )	Intensity <sup>g</sup> (obs) (calc)	$\Delta\nu^d$ ( $cm^{-1}$ )	Q	17328.9	-2.3		
					P	17300.4	-4.1		
(5,5) R <sup>+</sup>	20147.9	105.9	0.14	1.1	(5,6) R	16737.1	-5.7	$0.117 \times 10^{-1}$	
P <sup>+</sup>	20093.3	105.9	0.17	1.7	Q	16713.1	-4.2		
					P	16689.6	-1.1		
(5,6) R <sup>++</sup>	20228.5	29.2	0.09	-0.5	(5,7) R	16131.3	-5.1	$0.756 \times 10^{-1}$	
P <sup>++</sup>	20174.4	24.8	0.15	0.2	Q	16105.6	-5.3		
					P	16080.0	-4.7		
(5,6) R <sup>+</sup>	19562.5	-66.4	0.48	-0.3	(5,8) R	15529.4	-0.3	$0.624 \times 10^{-1}$	
P <sup>+</sup>	19507.1	-68.3	0.46	0.51	Q	15504.6	-7.9		
					P	15478.5	-8.1		

<sup>a</sup> The rotational quantum numbers are omitted. In Table Ib, for instance,  $R$ ,  $Q$ , and  $P$ , respectively, mean  $R(26)$ ,  $Q(27)$ , and  $P(28)$ .

<sup>b</sup>  $\Delta\nu = \nu_{obs} - \nu_{calc}$  where  $\nu_{calc}$  is the calculated frequency based on the spectroscopic constants of the  $X^1\Sigma^+$ ,  $A^1\Pi$ , and  $B^1\Sigma^+$  states reported in Ref. (4).

<sup>c</sup>  $q$  is the computed Franck-Condon factor based on the constants reported in Ref. (4).

<sup>d</sup>  $\Delta\nu'$  is the residual error after the least-squares treatment of the perturbation.

<sup>e</sup> Extra lines correspond to perturbation allowed transitions into levels of dominant  $a^3\Pi$  character. The vibrational quantum numbers shown are  $v'_B, v''_X$ ; the actual  $a^3\Pi$  vibrational quantum number is  $v''_X - 3$ . The + and ++ superscripts refer to the extra lines associated with the nominal  $a^3\Pi_0$  and  $a^3\Pi_1$  levels, respectively.

<sup>f</sup>  $\nu$  of main line minus  $\nu$  of extra line.

<sup>g</sup> Relative intensity of the extra line with respect to the main line.

<sup>h</sup> No Franck-Condon factors were calculated for the  $^{25}Mg^{16}O$  isotopic species. Value listed is average of values computed for  $^{26}Mg^{16}O$  and  $^{24}Mg^{16}O$ .

THIS PAGE IS BEST QUALITY PRACTICABLE  
FROM COPY FURNISHED TO DDC



514.5-nm excitation, the fluorescence spectrum shows four lines which are separated from the laser frequency by less than  $\omega''_e$ , and three of these lines are to the red of the laser, then the laser excites three  $R$  lines and one  $P$  line.

3. Fluorescence progressions originating from a common  $(v'_B, J'_B)$  level were identified by similar  $R(J' - 1) - P(J' + 1)$  separations.

4. If it were possible to be certain that the bluest member of a given fluorescence progression was a transition into a  $v'' = 0$  level, then it would be possible to use observed and isotopically corrected  $B''_0$  values for a level known to be perturbation free to determine  $J'_B$  from

$$R(J' - 1) - P(J' + 1) = B''_0(4J' + 2) - D''_0(8J'^2 + 12J' + 4). \quad (1)$$

It would also be possible to obtain  $v'_B$  from

$$T'_0(B'\Sigma^+) + \omega'_e(B'\Sigma^+)v'_B - \omega_e x'_e(v'_B + v'_B) \approx T''_0(A) + \nu_{RQP}, \quad (2)$$

where  $\nu_{RQP}$  is the average wavenumber of the  $R, Q, P$  triplet of transitions into the  $v'' = 0$  level. Franck-Condon factors, calculated using constants for the  $B'\Sigma^+$  and  $A''\Pi$  states from Ref. (4), indicate that fluorescence into  $A''\Pi$  ( $v''_A = 0$ ) will have intensity at least 5% that of the strongest  $(v'_B, v''_A)$  band for  $v'_B = 0-5$ . Thus the  $R-P$  separation in the shortest wavelength  $B-A$   $R, Q, P$  triplet determines three  $(J'_B, v'_B)_{\text{trial}}$  assignments,

TABLE Ib

Fluorescence Lines Due to the Coincidence of the 476.5-nm Laser Line with  $R(49)$  of the  $B-X$  (4,3) Band of  $^{24}\text{MgO}$

Band <sup>a</sup>	B-X System			$q^c$	$\Delta\nu^d$ (cm <sup>-1</sup> )	B-A System			$q$
	$\nu_{\text{obs}}^b$ (cm <sup>-1</sup> )	$\nu_{\text{calc}}^b$ (cm <sup>-1</sup> )	$\Delta\nu^b$ (cm <sup>-1</sup> )			Band	$\nu$ (cm <sup>-1</sup> )	$\Delta\nu$ (cm <sup>-1</sup> )	
(4,2) R	21719.8	-1.9		$0.179 \times 10^{-2}$		R 19997.3	-3.1		$0.458 \times 10^{-1}$
P	21625.7	-2.8				Q 19847.6	-2.8		
						P 19796.9	-3.0		
(4,3) R	20931.0	0.9		$0.804 \times 10^{-1}$	1.5	R 19252.1	-2.9		0.232
P	20859.7	0.7				Q 19203.6	-1.9		
						P 19152.9	-2.6		
(4,4) R	20257.8	8.9		0.806	0.1	R 18614.4	-3.0		$0.484 \times 10^{-1}$
P	20151.6	12.8				Q 18566.0	-2.4		
						P 18515.4	-3.4		
(4,5) R	19483.6	-38.4		0.108	0.4	R 17983.5	-4.2		0.120
P	19355.3	-33.6				Q 17936.4	-2.7		
						P 17886.0	-4.0		
(4,6) R	18733.5	-18.0		$0.347 \times 10^{-2}$	-1.1	R 17141.5	-3.9		$0.862 \times 10^{-1}$
P	18692.3	-17.4				Q 16992.6	-5.6		
						P 16945.9	-4.6		
Extra Lines <sup>e</sup>									
Band	$\nu_{\text{obs}}^f$ (cm <sup>-1</sup> )	$\nu_{\text{calc}}^f$ (cm <sup>-1</sup> )	Intensity <sup>g</sup> (obs)	Intensity <sup>g</sup> (calc)	$\Delta\nu^d$ (cm <sup>-1</sup> )	Band	$\nu$ (cm <sup>-1</sup> )	$\Delta\nu$ (cm <sup>-1</sup> )	
(4,4) R <sup>+</sup>	20137.0	120.8	-	0.09	0.4	R 16752.5	+0.8		$0.797 \times 10^{-1}$
P <sup>+</sup>	20036.1	115.5	0.13	0.12	0.3	R 16722.2	-29.5		
						Q 16699.1	-4.9		
R <sup>++</sup>	20225.4	32.4	-	0.17	3.3	P 16655.7	-0.2		
P <sup>++</sup>	20120.4	31.2	0.34	0.34	-0.4	P 16617.2	-38.7		
(4,5) R <sup>+</sup>	19553.3	-63.7	0.96	0.86	0.4	R 16141.5	-3.9		$0.862 \times 10^{-1}$
P <sup>+</sup>	19449.4	-64.1	0.84	0.64	0.1	Q 16092.6	-5.6		
						P 16045.9	-4.6		
						R 15539.3	-7.6		$0.232 \times 10^{-1}$
						Q 15492.1	-9.1		
						P 15445.5	-7.5		

Note. See Table Ia footnotes.

THIS PAGE IS BEST QUALITY PRACTICABLE  
FROM COPY FURNISHED TO DDC

one each for  $^{24}\text{MgO}$ ,  $^{25}\text{MgO}$ , and  $^{26}\text{MgO}$ . If the  $\tau''_A = 0$  band were detected but with insufficient intensity for  $\pm 1\%$  measurement of the  $R$ - $P$  separation, the more intense  $\tau''_A = 1$  or 2 band would be used.

5. Vibrational assignments were confirmed by matching the intensity variation within an observed  $B$ - $A$  progression against relative intensities calculated from  $q(\tau''_B, \tau''_A, \nu''_B, \nu''_A)$ . A weak or missing band in the middle of a  $B$ - $A$  progression was a sensitive indicator of the  $\tau''_B$  value independent of isotope. Counting from the bluest  $B$ - $A$  band, the predicted weakest bands originating from  $\tau_B = 1, 2, 3, 4, 5$  were, respectively, third (1,2), fifth (2,4), seventh (3,6), fifth (4,4), and fourth (5,3).

6. Once a set of plausible  $(\tau''_B, J''_B)$  assignments was obtained, they were tested against expected  $B$ - $A$  and  $B$ - $X$  fluorescence spectra calculated using constants for  $^{24}\text{MgO}$  determined by Lagerqvist and Uhler (4) for  $\tau''_B = 0-2$ ,  $\tau''_A = 0-2$ , and  $\nu''_X = 0-2$  and the isotopic formulas (42)

$$\begin{aligned}\omega_e^i &= \rho \omega_e, \\ \omega_e X_e^i &= \rho^2 \omega_e X_e, \\ B_e^i &= \rho^2 B_e, \\ \alpha_e^i &= \rho^2 \alpha_e, \\ D_e^i &= \rho^4 D_e, \\ \beta_e^i &= \rho^5 \beta_e, \\ \rho &= (\mu/\mu^i)^{1/2}.\end{aligned}\quad (3)$$

$B$ - $A$  were more valuable than  $B$ - $X$  fluorescence progressions in determining final rotation, vibration, and isotope assignments for several reasons. Most importantly, because

TABLE Ic  
Fluorescence Lines Due to the Coincidence of the 476.5-nm Laser Line with  $R(70)$   
of the  $B$ - $X$  (3,2) Band of  $^{24}\text{MgO}$

B-X System					B-A System		
Band <sup>a</sup>	$\nu''_{\text{obs}}$ ( $\text{cm}^{-1}$ )	$\nu''_{\text{calc}}$ ( $\text{cm}^{-1}$ )	$c^c$	$d$ ( $\text{cm}^{-1}$ )	Band	$\nu''_{\text{obs}}$ ( $\text{cm}^{-1}$ )	$q$
(3,2)	P 20951.0 P 20953.0	-1.5 -0.4	$0.576 \times 10^{-1}$	0.2 1.9	(3,0)	P 19303.0 C 19235.0 P 19163.9	0.140
(3,3)	P 20249.7 P 20099.0	-4.6 -0.3			0.857	(3,1)	R 18670.0 Q 18601.6 P 18530.2
(3,4)	P 19512.4 P 19503.0	-23.2 -9.4	$0.827 \times 10^{-1}$	1.0 2.4	(3,2)	R 18041.6 Q 17975.8 P 17905.9	$0.366 \times 10^{-1}$
Extra Lines <sup>e</sup>					(3,3)	R 17440.9 R 17412.2 Q 17357.5 P 17310.0 P 17260.2	$0.522 \times 10^{-1}$
Band	$\nu''_{\text{obs}}$ ( $\text{cm}^{-1}$ )	$\nu''_{\text{calc}}$ ( $\text{cm}^{-1}$ )	Intensity <sup>g</sup> (obs)	$d$ ( $\text{cm}^{-1}$ )	(3,4)	R 16917.6 Q 16746.9 P 16681.8	0.116
(3,3)	P* 20169.5 P* 20028.0	79.6 70.1	0.07 0.08	-1.3 -0.9			
	P** 20276.0 P** 20134.5	-27.1 -36.4	0.30 0.10	-1.0 -1.2			
(3,4)	P* 19674.7 P* 19431.7	-60.3 -68.6	0.65 0.39	1.36 0.23			

Note. See Table Ia footnotes.

THIS PAGE IS BEST QUALITY PRACTICABLE  
FROM COPY FURNISHED TO DDC



the rotational and vibrational constants for the  $B$  and  $X$  states are much more similar than for the  $B$  and  $A$  states, longer  $B-A$  than  $B-X$  progressions were observed. This ensured that  $B-A$  progressions would include transitions into the  $v_A = 0-2$  levels which are known to be free of perturbations and are well represented by constants from Ref. (4). The most useful information for isotopic assignments was derived from  $B-A$  bands with large  $|v_B - v_A|$  values, since these bands have the largest isotope shifts. Although  $A^1\Pi \sim X^1\Sigma^+$  perturbations were observed, these perturbations affected only  $B-A$   $R$ - and  $P$ -branch lines; the  $Q$  lines involve  $A^1\Pi$  levels of  $f$  Kronig symmetry (43) while  $X^1\Sigma^+$  levels all have  $e$  symmetry and, in the absence of external magnetic or electric fields and hyperfine effects,  $e \sim f$  perturbations are forbidden. Comparison of observed and calculated perturbation free  $Q$ -branch lines permitted testing of plausible assignments, guided extrapolation to  $v_A > 2$  bands, and enabled detection of  $A^1\Pi \sim X^1\Sigma^+$  perturbations in the  $R$  and  $P$  branches.

The coincidences of  $Ar^+$  laser lines with  $MgO$   $B^1\Sigma^+ - X^1\Sigma^+$  transitions are listed and discussed in the following paragraphs. Assignments of all observed photoluminescence lines in the  $B-X$ ,  $B-A^1\Pi$ , and  $B-A$  systems excited by the 476.5-, 496.5-, and 514.5-nm

TABLE II

Fluorescence Lines Due to the Coincidence of the 496.5-nm Laser Line with  $R(36)$  of the  $B-X$  (2,2) Band of  $^{26}MgO$

B-X System					B-A System					
Band <sup>a</sup>		$\nu_{obs}^b$ (cm <sup>-1</sup> )	$\nu_{calc}^b$ (cm <sup>-1</sup> )	$q^c$	Band	$\nu_{obs}^b$ (cm <sup>-1</sup> )	$\nu_{calc}^b$ (cm <sup>-1</sup> )	$q^c$		
(2,0)	R	21637.1	-1.0	0.254x10 <sup>-3</sup>	(2,0)	R	18221.2	-1.1		
	P	21553.6	-1.3			P	18185.7	-1.3	0.285	
							18149.1	-1.5		
(2,1)	R	20880.6	-1.0	0.375x10 <sup>-1</sup>	(2,1)	R	17580.3	-1.2	0.203x10 <sup>-1</sup>	
	P	20793.9	-0.9			P	17545.2	-1.4		
							17508.6	-1.6		
(2,2)	R	20135.0	-0.2	0.901	(2,2)	R	16947.3	-1.1	0.161	
	P	20053.4	-0.6			P	16912.7	-1.3		
							16875.8	-1.5		
(2,3)	R	19400.0	1.2	0.606x10 <sup>-1</sup>	(2,3)	R	16321.2	-1.7	0.665x10 <sup>-1</sup>	
	P	19319.0	0.7			P	16286.4	-1.4		
							16250.6	-1.6		
(2,4)	R	18675.2	2.7	0.105x10 <sup>-2</sup>	(2,4)	R			0.384x10 <sup>-4</sup>	
	P	18595.3	2.6			P				
					(2,5)	R	15091.1	-3.4	0.454x10 <sup>-1</sup>	
						P	15057.2	-2.9		
							15021.2	-3.9		
					(2,5)	R	14502.4	+10.7	0.937 x 10 <sup>-1</sup>	
						P	14482.2	-2.5		
							14452.8	-4.0		
						P	14429.9	-7.1		
							14410.7	-12.3		
					(2,7)	R	13792.0	-4.1	0.178	
						P	13657.3	-6.4		
							13623.6	-10.7		

Note. See Table Ia footnotes.

THIS PAGE IS BEST QUALITY PRACTICABLE  
FROM COPY FURNISHED TO DDC

TABLE IIIa

Fluorescence Lines Due to the Coincidence of the 514.5-nm Laser Line with  $P(10)$  of the  $B-X$  (4,5) Band of  $^{26}\text{MgO}$

B-X System					B-A System		
Band <sup>a</sup>	$\nu_{\text{obs}}$ ( $\text{cm}^{-1}$ )	$\Delta\nu^b$ ( $\text{cm}^{-1}$ )	$q^c$	$\Delta\nu^d$ ( $\text{cm}^{-1}$ )	Band	$\nu_{\text{obs}}$ ( $\text{cm}^{-1}$ )	$q$
(4,2)	R 21675.5 P 21655.3	0.7 0.8	0.179x10 <sup>-2</sup>		(4,0)	R 19716.6 Q 19707.2 P 19697.1	0.8 0.5 0.5 0.45x10 <sup>-1</sup>
(4,3)	R 20920.7 P 20901.9	0.5 0.9	0.804x10 <sup>-1</sup>	2.0 2.4	(4,1)	R 19059.9 Q 19051.2 P 19041.2	0.4 0.7 0.7 0.232
(4,4)	R 20180.7 P 20160.2	1.8 2.2	0.806	1.0 1.5	(4,2)	R 18411.2 Q 18402.2 P 18392.5	0.2 0.1 0.3 0.484x10 <sup>-1</sup>
(4,5)	R 19450.3 P 19429.9	4.3 4.6	0.108	-0.8 -0.6	(4,3)	R 17770.1 Q 17761.2 P 17751.7	-0.2 -0.3 -0.1 0.120
(4,6)	R 18741.0 P 18721.4	17.5 18.5	0.347x10 <sup>-2</sup>	-2.3 -1.9	(4,4)	R 16510.8 Q 16502.3 P 16492.8	-0.7 -1.6 -1.5 0.736x10 <sup>-4</sup>
Extra Lines					(4,5)	R 15892.6 Q 15884.3 P 15874.4	-2.7 -2.5 -2.8 0.862x10 <sup>-1</sup>
Band	$\nu_{\text{obs}}$ ( $\text{cm}^{-1}$ )	$\nu_{\text{calc}}$ ( $\text{cm}^{-1}$ )	Intensity <sup>e</sup> (obs)	$\Delta\nu^d$ (calc) ( $\text{cm}^{-1}$ )	(4,6)	R 15281.7 Q 15273.5 P 15264.2	-4.3 -4.0 -3.9 0.232x10 <sup>-1</sup>
(4,6)	R 18675.8 P 18655.4	55.5 65.0	0.28 ---	0.65 0.69 0.1 0.5			

Note. See Table Ia footnotes.

TABLE IIIb

Fluorescence Lines Due to the Coincidence of the 514.5-nm Laser Line with  $R(25)$  of the  $B-X$  (3,4) Band of  $^{26}\text{MgO}$

B-X System				B-A System		
Band <sup>a</sup>	$\nu_{\text{obs}}$ ( $\text{cm}^{-1}$ )	$\Delta\nu^b$ ( $\text{cm}^{-1}$ )	$q^c$	Band	$\nu_{\text{obs}}$ ( $\text{cm}^{-1}$ )	$q$
(3,2)	R 20540.2 P 20540.2	-0.3 0.1	0.593x10 <sup>-1</sup>	(3,0)	R 18294.6 Q 18294.6 P 18294.6	-0.5 -0.3 0.1 0.144
(3,3)	R 20159.0 P 20151.9	1.0 1.0	0.853	(3,1)	R 18277.2 Q 18277.2 P 18250.7	0.3 0.0 -0.5 0.199
(3,4)	R 19429.9 P 19373.9	1.5 2.1	0.850x10 <sup>-1</sup>	(3,2)	R 17665.4 Q 17641.1 P 17614.6	-0.8 -0.3 -1.0 0.406x10 <sup>-1</sup>
(3,5)	R 18711.4 P 18656.4	2.6 3.6	0.211x10 <sup>-2</sup>	(3,3)	R 17036.7 Q 17011.8 P 16986.6	-0.9 -1.2 -0.9 0.477x10 <sup>-1</sup>
				(3,4)	R 16414.9 Q 16390.7 P 16365.5	-1.7 -1.5 -1.5 0.116
				(3,5)	R 15800.3 Q 15776.5 P 15751.3	-2.5 -2.6 -2.7 0.427x10 <sup>-1</sup>

Note. See Table Ia footnotes.

THIS PAGE IS BEST QUALITY PRACTICABLE  
FROM COPY FURNISHED TO DDG

TABLE IIIc

Fluorescence Lines Due to the Coincidence of the 514.5-nm Laser Line with  $R(50)$  of the  $B-X$  (2,3) Band of  $^{25}\text{MgO}$

B-X System					B-A System				
Band <sup>a</sup>		$\nu_{\text{obs}}^b$ ( $\text{cm}^{-1}$ )	$\Delta\nu^b$ ( $\text{cm}^{-1}$ )	$q^{c,h}$	Band		$\nu_{\text{obs}}^b$ ( $\text{cm}^{-1}$ )	$\Delta\nu^b$ ( $\text{cm}^{-1}$ )	$q$
(2,1)	R	20907.9	-1.3	$0.370 \times 10^{-1}$	(2,0)	R	18331.6	-1.5	0.284
	P	20795.1	-0.5			Q	18282.5	-0.4	
(2,2)	R	20163.2	-0.2	0.902	(2,1)	R	17693.3	0.2	$0.220 \times 10^{-1}$
	P	20050.5	-0.4			Q	17643.2	-0.2	
(2,3)	R	19429.9	2.1	$0.598 \times 10^{-1}$	(2,2)	R	17059.1	-1.7	0.162
	P	19318.7	2.4			Q	17010.1	-1.5	
						P	16960.1	-1.8	
					(2,3)	R	16433.2	-3.0	$0.647 \times 10^{-1}$
						Q	16386.0	-1.4	
						P	16335.7	-2.5	

Note. See Table Ia footnotes.

$\text{Ar}^+$  lines are summarized, respectively, in Tables Ia-Ic, II, and IIIa-IIIId:

476.5 nm	excites	$^{24}\text{Mg}^{16}\text{O}$	$B-X$	(5,4)	$R(26)$
		$^{24}\text{Mg}^{16}\text{O}$	$B-X$	(4,3)	$R(49)$
		$^{24}\text{Mg}^{16}\text{O}$	$B-X$	(3,2)	$R(70)$
496.5 nm	excites	$^{26}\text{Mg}^{16}\text{O}$	$B-X$	(2,2)	$R(36)$
514.5 nm	excites	$^{24}\text{Mg}^{16}\text{O}$	$B-X$	(4,5)	$P(10)$
		$^{26}\text{Mg}^{16}\text{O}$	$B-X$	(3,4)	$R(25)$
		$^{25}\text{Mg}^{16}\text{O}$	$B-X$	(2,3)	$R(50)$
		$^{24}\text{Mg}^{16}\text{O}$	$B-X$	(1,2)	$R(70)$

The 476.5-nm line coincides with three  $\Delta r = +1$  MgO  $B-X$  transitions. All three assigned excitations involve the most abundant  $^{24}\text{Mg}^{16}\text{O}$  isotopic species.

TABLE IIIId

Fluorescence Lines Due to the Coincidence of the 514.5-nm Laser Line with  $R(70)$  of the  $B-X$  (1,2) Band of  $^{24}\text{MgO}$

B-X System				B-A System				
Band <sup>a</sup>		$\nu_{\text{obs}}^b$ ( $\text{cm}^{-1}$ )	$\Delta\nu^b$ ( $\text{cm}^{-1}$ )	$q^c$	Band	$\nu_{\text{obs}}^b$ ( $\text{cm}^{-1}$ )	$\Delta\nu^b$ ( $\text{cm}^{-1}$ )	$q$
(1,0)	R	20915.7	-1.9	$0.172 \times 10^{-1}$	(1,0)	R	17751.3	-2.3
	P	20756.2	-1.5			Q	17682.6	-1.2
(1,1)	R	20167.7	-0.6	0.945	(1,1)	P	17611.9	-1.2
	P	20009.5	-0.3			R	17117.9	-1.8
(1,2)	R	19429.3	0.0	$0.371 \times 10^{-1}$	(1,2)	Q	17050.2	-0.4
	P	19273.4	1.1			P	16978.5	-2.0

Note. See Table Ia footnotes.



The 496.5-nm line almost exclusively excites the less abundant  $^{26}\text{Mg}^{16}\text{O}$  isotopic species. This excitation involves larger Franck-Condon ( $q_{2,2}^{B-X} = 0.90$ ) and Boltzmann lower level population factors than the three transitions excited by the 476.5-nm line. Consequently fluorescence is strong despite the 1/7 abundance of  $^{26}\text{MgO}$  relative to  $^{24}\text{MgO}$ . This isotopically selective excitation of  $^{26}\text{MgO}$  may be of value in laser separation of Mg isotopes.

The 514.5-nm line excites four assignable transitions in the  $B-X$   $\Delta v = -1$  sequence. Three different isotopic species are excited.

Other  $\text{Ar}^+$  laser lines, including 488.0 nm, produced detectable photoluminescence which was too weak to be assigned.

Once the specific  $B-X$  transitions excited by the laser were assigned, it was possible to examine closely all of the photoluminescence spectra for perturbations and intercombination transitions. The wavenumbers of all observed fluorescence lines are compared against calculated values in Tables I-III. Two kinds of deviations are observed. The first is a smooth function of  $v''$  and is more apparent in the  $B-A$  system. These deviations are extrapolation errors which arise from the use of spectroscopic constants derived from  $v = 0-2$  levels in order to calculate transition frequencies involving higher  $v$  levels. The second sort of deviation, which is quite apparent in the  $B-X$  system, is larger, irregular, and results from perturbations. In the  $B-A$  system, extrapolation errors and perturbation effects are separable because  $Q$ -branch transitions are not affected by perturbations. A model  $X^1\Sigma \sim a^3\Pi$  perturbation calculation described in Section III.D.3 accounts for the observed deviations and extra lines in the  $B-X$  fluorescence. In Tables I-III, observed minus calculated values, listed as  $\Delta v$  and  $\Delta v'$ , respectively, exclude and include the calculated effects of  $X \sim a$  perturbations. No attempt was made to include effects of  $A \sim X$  perturbations.

#### B. Determination of the Ratio of Electronic Transition Dipole Moments For the $\text{MgO } B-X$ and $B-A$ Systems

As shown in Fig. 1, fluorescence lines in the  $B-X$  (5,6) and (4,5) bands and the  $B-A$  (5,2) and (4,1) bands excited by the 476.5-nm  $\text{Ar}^+$  line all fall into a narrow wavelength region and have comparable intensities. The  $B-X$  (5,6) and  $B-A$  (5,2) bands originate from a common rovibronic level ( $v'_B = 5$ ,  $J'_B = 27$ ). The  $B-X$  (4,5) and  $B-A$  (4,1) bands originate from ( $v'_B = 4$ ,  $J'_B = 50$ ). Because these fluorescence lines fall into such a narrow wavelength region, accurate measurements of their relative intensities do not require calibration of the wavelength response of the optical train, monochromator, and photomultiplier. We assume that in this region the instrumental response is constant and that the recorded peak heights are proportional to the number of photons per second emitted rather than to energy per second. Polarization effects are neglected.

The probability of spontaneous emission from a particular level ( $v'_B$ ,  $J'_B$ ) of the  $B^1\Sigma^+$  state to ( $v''_X$ ,  $J''_X$ ) of the  $X^1\Sigma^+$  state is

$$P_{BX} = k\nu_{BX}^3 q_{v'_B v''_X}^2 |R_{v'_B v''_X}|^2 S_{J'_B J''_X}^{\Sigma\Sigma} \quad (4)$$

where  $k$  is a proportionality constant,  $\nu_{BX}$  is the frequency,  $q$  is the Franck-Condon

factor,  $R_e^{BX}$  is the electronic transition moment, and  $S$  is the rotational line strength. A similar expression can be written for a transition from the same level of the  $B$  state to a level ( $v''_A, J''_A$ ) of the  $A$  state

$$P_{B,A} = k \nu_{B,A}^3 q_{v''_B v''_A} |R_e^{B,A}|^2 S_{J''_B J''_A}^{\Sigma\Pi}, \quad (5)$$

where the proportionality constant is identical to that in Eq. (4). Rotational line strength factors used are (+)

Line	$S_{J''_B J''_A}^{\Sigma\Pi}$	$S_{J''_B J''_A}^{\Sigma\Pi}$
$R(J)$	$J+1$	$J/2$
$Q(J)$	0	$(2J+1)/2$
$P(J)$	$J$	$(J+1)/2$

(6)

If the intensities of the  $B-X$  (5,6) and  $B-A$  (5,2) lines arising from ( $v'_B = 5, J'_B = 27$ ) are compared, the following relation is obtained:

$$\frac{I_{obs}^{BX}}{I_{obs}^{BA}} = \frac{89.0}{67.5} = \frac{q_{5,6}^{BX} |R_e^{BX}|^2 [\nu_{BX}^3 (R) S_{27,26}^{\Sigma\Pi} + \nu_{BX}^3 (P) S_{27,28}^{\Sigma\Pi}]}{q_{5,2}^{BA} |R_e^{BA}|^2 [\nu_{BA}^3 (R) S_{27,26}^{\Sigma\Pi} + \nu_{BA}^3 (Q) S_{27,27}^{\Sigma\Pi} + \nu_{BA}^3 (R) S_{27,28}^{\Sigma\Pi}]} \quad (7)$$

The  $B-X$  (5,6) band is strongly perturbed and the resulting extra lines have significant intensities which are therefore summed with the main line intensities. From Eq. (7)

$$R_e^{BX}/R_e^{BA} = 1.4 \pm 0.1. \quad (8)$$

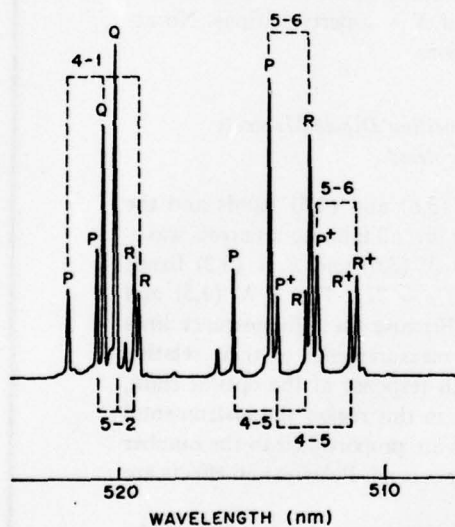


FIG. 1. Region of photoluminescence spectrum from which the ratio of  $B-X$  and  $B-A$  transition moments is obtained. Lines marked 5-6 and 5-2 are, respectively,  $B-X$  and  $B-A$  transitions originating from  $B^1\Sigma^+$  ( $v_B = 5, J_B = 27$ ). Lines marked 4-5 and 4-1 are  $B-X$  and  $B-A$  transitions originating from ( $v_B = 4, J_B = 50$ ). The two pairs of bands are excited by the  $Ar^+$  476.5-nm line. Extra lines due to  $X^1\Sigma \sim a^3\Pi$  perturbations are labeled  $P^+$  and  $R^+$ .

Comparison of the  $B-X$  (4,5) and  $B-A$  (4,1) line intensities gives

$$\frac{I_{\text{obs}}^{BX}}{I_{\text{obs}}^{BA}} = \frac{41.4}{50.0} \quad (9)$$

and

$$R_e^{BX}/R_e^{BA} = 1.3 \pm 0.1. \quad (10)$$

The relevant  $^{24}\text{Mg}^{16}\text{O}$  Franck-Condon factors and  $R$  centroids are

	$q_{e'v''}$	$R_{e'v''}$
$B-X$ (5, 6)	0.1347	1.530 Å
$B-A$ (5, 2)	0.2054	1.954
$B-X$ (4, 5)	0.1081	1.507
$B-A$ (4, 1)	0.2317	1.943.

(11)

Note that, in the  $R$ -centroid approximation, the observed ratios of  $R_e$  values sample  $R_e^{BA}$  and  $R_e^{BX}$  at considerably different values of internuclear separation. This ratio of transition moments should be compared against the ab initio (26) ratio of

$$R_e^{BX}/R_e^{BA} = 1.13,$$

where both transition moments were calculated at an internuclear separation of 1.74 Å.

A measurement of  $R_e^{BX}/R_e^{da} = 0.83$  has recently been reported (20).  $R_e^{da}$  refers to the  $d^3\Delta-a^3\Pi$  transition. The measured ratio agrees well with the ratio of ab initio values, 0.86 (26).

#### C. The $\text{MgO } B^1\Sigma^+-A^1\Pi$ Excitation Spectrum

The  $\text{MgO}$  red system overlaps the 570–620-nm tuning range of a cw Rhodamine 6G dye laser (41). The strongest bands in this region were expected to be  $B-A$  (1,0)  $\nu_{1,0} = 17\,314.85\text{ cm}^{-1}$ ,  $q_{1,0} = 0.338$ , and  $B-A$  (0,0)  $\nu_{0,0} = 16\,500.29\text{ cm}^{-1}$ ,  $q_{0,0} = 0.180$ . It was hoped, however, that a significant population of  $\text{MgO } a^3\Pi$  might be formed in the  $\text{Mg} + \text{N}_2\text{O}$  reaction and that transitions involving this state might appear in the excitation spectrum.

The only bands observed in the excitation spectrum were  $B-A$  (1,0) and (0,0). The  $B-A$  (2,1) and (1,1) bands were undetectable, probably because of a smaller population in  $\tau_A = 1$  combined with Franck-Condon factors, respectively, 14 and 4 times smaller than that for the (1,0) band. Predicted triplet transitions (24, 25) fell outside the tuning range of our laser, but the  $B^1\Sigma^+-a^3\Pi_1$  (0,0) intercombination band was expected to occur near  $17\,440\text{ cm}^{-1}$ . However, the estimated oscillator strength of this transition,

$$F_{0,0}^{B-a} = q_{0,0}^{B-A} [A_{\Pi}/(E_{\Pi^0} - E_{\Pi^0})]^2 = 0.180 (64/940)^2,$$

was 400-fold weaker than the  $B-A$  (1,0) band.

The  $B-A$  (1,0) and (0,0) bands in the excitation spectrum were examined using a single longitudinal mode dye laser. The laser was tuned to a feature in the  $B-A$  spectrum and the resultant  $B-X$   $\Delta v = 0$  photoluminescence spectrum was recorded.  $R(J-1)-P(J+1)$  separations permitted identification of the  $J'_B$  level excited. The dye laser was then tuned to the next line while the laser frequency was monitored by a spectrum analyzer with a 3-GHz free spectral range. In this way absolute  $J'_B$  assignments and



frequency separations accurate to  $0.015 \text{ cm}^{-1}$  for several features in the excitation spectrum were obtained. The line assignments and rotational constants for the  $\text{MgO } B^1\Sigma$  and  $A^1\Pi$  states were in complete agreement with the more extensive study of the  $B-A$  system by Lagerqvist and Uhler (4).

It is interesting that it was possible to excite detectable photoluminescence from a lower level  $3500 \text{ cm}^{-1}$  above  $X^1\Sigma \text{ } v_X = 0$ . Similar 1-10-Torr metal plus oxidant flames have been found to be characterized by vibrational temperatures on the order of 500 K. At that temperature the population ratio would be

$$N_{v_A=0}/N_{v_X=0} = 4 \times 10^{-5}.$$

The  $A^1\Pi \text{ } v_A = 0$  level lies just above  $X^1\Sigma \text{ } v_X = 4$ , and  $\text{Ar}^+$  laser excitation out of  $v_X = 4$  was also observed.

Recently Benard *et al.* (22) observed dramatic enhancement of  $A^1\Pi-X^1\Sigma$  chemiluminescence and the appearance of  $d^3\Delta-a^3\Pi$  chemiluminescence when CO was added to alkaline earth-nitrous oxide flames. It would be interesting to observe the effect of CO on the MgO excitation spectrum, in particular whether the population of  $a^3\Pi$  is increased sufficiently that  $B-a$  intercombination bands become detectable.

#### D. Analysis of Perturbations of $\text{MgO } X^1\Sigma^+$ by $a^3\Pi$ ; and $A^1\Pi$

##### 1. Review of Electronic Structure and Perturbations in Alkaline Earth Monoxides

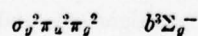
Analysis of perturbations normally provides fragmentary information about perturbing states. This information is often insufficient to yield a deductive electronic assignment in the absence of prior information. However, once a plausible and self-consistent assignment which accounts for all perturbation effects is obtained, it is possible for the experimental observations of perturbations to stand free of support from *ab initio* and semiempirical calculations. Although guided in its initial stages by theoretical considerations, a perturbation analysis is an *experimental* determination of the electronic symmetry, absolute vibrational numbering, and spectroscopic constants of the perturbing state.

Tables I-III show numerous level shifts and intensity anomalies characteristic of perturbations. The  $X^1\Sigma^+$  state is most significantly perturbed in the  $v''_X$  4-6 levels. The  $A^1\Pi$  state shows somewhat smaller and more localized  $e$ -parity-only perturbations. The low-lying electronic states responsible for these perturbations are suggested by a summary of the known perturbations and low-lying states of isoelectronic molecules.

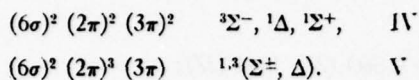
The expected low-lying states of MgO derive from the following configurations (23-25):

$(6\sigma)^2 (2\pi)^4$	$^1\Sigma^+ \text{ (I);}$	I
$(6\sigma)^2 (2\pi)^3 (7\sigma)$	$^3\Pi_i \text{ (I), } ^1\Pi \text{ (I);}$	II
$(6\sigma) (2\pi)^4 (7\sigma)$	$^3\Sigma^+ \text{ (I), } ^1\Sigma^+ \text{ (II).}$	III

Since the  $\text{Mg}(^1S) + \text{O}(^3P)$  ground state atoms combine adiabatically to form  $\text{MgO } ^3\Pi$  or  $^3\Sigma^-$ , and since the



state is known and low lying in the isovalent  $C_2$  molecule, Brewer (45) has argued that it will also be necessary to consider configurations such as



The observed energies of the  $MgO$   $C^1\Sigma^+$  (14),  $D^1\Delta$  (14), and  $d^3\Delta$  (20-22) states derived from configuration V are accurately predicted by ab initio calculations by Schamps and Lefebvre-Brion (24). The remaining states will occur at energies much too high to perturb the observed levels of  $A^1\Pi$  and  $X^1\Sigma^+$ . Configuration IV is only superficially analogous to the  $C_2$   $\sigma_g^2 \pi_u^2 \pi_g^2$  configuration. Bonding in  $C_2$  is covalent but in  $MgO$  is primarily ionic; in  $MgO$  only repulsive states arise when two electrons are transferred from the  $2\pi$  ( $2p_{O\pi}$ ) into the  $3\pi$  ( $3p_{Mg\pi}$ ) orbital.

The only plausible candidates for the  $X^1\Sigma^+$  perturbations are  ${}^3\Pi_i$  (I),  ${}^1\Pi$  (I), and  ${}^3\Sigma^+$  (I). The  ${}^3\Sigma^+$  (I) state can be immediately ruled out because spin-orbit perturbations between  ${}^1\Sigma^+$  and  ${}^3\Sigma^+$  states are forbidden in first order (one of the states must first be mixed with a  $\Pi$  or  ${}^3\Sigma^-$  state for perturbations to be observable). Since the  $A^1\Pi$  state is well known and its extrapolated energy levels do not match the positions of most of the large  $X^1\Sigma^+$  perturbations, these perturbations must be due to the  ${}^3\Pi_i$  (I) state.

Ab initio calculations (24) indicate that the  ${}^3\Pi_i$  (I) state must be an inverted state and that it must lie below  $A^1\Pi$ . The  ${}^3\Pi$  state is inverted because the open shell  $2\pi$  orbital lies primarily on oxygen, in contrast to the situation for the  $BeF$  and  $MgF$   $A^2\Pi$  states, for which the regular or inverted character was until recently in doubt (46, 47), where the  $\pi$  orbital is centered primarily on the metal. Brewer (45) has suggested that the energy separation between  ${}^3\Pi$  (I) and  ${}^1\Pi$  (I) for the alkaline earth monoxides will be large, comparable to the  $7675\text{-cm}^{-1}$  separation observed between the  $A^1\Pi_u$  and  $a^3\Pi_u$  states of  $C_2$  (32). Ab initio calculations on  $BeO$  (28, 29) and  $MgO$  (24, 25) and the results of analyses of perturbations in  $CaO$ ,  $SrO$ , and  $BaO$  (27) indicate that Brewer's estimate is much too large. The  ${}^1\Pi$ - ${}^3\Pi$  splitting arises from two sources, an exchange integral involving the  $2\pi$  and  $7\sigma$  orbitals and differential pair correlation, both of which are unusually small for the highly ionic  $MgO$  molecule. The exchange integral is small because the  $2\pi$  and  $7\sigma$  orbitals are centered, respectively, on oxygen and magnesium. The pair correlation energy for the  ${}^3\Pi$  and  ${}^1\Pi$  states is small and similar because the electrons in the  $2\pi$  and  $7\sigma$  orbitals are widely separated. In this special case, simple SCF calculations should give reliable estimates of  ${}^1\Pi$ - ${}^3\Pi$  splittings.

The best estimate of the  ${}^1\Pi$ - ${}^3\Pi$  splitting indicates that  $X^1\Sigma^+ \sim a^3\Pi_i$  perturbations should be observable in the  $X^1\Sigma^+ v_x = 3$  level. Such a perturbation was, in fact, observed. It is ironic that the only vibrational levels of the  $MgO$   $X^1\Sigma^+$  state for which a rotational analysis has been reported (4) are  $v_x = 0-2$ .

The only plausible candidates for the  $A^1\Pi$  perturbations are  $X^1\Sigma^+$ ,  $a^3\Pi_i$ , and  ${}^3\Sigma^+$  (I). The  $a^3\Pi$  possibility can be immediately ruled out because perturbations affect only the  $e$ -parity levels;  ${}^3\Pi \sim {}^1\Pi$  perturbations would involve both  $e$  and  $f$  levels at the same  $J$  value. All of the observed deviations occur near  $J$  values where extrapolated levels of  $X^1\Sigma^+$  are nearly degenerate with those of  $A^1\Pi$ . These perturbations will be discussed further in Section III.D.6.



Numerous perturbations involving the  $A^1\Pi$  and  $a^3\Pi$  states of isovalent molecules have been observed. Following is a summary of the analyses of these perturbations:

$^3\Pi(I) \sim ^1\Sigma^+(I)$	MgO;
$^3\Pi(I) \sim ^1\Sigma^+(II)$	BeO (28, 48), CaO (27), SrO (27), BaO (27);
$^3\Pi(I) \sim ^1\Pi(I)$	BeO (28, 48), BeS (49, 50);
$^1\Pi(I) \sim ^1\Sigma^+(I)$	BeO (27, 28, 48), MgO, BeS (49, 50);
$^1\Pi(I) \sim ^1\Sigma^+(II)$	BeO (28, 48), CaO (27), SrO (27), BaO (27).

A comprehensive discussion of these types of perturbations and the methods used for obtaining electronic and vibrational assignments from the analysis of perturbations is contained in Ref. (27). The magnitudes of MgO perturbations are compared to those of isovalent molecules in Section IV.

## 2. Assignment of Perturbed $B^1\Sigma^+-X^1\Sigma^+$ and $B^1\Sigma^+-a^3\Pi$ ; Photoluminescence Lines

The laser induced photoluminescence spectrum, although it contains emission from several ( $v'_B, J'_B$ ) levels, overlapping vibrational progressions from the  $B-A$  and  $B-X$  systems, and several highly perturbed transitions sometimes accompanied by one or two "extra lines," is much less complex than an ordinary emission spectrum. The relative simplicity of the laser spectrum would seem to suggest that it contains less information. For purposes of detection and analysis of relatively strong perturbations, there are two reasons to the contrary: unambiguous assignment and dynamic range. Much of the information in an ordinary emission spectrum is redundant, its value being solely that of confirming the assignments of important lines. In a laser photoluminescence spectrum, as described in Section III.A, a few of the well-behaved transitions are utilized to determine absolutely the isotopic species, term energy, and rotation-vibration assignment of the upper level(s) from which fluorescence originates. The perturbed lines, diminished in intensity and shifted from their expected frequencies, are easily lost amidst a complex emission spectrum, yet are easily located in a much sparser laser spectrum. The most valuable sources of information about the perturbing state, the so-called "extra lines" which are normally forbidden transitions made observable by perturbation mixing of the basis functions associated with the perturbed and perturbing levels, are often so weak that they could never be detected in a photographically recorded emission spectrum even if their exact frequencies were known. The relative sparsity of lines in a laser spectrum decreases the probability that a much stronger line will occur unresolvably near an extra line. The large dynamic range of photoelectric detection, combined with the possibility of widening slits for lower resolution but higher sensitivity, maximizes the possibility of detecting extremely weak extra lines.

In cases where the laser populates simultaneously more than one ( $v'_B, J'_B$ ) level and where perturbations distort the expected  $R(J-1)-P(J+1)$  separations and intensity relationships by which fluorescence lines would normally be assigned, all transitions associated with a common ( $v'_B, J'_B$ ) upper level are identified by causing the  $Ar^+$  laser to oscillate on a single longitudinal mode. Insertion of an air-spaced etalon inside the cavity of the  $Ar^+$  laser narrows the spectral width of the output beam from  $0.3\text{ cm}^{-1}$  to

much less than the  $0.02 \text{ cm}^{-1}$  Doppler half-width of the MgO transitions. The laser may be tuned  $0.2 \text{ cm}^{-1}$  by changing the length of the etalon. Provided that the  $B-X$  transitions excited simultaneously by the broad band laser do not have completely overlapping Doppler profiles, the intensity of fluorescence features originating from different ( $v'_B, J'_B$ ) levels will vary separately as the narrow bandwidth laser is tuned. The intensities of all of the lines, regardless of whether they are perturbed or extra lines,

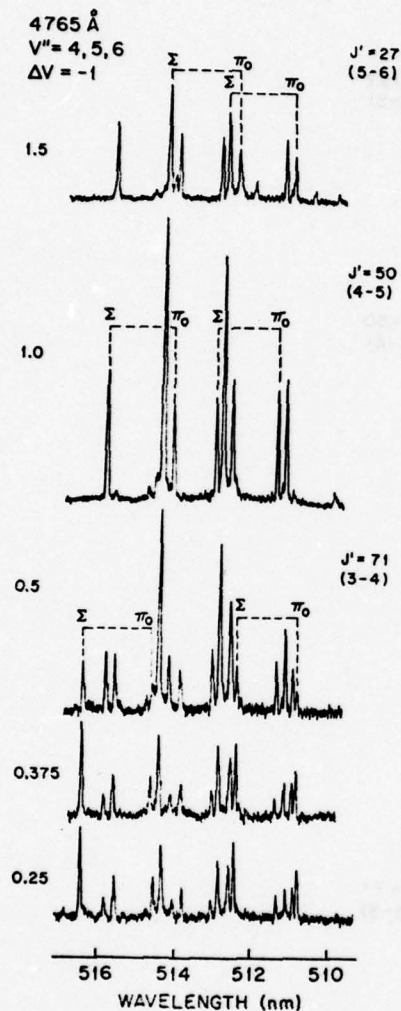


FIG. 2.  $B^1\Sigma-X^1\Sigma \Delta v = -1$  photoluminescence excited by the 476.5-nm line of a single mode  $\text{Ar}^+$  laser. Lines marked by dotted lines on the first, second, and third spectra are main and extra lines of, respectively, the  $B-X$ , 5-6, 4-5, and 3-4 bands. The number to the left of each spectrum is a relative indication of the laser frequency as the laser is tuned across its  $0.2\text{-cm}^{-1}$  gain width. Note that the intensity ratios of the four lines associated with each band do not vary as the laser is tuned.

originating from a common ( $v'_B, J'_B$ ) level are maximized or minimized at the same etalon setting.

The 476.5-nm  $\text{Ar}^+$  line excites three transitions. The  $B-X$  (5,4)  $R(26)$  and (4,3)  $R(49)$  lines partially overlap so that one cannot be excited completely separately from the other. However, the relative intensities of the two excitations can be varied. Fluorescence

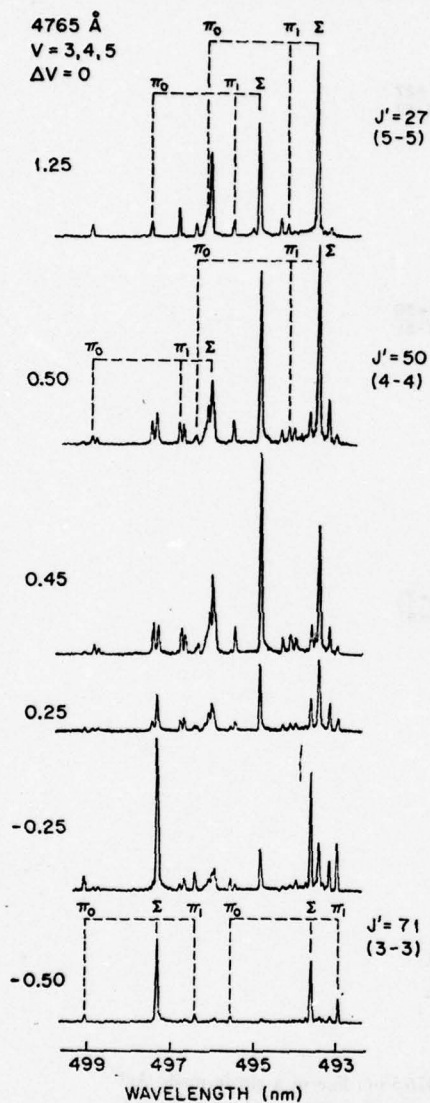


FIG. 3.  $B^1\Sigma-X^1\Sigma \Delta v = 0$  photoluminescence excited by the 476.5-nm line of a single mode  $\text{Ar}^+$  laser. Lines marked by dotted lines of the first, second, and sixth spectra are main and extra lines of, respectively, the  $B-X$  5-5, 4-4, and 3-3 bands. Each main line is accompanied by two extra lines.



spectra of the  $B-X \Delta v = -1$  region recorded at various etalon settings are shown in Fig. 2. At the left of the figure are numbers representing the number of rotations of a knob which controls the etalon spacing. About six rotations are required to tune the laser across its gain profile. Spectra of the  $B-X \Delta v = 0$  region are shown in Fig. 3. Figures 2 and 3 are included because they show that the relative intensities of the three coincident 476.5-nm excitations can be controlled and because they show the most strongly perturbed bands, particularly those in which most of the extra lines were detected.

In Fig. 2, six extra lines are evident, one for each of the six  $B-X$  (5,6)  $R(26)$  and  $P(28)$ , (4,5)  $R(49)$  and  $P(51)$ , and (3,4)  $R(70)$ , and  $P(72)$  main lines. Each extra line has a ratio of intensity to the main line which is invariant as the etalon is tuned. In Fig. 3, each of the six  $B-X$  (5,5) (4,4), and (3,3) main lines is accompanied by *two* extra lines. A total of 18 extra lines are assigned from fluorescence excited by the 476.5-nm line. Two additional extra lines accompany the  $B-X$  (4,6)  $R(8)$  and  $P(10)$  lines excited by the 514.5-nm line. Several unassigned peaks are evident in Figs. 2 and 3. None of these lines have a fixed intensity ratio to any of the assigned lines and are due to other coincidences of  $\text{Ar}^+$  lines with  $\text{MgO}$  transitions which were unassignably weak.

The extra lines are listed in Tables I-III. Also included are observed intensities relative to the main lines and frequency separations from the main lines. One-half of this

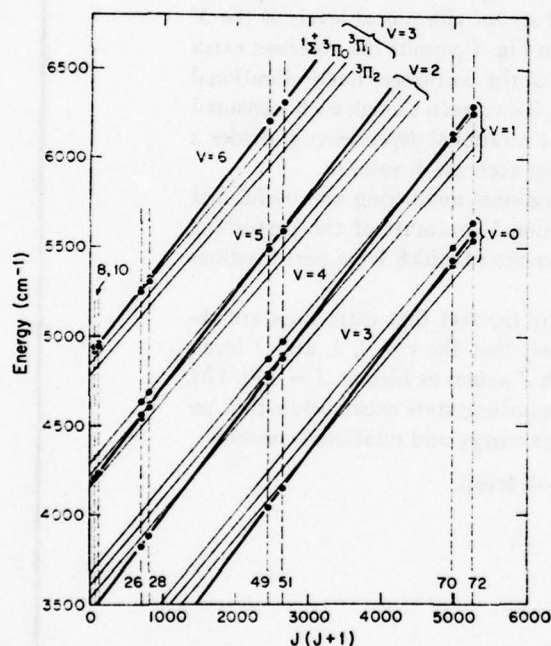


FIG. 4. Summary of the  $X^1\Sigma^+ \sim a^3\Pi_1$  perturbations. Heavy and light lines correspond, respectively, to the term energies of  $X^1\Sigma^+ v_X = 3-6$  and  $a^3\Pi_{0,1,2} v_a = 0-3$ . Each coincidence of an  $\text{Ar}^+$  laser line with a  $^{24}\text{Mg}^{16}\text{O}$   $B-X$  transition samples two  $J''$  levels for each of several  $X^1\Sigma^+$  and  $a^3\Pi$  vibrational levels. Observed energy levels are represented by solid circles, and vertical lines group levels belonging to the same  $J$  value.

frequency difference,  $\nu_{\text{main}} - \nu_{\text{extra}}$ , provides a useful upper limit to the interaction matrix element between the perturbed and perturbing states. When two extra lines are observed, the one at lower frequency (corresponding to the perturbing level with the higher term energy) is designated  $R^+$  or  $P^+$ , and the one at higher frequency by  $R^{++}$  or  $P^{++}$ .

Since transitions from  $B^1\Sigma^+$  into the perturbing state are forbidden, extra lines are always less intense than the main line with the same  $J''$  value. The sum of intensities of main and extra lines for the same  $J''$  is equal to the unperturbed intensity, thus the intensity sum for  $R(J' - 1)$  lines should be similar to that for  $P(J' + 1)$  lines. The  $J''$  assignment of the perturbing level is obtained from the  $\Delta J = 0$  perturbation selection rule and from the fact that the  $P(J' + 1)$  line is always to the red of the  $R(J' - 1)$  line.

The information derived from the rotationally assigned perturbed main and extra lines is displayed in Fig. 4. The term energy,  $T''_{v,J}$ , associated with the lower level of each line is plotted vs  $J(J + 1)$ . Neglecting centrifugal distortion and perturbation effects, term values associated with a given vibrational level should fall on a straight line with slope  $B''$ , and intercept  $T''_v$ , where  $B$  and  $T$  are, respectively, the rotational constant and rotationless term energy. The term energy is given by

$$T''_{v,J} = T_{vX,JX} + \nu_{\text{Laser}} - \nu_{\text{Fluorescence}} \quad (12)$$

Note that each  $(v'_R, J'_R)$  level populated by the  $\text{Ar}^+$  laser gives rise to fluorescence lines which determine the energy of the  $J'_R \pm 1$  levels of several vibrational levels of the  $X$  and perturbing states. The crossing diagram shown in Fig. 4 permits the observed extra lines to be grouped into common vibrational levels of the perturber. Each vibrational level is sampled at several widely separated  $J$  values. Thus, even though each measured frequency is only accurate to  $0.5 \text{ cm}^{-1}$ , the  $J(J + 1)$  rotational dependence provides a large lever arm which permits determination of rather accurate  $B$  values.

Figure 4 provides a relative but not absolute vibrational numbering and useful first approximation values for the vibrational and rotational constants of the perturbing state. It also permits prediction of other  $(v_X, J_X)$  values at which large perturbations should be observable.

An absolute vibrational numbering is suggested by the fact that extra lines are observed for perturbations of the  $X^1\Sigma \ v_X = 3$  level but that the  $v = 0, 1$ , and  $2$  levels were observed (3, 4) to be perturbation free through  $J$  values as high as  $J = 130, 120$ , and  $90$ , respectively. If a vibrational level of the perturbing state exists below that responsible for the perturbation of the  $v_X = 3$  level, its energy and rotational constant

$$\begin{aligned} T_{\text{pert}} &= 2300 \text{ cm}^{-1} \quad (+ + \text{ level}), \\ B_{\text{pert}} &= 0.508 \text{ cm}^{-1}, \end{aligned}$$

compared to those of the  $v_X = 2$  level

$$\begin{aligned} T_2 &= 1930 \text{ cm}^{-1}, \\ B_2 &= 0.5618 \text{ cm}^{-1}, \end{aligned}$$

using

$$T_{\text{pert}} - T_2 = (B_2 - B_{\text{pert}})J^0(J^0 + 1) \quad (13)$$

require that the perturbing level would become degenerate with  $v_X = 2$  near  $J_X = 83$

(++ level) and  $J_X = 90$  (+ level). The absence of any perturbation in  $v_X = 2$  through  $J_X = 90$  suggests that the level responsible for the  $v_X = 3$  perturbation is in fact  $v = 0$ . Confirming evidence for this assignment is presented in Section III.D.4.

The first approximation vibrational and rotational constants of the perturbing state obtained from Fig. 4 resemble those of the  $A$  state. Ab initio constants for the  ${}^1\Pi$  (I) and  ${}^3\Pi_i$  (I) states are nearly identical (23-25). Assuming that the  $v = 0$  level in fact perturbs  $v_X = 3$ , then the  $v = 0$  perturber lies approximately  $950\text{ cm}^{-1}$  below  $A^1\Pi$   $v_A = 0$ , in good agreement with the  $1200\text{ cm}^{-1}$   ${}^1\Pi$  (I)- ${}^3\Pi_i$  (I) splitting calculated by Schamps and Lefebvre-Brion (24). The  $\nu_{\text{main}} - \nu_{\text{extra}}$  values and relative intensities for the + and ++ perturbations indicate that the + perturbations involve a larger interaction matrix element. The matrix elements for perturbations of a  ${}^1\Sigma^+$  state by an intermediate Hund's case "a-b"  ${}^3\Pi$  state are largest for the nominal  ${}^3\Pi_0$  substate, small and  $J$  dependent for  ${}^3\Pi_1$ , and very small and usually undetectable except at high  $J$  values for  ${}^3\Pi_2$ . This means that + extra lines are due to  ${}^3\Pi_0$  and ++ to  ${}^3\Pi_1$ . No  ${}^3\Pi_2$  perturbations were detected. This identification is consistent only with an inverted  ${}^3\Pi$  state with  $A_{\Pi} \approx -70\text{ cm}^{-1}$ . An alternative assignment as a regular  ${}^3\Pi$  state with  $A_{\Pi} \approx 580\text{ cm}^{-1}$  can be ruled out by analogy with the  $a^3\Pi$  states of CaO, SrO, and BaO (27) and by the fact that such a state would be at the case 'a' limit and  ${}^3\Pi_1 \sim {}^1\Sigma^+$  perturbations would be much weaker than observed here.

It is evident that all of the important information about the  $a^3\Pi_i$  state is obtainable directly from Fig. 4. However, in order to obtain the best possible deperturbed spectroscopic constants for the  $a^3\Pi$  and  $X^1\Sigma^+$  states, it is necessary to construct a model perturbation Hamiltonian matrix and least-squares fit the eigenvalues of this matrix to the observed term energies.

### 3. Effective Hamiltonian Matrix and Least-Squares-Fitting Model

An effective Hamiltonian is constructed in a Hund's case "a" basis set consisting of one each of the following basis functions:

$$\begin{aligned} X^1\Sigma^+ (v_X = v_a + 3, J), \\ a^3\Pi_{0e} (v_a, J), \\ a^3\Pi_{1e} (v_a, J), \\ a^3\Pi_{2e} (v_a, J), \\ A^1\Pi_e (v_A = v_a, J). \end{aligned} \quad (14)$$

Choice of a case "a" representation is purely a matter of taste and is completely irrelevant to the ultimately obtained eigenvalues and molecular constants. For perturbations,  $J$  and  $e/f$  parity are rigorously good quantum numbers. Since the  ${}^1\Sigma^+$  state possesses only  $e$ -parity levels and only the  $e$  levels of  $a^3\Pi$  are sampled by the observable extra lines,  $f$ -parity basis functions are excluded. Thus a doubling in the  $a^3\Pi$  and  $A^1\Pi$  states is neglected. Although perturbations between  $A^1\Pi$  and  $X^1\Sigma^+$  involving pairs of levels  $v_X \sim v_A = v_X - 4$  rather than  $v_X \sim v_A = v_X - 3$  are observed, these perturbations are neglected here. The reason for including the  $v_A = v_a$  level here is that, due to the similarity of the  $A^1\Pi$  and  $a^3\Pi$  potential energy curves, the  $\langle v_A = v_a | v_a \rangle$



vibrational overlaps are near unity and all others are vanishingly small. There is a significant  $J$ -independent spin-orbit interaction between the  $950\text{-cm}^{-1}$  distant  $v_A = v_a$  levels which causes an asymmetry in the  $a^3\Pi$  spin-orbit splitting. Since the immediate goal is characterization of a deperturbed  $a^3\Pi$  state, the  $v_A = v_a$  basis functions are included here and the  $v_X \sim v_A = v_X - 4$  interactions are considered separately in Section III.D.6.

Only a small number of rotational levels of each  $X$ ,  $A$ , and a state vibrational level are sampled here, thus all of the term energies obtained from the photoluminescence spectra are least-squares fitted simultaneously rather than as one group of near-degenerate vibrational levels at a time. The data set consists of 40 predominantly  $^1\Sigma^+$  rovibronic levels, and 20  $^3\Pi$  levels. Rather than including observed  $A^1\Pi$  term energies, the  $A^1\Pi$  levels are represented by constants from Ref. (4). The effective Hamiltonian is expressed in terms of six least-squares variable parameters,  $T_e(a^3\Pi)$ ,  $\omega_e(a)$ ,  $\omega_e x_e(a)$ ,  $B_e(a)$ ,  $A_{II}(a)$ , and the electronic part of the spin-orbit perturbation parameter  $H^{el}$ , and several fixed, constrained, and separately calculated parameters.

	$^3\Pi_0$	$^3\Pi_1$	$^3\Pi_2$	$^1\Sigma^+$	$^1\Pi$
$^3\Pi_0$	$T_0$	$H_{01}$	0	$H^{el}\langle v_X   v_a \rangle$	0
$^3\Pi_1$	$H_{01}$	$T_1$	$H_{12}$	0	$-A_{II}$ (15)
$^3\Pi_2$	0	$H_{12}$	$T_2$	0	0
$^1\Sigma^+$	$H^{el}\langle v_X   v_a \rangle$	0	0	$T_X$	0
$^1\Pi$	0	$-A_{II}$	0	0	$T_A$

$T_0$ ,  $T_1$ , and  $T_2$  are the deperturbed  $a^3\Pi$  case "a" term energies

$$T_0 = T_e(a^3\Pi) + G_a(v_a) - A_{II} + B_{ra}[J(J+1) + 1] - D_{ra}J^2(J+1)^2, \quad (16a)$$

$$T_1 = T_0 + A_{II}, \quad (16b)$$

$$T_2 = T_0 + 2A_{II} - 3B_{ra}, \quad (16c)$$

$$G_a(v_a) = \omega_e(a)(v_a + \frac{1}{2}) - \omega_e x_e(a)(v_a + \frac{1}{2})^2. \quad (17)$$

$H_{01}$  and  $H_{12}$  are spin-uncoupling terms

$$H_{01} = B_{ra}[2J(J+1)]^{\frac{1}{2}}, \quad (18a)$$

$$H_{12} = B_{ra}[2J(J+1) - 4]^{\frac{1}{2}}. \quad (18b)$$

Centrifugal distortion contributions to  $H_{01}$ ,  $H_{12}$ , and  $H_{02}$  are ignored.  $T_X$  and  $T_A$  are the deperturbed term values of the  $X^1\Sigma^+$  and  $A^1\Pi$  states (see Section III.D.5)

$$T_X = T_e(X^1\Sigma) + \omega_e(X)(v_X + \frac{1}{2}) - \omega_e x_e(X)(v_X + \frac{1}{2})^2 + B_{rX}J(J+1) - D_{rX}J^2(J+1)^2, \quad (19)$$

$$T_A = T_e(A^1\Pi) + \omega_e(A)(v_A + \frac{1}{2}) - \omega_e x_e(A)(v_A + \frac{1}{2})^2 + B_{rA}J(J+1) - D_{rA}J^2(J+1)^2. \quad (20)$$

The spin-orbit perturbation matrix element (27)

$$\langle ^1\Sigma^+ | H^{so} | ^3\Pi_{0e} \rangle = H^{el}\langle v_X | v_{II} \rangle \quad (21)$$

is factored into an assumed constant electronic part and a rotation independent vibrational overlap. This is the *only* nonzero matrix element between case "a"  $^1\Sigma$  and  $^3\Pi$  basis functions; the spin-uncoupling terms,  $H_{01}$  and  $H_{12}$ , mix  $\Omega = 0$  character into the nominally  $\Omega = 1$  and 2 substrates, thereby causing observable perturbations between  $^1\Sigma^+$  and dominantly  $^3\Pi_1$  and  $^3\Pi_2$  eigenstates. The  $\langle ^3\Pi_1 | H^{so} | ^1\Pi \rangle$  perturbation parameter,  $-A_{11}$ , arises from the assumption that the  $A^1\Pi$  and  $a^3\Pi$  states are represented by a single electronic configuration and that the molecular orbitals for both states are identical. With the additional assumption that the  $\langle r_A = r_a | r_a \rangle$  vibrational overlap is unity, this perturbation parameter is identical to the spin-orbit constant of the  $a^3\Pi$  state (27)

$$A_{11} = \langle ^3\Pi_2 | H^{so} | ^3\Pi_2 \rangle. \quad (22)$$

Other spectroscopic constants of the  $a^3\Pi$  state are subject to the following restrictions: the Pekeris relation (42),

$$\alpha_e = [(B_e \omega_e r_e)^2 - B_e] 6 B_e / \omega_e, \quad (23)$$

the Kratzer relation (42),

$$D_e = 4 B_e^2 / \omega_e^2, \quad (24)$$

and the  $\beta_e$  value of the  $A^1\Pi$  state (4),

$$\beta_e = -5.0 \times 10^{-9} \text{ cm}^{-1}. \quad (25)$$

Initial values of all  $a^3\Pi$  constants except  $T_e(a^3\Pi)$  were set identical to those for the  $A^1\Pi$  state. Vibrational overlaps  $\langle r_a | r_X \rangle$  were initially approximated by the corresponding  $\langle r_A = r_a | r_X \rangle$  overlaps calculated from RKR curves for the  $A^1\Pi$  and  $X^1\Sigma^+$  states. The matrix was set up and diagonalized for vibrational levels  $v_X = 3-7$ ,  $J = 8, 10, 26$ ,

TABLE IV  
Comparison of Calculated Vibrational Overlap Integrals Relevant to Analysis of  
 $X^1\Sigma^+ \sim a^3\Pi_1$  Perturbations

$v_X$	$v_a$	Initial <sup>a</sup>	Intermediate <sup>b</sup>		Final <sup>c</sup>		R-centroid <sup>d</sup>
		$\langle r_X   r_a \rangle$	$\langle r_X   r_a \rangle$	$\langle r_X   r_a \rangle$	$\langle r_X   r_a \rangle$	$\langle r_X   r_a \rangle$	
3	0 <sup>d</sup>	0.296	0.314	0.318	0.327	1.96	
4	1 <sup>d</sup>	0.437	0.453	0.456	0.459	1.97	
5	2 <sup>d</sup>	0.499	0.498	0.497	0.495	1.95	
5	3	0.251	0.178	0.156	0.165	1.93	
6	3 <sup>d</sup>	0.494	0.465	0.460	0.458	1.99	
6	4	0.070	-0.019	-0.032	-0.020	1.72	
7	4 <sup>d</sup>	0.439	0.375	0.360	0.374	1.90	
7	5	-0.089	-0.179	-0.189	-0.168	1.92	
8	6	-0.211	-0.285	-0.291	-0.267	1.94	
9	7	-0.291	-0.333	-0.334	-0.319	1.96	
10	8	-0.329	-0.327	-0.324	-0.329	1.97	

a. Vibrational overlaps calculated using constants for  $A^1\Pi$  state as initial estimates of  $\langle r_X | r_a \rangle$ .

b. Overlaps used in final least squares fit to observed perturbations.

c.  $\langle r_X | r_a \rangle$  and R-centroid calculated using deperturbed  $X^1\Sigma^+$  constants and constants for  $a^3\Pi$  from Table V.

d. Explicitly included in effective Hamiltonian.

THIS PAGE IS BEST QUALITY PRACTICABLE  
FROM COPY FURNISHED TO DDG

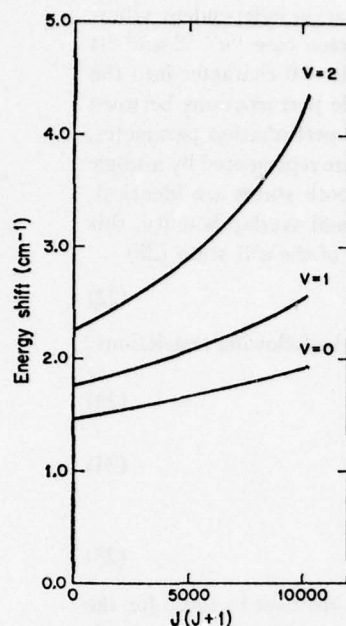


FIG. 5. Energy shifts of  $X^1\Sigma v_X = 0-2$  due to  $a^3\Pi$ . Although the previously known levels of  $X^1\Sigma$  are free of perturbations, the observed levels are depressed by interaction with higher lying  $a^3\Pi$  levels. Plotted are the energy corrections that should be added to the observed energy levels to obtain deperturbed energies. Energy corrections plotted here differ slightly from the final values listed in Table VI.

28, 49, 51, 70, and 72 for  $^{24}\text{MgO}$  and  $J = 25, 27, 36$ , and 38 for  $^{26}\text{MgO}$ . The calculation was limited to the  $v, J$  term energies sampled by the laser induced photoluminescence and to vibrational levels in which  $X^1\Sigma^+ \sim a^3\Pi$  perturbations are observed.

The least-squares-fitting procedure was necessarily iterative. Once approximate values of the  $a^3\Pi$  state vibrational and rotational constants were known, a set of  $\langle v_a | v_X \rangle$  overlaps could be calculated. These overlaps gave a better representation of the vibrational variation of  $a \sim X$  perturbation matrix elements than the initially used  $\langle v_A | v_X \rangle$  overlaps. Convergence of the  $\langle v_a | v_X \rangle$  overlaps to stable values is demonstrated in Table IV in which the  $\langle v_A | v_X \rangle$ , intermediate  $\langle v_a | v_X \rangle$ , and final  $\langle v_a | v_X \rangle$  overlaps are compared.

Once estimates of the electronic parts of the  $a^3\Pi \sim X^1\Sigma^+$  and  $a^3\Pi \sim A^1\Pi$  perturbation matrix elements were obtained from a preliminary fitting of the perturbed lines, it was possible to obtain deperturbed vibrational and rotational constants for the  $X^1\Sigma^+$  and  $A^1\Pi$  states. These deperturbed constants were needed in order to extrapolate reliably from the well-characterized  $v_X = 0-2$  and  $v_A = 0-2$  levels (4) up to  $v_X = 7$  and  $v_A = 10$  without recourse to least-squares variation of additional  $X^1\Sigma^+$  and  $A^1\Pi$  constants.

The deperturbation procedure involves correction for interaction with energetically remote vibrational levels of  $a^3\Pi$  and is described in Section III.D.5. The necessity for such deperturbation is illustrated by Fig. 5, which displays the energy shifts of the  $v_X = 0-2, J_X = 0-101$  levels due to repulsion by the  $a^3\Pi$  levels  $v_a = 0-12$ . These level



TABLE V  
Spectroscopic Constants<sup>a</sup> for  $^{24}\text{Mg}^{16}\text{O } a^3\Pi$  and  $A^1\Pi$  (in  $\text{cm}^{-1}$ )

	$a^3\Pi$	$A^1\Pi$ <sup>b</sup>
$T_e$	2523(7)	3557.5 <sup>c</sup>
$\nu_e$	643(5)	664.44
$\nu_e x_e$	3.9(9)	3.91
$B_e$	0.5022(13)	0.5056
$\nu_e$	0.0042(8) <sup>d</sup>	0.0046
$A_{\text{so}}$	-64(1) <sup>f</sup>	—
$H^{\text{el}}$	71.78(8) <sup>e</sup>	—

a. Uncertainties (1 $\sigma$ ) in parentheses.

b. From Reference [4].

c. Deperturbed, see Section III.0.5.

d. Calculated using Pekeris' relation.

e. Electronic part of the  $X^1\Sigma^+ \sim a^3\Pi$  spin-orbit perturbation matrix element.

f. This value is uncertain by an additional 3  $\text{cm}^{-1}$  due to neglect of  $\Lambda$ -doubling effects. Probable deperturbed value is -61.5  $\text{cm}^{-1}$ .

shifts are so large and  $J$  dependent that it is remarkable that Lagerqvist and Uhler (4) were not led to search for perturbations in  $v_X = 3$ .

The  $\langle v_a | v_X \rangle$  overlaps and the deperturbed  $X^1\Sigma^+$  and  $A^1\Pi$  constants, calculated separately from the results of the preliminary least-squares fit, were used in the final six parameter, nonlinear least-squares fit to 60 data points. The standard deviation of the fit was 1.6  $\text{cm}^{-1}$  which is larger than the estimated 0.5- $\text{cm}^{-1}$  measurement error for individual photoluminescence lines. Residual error arises from neglect of  $X^1\Sigma^+ \sim A^1\Pi$  perturbations and from the highly constrained nature of the effective Hamiltonian. Final values of the  $a^3\Pi$  molecular constants and the  $a \sim X$  electric perturbation parameter are listed in Table V and compared with the known constants of the isoconfigurational  $A^1\Pi$  state (4). The success of the fitting procedure is illustrated two ways in Tables I-III. First, comparison of observed minus calculated values before,  $\Delta\nu$ , and after,  $\Delta\nu'$ , taking  $a \sim X$  perturbations into account shows that the largest deviations are well accounted for. Even though separations between main and extra lines are often larger than 50  $\text{cm}^{-1}$ , the extra lines are typically fitted to 1  $\text{cm}^{-1}$ . Second, relative intensities of extra lines are calculated using the fractional  $X^1\Sigma^+$  character obtained from the eigenfunctions of the effective Hamiltonian. The extra line intensities are tabulated as fractions of main line intensities. For example, the (4,5)  $R^+$  (49) extra line is observed to be 96% as intense as the corresponding main line, implying that the  $J = 49$  eigenfunction is nearly a 50-50 mixture of  $X^1\Sigma^+ v_X = 5$  and  $a^3\Pi_0 v_a = 2$ . Intensities of transitions into predominantly  $a^3\Pi \Omega = 2$  levels were calculated and, without exception, were found to be undetectably weak.

#### 4. Vibrational Assignment of the $a^3\Pi$ State

As discussed in Section III.D.2, the absolute vibrational numbering of the  $a^3\Pi$  state is tentatively determined by the absence of  $X \sim a$  perturbations in  $X^1\Sigma^+ v_X = 0-2$  and

the presence of one in  $v_X = 3$ . This assignment is confirmed by examination of vibrational overlap integrals calculated using various trial numberings of the observed  $a^3\Pi$  levels.

Figure 4 shows that an  $a^3\Pi_i$  level crosses  $X^1\Sigma^+ v_X = 3$  near  $J_X = 67$ . This crossing places an upper bound on the energy of the  $v_a = 0$  level because the observed perturbing level must belong to  $v_a = 0$  or some higher  $v_a$  value. The absence of a perturbation in  $v_X = 2$  would seem to put a lower bound on the energy of  $v_a = 0$ . Provided that the perturbation matrix element is large enough and that the  $X^1\Sigma^+ v_X = 2$  level is known to high enough  $J$  values, then a perturbation would necessarily be observable involving a level of  $a^3\Pi$  lower than the one responsible for the  $v_X = 3$  perturbation. Using the  $\Delta G$ ,  $B_v$ , and  $\alpha_e$  values obtained from Fig. 4 for the observed  $X \sim a$  perturbations, the energy and rotational constants of a possible  $a^3\Pi$  level below the lowest observed one are calculated. The predicted  $\Omega = 0$  and 1 crossings (locations of maximum rotational level shifts and intensity alterations) between this possible  $a^3\Pi$  vibrational level and  $X^1\Sigma^+ v_X = 2$  occur within the observed (4) range of  $J$  values. In order for these crossings to occur without any evidence of perturbation, the matrix element

$$H_{v_X=2, v_a} = H^{el}(v_X = 2 | v_a)$$

would necessarily be much smaller than the observed  $v_X = 3$  matrix element,  $H_{v_X=3, v_a+1}^{obs}$ . Until the absolute vibrational numbering of the  $a^3\Pi$  state is established, neither  $H^{el}$  nor  $\langle v_X v_a \rangle$  is known. However,  $X \sim a$  overlaps should be approximated well by  $X \sim A$  overlaps because of the predicted similarity of the  $a^3\Pi$  and  $A^1\Pi$  potential energy curves. The interaction strength for the possible  $v_X = 2 \sim v_a$  crossing is estimated by

$$H_{v_X=2, v_a} \approx H_{v_X=3, v_a+1}^{obs} \frac{\langle v_X = 2 | v_a \rangle}{\langle v_X = 3 | v_a + 1 \rangle}, \quad (26)$$

where the ratios of vibrational overlaps are 0.94, 30., and 1.1, respectively, for  $v_a = 0, 1$ , and 2. Thus the absence of a detected perturbation in  $v_X = 2$  implies that the level responsible for the perturbations of  $v_X = 3$  is  $v_a = 0$ .

This assignment is confirmed from the observed vibrational variation of the perturbation strengths for  $v_X = 3-7$ . Figure 4 shows that main and extra lines are observed fortuitously close to several  $X^1\Sigma^+ \sim a^3\Pi_0$  crossings. At a crossing, the separation between main and extra lines is twice the interaction matrix element. Inspection of the frequency differences between main and extra lines for strongly perturbed levels  $v_X = 4$   $J_X = 70, 72$ ,  $v_X = 5$   $J_X = 49, 51$ , and  $v_X = 6$   $J_X = 26, 28$  indicates that whatever the vibrational numbering of  $a^3\Pi$  might be, the three overlap integrals  $\langle v_X = 4 | v_a \rangle$ ,  $\langle v_X = 5 | v_a + 1 \rangle$ , and  $\langle v_X = 6 | v_a + 2 \rangle$  must have similar values. Again using overlaps calculated from  $A^1\Pi$  rather than  $a^3\Pi$  constants,

$v_X$	$v_a$	$\langle v_X   v_a \rangle$		
		$v_a = v_X - 2$	$v_a = v_X - 3$	$v_a = v_X - 4$
4	$v_a$	0.422	0.437	0.137
5	$v_a + 1$	0.251	0.499	0.248
6	$v_a + 2$	0.070	0.494	0.345

(27)

it is evident that the only acceptable vibrational numbering of these  $a^3\Pi$  perturbing levels is  $v_a = v_X - 3$ .

### 5. Deperturbed Constants

The constants for the  $B^1\Sigma$ ,  $A^1\Pi$ , and  $X^1\Sigma$  states were obtained in the usual way for the apparently perturbation free  $v = 0-2$  vibrational levels of each state (4). These constants, although they accurately reproduce the observed  $v = 0-2$  energy levels, have compromised mechanical significance (51). They are not suitable for extrapolation to higher vibrational levels nor for construction of realistic potential energy curves. It is possible to obtain constants deperturbed with respect to energetically remote levels of the  $a^3\Pi$  state. These deperturbed constants, *when supplemented by the necessary interaction matrix elements*, represent the observed  $v = 0-2$  energy levels equally as well as those of Ref. (4), and also provide a better mechanical representation which is more suitable for extrapolation and construction of potential curves.

The second order perturbation theoretic energy correction is

$$E_i^{(2)} = \sum_j \frac{|H_{ij}|^2}{E_i^0(J) - E_j^0(J)}. \quad (28)$$

If  $H_{ij}$  can be factored into a constant electronic part and a vibrational overlap, Eq. (28) reduces to

$$E_i^{(2)} = |H^{el}|^2 \sum_j \frac{q_{ij}}{E_i^0(J) - E_j^0(J)}, \quad (29)$$

where  $q$  is a vibrational overlap squared. Shifts of the  $X^1\Sigma$   $v_X = 0-2$   $J_X = 0-161$  levels due to  $a^3\Pi_0$   $v = 0-12$  are calculated using  $H^{el} = 71.7 \text{ cm}^{-1}$  and displayed in Fig. 5. Energy shifts are  $v$  and  $J$  dependent and range from 1.4 to  $4.3 \text{ cm}^{-1}$ .

Equation (29) can be separated, by considering the  $J$  dependence of the denominator, into three terms which are, respectively, corrections to vibrational energies, rotational constants, and centrifugal distortion constants

$$E_i^{(2)} = |H^{el}|^2 \sum_j \left[ \frac{q_{ij}}{\Delta E_{ij}^0} - \frac{q_{ij} \Delta B_{ij}^0 J(J+1)}{(\Delta E_{ij}^0)^2} + \frac{q_{ij} (\Delta B_{ij}^0)^2 J^2(J+1)^2}{(\Delta E_{ij}^0)^3} \right], \quad (30)$$

where  $\Delta E_{ij}^0 = E_i^0 - E_j^0$  and  $\Delta B_{ij}^0 = B_i^0 - B_j^0$ . The mechanical or deperturbed constants are

$$E = E_{obs} - |H^{el}|^2 \sum \frac{q}{\Delta E}, \quad (31a)$$

$$B = B_{obs} + |H^{el}|^2 \sum \frac{q \Delta B}{\Delta E^2}, \quad (31b)$$

$$D = D_{obs} + |H^{el}|^2 \sum \frac{q \Delta B^2}{\Delta E^3}, \quad (31c)$$

where the obs subscript refers to constants from Ref. (4). Correction terms for  $v_X = 0-7$



TABLE VI  
Mutual Deperturbation of  $^2\text{Mg}^{16}\text{O } X^1\Sigma^+$  and  $a^3\Pi$

Deperturbed <sup>a</sup> Level	$E-E_{\text{obs}}^b$ ( $\text{cm}^{-1}$ )	$B-B_{\text{obs}}^b$ ( $10^{-3}\text{cm}^{-1}$ )	$D-D_{\text{obs}}^b$ ( $10^{-8}\text{cm}^{-1}$ )	Excluded <sup>c</sup> Level
$X^1\Sigma^+$				$a^3\Pi$
$v_X = 0$	1.51	3.6	-0.09	
1	1.85	5.7	-0.19	
2	2.47	11.2	-0.58	
3	2.39	12.1	-0.73	$v_a = 0$
4	1.51	12.2	-0.26	1
5	0.55	11.9	+0.27	2
6	-0.13	12.7	+0.44	3
7	-0.18	16.7	-0.06	4
$a^3\Pi$				$X^1\Sigma^+$
$v_a = 0$	-2.56	-16.6	0.35	$v_X = 3$
1	-1.50	-19.0	0.18	4
2	-0.30	-17.3	-0.10	5
3	+0.53	-14.2	-0.33	6
4	0.81	-12.7	-0.33	7
5 <sup>d</sup>	2.34	-44.5	-7.46	7

- a. Levels of  $X^1\Sigma^+$  are deperturbed with respect to  $v_a=0-20$  of  $a^3\Pi$ .  
e-parity levels of  $a^3\Pi$  are deperturbed with respect to  $v_X=0-20$  of  $X^1\Sigma^+$ .
- b. Calculated deperturbation corrections. Tabulated quantities are differences between the deperturbed value and the value that would be obtained from a least squares fit in which remote perturbing levels are excluded from the effective Hamiltonian.
- c. One level is excluded from the perturbation summation because it should be explicitly included in the effective Hamiltonian.
- d. Perturbation summation valid only at low  $J$ -values. Effective Hamiltonian should include  $v_a=5$ ,  $v_X=7$  and 8.

are listed in Table VI. For  $v_X = 3-7$  the obs subscript refers to constants that would be obtained in a least-squares fit if only the nearest higher energy  $a^3\Pi$  vibrational level were included in the effective Hamiltonian matrix. Note that the effect of remote  $a^3\Pi$  levels on  $B$  and  $D$  values is small, but that band origins are significantly affected.

The observed energies of  $v_X = 0-2$  (4) are converted to deperturbed energies and new values of the following constants are obtained (constants from Ref. (4) are in parentheses):

$$\begin{aligned}
 \omega_e(X^1\Sigma) &= 785.14 \quad (785.06) \text{ cm}^{-1}, \\
 \omega_e v_e(X^1\Sigma) &= 5.07 \quad (5.18) \text{ cm}^{-1}, \\
 T_e(A^1\Pi) &= 3561.9 \quad (3563.3) \text{ cm}^{-1}, \\
 T_e(B^1\Sigma) &= 19\,982.6 \quad (19\,984.0) \text{ cm}^{-1}.
 \end{aligned} \tag{32}$$

The  $T_e$  values for  $A$  and  $B$  states are decreased by  $1.4 \text{ cm}^{-1}$  because the position of the minimum of the  $X^1\Sigma^+$  potential is raised  $1.4 \text{ cm}^{-1}$  by deperturbation. The new vibrational constants for the  $X^1\Sigma$  state provide significantly improved extrapolated energies for  $v_X = 3-7$ ; the shift for  $v_X = 7$  is  $7 \text{ cm}^{-1}$ .

The interaction between  $A^1\Pi$  and remote levels of  $a^3\Pi$ , although comparable in magnitude to the  $X \sim a$  interaction, has a much less dramatic effect on the constants of the  $A^1\Pi$  state. The vibrational and rotational constants of the  $A$  and  $a$  states are nearly identical. As a result, the vibrational overlap factor is large only for  $v_A = v_a$  interactions. Only the  $\Delta v = 0$  terms in the Eq. (31) summations are significant, and, since  $\Delta B \approx 0$  for  $\Delta v = 0$ , the corrections to  $B$  and  $D$  vanish. Assuming that  $H^{e1}$  for the  $A \sim a$  interaction is  $64 \text{ cm}^{-1}$  (equal in magnitude to the observed spin-orbit coupling constant for  $a^3\Pi$ ) and  $\Delta E = 940 \text{ cm}^{-1}$ , a constant  $v$ - and  $J$ -independent energy shift.

$$E(A^1\Pi) = E_{\text{obs}} - 4.4 \text{ cm}^{-1} \quad (33a)$$

is obtained. The only deperturbed constant of  $A^1\Pi$  which differs from the observed constants ( $f$ ) is

$$T_e(A^1\Pi) = 3557.5 \text{ cm}^{-1}. \quad (33b)$$

Deperturbation of  $A^1\Pi$  with respect to levels of the  $X^1\Sigma$  state is discussed in Section III.D.6.

The constants for the  $a^3\Pi$  state given in Table V are only partially deperturbed. Effects of interaction with all  $A^1\Pi$  levels and only the nearest  $X^1\Sigma$  vibrational level are included.  $A^1\Pi$  causes the deperturbed  $a^3\Pi$  energy to be  $4.4 \text{ cm}^{-1}$  higher than the apparent energy and also causes an asymmetry in the  $a^3\Pi$  spin splitting. The  $^3\Pi_0 - ^3\Pi_1$  and  $^3\Pi_1 - ^3\Pi_2$  splittings are, respectively,  $4.4 \text{ cm}^{-1}$  larger and smaller than in an unperturbed  $^3\Pi_i$  state. The  $^3\Pi \sim ^1\Sigma^+$  interaction contributes to the  $J$ -independent  $\Lambda$  doubling of  $^3\Pi_0$ . The bottom half of Table VI lists the effect of remote  $X^1\Sigma$  levels on  $^3\Pi_{0e}$ . For example, in  $v_a = 0$  the  $^3\Pi_{0e}$  levels are raised above  $^3\Pi_{0f}$  by  $2.56 \text{ cm}^{-1}$ . There is an additional  $1.70 \text{ cm}^{-1}$  contribution to the  $v_a = 0$ ,  $\Omega = 0$  doubling at  $J_a = 0$  due to the near degenerate  $v_a = 0 \sim v_X = 3$  interaction. Since only  $e$ -parity levels are observed here, it is not possible to experimentally sample the  $a^3\Pi$   $\Lambda$  doubling, but it is likely that the  $v_a = 0$ ,  $\Omega = 0$  doubling is  $4 \text{ cm}^{-1}$ . Contributions from the  $B^1\Sigma^+$  and  $^3\Sigma^+(1)$  states are expected to be small and of opposite signs, but a direct spin-spin contribution,  $\alpha$  (52), could alter the predicted doubling by  $\pm 2 \text{ cm}^{-1}$ . Uncertainty about the magnitude and physical origin of the  $a^3\Pi$   $\Lambda$  doubling, combined with observance of only  $e$ -parity levels, results in an uncertainty in the deperturbed value of the spin-orbit constant  $A_{\Pi}$ . If the  $\Omega = 0$  doubling were  $2.56 + 1.70 \text{ cm}^{-1}$ , then the deperturbed value of  $A_{\Pi}$  would be  $-61.5 \text{ cm}^{-1}$  rather than the value  $-64 \text{ cm}^{-1}$  given in Table V.

#### 6. Analysis of $A^1\Pi \sim X^1\Sigma^+$ Perturbations

The  $A^1\Pi$  state interacts with both  $X^1\Sigma^+$  and  $B^1\Sigma^+$ . The ordinary  $\Lambda$  doubling of the  $A$  state

$$E_{J_e} - E_{J_f} = q_e J(J+1) - q_o J^2(J+1)^2 \quad (34)$$

is dominated by contributions from the  $X$  and  $B$  states. Several  $X \sim A$  perturbations are recognized by the resultant anomalous  $\Lambda$  doubling which increases rapidly with  $J$ , changes discontinuously from large positive to large negative, and then decreases in magnitude to the asymptotic doubling of Eq. (34). Franck-Condon forbidden but perturbation allowed  $B \sim X$  transitions are observed as extra lines at  $^{24}\text{MgO } v_X = 7 \sim v_A = 3$ ,  $v_X = 9 \sim v_A = 5$ , and  $^{26}\text{MgO } v_X = 10 \sim v_A = 6$  perturbations.

Only the  $e$ -parity ( $4J$ ) levels of  $A^1\Pi$  are affected by a  $^1\Sigma^+$  perturber, thus only the  $B-A$   $R$ - and  $P$ -branch lines are shifted. The interaction matrix element is  $J$  dependent (44)

$$\langle ^1\Pi_e | H | ^1\Sigma^+ \rangle = [2J(J+1)]^{1/2} \eta \quad (35)$$

and may be factored into an electronic and a calculable vibrational part (27)

$$2\eta = b \langle v_{\Pi} | h/8\pi^2 c \mu r^2 | v_{\Sigma} \rangle \equiv b B_{v_{\Pi} v_{\Sigma}} \quad (36)$$

If one assumes that the electronic factor,  $b$ , is independent of internuclear distance, then

$$q_{v_{\Pi}} = 2b^2 \sum_{v_{\Sigma}} \frac{(B_{v_{\Pi} v_{\Sigma}})^2}{E_{v_{\Pi}}^0 - E_{v_{\Sigma}}^0}, \quad (37a)$$

$$q_{Dv_{\Pi}} = 2b^2 \sum_{v_{\Sigma}} \frac{(B_{v_{\Pi} v_{\Sigma}})^2 (B_{v_{\Pi}}^0 - B_{v_{\Sigma}}^0)}{(E_{v_{\Pi}}^0 - E_{v_{\Sigma}}^0)^2}, \quad (37b)$$

thus it is possible to estimate the contribution of remote  $X^1\Sigma^+$  levels to the  $A^1\Pi$   $\Lambda$  doubling once a value of  $b$  is obtained from analysis of  $X \sim A$  perturbations.

The following  $b$  values are obtained from the observed  $X \sim A$  perturbations at which extra lines are found:

	$v_X$	$v_A$	$J^0$	$B_{v_{\Pi} v_{\Sigma}}$ ( $\text{cm}^{-1}$ )	$R$ centroid ( $\text{\AA}$ )	$b$
$^{24}\text{MgO}$	7	3	70.2	0.1743	2.054	0.83 (2)
	9	5	44.6	0.2000	2.075	0.86 (4)
$^{26}\text{MgO}$	10	6	39.2	0.1901	2.082	0.89 (4)

(38)

Perturbation matrix elements are derived from measured separations between main and extra lines

$$|\nu_{\text{main}} - \nu_{\text{extra}}| = |E_{\Pi}^0 - E_{\Sigma}^0| + 2|\delta| \quad (39)$$

and level shifts

$$\delta = E_{\Pi}^0 - E_{\Pi}^{\text{obs}} \quad (40)$$

$$= [H^2 + (\Delta E_{\Pi \Sigma}^0/2)^2]^{1/2} - \Delta E_{\Pi \Sigma}^0/2, \quad (41)$$

where the zero superscript denotes the extrapolated (unperturbed) level position which is estimated from perturbation-free  $Q$ -branch lines. The uncertainty estimate for  $b$  is obtained by shifting one of the four main or extra lines by  $0.5 \text{ cm}^{-1}$ .

An average value of the electronic perturbation parameter

$$b^{X \sim A} = 0.85$$

means that  $X \sim A$  interactions contribute

$$q_v^{X \sim A} = 1.5 \times 10^{-4} \text{ cm}^{-1},$$

$$q_{Dv}^{X \sim A} = -6 \times 10^{-9} \text{ cm}^{-1}$$

to the  $\Lambda$ -doubling constants  $q_v$  and  $q_{Dv}$  for  $A^1\Pi$   $v_A = 0-2$ . After removing the effects of high- $J$   $X \sim A$  perturbations (at  $J^0 = 97, 89$ , and  $80$ , respectively) from  $v_A = 0-2$  term energies (4),

$$q_v = 0.6 \times 10^{-4} \text{ cm}^{-1}$$



is obtained. It is not surprising that the observed  $q_r$  value is smaller than the  $X \sim A$  contributions. All  ${}^1\Sigma$  states contribute to  $q_r$ ; higher-lying  ${}^1\Sigma^+$  and lower lying  ${}^1\Sigma^-$  states make negative contributions. Assuming a maximum value for the  $B \sim A$  interaction (27)

$$b^{B \sim A} = \langle 2p_0\pi | I_z | 2p_0\sigma \rangle = 2^1,$$

the  $B \sim A$  contribution for  $r_{11} = 0.5$  is found, by explicit evaluation of the Eq. (37) perturbation sums, to be

$$q_r^{B \sim A} = -6 \times 10^{-3} \text{ cm}^{-1},$$

$$q_{Dr}^{B \sim A} = -2 \times 10^{-10} \text{ cm}^{-1}.$$

Thus all remaining higher-lying  ${}^1\Sigma$  states make a net contribution of  $-3 \times 10^{-3} \text{ cm}^{-1}$  to  $q_r$  and a negligible contribution to  $q_{Dr}$ . There is no need to deperturb the constants

TABLE VII  
Summary of  ${}^{24}\text{MgO } X^1\Sigma^+$  Perturbations ( $J_X < 100$ )

$J_X$	$J^{\text{a}}$	$v_A$	$v_A' (=2)$	$v_A' (=1)$	$v_A' (=0)$	Matrix Element <sup>c</sup>	
						Vibronic Part <sup>b</sup> ( $\text{cm}^{-1}$ )	Rotational Factor <sup>d</sup>
3	34 47 81		0	0°	0°	23.4 23.4 23.4	0.15 0.47 0.86
4	37 52 67 97		1	1°	1°	32.9 32.9 32.9 0.113	0.08 0.41 0.88 1.33
5	40 51 59 89		2	2°	2°	35.5 35.5 35.5 11.8	0.06 0.30 0.91 0.32
6	19 30 37 93		3	3°	3°	32.9 0.173 -1.4 -1.4	0.08 1.31 0.29 0.54
7	70 78 89		4	4°	4°	0.145 -12.3 -12.0	1.33 0.25 0.52
8	59 63 79 92		5	5°	5°	0.145 -19.2 -19.2 -19.2	0.11 0.21 0.50 0.93
9	45 55 68 81		6	6°	6°	0.173 -22.9 -22.0 -22.0	0.11 0.15 0.47 0.86
10	26 19 54 69		7	7°	7°	0.150 -21.6 -21.6 -21.6	0.11 0.08 0.42 0.88

<sup>a</sup> Calculated value of  $J$  at which levels of the perturbed and perturbing states with the same  $J$  values are most nearly degenerate.

<sup>b</sup> For the  $X \sim A$  perturbations this is  $b B_{v_X v_A}$ . For the  $X \sim a$  perturbations, this is  $\langle {}^2\Pi_g | H^{\infty} | {}^1\Sigma^+ \rangle \times \langle v_X | v_A \rangle$ . Calculated using  $H^{\infty} = 71.7 \text{ cm}^{-1}$  and  $b = 0.85$ .

<sup>c</sup> For the  $X \sim A$  perturbations, this is  $[2J(J+1)]^{\frac{1}{2}}$ . For the  $X \sim a$  perturbations this is a spin uncoupling factor, see Ref. (44), pp. 68-70.

<sup>d</sup> Actual matrix element for the specific  $v, J(v)$  level is given by the product of the vibronic part times the rotational factor.

<sup>e</sup> Extra lines observed.

<sup>f</sup> Extra lines observed for  ${}^{24}\text{MgO}$  at  $J^0 = 39.2$ .

THIS PAGE IS BEST QUALITY PRACTICABLE  
FROM COPY FURNISHED TO DDG

for  $A^1\Pi$  with respect to  $^1\Sigma$  states, provided that only the  $f$ -parity levels obtained from  $Q$  branches of the  $B^1\Sigma^+-A^1\Pi$  transition (4) are used to obtain  $B_r$  values.

The effect of  $^1\Sigma$  states is small, except for a  $\Lambda$  doubling that amounts to about  $2\text{ cm}^{-1}$  at  $J = 100$  and several local  $X \sim A$  perturbations accompanied by  $e$ -level shifts as large as  $15\text{ cm}^{-1}$ . One of the largest of these perturbations may have been noticed in the  $C^1\Sigma^+-A^1\Pi$  (4,4) band by Brewer and Trajmar (10) at which the  $v_X = 8$  and  $v_A = 4$  levels cross near  $J = 59$  with an interaction matrix element of  $14\text{ cm}^{-1}$ .

All of the perturbations involving  $X^1\Sigma$   $v_X = 0-10$ ,  $A^1\Pi$   $v_A = 0-6$ , and  $a^3\Pi_{0,1,2}$   $v_a = 0-8$  for  $J = 0-100$  are summarized in Table VII.  $J$  values at which perturbing levels cross and estimated matrix elements at  $J^0$  are included.

#### IV. DISCUSSION

The most important result of the work presented here is a set of preliminary values of the MgO  $a^3\Pi$  molecular constants. The  $a^3\Pi$  constants are found to be nearly identical with those for  $A^1\Pi$ , and the differences between constants agree in sign and magnitude with ab initio calculations:

	Observed	Ref. (24)
$T_e(^1\Pi) - T_e(^3\Pi)$	$934\text{ cm}^{-1}$	$1203\text{ cm}^{-1}$
$\omega_e(^1\Pi) - \omega_e(^3\Pi)$	$2.4\%$	$0.9\%$
$r_e(^1\Pi) - r_e(^3\Pi)$	$-0.33\%$	$-0.11\%$

(42)

Similar agreement exists between observed,  $A_{II} = -64\text{ cm}^{-1}$ , and ab initio (21),  $A_{II} = -53.5\text{ cm}^{-1}$ , values of the spin-orbit constant. There have been no ab initio calculations of MgO perturbation parameters.

The  $a^3\Pi$  spin-orbit constant for MgO may be compared against values for the following isovalent molecules:

	$A_{II}\text{ (cm}^{-1}\text{)}$
BeO	$-62\text{ (53)}$
C <sub>2</sub>	$-16.4\text{ (33)}$
BeS	$-159\text{ (53)}$
MgO	$-64\text{ (43)}$
CaO	$-58\text{ (27)}$
SrO	$-70\text{ (27)}$
BaO	$-105\text{ (27)}$

The BeO, MgO, and CaO  $A_{II}$  values are nearly identical because of the negligible metal atom character in the only incompletely filled  $\pi$  orbital.

Transitions involving  $a^3\Pi$  as the lower state have been reported (20-22). A partial analysis of the  $d^3\Delta-a^3\Pi$  (0,0) band is reported in Ref. (21). Information obtained here about the  $a^3\Pi$  state suggests that the analysis in Ref. (21) may be incorrect in a minor detail. Two of several plausible bandhead assignments are compared:

	Ref. (21)	More probable
3721.39 Å	$^3\Delta_3-^3\Pi_2\text{ (Q)}$	$^3\Delta_3-^3\Pi_1\text{ (Q)}$
3720.94	$^3\Delta_3-^3\Pi_1\text{ (Q)}$	$^3\Delta_1-^3\Pi_{0e}\text{ (Q)}$
3720.64	$^3\Delta_1-^3\Pi_{0e}\text{ (Q)}$	$^3\Delta_3-^3\Pi_2\text{ (Q)}$
3720.56	$^3\Delta_1-^3\Pi_{0f}\text{ (Q)}$	$^3\Delta_1-^3\Pi_{0f}\text{ (Q)}$
3724.9	Superimposed $P$	Superimposed $P$
$^3\Pi_{0e}-^3\Pi_{0f}$	$0.5\text{ cm}^{-1}$	$3\text{ cm}^{-1}$
$A_{\Delta}$	$-32.5\text{ cm}^{-1}$	$-30.5\text{ cm}^{-1}$
$^3\Delta$ asymmetry	$6.5\text{ cm}^{-1}$	$11.5\text{ cm}^{-1}$

(44)

The alternative assignment is supported by its larger  $^3\Pi_0$   $\Lambda$  doubling and  $^3\Delta$  asymmetry. The  $^3\Delta$  asymmetry is caused by spin-orbit interaction between  $D^1\Delta$  at  $T_{0e} = 30\,160\text{ cm}^{-1}$  and  $d^3\Delta_2$  at  $T_{0e} = 29\,812\text{ cm}^{-1}$  with a matrix element

$$\langle ^1\Delta | H^{so} | ^3\Delta_2 \rangle \approx -2.1\Delta.$$

The  $^3\Delta_2$  substate should be depressed  $11\text{ cm}^{-1}$  below its deperturbed position. A simple experimental verification of one of the above alternative assignments is possible. The intensity of the two  $^3\Delta_1$ - $^3\Pi_0$  Q heads should be one-half that of the  $^3\Delta_3$ - $^3\Pi_2$  and  $^3\Delta_2$ - $^3\Pi_1$  heads.

The MgO  $a^3\Pi \sim X^1\Sigma$  perturbations are the first observed  $^3\Pi$  (I)  $\sim$   $^1\Sigma$  (I) perturbations for the eight valence electron group of diatomic molecules. A surprisingly large electronic matrix element,  $71.7\text{ cm}^{-1}$ , is observed. Single configuration, dominant atomic orbital character arguments predict that the  $^3\Pi$  (I)  $\sim$   $^1\Sigma^+$  (I) matrix element for MgO

$$\langle ^3\Pi_0 \text{ (I)} | H^{so} | ^1\Sigma^+ \text{ (I)} \rangle = -\frac{1}{2} \langle 2\pi | \hat{a}l_+ | 7\sigma \rangle \quad (45a)$$

should be smaller than

$$\langle ^3\Pi_0 \text{ (I)} | H^{so} | ^1\Sigma^+ \text{ (II)} \rangle = -\frac{1}{2} \langle 2\pi | \hat{a}l_+ | 6\sigma \rangle \quad (45b)$$

because the  $2\pi$ ,  $6\sigma$ , and  $7\sigma$  orbitals are dominated, respectively, by  $2p_{0\pi}$ ,  $2p_{0\sigma}$ ,  $3s_{Mg}\sigma$  atomic character.  $^3\Pi$  (I)  $\sim$   $^1\Sigma$  (II) matrix element is not known for MgO, but values of 55, 31, and  $35\text{ cm}^{-1}$  are found for CaO, SrO, and BaO (27). Ab initio calculations (53) for BeO and BeS show the  $^3\Pi$  (I)  $\sim$   $^1\Sigma^+$  (I) interaction to be smaller than the  $^3\Pi$  (I)  $\sim$   $^1\Sigma^+$  (II). Both  $^3\Pi \sim ^1\Sigma$  matrix elements are found (53) smaller for BeO and larger for BeS than  $71.7\text{ cm}^{-1}$ . It will be interesting to discover whether the MgO  $a \sim X$  interaction is larger or smaller than the  $a \sim B$  and to find the reason for the large  $a \sim X$  matrix element.

Considerable interest has focused recently on chemiluminescent photon yields and collision induced transfer from nonradiating energy reservoir states into radiating states. For all of the alkaline earth monoxides and many other molecules, the lowest triplet state and high vibrational levels of the electronic ground state act as reservoir levels. Often the lowest triplet also acts as a conduit through which population is transferred from reservoir to radiating states. Locations of potential energy curve crossings and magnitudes of spin-orbit matrix elements between  $^3\Pi$  (I) and  $^1\Sigma^+$  (I and II) states are of paramount importance in determining the rates, efficiency, and specificity of energy funneling from reservoir to radiating levels. All of the relevant potential energy curves for the alkaline earth monoxides are now known [excluding  $^3\Sigma^+$  (I)]. Several of the spin-orbit matrix elements are known and the remainder will be, within a factor of 2,  $40\text{ cm}^{-1}$ .

The MgO  $A^1\Pi \sim X^1\Sigma^+$  perturbations are also characterized by a surprisingly large matrix element. For the same reason that the  $^3\Pi$  (I)  $\sim$   $^1\Sigma$  (I) matrix element should be smaller than  $^3\Pi$  (I)  $\sim$   $^1\Sigma$  (II), the  $^1\Pi$  (I)  $\sim$   $^1\Sigma^+$  (I) interaction should be weaker than the  $^1\Pi$  (I)  $\sim$   $^1\Sigma^+$  (II). In the single configuration approximation, the  $b$  values defined by Eqs. (35) and (36) are

$$b[^1\Pi \text{ (I)}, ^1\Sigma \text{ (I)}] = \langle 2\pi | l_+ | 7\sigma \rangle, \quad (46a)$$

$$b[^1\Pi \text{ (I)}, ^1\Sigma \text{ (II)}] = \langle 2\pi | l_+ | 6\sigma \rangle. \quad (46b)$$



The value  $b^4 \sim X = 0.85$  is much larger than the corresponding value, 0.41, for BeO (27). Similar perturbations have been observed for BeS (50), but no  $b$  value is available for comparison.  $^1\Pi(I) \sim ^1\Sigma(II)$  perturbations are unknown for MgO, but it is likely that  $b^4 \sim X$  will be similar to the values 1.23, 1.30, 1.17 found for BeO, CaO, and SrO, respectively (27). Because of the large  $b^4 \sim X$  value and unusually low energy of MgO  $A^1\Pi$ , the lambda doubling for the  $^1\Pi(I)$  state is dominated by  $^1\Sigma^+(I)$  rather than  $^1\Sigma^+(II)$  as occurs for BeO, CaO, SrO, and BaO.

Little is known about transition moments for the alkaline earth monoxides. Radiative lifetimes have been measured for BeO  $^1\Sigma^+(II)$ ,  $\tau = 9 \times 10^{-8}$  sec (54), BaO  $^1\Sigma^+(II)$ ,  $\tau = 3 \times 10^{-7}$  sec (55), and BaO  $^1\Pi(I)$ ,  $\tau = 1 \times 10^{-5}$  sec (56). Transition moment ratios have been measured for MgO and were shown in Section III.B to agree well with ab initio values (26). It is interesting that the observed BaO  $^1\Sigma^+(II) \rightarrow ^1\Sigma^+(I)$  to  $^1\Pi(I) \rightarrow ^1\Sigma^+(I)$  transition moment ratio, 2.5, is nearly identical to the corresponding ratio of calculated MgO moments, 3.1 (26). The radiative lifetimes of the MgO  $B^1\Sigma$  and  $A^1\Pi$  states, estimated using the calculated transition moments, are  $3.6 \times 10^{-8}$  and  $4 \times 10^{-4}$  sec (57). A final indication that the single-configuration, dominant atomic character approximation is invalid for MgO is the strength of the  $B^1\Sigma \rightarrow A^1\Pi$  transition. In the separated atom limit this would be a forbidden  $2p_0\pi \rightarrow 2p_0\sigma$  transition, yet the calculated  $B \rightarrow A$  moment is a factor of three larger than the allowed charge transfer  $3s_{Mg}\sigma \rightarrow 2p_{O}\pi A \rightarrow X$  transition.

The Ar<sup>+</sup> laser induced photoluminescence spectra described here are an excellent illustration of the dynamic range of laser spectroscopy. Spectra of rare isotopes are observed in natural abundance. Intercombination lines due to perturbations are recorded and unambiguously assigned in spite of the fact that these extra lines are often found far from the  $J$  levels where the mixing coefficients are largest. It is not necessary to sample the perturbation culmination in order to assign the extra lines and characterize the perturbing state. The energy level diagram for the mutually perturbing  $X^1\Sigma^+$ ,  $A^1\Pi$ , and  $a^3\Pi$  states is sampled at only a few  $J$  values, yet a complete characterization of these states and their interactions is achieved. Molecular constants are obtained at about a factor of 10 inferior precision to that typical of a full rotational analysis, but this lower precision is due to a  $\pm 0.02$ -nm measurement uncertainty rather than the limited number of lines recorded.

In this work the MgO  $a^3\Pi$  state was observable because of its perturbations by the  $X^1\Sigma^+$  state. Only parity levels of  $\Omega = 0$  and 1 could be sampled. However, the  $a^3\Pi$  state is now sufficiently well characterized that it may prove possible to complete a rotational analysis of an electronic transition involving this state. There appear to be three attractive possibilities:  $a^3\Pi \rightarrow a^3\Pi$  at 372.1 nm (21);  $b^3\Sigma^+ \rightarrow a^3\Pi$  near 901 nm (24); and the intercombination subband  $B^1\Sigma^+ \rightarrow a^3\Pi_1(0,0)$  at 573.1 nm. The  $B \rightarrow a_1$  transition borrows oscillator strength from the  $B \rightarrow A(0,0)$  band by spin-orbit mixing,

$$f_{B \rightarrow a_1} / f_{B \rightarrow A} = [A_{II} / (E_{II}^0 - E_{II}^0)]^2 = 5 \times 10^{-3}.$$

In a laser excitation spectrum recorded at a temperature of 500 K, the  $B \rightarrow a_1(0,0)$  band at 573.1 nm should be 5% as strong as the  $B \rightarrow A(1,0)$  band at 577.5 nm.

#### ACKNOWLEDGMENTS

We thank Mr. J. Wyss for photographing part of the MgO Spectrum, Dr. Peter Domaille for verifying many of the fluorescence assignments, Dr. Michael Revelli for experimental assistance, and Mr. R. Wormsbecher and Mr. M. Trkula for locating several extra lines at  $A^1\Pi \sim X^1\Sigma$  perturbations. Dr. B.

Wicke generously provided RKR and Franck-Condon computer programs. We also express our appreciation to Professor H. P. Broida for his continued interest in this work. Dr. H. Lefebvre-Brion and Mr. Richard Gottscho made several valuable suggestions.

RECEIVED: June 17, 1977

## REFERENCES

1. P. N. GHOSH, P. C. MAHANTI, AND B. C. MUKHERJEE, *Phys. Rev.* **35**, 1491 (1930).
2. P. C. MAHANTI, *Phys. Rev.* **42**, 609 (1932).
3. A. LAGERQVIST, *Ark. Mat. Astron. Fys. A* **29**, 1 (1943).
4. A. LAGERQVIST AND U. UHLER, *Ark. Fys.* **1**, 459 (1949).
5. R. F. BARROW AND D. V. CRAWFORD, *Proc. Phys. Soc. London* **57**, 12 (1945).
6. D. PEŠIĆ, *Proc. Phys. Soc. London* **76**, 844 (1960).
7. D. PEŠIĆ, *Proc. Phys. Soc. London* **83**, 885 (1964).
8. A. LAGERQVIST AND U. UHLER, *Nature (London)* **164**, 665 (1949).
9. P. C. MAHANTI, *Indian J. Phys.* **9**, 455 (1935).
10. L. BREWER AND S. TRAJMAR, *J. Chem. Phys.* **36**, 1585 (1962).
11. L. BREWER, S. TRAJMAR, AND R. A. BERG, *Astrophys. J.* **135**, 955 (1962).
12. S. TRAJMAR AND G. E. EWING, *J. Chem. Phys.* **40**, 1170 (1964).
13. D. PEŠIĆ AND A. G. GAYDON, *Proc. Phys. Soc. London* **73**, 244 (1959).
14. S. TRAJMAR AND G. E. EWING, *Astrophys. J.* **142**, 77 (1965).
15. J. SCHAMPS, G. GANDARA, AND M. BÉCART, *Canad. Spectrosc.* **14**, 13 (1969).
16. (a) M. SINGH, *J. Phys. B.* **4**, 565 (1971). (b) A. ANTIĆ-JOVANOVIĆ, D. S. PEŠIĆ, AND V. BOJOVIĆ, *J. Mol. Spectrosc.* **60**, 416 (1976).
17. M. SINGH, *J. Phys. B.* **6**, 1339 (1973).
18. M. SINGH, *J. Phys. B.* **6**, 1917 (1973).
19. N. B. WONG, T. IKEDA, AND D. O. HARRIS, Symposium on Molecular Structure and Spectra, The Ohio State University, Paper TE8 (1975).
20. P. J. EVANS AND J. C. MACKIE, *Chem. Phys.* **5**, 277 (1974); *J. Mol. Spectrosc.* **65**, 169 (1977).
21. J. SCHAMPS AND G. GANDARA, *J. Mol. Spectrosc.* **62**, 80 (1976).
22. (a) D. J. BENARD, W. D. SLAFER, AND J. HECHT, *J. Chem. Phys.* **66**, 1012 (1977). (b) D. J. BENARD AND W. D. SLAFER, *J. Chem. Phys.* **66**, 1017 (1977).
23. W. G. RICHARDS, G. VERHAEGEN, AND C. M. MOSER, *J. Chem. Phys.* **45**, 3226 (1966).
24. J. SCHAMPS AND H. LEFEBVRE-BRION, *J. Chem. Phys.* **56**, 573 (1972).
25. B. HURON AND P. RANCUREL, *Chem. Phys. Lett.* **13**, 515 (1972).
26. B. HURON, J. P. MALRIEU, AND P. RANCUREL, *Chem. Phys.* **3**, 277 (1974).
27. R. W. FIELD, *J. Chem. Phys.* **60**, 2400 (1974).
28. W. M. HUO, K. F. FREED, AND W. KLEMPERER, *J. Chem. Phys.* **46**, 1967 (1967).
29. (a) P. K. PEARSON, S. V. O'NEIL, AND H. F. SCHAEFER III, *J. Chem. Phys.* **56**, 3938 (1972). (b) H. F. SCHAEFER III, *J. Chem. Phys.* **55**, 176 (1971). (c) S. V. O'NEIL, P. K. PEARSON, AND H. F. SCHAEFER III, *Chem. Phys. Lett.* **10**, 404 (1971).
30. J. DROWART, G. ENSTEEN, AND G. VERHAEGEN, *Trans. Faraday Soc.* **60**, 1920 (1964).
31. E. A. BALLIK AND D. A. RAMSAY, *J. Chem. Phys.* **31**, 1128 (1959).
32. E. A. BALLIK AND D. A. RAMSAY, *Astrophys. J.* **137**, 84 (1963).
33. E. A. BALLIK AND D. A. RAMSAY, *Astrophys. J.* **137**, 61 (1963).
34. M. HULTIN AND A. LAGERQVIST, *Ark. Fys.* **2**, 471 (1951).
35. H. JOHANSEN, Ph.D. thesis, University of California, Berkeley, 1970.
36. G. ALMKVIST AND A. LAGERQVIST, *Ark. Fys.* **1**, 477 (1949).
37. G. ALMKVIST AND A. LAGERQVIST, *Ark. Fys.* **2**, 233 (1950).
38. A. LAGERQVIST AND L. -E. SELIN, *Ark. Fys.* **11**, 323 (1959).
39. A. LAGERQVIST, E. LIND, AND R. F. BARROW, *Proc. Phys. Soc. London Sect. A* **63**, 1132 (1950).
40. I. KOVÁCS AND A. LAGERQVIST, *Ark. Fys.* **2**, 411 (1951).
41. R. W. FIELD, A. D. ENGLISH, T. TANAKA, D. O. HARRIS, AND D. A. JENNINGS, *J. Chem. Phys.* **59**, 2191 (1973).

42. G. HERZBERG, "Spectra of Diatomic Molecules," Chap. 3, Van Nostrand, New York, 1950.
43. J. M. BROWN, J. T. HOUGEN, K.-P. HUBER, J. W. C. JOHNS, I. KOPP, H. LEFEBVRE-BRION, A. J. MERER, D. A. RAMSAY, J. ROSTAS, AND R. N. ZARE, *J. Mol. Spectrosc.* **55**, 500 (1975).
44. I. KOVÁCS, "Rotational Structure in the Spectra of Diatomic Molecules," American Elsevier, New York, 1969.
45. L. BREWER, in "Proceedings of the Robert A. Welch Foundation Conferences on Chemical Research, VI, Topics in Modern Inorganic Chemistry," pp. 47-92. 1962.
46. R. F. BARROW AND J. R. BEALE, *Proc. Phys. Soc. London* **91**, 483 (1967); T. E. H. WALKER AND R. F. BARROW, *J. Phys. B* **2**, 102 (1969).
47. T. E. H. WALKER AND W. G. RICHARDS, *J. Phys. B* **3**, 271 (1970).
48. A. LAGERQVIST AND R. WESTÖÖ, *Ark. Mat. Astron. Fys. A* **31**, No. 21 (1945); **32**, No. 10 (1945); A. LAGERQVIST, *Ark. Mat. Astron. Fys. A* **33**, No. 8 (1946); *Ark. Mat. Astron. Fys. B* **34**, No. 23 (1947).
49. C. J. CHEETHAM, W. J. M. GISSANE, AND R. F. BARROW, *Trans. Faraday Soc.* **61**, 1308 (1965).
50. L. YOUNG, J. SCHAMPS, J. M. ROBEE, AND R. W. FIELD, unpublished results.
51. R. N. ZARE, A. L. SCHMELTEKOPF, W. J. HARROP, AND D. L. ALBRITTON, *J. Mol. Spectrosc.* **46**, 37 (1973).
52. M. H. HEBB, *Phys. Rev.* **49**, 610 (1936).
53. J. SCHAMPS, private communication.
54. G. A. CAPELLE, S. E. JOHNSON, AND H. P. BROIDA, *J. Chem. Phys.* **56**, 6264 (1972).
55. S. E. JOHNSON, *J. Chem. Phys.* **56**, 149 (1972).
56. J. G. PRUETT AND R. N. ZARE, *J. Chem. Phys.* **62**, 2050 (1975).
57. P. DOMAILLE (private communication) reports a lifetime of MgO B $\Sigma^+$  of  $24 \pm 5$  nsec.



## High-Resolution Laser Excitation Spectroscopy

Analysis of the  $B^2\Sigma^+-X^2\Sigma^+$  System of  $\text{CaCl}^1$ PETER J. DOMAILLE, TIMOTHY C. STEIMLE, NING BEW WONG,  
AND DAVID O. HARRISQuantum Institute and Chemistry Department, University of California,  
Santa Barbara, California, 93106

Single-mode cw dye laser excitation spectra of the (0, 0), (1, 1), and (2, 2) bands of the  $B^2\Sigma^+-X^2\Sigma^+$  system of  $\text{CaCl}$  have been observed and assigned. Some 300 independent photoluminescence spectra have been used in making the rotational assignment and demonstrate the power of the technique of line-by-line analysis in unraveling complex spectra. Spectroscopic constants ( $\text{cm}^{-1}$ ) obtained from a weighted least squares fit of the data are given below. Numbers in parentheses refer to 95% confidence limits in the last digit.

	$X^2\Sigma^+$	$B^2\Sigma^+$
$T_e$	0	16856.69(2)
$\omega_e$	369.8(10)	366.8(10)
$\omega_e x_e$	1.13(20)	1.28(20)
$B_e$	0.15200(54)	0.15448(54)
$\alpha_e$	0.00063(34)	0.00073(35)
$D_e$	$1.027(16) \times 10^{-7}$	$1.097(17) \times 10^{-7}$
$\gamma_e$ (spin-rotation)	+0.003	-0.0630(16)

The ground-state rotational constant is in excellent agreement with the previous value obtained from the analysis of the  $C^2\Pi-X^2\Sigma^+$ . The  $B$ -state spin-rotation interaction constant is consistent with the pure precession estimate of the interaction between the  $A^2\Pi$ , and  $B^2\Sigma^+$  states, which, in the one electron approximation, both have the unpaired electron in a calcium  $4p$  orbital.

## I. INTRODUCTION

Rotational analyses of the  $A-X$  and  $B-X$  band systems of the alkaline earth halides have previously proved to be a formidable task using conventional spectroscopy because of the complex overlapped nature of the spectra. This complexity arises because the one electron promotion is primarily from a metal  $ns\sigma(X^2\Sigma^+)$  orbital to a metal  $np\pi(A^2\Pi)$  or  $np\sigma(B^2\Sigma^+)$  orbital. The localization of the electron promotion to the metal atom leads to very similar spectroscopic constants in all three states with only slight differences in the potential energy curves. The spectra thus consist of strong  $\Delta v = 0$  sequences with heavily overlapped rotational structure. The spectrum of  $\text{CaCl}$  is particularly

<sup>1</sup> This research was supported by the AFOSR and the National Science Foundation, Grants AFOSR-73-2365 and NSF-MPS-72-04978, respectively.

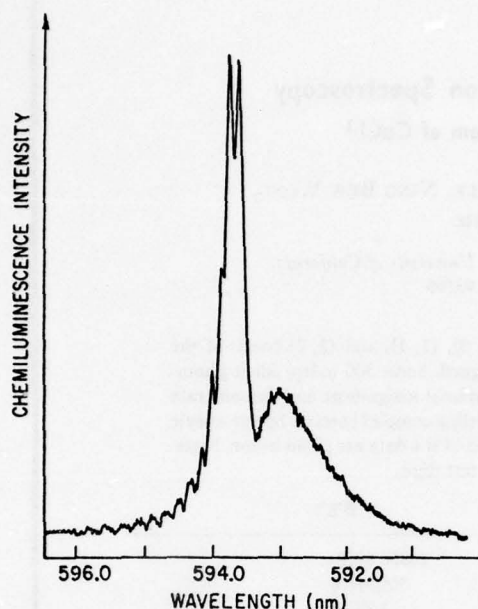


FIG. 1. Low-resolution trace of the  $\Delta v = 0$  sequence of the  $B^2\Sigma^+-X^2\Sigma^+$  system of  $\text{CaCl}$  produced in the chemiluminescent  $\text{Ca} + \text{Cl}_2$  reaction. The peaks are the  $P$ -branch heads of the  $(0,0)$ ,  $(1,1)$ ,  $(2,2)$ , etc., bands extending successively to longer wavelength. The broad hump to shorter wavelength is heavily overlapped  $R$ -branch structure.

congested, as indicated in Fig. 1, where a low-resolution spectrum of the chemiluminescence from the  $\text{Ca} + \text{Cl}_2$  reaction is shown. The sharp peaks are successive  $P$ -branch heads of the  $\Delta v = 0$  sequence of the  $B^2\Sigma^+-X^2\Sigma^+$  system and the broad band extending to the blue is overlapped  $R$ -branch structure. In addition to the almost vertical displacement of the potential curves, further complications arise in the  $\text{CaCl } B-X$  system because the unpaired electron produces spin doubling of the levels in both states. The natural abundance of the two chlorine isotopes,  $^{35}\text{Cl}$  and  $^{37}\text{Cl}$ , also contributes to further spectral overlap.

The technique of single-mode cw dye laser excitation spectroscopy has been demonstrated previously (1-3) in the analysis of complex spectra. The advantages of being able to record Doppler width limited high-resolution excitation spectra, and the independent assignment of each line from the resolved photoluminescence have been discussed by Field *et al.* (1). A line-by-line rotational assignment is obtained by tuning the laser to a particular line in the excitation spectrum and recording the resolved photoluminescence. Measurement of the  $P$ - $R$  separation and a knowledge of  $B''$  then allow an  $N'$  assignment. Noting whether the laser is tuned to coincide with the higher (lower) frequency member of the doublet allows an unambiguous assignment of the line as  $R(N'')$  [ $P(N'')$ ] in the excitation spectrum. The laser is then tuned to the next rotational coincidence and the process repeated.

No rotational analysis of the  $B^2\Sigma^+-X^2\Sigma^+$  system of  $\text{CaCl}$  has previously been reported; however, Menzinger (4) quotes a value of  $B_0(B) = 0.1538 \text{ cm}^{-1}$  based on the measure-

ment of head separations in the  $A^2\Pi_r-X^2\Sigma^+$  system and assuming  $B_0(A) = B_0(B)$ . However, there is no a priori reason for this assumption.

Morgan and Barrow (5) have reported a rotational analysis of the  $C^2\Pi_r-X^2\Sigma^+$  system and have obtained a value of  $B_0(X) = 0.1516 \text{ cm}^{-1}$ . This analysis proved a valuable asset to our rotational assignment of the excitation spectrum.

## II. EXPERIMENTAL DETAILS

### A. Production of CaCl

CaCl was produced in a conventional (6) flowing metal vapor flame of  $\text{Ca} + \text{Cl}_2$  using argon as a carrier gas. The exothermic reaction produces a red chemiluminescent glow characteristic of the  $A-X$  system at 620 nm.  $B-X$  chemiluminescence at 595 nm is also observed, but is of lower intensity. Because the intensity of the chemiluminescence is about 100 times less intense than the laser induced photoluminescence it does not interfere with the recording and measurement of the  $P-R$  doublets. In addition, the laser was chopped at 6 kHz and only the ac photoluminescence was detected.

### B. Optical Arrangement

A Spectra Physics Model 580 single-mode cw dye laser operating with rhodamine-6G was used for all experiments. The dye laser was pumped with about 1 W of the 514.5 nm line from a Spectra Physics Model 164 argon-ion laser. Typical output power from the dye laser was 20 mW. Rather than scanning the laser continuously by simultaneously tuning the cavity and intracavity etalon electronically, the laser was swept by mechanically driving the dc offset to the etalon with a 1 rpm clock motor. The laser output consisted then of a single line with width  $\sim 20 \text{ MHz}$  stepped along in 500 MHz increments. Since the Doppler width of lines in the excitation spectrum is 1000–1500 MHz, the 500 MHz steps produce a faithful representation of the spectrum. The laser could be scanned about 200 GHz before jumping to an adjacent etalon mode.

About 4% of the dye laser output was split off and directed to a 3 GHz FSR spectrum analyzer which was swept by a synchronous voltage ramp and displayed on an oscilloscope. Initially, the spectrum analyzer was used for frequency measurements, however, oscilloscope drift and an imprecise knowledge of the free spectral range meant that frequency differences were only known to about 1% accuracy. The spectrum analyzer was necessary though, to ensure the single-mode nature of the laser output. Precise frequency measurements were obtained by simultaneously recording a separate excitation spectrum of  $\text{I}_2$  vapor along with that of CaCl on a dual trace recorder. This comparative display and the accurate measurements of the  $\text{I}_2$  spectrum by Simmons and Hougén (24) were used for final line position measurements. Unblended lines in the excitation spectrum could be measured to  $\pm 500 \text{ MHz}$  ( $\pm 0.02 \text{ cm}^{-1}$ ).

The main laser beam was directed through a 6 kHz mechanical chopper and then vertically into the reaction cell through a Brewster window. Resolved photoluminescence was monitored through a 1 m McPherson monochromator with a typical bandpass of 0.02–0.05 nm. Broadbanded photoluminescence was monitored through a 20 nm bandpass interference filter centered at 600 nm. Both broadbanded and resolved photoluminescence were detected with an RCA 1P28 photomultiplier and the ac signal directed to a PAR Model HR-8 lock-in amplifier and strip chart recorder combination.





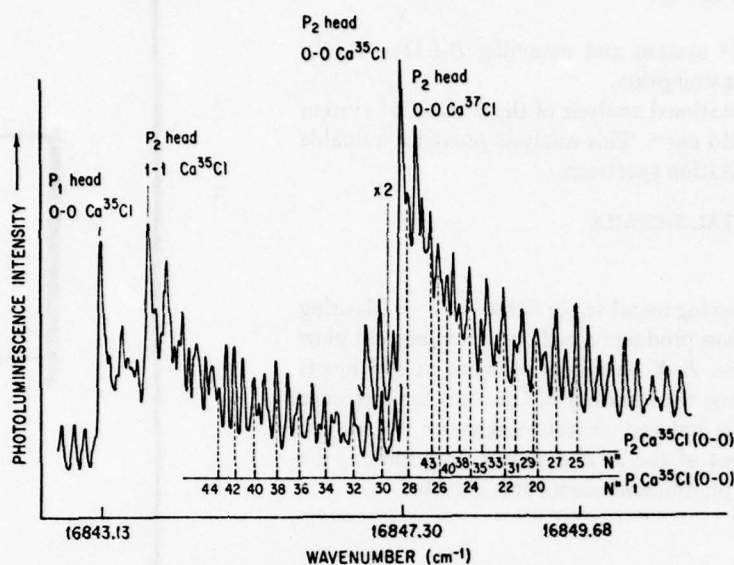


FIG. 2. A simple portion of the single-mode cw dye laser excitation spectrum of  $\text{CaCl}$ . Most spectra appear more complex. The  $P$ -branch heads due to both  $\text{Ca}^{35}\text{Cl}$  and  $\text{Ca}^{37}\text{Cl}$  are visible and the near coincidence of the  $P_2$  head of (1, 1) and the  $P_1$  head of (0, 0) is apparent. The  $\times 2$  scale change is only approximate.

A typical trace of the excitation spectrum obtained by sweeping the laser while monitoring the total photoluminescence intensity through the filter is shown in Fig. 2. Typical S/N is about 100. After completion of such a scan, the laser was reset to a particular feature in the excitation spectrum and the resolved photoluminescence was recorded with the monochromator. Typical S/N of the resolved  $P$ - $R$  doublets was also 100 and the line separations could be measured to  $\pm 0.2 \text{ cm}^{-1}$ . The laser was then tuned to the next line in the excitation spectrum and the process repeated.

### III. DESCRIPTION OF THE SPECTRUM

Beginning at high frequency and stepping the laser to lower frequency results in excitation of steadily decreasing  $R(N'')$  lines, as evidenced by the corresponding  $P(N'' + 2)$  appearing at lower frequency than the laser line in the photoluminescence. It is important to realize that because the spectrum is badly overlapped it is not unusual to simultaneously excite several different rotational transitions of different  $(v', v'')$  bands. Indeed, up to 10 different rotational coincidences of comparable intensity have been excited simultaneously in portions of the spectrum. Successive lines in a particular branch were often separated by several other  $(v'J', v''J'')$  coincidences, thus making pattern recognition impossible; photoluminescence from every line had to be recorded. The onset of the first low- $N$   $P$ -branch coincidences is due to excitation in the (0, 0) band. Additional evidence for excitation into the (0, 0) band is a corresponding  $P$ - $R$  doublet in the  $\Delta v = -1$  sequence and the necessary absence in the  $\Delta v = +1$  sequence. As the laser is stepped to even lower frequency than the (0, 0) band origin, the next

low- $N$   $P$ -branch coincidences observed are due to the (1, 1) and (2, 2) bands, respectively.

At low- $N$  values the isotope splitting and the spin rotation splitting are less than the Doppler width and are not resolved for the (0, 0) band. The simultaneous excitation of the same (0, 0)  $\text{Ca}^{37}\text{Cl}$  transition as that of  $\text{Ca}^{35}\text{Cl}$  is apparent, however, when the (0, 1) band is observed in the photoluminescence. Two identical  $P$ - $R$  doublets arise, displaced from each other by

$$5.16 \pm 0.10 \text{ cm}^{-1} = \omega_e''(1 - \rho) - 2\omega_e x_e''(1 - \rho^2), \quad (1)$$

where the symbols have their usual meanings (7).

At higher  $N$  values the isotope splitting and the spin-rotation splitting are resolved in the excitation spectrum. The  $P_1$  ( $J = N + \frac{1}{2}$ ) and  $P_2$  ( $J = N - \frac{1}{2}$ ) branches can be followed out to their respective heads, as shown in Fig. 2. Because of laser power fluctuations, our intensity measurements are unreliable; consequently it was not possible to differentiate between  $P_1$ ,  $R_1$ ,  $P_2$ , and  $R_2$  lines. Thus, our experiments cannot unambiguously determine the sign of the upper-state spin-rotation constant,  $\gamma'$ . Also the  $^4Q_{12}$  and  $^4Q_{21}$  branches were not observed because of the unfavorable Hönl-London (8) and partition function factors. The upper-state spin-rotation constant  $\gamma'$  was assumed to be negative on the basis of Van Vleck's pure precession estimate, (9) an assumption well borne out previously from the sign of the  $\Lambda$ -doubling constant,  $p$ , in the  $A^2\Pi$ , state of  $\text{CaF}$  (1). The final values of  $\gamma'$  and  $\gamma''$  obtained from the analysis of the  $B$ - $X$  system of  $\text{CaCl}$  also fully support this assumption. Thus, the  $P_2$  head of the (0, 0) band forms closest to the band origin, while the  $P_1$  head is almost coincident with the  $P_2$  head of the (1, 1) band. This near overlap has interesting consequences in terms of a previous determination (4) of vibrational temperatures from chemiluminescence spectra. Discussion of this point is deferred until Section V.

Continuous series of lines due to  $\text{Ca}^{37}\text{Cl}$  were not evident because of their lower intensity and were thus not used in the determination of the constants. However, the heads due to  $\text{Ca}^{37}\text{Cl}$  are particularly apparent in the excitation spectrum. The (0, 0)  $P_2$  head of  $\text{Ca}^{37}\text{Cl}$  is  $0.183 \pm 0.017 \text{ cm}^{-1}$  to the blue of the corresponding head of  $\text{Ca}^{35}\text{Cl}$ , as shown in Fig. 2.

The informative photoluminescence spectrum shown in Fig. 3a is obtained by pumping slightly to the blue of the  $P_2$  head of the  $\text{Ca}^{35}\text{Cl}$  (0, 0) band. The laser simultaneously pumps  $P_2$  (52) through  $P_2$  (61) near the vertex of the Fortrat parabola and the corresponding  $R_2$  (50) through  $R_2$  (59) are observed in the photoluminescence. The lowest intensity line,  $R_2$  (54), is due to pumping  $P_2$  (56) about 1 GHz ( $0.03 \text{ cm}^{-1}$ ) off its center frequency, but still within its Doppler profile. The fact that the intensity of  $R_2$  (53) and  $R_2$  (55) is greater than that of  $R_2$  (54) shows that the head of the  $P_2$  branch forms at  $N'' \approx 56$ . Figure 3b shows the photoluminescence with the laser tuned 1 GHz further to the red. The  $R_2$  (54) is now most intense because  $P_2$  (56) now has the most favorable Doppler overlap with the laser. This value of  $N_{\text{max}}''$  at the  $P_2$  head, in conjunction with Morgan and Barrow's (5) value of  $B_0''$  and estimated  $\gamma_0'$  and  $\gamma_0''$ , can be used to obtain an initial value of  $B_0' = 0.154 \text{ cm}^{-1}$  from the expression

$$N_{\text{max}}'' = \frac{B_0' + B_0'' + \frac{1}{2}(\gamma_0' - \gamma_0'')}{2(B_0' - B_0'')} \quad (2)$$

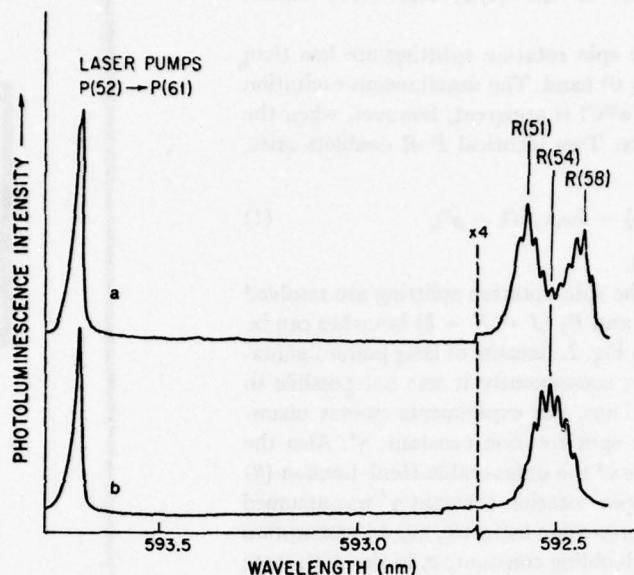


FIG. 3. (a) Photoluminescence spectrum of  $\text{CaCl}$  excited by a single-mode cw dye laser tuned 1 GHz ( $0.03 \text{ cm}^{-1}$ ) to the blue of the  $P_2$  head of the  $(0,0)$  band. (b) Laser tuned to the  $P_2$  head of the  $(0,0)$  band.

This initial estimate proved particularly useful in understanding general features of the spectrum such as the position of the  $\text{Ca}^{37}\text{Cl}$  heads and the spin-rotation splitting of the heads. In addition, Eq. (2) provides an uncertainty estimate of  $B'$ , which was used in the diagnostic least squares (12) data treatment described later.

Similar features to those described above for the  $(0,0)$  band were also observed for the  $(1,1)$  and  $(2,2)$  bands. Approximately 300 independent photoluminescence spectra were recorded over about a  $20 \text{ cm}^{-1}$  region extending from the  $P_1$  head of the  $(1,1)$  band to higher frequencies in the  $R$  branch. Observation of rotational structure in this region has resulted in a complete analysis of the  $(0,0)$ ,  $(1,1)$ , and  $(2,2)$  bands of  $\text{Ca}^{35}\text{Cl}$ . Excitation spectra were not recorded in any  $\Delta v > 0$  sequences because of the smaller Franck-Condon factors. Furthermore, data from these other sequences do not yield any additional spectroscopic parameters.

#### IV. ANALYSIS

The  $P$ - $R$  separations measured from the resolved photoluminescence were fitted to the expression (13)

$$\begin{aligned} \Delta_2 F(N'') &= F(N'' + 1) - F(N'' - 1) \\ &= (4B_r'' - 6D_r'')(N'' + \tfrac{1}{2}) - 8D_r''(N'' + \tfrac{1}{2})^3, \end{aligned} \quad (3)$$

using a standard weighted least squares procedure. The values of  $B_r''$  and the accuracy of the fit were used primarily to confirm the assignment, as the errors in measured  $P$ - $R$  separations are at least an order of magnitude larger than the measured frequency differences in the excitation spectrum.



The assigned transition frequencies in the excitation spectrum were fitted to the normal expressions for the  $P_1$ ,  $P_2$ ,  $R_1$ , and  $R_2$  branches (8) using a weighted least squares procedure. The  ${}^PQ_{12}$  and  ${}^RQ_{21}$  satellite branches were not observed; the expected intensity of the strongest  $Q$  branch is more than three times weaker than the intensity of the weakest observed  $P$  or  $R$  branches. Terms due to centrifugal distortion were included as fixed parameters and the equations used to fit only  $\nu_0$ ,  $B_v'$ ,  $B_v''$ ,  $\gamma_v'$ , and  $\gamma_v''$ . Assigned weights were the reciprocal of the uncertainty squared. Uncertainties in the measured frequencies of lines in the excitation spectrum were estimated as follows: (i) Unblended lines were deemed to be accurately positioned within  $\pm 0.02 \text{ cm}^{-1}$  (the dye laser cavity mode spacing) because tuning the laser to an adjacent mode produced a substantial decrease in photoluminescence. The worst case is that of two adjacent modes producing the same intensity of photoluminescence. (ii) When a line consisted of overlapped transitions the relative intensity of each was determined from the photoluminescence spectrum. The relative intensity *expected*, based on considerations of line strengths and Boltzmann factors, was then computed. A low measured relative intensity was then an indication that although the laser was tuned to within  $0.02 \text{ cm}^{-1}$  of the maximum in the excitation spectrum it was off the line center of the particular line of interest. The relative intensity and the Doppler width provide an estimate of how far off the center frequency the laser is tuned and  $0.02 \text{ cm}^{-1}$  is added to this value to account for picking the overlapped line maximum in the excitation spectrum. This method has one obvious shortcoming; that is, *all* the overlapped transitions need to be assigned to calculate the expected relative intensity. In those cases where the problem of unassigned lines was encountered, the worst situation was chosen; that is, the unassigned lines were given zero expected intensity, thus overestimating the expected relative intensity and maximizing the uncertainty. Note that accurate relative weights are important in a problem of this kind because the Jacobians of the parameters  $B_v'$ ,  $B_v''$ ,  $\gamma_v'$ , and  $\gamma_v''$  are  $N$  dependent. Low- $N$  values are less correlated than higher- $N$  values, thus the values of the parameters are sensitive functions of the uncertainty estimates of low- $N$  value transitions.

The form of the equations for the various branches of interest produces problems in the least squares method of data treatment. The normal  $B$  matrix of least squares (15) is near singular because the Jacobians of similar parameters ( $B_v'$  and  $B_v''$ ,  $\gamma_v'$  and  $\gamma_v''$ ) are almost identical in magnitude. The inversion of  $B$  to obtain the solution for the parameters and the covariance matrix is thus unreliable and the method of diagnostic least squares described by Curl (12) is more appropriate. In fact, the diagnostic option for constraining poorly determined parameters proved unnecessary, but the pre-diagonalization of the  $B$  matrix prior to inversion was necessary to alleviate the numerical problems of the near singularity. The similarity of the Jacobians means that the variables are highly correlated. Examination of the transformation matrix of the diagnostic least squares procedure (12) serves as a reminder that ( $B_v' - B_v''$ ) is a sensitive function of the input data but that the independent values of the  $B_v'$  and  $B_v''$  are not as well determined. The same problem occurs in the case of  $\gamma_v'$  and  $\gamma_v''$ . It is encouraging, however, that the values of the  $B_v''$  determined from  $\Delta_2 F''(N)/(N + \frac{1}{2})$ , where the correlation problem does not exist, agree well within the uncertainty limits with those obtained from the direct fit. The improved statistics obtained by fitting to many data points in the excitation spectrum have minimized the effects of the correlation problem.



60

The  $B_v''$  values obtained from the photoluminescence data are slightly higher than those obtained from the excitation spectra and the uncertainty limits do not overlap. We attribute this slight discrepancy to an underestimation of measurement errors in the photoluminescence data.

Table I lists the measured transition frequencies used in the diagnostic least squares fit along with the deviation from the calculated values. The rms deviation of the fits to the (0, 0), (1, 1), and (2, 2) bands are 0.017, 0.016, and 0.013  $\text{cm}^{-1}$ , respectively.

The rotational constants and spin-rotation interaction constants obtained from the fit are given in Table II. Uncertainties are 95% confidence limits in the last digit. The

TABLE I - Measured transition frequencies ( $\text{cm}^{-1}$ ) and deviation<sup>a</sup> from fitted value in the excitation spectrum of  $\text{Ca}^{85}\text{Cl}$ .

Line	Frequency	$\Delta v$	Line	Frequency	$\Delta v$	Line	Frequency	$\Delta v$	Line	Frequency	$\Delta v$
<b>(0, 0) Band</b>											
$P_2(1)$	1564.54	-0.11	$P_2(1)$	1564.53	0.00	$P_2(14)$	1564.50	0.00	$P_2(40)$	1564.481	0.00
"	54.17	-0.13	"	48.90	-0.01	"	50.15	0.00	"	48.10	-0.05
"	53.35	0.00	"	48.79	-0.02	"	50.16	0.00	"	48.01	-0.01
"	53.11	0.00	"	48.70	-0.02	"	49.98	0.01	"	47.98	0.00
"	53.11	-0.11	"	48.58	-0.01	"	49.85	-0.05	"	47.89	0.00
"	53.11	-0.13	"	48.47	0.00	"	49.72	0.01	"		
"	53.09	0.00	"	48.38	-0.01	"	49.59	0.02	$P_2(41)$	1564.484	-0.05
"			"	48.28	-0.01	"	49.46	0.01	"	47.81	-0.05
"	53.02	-0.12	"	48.11	-0.01	"	49.33	0.00	"	47.70	0.02
"	52.97	0.00	"	47.97	-0.02	"	49.21	-0.01	"	47.59	0.02
"	52.91	0.00	"	47.83	0.00	"	49.07	0.00	$P_2(42)$	1564.470	0.00
"	52.81	-0.11	"	47.69	0.00	"	48.94	0.00	"	47.48	-0.02
"	52.71	-0.10	"	47.55	-0.01	"	48.80	0.01	"	47.37	-0.00
"	52.61	-0.10	"	47.40	-0.02	"	48.67	-0.02	"	47.26	0.00
"	52.51	-0.10	"	47.26	-0.01	"	48.53	0.00	"	47.15	-0.04
"	52.41	0.00	"	47.11	-0.01	"	48.40	-0.01	"	47.04	0.00
"	52.31	-0.11	"	46.97	-0.01	"	48.26	0.00	"	46.93	0.00
"	52.21	-0.11	"	46.83	0.00	"	48.13	0.00	"	46.82	0.00
"	52.11	-0.11	"	46.69	-0.01	"	47.99	0.00	"	46.71	0.00
"	52.01	-0.11	"	46.55	-0.01	"	47.86	0.00	"	46.60	0.00
"	51.91	-0.11	"	46.41	-0.01	"	47.72	0.00	"	46.49	0.00
"	51.81	-0.11	"	46.27	-0.01	"	47.59	0.00	"	46.38	0.00
"	51.71	-0.11	"	46.13	-0.01	"	47.45	0.00	"	46.27	0.00
"	51.61	-0.11	"	45.99	-0.01	"	47.32	0.00	"	46.16	0.00
"	51.51	-0.11	"	45.85	-0.01	"	47.18	0.00	"	46.05	0.00
"	51.41	-0.11	"	45.71	-0.01	"	47.05	0.00	"	45.94	0.00
"	51.31	-0.11	"	45.57	-0.01	"	46.91	0.00	"	45.83	0.00
"	51.21	-0.11	"	45.43	-0.01	"	46.78	0.00	"	45.72	0.00
"	51.11	-0.11	"	45.29	-0.01	"	46.64	0.00	"	45.61	0.00
"	51.01	-0.11	"	45.15	-0.01	"	46.51	0.00	"	45.50	0.00
"	50.91	-0.11	"	45.01	-0.01	"	46.37	0.00	"	45.39	0.00
"	50.81	-0.11	"	44.87	-0.01	"	46.24	0.00	"	45.28	0.00
"	50.71	-0.11	"	44.73	-0.01	"	46.10	0.00	"	45.17	0.00
"	50.61	-0.11	"	44.59	-0.01	"	45.97	0.00	"	45.06	0.00
"	50.51	-0.11	"	44.45	-0.01	"	45.83	0.00	"	44.95	0.00
"	50.41	-0.11	"	44.31	-0.01	"	45.70	0.00	"	44.84	0.00
"	50.31	-0.11	"	44.17	-0.01	"	45.56	0.00	"	44.73	0.00
"	50.21	-0.11	"	44.03	-0.01	"	45.43	0.00	"	44.62	0.00
"	50.11	-0.11	"	43.89	-0.01	"	45.29	0.00	"	44.51	0.00
"	50.01	-0.11	"	43.75	-0.01	"	45.16	0.00	"	44.40	0.00
"	49.91	-0.11	"	43.61	-0.01	"	45.02	0.00	"	44.29	0.00
"	49.81	-0.11	"	43.47	-0.01	"	44.89	0.00	"	44.18	0.00
"	49.71	-0.11	"	43.33	-0.01	"	44.75	0.00	"	44.07	0.00
"	49.61	-0.11	"	43.19	-0.01	"	44.62	0.00	"	43.96	0.00
"	49.51	-0.11	"	43.05	-0.01	"	44.48	0.00	"	43.85	0.00
"	49.41	-0.11	"	42.91	-0.01	"	44.35	0.00	"	43.74	0.00
"	49.31	-0.11	"	42.77	-0.01	"	44.21	0.00	"	43.63	0.00
"	49.21	-0.11	"	42.63	-0.01	"	44.08	0.00	"	43.52	0.00
"	49.11	-0.11	"	42.49	-0.01	"	43.94	0.00	"	43.41	0.00
"	49.01	-0.11	"	42.35	-0.01	"	43.81	0.00	"	43.30	0.00
"	48.91	-0.11	"	42.21	-0.01	"	43.67	0.00	"	43.19	0.00
"	48.81	-0.11	"	42.07	-0.01	"	43.54	0.00	"	43.08	0.00
"	48.71	-0.11	"	41.93	-0.01	"	43.40	0.00	"	42.97	0.00
"	48.61	-0.11	"	41.79	-0.01	"	43.27	0.00	"	42.86	0.00
"	48.51	-0.11	"	41.65	-0.01	"	43.13	0.00	"	42.75	0.00
"	48.41	-0.11	"	41.51	-0.01	"	43.00	0.00	"	42.64	0.00
"	48.31	-0.11	"	41.37	-0.01	"	42.86	0.00	"	42.53	0.00
"	48.21	-0.11	"	41.23	-0.01	"	42.73	0.00	"	42.42	0.00
"	48.11	-0.11	"	41.09	-0.01	"	42.59	0.00	"	42.31	0.00
"	48.01	-0.11	"	40.95	-0.01	"	42.46	0.00	"	42.20	0.00
"	47.91	-0.11	"	40.81	-0.01	"	42.32	0.00	"	42.09	0.00
"	47.81	-0.11	"	40.67	-0.01	"	42.19	0.00	"	41.98	0.00
"	47.71	-0.11	"	40.53	-0.01	"	42.05	0.00	"	41.87	0.00
"	47.61	-0.11	"	40.39	-0.01	"	41.92	0.00	"	41.76	0.00
"	47.51	-0.11	"	40.25	-0.01	"	41.78	0.00	"	41.65	0.00
"	47.41	-0.11	"	40.11	-0.01	"	41.65	0.00	"	41.54	0.00
"	47.31	-0.11	"	39.97	-0.01	"	41.51	0.00	"	41.43	0.00
"	47.21	-0.11	"	39.83	-0.01	"	41.38	0.00	"	41.32	0.00
"	47.11	-0.11	"	39.69	-0.01	"	41.24	0.00	"	41.21	0.00
"	47.01	-0.11	"	39.55	-0.01	"	41.11	0.00	"	41.10	0.00
"	46.91	-0.11	"	39.41	-0.01	"	40.97	0.00	"	40.99	0.00
"	46.81	-0.11	"	39.27	-0.01	"	40.84	0.00	"	40.88	0.00
"	46.71	-0.11	"	39.13	-0.01	"	40.70	0.00	"	40.77	0.00
"	46.61	-0.11	"	38.99	-0.01	"	40.57	0.00	"	40.66	0.00
"	46.51	-0.11	"	38.85	-0.01	"	40.43	0.00	"	40.55	0.00
"	46.41	-0.11	"	38.71	-0.01	"	40.30	0.00	"	40.44	0.00
"	46.31	-0.11	"	38.57	-0.01	"	40.16	0.00	"	40.33	0.00
"	46.21	-0.11	"	38.43	-0.01	"	40.03	0.00	"	40.22	0.00
"	46.11	-0.11	"	38.29	-0.01	"	39.89	0.00	"	40.11	0.00
"	46.01	-0.11	"	38.15	-0.01	"	39.76	0.00	"	40.00	0.00
"	45.91	-0.11	"	38.01	-0.01	"	39.62	0.00	"	39.89	0.00
"	45.81	-0.11	"	37.87	-0.01	"	39.49	0.00	"	39.78	0.00
"	45.71	-0.11	"	37.73	-0.01	"	39.35	0.00	"	39.67	0.00
"	45.61	-0.11	"	37.59	-0.01	"	39.22	0.00	"	39.56	0.00
"	45.51	-0.11	"	37.45	-0.01	"	39.08	0.00	"	39.45	0.00
"	45.41	-0.11	"	37.31	-0.01	"	38.95	0.00	"	39.34	0.00
"	45.31	-0.11	"	37.17	-0.01	"	38.81	0.00	"	39.23	0.00
"	45.21	-0.11	"	37.03	-0.01	"	38.68	0.00	"	39.12	0.00
"	45.11	-0.11	"	36.89	-0.01	"	38.54	0.00	"	39.01	0.00
"	45.01	-0.11	"	36.75	-0.01	"	38.41	0.00	"	38.90	0.00
"	44.91	-0.11	"	36.61	-0.01	"	38.27	0.00	"	38.79	0.00
"	44.81	-0.11	"	36.47	-0.01	"	38.14	0.00	"	38.68	0.00
"	44.71	-0.11	"	36.33	-0.01	"	38.00	0.00	"	38.57	0.00
"	44.61	-0.11	"	36.19	-0.01	"	37.87	0.00	"	38.46	0.00
"	44.51	-0.11	"	36.05	-0.01	"	37.73	0.00	"	38.35	0.00
"	44.41	-0.11	"	35.91	-0.01	"	37.60	0.00	"	38.24	0.00
"	44.31	-0.11	"	35.77	-0.01	"	37.46	0.00	"	38.13	0.00
"	44.21	-0.11	"	35.63	-0.01	"	37.33	0.00	"	38.02	0.00
"	44.11	-0.11	"	35.49	-0.01	"	37.19	0.00	"	37.91	0.00
"	44.01	-0.11	"	35.35	-0.01	"	37.06	0.00	"	37.80	0.00
"	43.91	-0.11	"	35.21	-0.01	"	36.92	0.00	"	37.69	0.00
"	43.81	-0.11	"	35.07	-0.01	"	36.79	0.00	"	37.58	0.00
"	43.71	-0.11	"	34.93	-0.01	"	36.65	0.00	"	37.47	0.00
"	43.61	-0.11	"	34.79	-0.01	"	36.52	0.00	"	37.36	0.00
"	43.51	-0.11	"	34.65	-0.01	"	36.38	0.00	"	37.25	0.00
"	43.41	-0.11	"	34.51	-0.01	"	36.25	0.00	"	37.14	0.00
"	43.31	-0.11	"	34.37	-0.01	"	36.11	0.00	"	37.03	0.00
"	43.21	-0.11	"	34.23	-0.01	"	35.98	0.00	"	36.92	0.00
"	43.11	-0.11	"	34.09	-0.01	"	35.84	0.00	"	36.81	0.00
"	43.01	-0.11	"	33.95	-0.01	"	35.71	0.00	"	36.70	0.00
"	42.91	-0.11	"	33.81	-0.01	"	35.57	0.00	"	36.59	0.00
"	42.81	-0.11	"	33.67	-0.01	"	35.44	0.00	"	36.48	0.00
"	42.71	-0.11	"	33.53	-0.01	"	35.30	0.00	"	36.37	0.00
"	42.61	-0.11	"	33.39	-0.01	"	35.17	0.00	"	36.26	0.00</

all-important correlation coefficients between the parameters are also tabulated. For comparison purposes the  $B_v''$  values obtained from the fit to the  $P$ - $R$  separations are also quoted. The  $B_0''$  value of  $0.15152 \text{ cm}^{-1}$  is in very good agreement with Morgan and Barrow's (5) value of  $0.15156 \text{ cm}^{-1}$  from analysis of the  $C^2H_2-X^2\Sigma^+$  system.  $B_v$  and  $\alpha_v$  were obtained from a fit of the  $B_0$ ,  $B_1$ , and  $B_2$  to the expression (7)

$$B_v = B_0 - \alpha_v(v + \frac{1}{2}). \quad (4)$$

$D_v$  was obtained from the relation (14)

$$D_v = 4B_v^3/\omega_v^2. \quad (5)$$

The three band origins are also obtained from the fit and are used to obtain  $T_v$ ,  $(\omega_v' - \omega_v'')$  and  $(\omega_v x_v' - \omega_v x_v'')$ . Measurement of the line positions of some low- $N$   $P$ - $R$  doublets in the (1, 0), (1, 1), and (1, 2) bands gave values of  $\omega_v''$  and  $\omega_v x_v''$  limited by monochromator accuracy. The vibrational constants and their estimated uncertainties are listed in Table III. Note that correlation is not a problem in this case, as the band origin is not strongly dependent on any of the other molecular constants. The

TABLE II - Rotational, spin-rotation interaction, vibration-rotation interaction and centrifugal distortion constants ( $\text{cm}^{-1}$ )<sup>a</sup> of  $\text{Ca}^{35}\text{Cl}$ .

	$B_v''$ <sup>a</sup>	$B_v \text{ (cm}^{-1}\text{)}$ <sup>a</sup>	$B_v''$ <sup>a</sup>	$x_v(\text{K})$ <sup>b</sup>
$B_0$	0.15152 (10)	0.15152 (10)	0.15152 (10)	0.0000
$B_1$	0.15109 (10)	0.15137 (11)	0.15133 (11)	0.0000
$B_2$	0.15069 (20)	0.15140 (21)	0.15147 (21)	0.0001
$\gamma_0$	0.0000 (0)		-0.0000 (0)	0.0000
$\gamma_1$	-0.0011 (0)		-0.0000 (0)	0.0000
$\gamma_2$	0.0000 (14)		-0.0003 (14)	0.0003
$D_0$	0.15152 (54)		0.15144 (54)	
$\gamma_0$	assumed 0.003		-0.0030 (10)	
$D_1$	$1.12 \times 10^{-7}$ (10)		$1.09 \times 10^{-7}$ (17)	
$D_2$	0.0003 (34)		0.0003 (39)	

$$B_0' - B_0'' = 0.00412(10)$$

$$B_1' - B_1'' = 0.00254(10)$$

$$B_2' - B_2'' = 0.00217(20)$$

$$\gamma_0' - \gamma_0'' = -0.0044(20)$$

$$\gamma_1' - \gamma_1'' = -0.0030(20)$$

$$B_0' - B_0'' = 0.00468(12)$$

$$D_0' - D_0'' = 0.00007(20)$$

<sup>a</sup>From fit to 13 separations in photoluminescence spectra.

<sup>b</sup>Correlation coefficient between parameters in the  $X$  and  $B$  states.

<sup>c</sup>Uncertainties are 95% confidence limits in the last digit.

THIS PAGE IS BEST QUALITY PRACTICABLE  
FROM COPY FURNISHED TO DDC



TABLE III - Vibrational constants ( $\text{cm}^{-1}$ ) of  $\text{CaCl } B^2\Sigma^+$ 

	$X^2\Sigma^+$	$B^2\Sigma^+$
$\bar{\nu}_0$	0	10957.09(2)
$x_0$	369.8(10)	366.8(10)
$x_0 x_0'$	1.15(20)	1.28(20)
	$x_0' - x_0'' = -3.033(10)$	
	$x_0 x_0' - x_0 x_0'' = 0.14(10)$	

<sup>a</sup>Uncertainties are 95% confidence limits in the last digit.

ground-state constants are in excellent agreement with previously accepted values (16-18). Those obtained from the recent vibrational analysis of Darji and Shah (19) based on bandhead measurements are inconsistent with the present findings and reflect the dangers of using high- $N$  bandhead data for an accurate vibrational analysis.

#### V. DISCUSSION

The power of single-line excited photoluminescence in the analysis of a severely overlapped spectrum has been demonstrated. It should be emphasized that overlapped lines may not only be detected and unambiguously assigned by this technique but that their frequency can also be precisely measured by tuning a monochromator to only the  $P$  or  $R$  partner of the line excited and peaking the photoluminescence of *that line only*. For example, consider an overlapped line in the excitation spectrum consisting of  $P(7)$  (0, 0) and  $R(3)$  (1, 1). The precise frequency of the  $P(7)$  line may be determined by monitoring only  $R(5)$  through a monochromator and tuning the frequency of the laser to maximize that intensity. Similarly the frequency of  $R(3)$  may be measured by setting the monochromator to maximize  $P(5)$  only. The monochromator may then be tuned to detect only the next line in a series and the process repeated. In principle, the technique could be used to assign and measure rotational structure in an unresolved Doppler overlapped spectrum. Fortunately this tedious approach was not necessary in the present case; however, it could have been employed to decrease the uncertainty limits of overlapped lines.

The equilibrium rotational constant is reasonably well determined by our fitting procedure; however, the first-order vibration-rotation interaction constant,  $\alpha_e$ , is poorly determined. This arises as a natural result of a  $\alpha_e$  being a difference between already small numbers. Another estimate of the  $\alpha_e$ 's is possible using the Pekeris relation (14)

$$\alpha_e = 6 \omega_e [(B_e^3 \omega_e x_e)^{1/2} - B_e^2] \quad (6)$$

and our experimental values of  $B_v$ ,  $\omega_v$ , and  $\omega_e x_e$ . The excellent agreement between these values of

$$\alpha_e(X) = 0.00065(6) \text{ cm}^{-1},^2$$

$$\alpha_e(B) = 0.00073(6) \text{ cm}^{-1},$$

is probably more fortuitous than anything else because of the large experimental uncertainty. However, the agreement does serve the useful purpose of providing an internal consistency test of the experimental vibrational and rotational constants. A further calculation of  $\alpha_e$  based on the Rittner ionic model (20, 21) is also in agreement with that obtained from the Morse potential to which Eq. (6) applies.

The  $B$ -state spin-rotation interaction constant,  $\gamma_0'$ , is in good agreement with the value expected on the basis of the Van Vleck "pure precession" (9) and the Zare "unique perturber" (11) approximation. The calculated value (based on our constants of  $A_{II}$  (spin-orbit)<sup>2</sup> = +71.0 cm<sup>-1</sup>,  $B_0' = 0.1539$  cm<sup>-1</sup>,  $E_{II} - E_{\Sigma} = -722$  cm<sup>-1</sup>) and the  $p$ -electron value ( $l = 1$ ) is  $\gamma_0' = -0.061$  cm<sup>-1</sup>. The agreement between this and the experimental value of  $\gamma_0' = -0.059$  cm<sup>-1</sup> indicates the one electron description of  $A^2\Pi$ , as  $\omega\pi^4 4p\pi$  and  $B^2\Sigma^+$  as  $\omega\pi^4 4p\sigma$  is particularly appropriate. Similar conclusions have been reached previously in studies of CaF (1) and BaF (22). The agreement of the pure precession-unique perturber model (9, 11) suggests that it is useful to define  $\gamma_e'$  in a similar manner to  $B_e'$  as

$$\gamma_e' = \gamma_e' - \delta_e'(v + \frac{1}{2}). \quad (7)$$

The  $\gamma_e'$  value quoted in Table II was obtained from  $\gamma_0'$ ,  $\gamma_1'$ , and  $\gamma_2'$  using Eq. (7).  $\gamma_e''$  is the assumed value of 0.003 cm<sup>-1</sup>. However, our data are not sufficiently precise to confirm the above expression. An accurate determination of the variation of  $\gamma_e'$  and  $\gamma_e''$  with vibrational state must await accurate microwave data. Note that the beautiful work of Dixon and Woods (23) on the microwave spectrum of the  $X^2\Sigma^+$  state of CN reaches a similar conclusion to that above as to the vibrational dependence of  $\gamma_e''$ .

One consequence of the large value of  $\gamma'$  and the small difference in rotational constants is that the  $P_1$  and  $P_2$  heads are split by about 3 cm<sup>-1</sup>. As a result, the  $P_1$  head of a ( $v'$ ,  $v''$ ) band nearly overlaps the  $P_2$  head of ( $v' + 1$ ,  $v'' + 1$ ) bands because the difference in vibrational frequencies is also about 3 cm<sup>-1</sup>. Low-resolution chemiluminescence spectra (see Fig. 1) then have the interesting feature that the (0, 0) head appears less intense than the (1, 1) head. The ( $v'$ ,  $v''$ ) bands, where  $v', v'' \geq 1$ , show an exponential decrease in intensity with  $v$  from which the vibrational temperature has previously been derived by Menzinger (4). The deviation of the (0, 0) band from a Boltzmann fit was ascribed to a slight population inversion between  $v' = 1$  and  $v' = 0$  (4). However, it is the near overlap which makes the (1, 1) head appear more intense than the (0, 0) head.

Finally, it should be mentioned that ultraviolet photoluminescence has also been observed when CaCl is excited with a rhodamine-6G dye laser; a result of optical-optical double resonance which initially pumps  $X^2\Sigma^+ \rightarrow B^2\Sigma^+$  and then  $B^2\Sigma^+ \rightarrow E^2\Sigma^+$ . This immediately suggests the experiment of using two dye lasers; the first tuned to select a particular rotational state of  $B^2\Sigma^+$ , and the second scanned over its tuning range to

<sup>2</sup> Uncertainties are 95% confidence limits in the last digit.

<sup>3</sup> From  $A = \nu_0(\Omega = \frac{1}{2}) - \nu_0(\Omega = \frac{1}{2}) + 2B$  and measurement of the spacing of the  $Q$  heads in the Ca + Cl<sub>2</sub> luminescence.

obtain a  $B^2\Sigma^+-E^2\Sigma^+$  excitation spectrum. Rotational analysis of the  $E^2\Sigma^+$  state is then particularly simple as a result of knowing the intermediate ( $B^2\Sigma^+$ ) state rotational level and measuring the  $P$ - $R$  separation in the excitation spectrum. Another double-resonance experiment to be attempted is the microwave-optical double-resonance (MODR) (2) spectrum to obtain both ground-state  $X^2\Sigma^+$  and excited-state  $B^2\Sigma^+$  spectroscopic constants more precisely. Both states have the interesting complication of nuclear spin-electron spin interactions and nuclear quadrupole hyperfine structure, both of which provide additional information on the molecular structure.

## ACKNOWLEDGMENTS

We thank Dr. Katsumi Sakurai and Professor H. P. Broida for initial discussions and their continued interest in this work. We are indebted to Professor R. F. Barrow for supplying us with data which indicated a reappraisal of our frequency measurements and to Dr. J. T. Hougen for promptly supplying us with his unpublished iodine frequency measurements.

RECEIVED: December 15, 1976

## REFERENCES

1. R. W. FIELD, D. O. HARRIS, AND T. TANAKA, *J. Mol. Spectrosc.* **57**, 107 (1975).
2. R. W. FIELD, A. D. ENGLISH, T. TANAKA, D. O. HARRIS, AND D. A. JENNINGS, *J. Chem. Phys.* **59**, 2191 (1973).
3. T. TANAKA, A. D. ENGLISH, R. W. FIELD, D. A. JENNINGS, AND D. O. HARRIS, *J. Chem. Phys.* **59**, 5217 (1973).
4. M. MENZINGER, *Chem. Phys.* **5**, 350 (1974).
5. E. MORGAN AND R. F. BARROW, *Nature (London)* **185**, 754 (1960).
6. J. B. WEST, R. S. BRADFORD, JR., J. D. EVERSOLE, AND C. R. JONES, *Rev. Sci. Instrum.* **46**, 164 (1975).
7. G. HERZBERG, "Spectra of Diatomic Molecules," Van Nostrand, Princeton, N. J., 1950.
8. Ref. (7), pp. 247-250.
9. J. H. VAN VLECK, *Phys. Rev.* **33**, 467 (1929).
10. R. S. MULLIKEN AND A. CHRISTY, *Phys. Rev.* **38**, 87 (1931).
11. R. N. ZARE, A. L. SCHMELTEKOPF, W. J. HARROP, AND D. L. ALBRITTON, *J. Mol. Spectrosc.* **46**, 37 (1973).
12. R. F. CURL, JR., *J. Comp. Phys.* **6**, 367 (1970).
13. Ref. (7), pp. 181.
14. C. L. PEKERIS, *Phys. Rev.* **45**, 98 (1934).
15. W. E. WENTWORTH, *J. Chem. Educ.* **42**, 96 (1965).
16. S. N. SUCHARD, "Spectroscopic Data," Plenum, New York, 1975.
17. B. ROSEN, "Spectroscopic Data Relative to Diatomic Molecules," Pergamon, New York, 1970.
18. L. L. KHANNA AND V. S. DUBEY, *Indian J. Pure Appl. Phys.* **13**, 603 (1975).
19. A. B. DARJI AND S. G. SHAH, *Indian J. Pure Appl. Phys.* **13**, 187 (1975).
20. E. S. RITTNER, *J. Chem. Phys.* **19**, 1030 (1951).
21. A. HONIG, M. MANDEL, M. L. STITCH, AND C. H. TOWNES, *Phys. Rev.* **96**, 629 (1954).
22. R. F. BARROW, M. W. BASTIN, AND B. LONGBOROUGH, *Proc. Phys. Soc. London* **92**, 518 (1967).
23. T. A. DIXON AND R. C. WOODS, in press.
24. J. D. SIMMONS AND J. T. HOUGEN, in press; J. T. HOUGEN, private communication.



## LETTER TO THE EDITOR

The Rotational Spectrum of the  $X^2\Sigma^+$  State of the  $\text{Ca}^{35}\text{Cl}$  Radical Using Laser Microwave Optical Double Resonance<sup>1</sup>

PETER J. DOMAILLE, TIMOTHY C. STEIMLE, AND DAVID O. HARRIS

*Quantum Institute and Department of Chemistry, University of California, Santa Barbara, Santa Barbara, California 93106*

In a recent paper we reported a rotational analysis of the  $B^2\Sigma^+-X^2\Sigma^+$  system of  $\text{CaCl}$  using cw dye laser excitation spectroscopy (1). At that time we indicated that microwave optical double resonance (MODR) (2, 3) could be performed to yield more precise ground state rotational constants. That study has since been completed and we report here more accurate constants for the  $X^2\Sigma^+$  and  $B^2\Sigma^+$  states derived from the combined optical and microwave measurements.

Because a laser excitation study of the  $B^2\Sigma^+-X^2\Sigma^+$  system of  $\text{SrF}$  (4) and a corresponding MODR study (3) of the  $X^2\Sigma^+$  state were completed nearly simultaneously with this

TABLE I

Measured and fitted line positions (MHz) in the rotational spectrum of  $^{35}\text{Cl}$  in the  $X^2\Sigma^+$  state.

TRANSITION <sup>a</sup>	MEASURED <sup>b</sup>	CALCULATED
$v=0$ 5, 9 (2) - 4, 7 (2)	45496.7(2.5)	45496.5
$v=0$ 5, 11 (2) - 4, 9 (2)	45538.7(2.4)	45537.4
$v=0$ 6, 11 (2) - 5, 9 (2)	54596.9(3.3)	54599.1
$v=0$ 6, 13 (2) - 5, 11 (2)	54639.9(2.4)	54640.0
$v=0$ 7, 11 (2) - 6, 11 (2)	63701.8(2.0)	63701.2
$v=0$ 7, 13 (2) - 6, 13 (2)	63741.0(2.4)	63742.1
$v=1$ 5, 9 (2) - 4, 7 (2)	45254.7(2.9)	45257.0
$v=1$ 5, 11 (2) - 4, 9 (2)	45297.4(7.4)	45297.2
$v=1$ 6, 11 (2) - 5, 9 (2)	54312.4(2.1)	54311.6
$v=1$ 6, 13 (2) - 5, 11 (2)	54351.7(1.2)	54351.8
$v=1$ 7, 11 (2) - 6, 11 (2)	63367.0(4.3)	63365.8
$v=1$ 7, 13 (2) - 6, 13 (2)	63406.1(1.4)	63406.0

<sup>a</sup>Transitions are labelled as  $(N', J') - (N'', J'')$ ; hyperfine structure is not resolved.

<sup>b</sup>The line position uncertainties, in parentheses, represent 95% confidence limits derived from several repeat measurements.

<sup>1</sup>This research was supported by grants from the National Science Foundation NSF-MPS-72-04978 and the Air Force Office of Scientific Research USAF-OSR-73-2565.

TABLE II

Rotational constants of  $\text{Ca}^{35}\text{Cl}$  from fitting measured microwave frequencies. Uncertainties are 95% confidence limits in the last digit.

CONSTANT	FREQUENCY (MHz)	WAVENUMBER ( $\text{cm}^{-1}$ )
$B_0''$	4551.85 (11)	0.151833 (4)
$B_1''$	4527.86 (10)	0.151033 (3)
$\gamma_0''$	40.9 (27)	0.00136 (9)
$\gamma_1''$	40.2 (24)	0.00134 (8)
$D$ (fixed)	$3.09 \times 10^{-3}$	$1.03 \times 10^{-7}$

work, no detailed discussion of the experiments or the methods used to treat the  $\text{CaCl}$  data are given here.

The measured microwave transition frequencies and their associated uncertainties are listed in Table I. The broad MODR linewidths prevented measurements of any hyperfine structure, hence line positions were fitted to the simple expression (3, 5)

$$\nu(N \rightarrow N+1) = 2B_r(N+1) - 4D(N+1)^3 \pm \gamma_r/2 \quad (1)$$

using a weighted least squares procedure. The data are not sufficiently precise to derive an accurate value of  $D$ , hence it was fixed ( $4B^2/\omega^2$ ) and Eq. (1) used to fit  $B''$ , and  $\gamma''$ , for  $r'' = 0$  and 1. The constants derived from the fit are collected in Table II. The values are in good agreement with those derived from the optical study (1) but represent a 50-fold increase in precision. Because of the increased accuracy of the microwave results and the high degree of correlation of the constants obtained from the optical study, the two sets of data (1) have been merged (6) to obtain more precise constants for both the  $X^2\Sigma^-$  and  $B^2\Sigma^+$  states. Results are collected in Table III.

A word of caution concerning the  $B$  parameters in the  $B^2\Sigma^+$  state is necessary. The value listed is simply the  $N(N+1)$  coefficient in the rotational energy expression and does not directly represent  $\langle 1/r^2 \rangle$ , for the  $B^2\Sigma^+$  state. The  $B^2\Sigma$  and  $A^2\Pi$  states are in pure precession (1, 7) and hence the true rotational constant is contaminated by an electronic contribution,  $q_2$ . The pure precession estimate (7) of  $q_2 \approx -\gamma B/A$  must be

TABLE III

$\text{Ca}^{35}\text{Cl}$  spectroscopic constants for the  $X^2\Sigma^+$  and  $B^2\Sigma^+$  states from combining microwave and optical data.

	$X^2\Sigma^+$	$B^2\Sigma^+$
$B_0$	0.151833 (2)	0.154256 (5)
$B_1$	0.151033 (2)	0.153367 (7)
$\gamma_0$	0.00136 (5)	-0.0652 (2)
$\gamma_1$	0.00134 (4)	-0.0656 (3)
$B_e$	0.152233 (3)	0.154700 (8)
$q_2$	$2.00 (3) \times 10^{-4}$	$2.59 (9) \times 10^{-4}$
$A$		0.00013

subtracted from the quoted  $B$  value to retain a strictly mechanical significance. This is an important consideration, for example, when calculating Franck-Condon factors.

RECEIVED: April 11, 1977

## REFERENCES

1. P. J. DOMAILLE, T. C. STEIMLE, N. B. WONG, AND D. O. HARRIS, *J. Mol. Spectrosc.* **65**, 354-365 (1977).
2. R. W. FIELD, A. D. ENGLISH, T. TANAKA, D. O. HARRIS, AND D. A. JENNINGS, *J. Chem. Phys.* **59**, 2191 (1973).
3. P. J. DOMAILLE, T. C. STEIMLE, AND D. O. HARRIS, submitted for publication.
4. T. C. STEIMLE, P. J. DOMAILLE, AND D. O. HARRIS, submitted for publication.
5. W. GORDY AND R. L. COOK, "Microwave Molecular Spectra," Interscience, New York, 1970.
6. D. L. ALBRITTON, A. L. SCHMELTEKOPF, AND R. N. ZARE, "Molecular Spectroscopy: Modern Research" (K. Narahari Rao and K. W. Matthews, Eds.), Vol. II, Academic Press, New York, 1976.
7. R. N. ZARE, A. L. SCHMELTEKOPF, W. J. HARROP, AND D. L. ALBRITTON, *J. Mol. Spectrosc.* **46**, 37 (1973).



# Optical-optical double resonance with two dye lasers: Rotational analysis of the $E^2\Sigma-B^2\Sigma$ system of $\text{Ca}^{35}\text{Cl}$

Peter J. Domaille, Timothy C. Steimle, and David O. Harris

Department of Chemistry and Quantum Institute, University of California, Santa Barbara, California 93106

(Received 13 September 1977)

A complete rotational analysis of the  $E^2\Sigma-B^2\Sigma$  system of  $\text{CaCl}$  has been accomplished using two tunable dye lasers. The first cw laser is tuned to a known  $B^2\Sigma-X^2\Sigma$  transition to produce a finite concentration of molecules in a particular quantum state. Subsequently, a second pulsed dye laser is used to record the  $E^2\Sigma-B^2\Sigma$  excitation spectrum from this state prepared level. The method vastly simplifies an otherwise congested molecular spectrum. The data are combined with previous microwave measurements on the  $X^2\Sigma$  state and optical data on the  $B^2\Sigma-X^2\Sigma$  system to give the following molecular constants ( $\text{cm}^{-1}$ ). Uncertainties are 95% confidence limits in the last digit.

	$X^2\Sigma$	$B^2\Sigma$	$E^2\Sigma$
$T_e$	0	16856.69(2)	34268.17(98)
$\omega_e$	369.8(10)	366.8(10)	413.7(16)
$\omega_e x_e$	1.13(20)	1.28(20)	1.67(82)
$B_e$	0.1522325(45)	0.1546940(82)	0.163412(17)
$\alpha_e$	$7.998(39) \times 10^{-4}$	$8.839(67) \times 10^{-4}$	$8.66(10) \times 10^{-4}$
$\gamma_{\text{av}}$ (spin rotation)	0.00135(6)	-0.0652(2)	0.0046(5)

## I. INTRODUCTION

The realm of laser excitation spectroscopy can be greatly extended in energy coverage with the use of two lasers to perform optical-optical double resonance (OODR). Usually, spectroscopic states with energies greater than 2.5 eV are not readily accessible from the ground state by a single resonance because of the limited wavelength range of present laser systems. However, the use of two lasers in a double resonance experiment, extends this limit to about 5 eV by utilizing an intermediate state as a "stepping stone." Furthermore, if these intermediate states of a molecule are well characterized spectroscopically, the assignment of double resonance transitions becomes a trivial task and the subsequent analysis is greatly simplified.

The principal information to be gained from OODR experiments is exemplified in the study of Field and co-workers.<sup>1</sup> Specifically, two types of experiments may be performed, each providing data on different electronic states. First, the dispersed photoluminescence from the terminal level ( $v^*, J^*$ ) may be recorded with both lasers held at fixed frequencies, or, alternatively, the laser connecting the intermediate state ( $v', J'$ ) to the final state ( $v^*, J^*$ ) may be swept in frequency to produce an excitation spectrum. These possibilities are depicted schematically in the three level system shown in Fig. 1. Measurement of the resolved photoluminescence gives information about the ground state ( $v'', J''$ ), or other low lying states, while the excitation spectrum, ( $v^*, J^*$ ) - ( $v', J'$ ), probes the structure of the intermediate and final states.

In addition to the increased energy coverage, the fundamental advantage of the OODR method over conventional laser excitation spectroscopy is due to the state selectivity of the method. In an OODR experiment the first laser prepares one particular quantum state of the

molecule for the subsequent excitation spectrum. In contrast, excitation spectroscopy of a gas phase molecule at room temperature involves transitions from many rotational and vibrational levels of all isotopic species. Hence, the advantage of the two laser excitation spectrum is the simplification of the spectroscopy.

On completion of the laser excitation study of the  $B^2\Sigma-X^2\Sigma$  system of  $\text{CaCl}^{2,3}$  it was apparent that the  $3^2\Sigma$  state was an ideal intermediate state for excitation

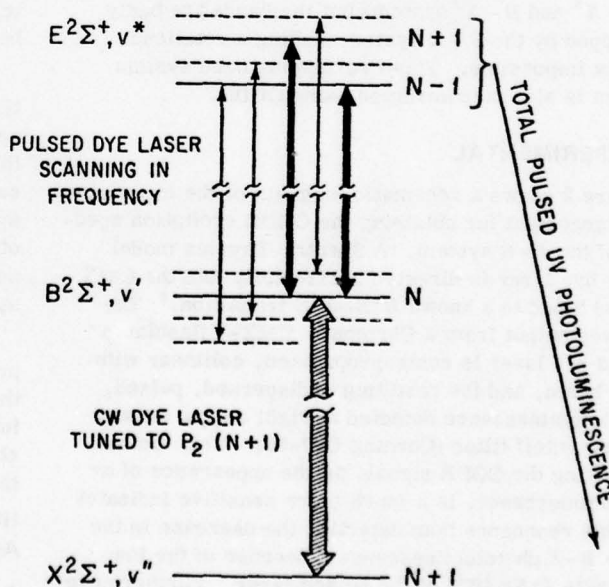


FIG. 1. Schematic diagram of the energy levels involved in a typical OODR experiment. The heavy line full arrows correspond to the PR doublet observed at low pressures while the lighter line full arrows refer to additional transitions caused by collisional relaxation in the  $B^2\Sigma, v'$  state.

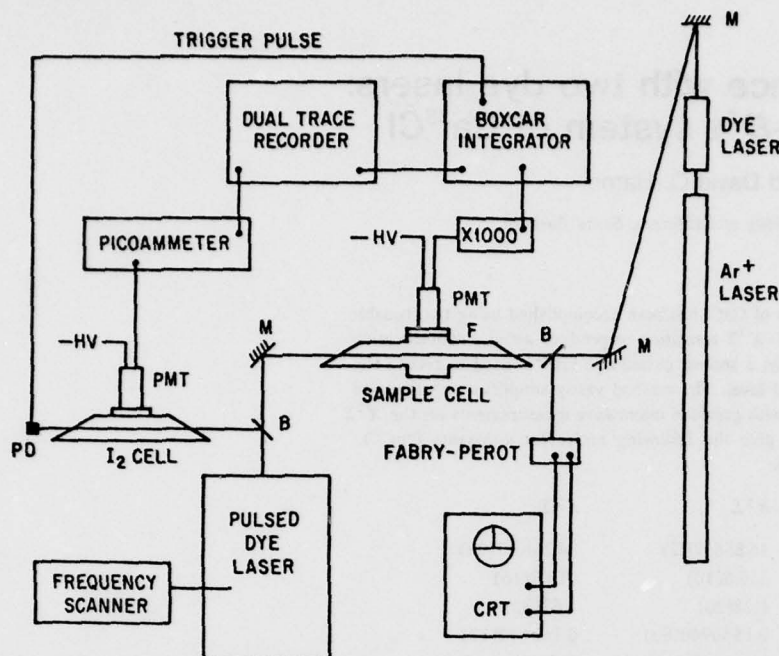


FIG. 2. Schematic of experimental arrangement for obtaining OODR. The following abbreviations have been used: M—mirror; B—beam splitter; F—filter; PD—photodiode; PMT—photomultiplier; CRT—oscilloscope to monitor the single frequency cw dye laser. The picoammeter detects the iodine excitation spectrum for frequency calibration of the pulsed dye laser.

into the higher lying electronic states,  $D^2\Sigma$ ,  $E^2\Sigma$  and  $F^2\Pi$ . All of these states are amenable to study, via the  $B^2\Sigma$  state, using a second laser in the 530–700 nm range. We report here a complete rotational analysis of the  $E^2\Sigma$ – $B^2\Sigma$  band system using an additional laser, operating between 555–575 nm, to obtain excitation spectra from several ( $v'$ ,  $J'$ ) levels of the  $B^2\Sigma$  state. The results indicate the dramatic simplification obtainable in an otherwise severely overlapped band system.

The only previous report of the  $E$ – $B$  system was the study of Khanna and Dubey<sup>4</sup> where the band system was obtained in emission from a  $\text{CaCl}_2$  arc. The identification of the bands is consistent with the known positions of the  $E$ – $X^5$  and  $B$ – $X^2$  systems but the bands are badly overlapped by the  $B$ – $X$  system making a rotational analysis impossible. This overlapping band system problem is also circumvented using OODR.

## II. EXPERIMENTAL

Figure 2 shows a schematic diagram of the experimental arrangement for obtaining the OODR excitation spectrum of the  $E$ – $B$  system. A Spectra-Physics model 580 cw dye laser is directed horizontally into the  $\text{CaCl}$  cell and tuned to a known  $B^2\Sigma$ – $X^2\Sigma$  transition.<sup>2</sup> The narrowed output from a Chromatix CMX-4 flashlamp pumped dye laser is contrapropagated, collinear with the cw beam, and the resulting undispersed, pulsed, uv photoluminescence detected at right angles through a visible cutoff filter (Corning CS7-51). This method of detecting the OODR signal, as the appearance of uv photoluminescence, is a much more sensitive indicator of double resonance than detecting the decrease in the visible  $B$ – $X$  photoluminescence,<sup>1</sup> because of the low duty cycle ( $\sim 5 \times 10^{-5}$ ) of the pulsed laser. Furthermore, detecting the appearance of emission over a zero background light-level is much easier than observing a decrease of intensity against a strong background.

The cw laser was operated with about 35 mW of power concentrated in a single longitudinal mode, producing a bandwidth of about 20 MHz. The pulsed dye laser, using Fluorol 555,<sup>6</sup> was also operated with an intracavity etalon, reducing the bandwidth to about  $0.08 \text{ cm}^{-1}$  over a tuning range of between 50 and  $100 \text{ cm}^{-1}$ . Scanning the frequency of the pulsed laser produces an  $E$ – $B$  excitation spectrum originating in a particular  $B^2\Sigma(v', J')$  level. No attempt was made to measure the dispersed photoluminescence.

The pulsed OODR signal was processed through a PAR model CW-1 boxcar integrator and recorded on one channel of a dual trace recorder. The boxcar was triggered externally by directing a portion of the pulsed beam to a photodiode.

For precise line position measurements, an excitation spectrum of molecular iodine was simultaneously recorded by directing a portion of the pulsed beam through a cell containing  $\text{I}_2$  vapor. The resulting photocurrent was directed to a Keithley picoammeter, smoothed by a 3 sec time constant, and displayed on the other channel of the dual trace recorder. To compensate for any difference in response time, the superimposed spectra were obtained for both directions of laser sweeps.

The production of  $\text{CaCl}$  is identical to that described previously.<sup>2</sup> Calcium metal is resistively heated, and the vapor entrained in an argon carrier gas and swept into the reaction zone where it is mixed with molecular chlorine. The pressure in the reaction cell was maintained at between 0.3 and 3 torr.

## III. EXCITATION SPECTRUM AND NUMERICAL ANALYSIS

### A. Description of the excitation spectrum

A typical OODR excitation spectrum is illustrated in Fig. 3. Compared with the previous  $B^2\Sigma$ – $X^2\Sigma$  excita-



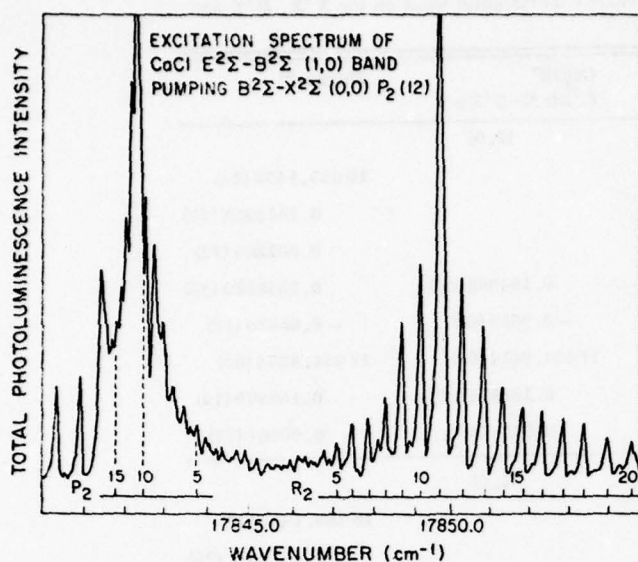


FIG. 3. A typical  $E^2\Sigma-B^2\Sigma$  excitation spectrum from a pseudo-state selected  $B^2\Sigma$  state. The cw laser selects  $v'=0$ ,  $N'=11$ ,  $J'=10.5$  by pumping  $B^2\Sigma-X^2\Sigma(0,0)P_2(12)$ . The pressure in the cell is around 2 torr so that rotational relaxation into adjacent states occurs producing a much simplified portion of the  $E-B$  band system. The two lines beyond the  $P_2$  head (at  $17845.7\text{ cm}^{-1}$ ) are due to additional unassigned  $B-X$  coincidences and subsequent double resonance. Line asymmetry is due to the response time of the detection system in recording this survey scan. Line position measurements were made on scans taken at one tenth of the above rate.

tion scans,<sup>2</sup> the spectrum is remarkably simple due to the selective population of the  $B^2\Sigma v'=0$ ,  $N'=11$  state of  $\text{Ca}^{35}\text{Cl}$ . In fact, in the absence of any rotational relaxation, this spectrum would contain only two lines,  $P_2(11)$  and  $R_2(11)$ , following from the selection rules and intensity considerations for a  $^2\Sigma-^2\Sigma$  transition.<sup>8</sup> However in Fig. 3, the pressure in the cell has been deliberately increased to  $\sim 2$  torr to enhance the intensity of the collisionally relaxed lines. The advantage of operating at these moderate pressures is that many lines of a band system can be obtained in one excitation scan while still retaining enough state specificity to maintain the simplicity of the rotational assignment. The labeling of rotational quantum numbers is trivially simple because the  $B^2\Sigma$  state ( $v'$ ,  $J'$ ) level is already assigned from the  $B-X$  analysis.<sup>2</sup>

Two other features of Fig. 3 warrant further discussion. First, the magnitude of the rotational relaxation cross section, and second, the absence of the more energetically favorable  $F_2-F_1$  transfer.

The radiative lifetime of the  $B^2\Sigma$  state is known to be  $38.2\text{ nsec}^7$  corresponding to a fluorescent rate constant of about  $2.6 \times 10^7\text{ sec}^{-1}$ . At a total pressure of 2 torr the hard sphere collision rate is also around  $2.6 \times 10^7\text{ sec}^{-1}$ . Thus, in the absence of electronic quenching, the rotational relaxation cross section is around one in five hard sphere collisions because the intensity of the relaxed lines is about 20% of the directly pumped state. These considerations are indeed approximate but the observations do demonstrate the feasibility of using high resolu-

tion OODR methods in evaluating detailed rotational relaxation kinetics.

To a trained pattern recognition spectroscopist, the spectrum in Fig. 3 could well be mistakenly identified as a  $^1\Sigma-^1\Sigma$  transition because the characteristic doubling of branches encountered in  $^2\Sigma-^2\Sigma$  systems<sup>8</sup> is absent. This occurs because the rotational relaxation is restricted to the spin manifold ( $J=N \pm S$ ) in which the molecule was originally prepared; there are no apparent  $F_1(J=N+S) \rightarrow F_2(J=N-S)$  transfers. Had there been transfer, the spectrum would have appeared more complex. Energetically this phenomenon is somewhat surprising since the rotational spacings are between 10 and 200 times larger than the spin doubling splittings. The rotational relaxation, resulting from collisions with the argon carrier gas, appears to obey the propensity rules  $\Delta J = \pm 1$  and parity  $\pm = -$  which implies that they are of "dipole type." Although chemical systems, in which collisional relaxation processes adhere to certain propensity rules, have been previously investigated,<sup>9,10</sup> we are not aware of any prior studies on excited  $^2\Sigma$  states.

It would be worth while pursuing this observation with additional experimental studies to attempt to unravel the details of rotational relaxation in open shell molecules.

Based on the reproducibility of the data from careful interpolation between reference iodine lines,<sup>11</sup> the estimated standard deviation of the measurement error distribution is  $\sim 0.02\text{ cm}^{-1}$ . The linewidth limitation in the excitation spectrum is due to the  $0.08\text{ cm}^{-1}$  bandwidth of the pulsed laser. Naturally, with two single mode cw lasers a substantial decrease in this linewidth would be realized because of the partial Doppler width cancellation.<sup>12</sup> Further pursuit of this aspect of OODR could well provide higher precision measurements of uv states relative to the precise iodine visible frequency standards.<sup>11</sup>

## B. Numerical procedures

Approximately 100 lines in each of the (0,0), (1,0) and (2,1) bands of the  $E-B$  system were used in the numerical analysis. Line position measurements were least squares fitted using the "direct approach" method described by Zare *et al.*<sup>13</sup> to obtain  $T_{\text{rot}}^*, B_v^*, \gamma_v^*, B_v'$ , and  $\gamma_v'$ . The parameters superscripted with an asterisk designate those of the  $E^2\Sigma$  state while those with a single prime superscript refer to the  $B^2\Sigma$  state.  $D_v$  was included in the fits but was held fixed at  $4B_v^3/\omega_v^2$  in all cases.

Line positions, which are available from the authors upon request list the measured raw data used in the fits along with deviations from the fitted values. The standard deviation of the fits to the (0,0), (1,0), and (2,1) bands are 0.020, 0.018, and  $0.020\text{ cm}^{-1}$ , respectively. In spite of the high precision of these fitted data, parameter correlation must be considered when interpreting the accuracy of the derived constants; the difference in constants is the most precisely determined quantity. Fortunately, an independent precise measurement of the microwave spectrum<sup>3</sup> yields accurate absolute  $X$ -state constants so that with the strong correlation, this



TABLE I. Spectroscopic constants<sup>a</sup> derived from the present and previous experimental work on the  $X^2\Sigma$ ,  $B^2\Sigma$  and  $E^2\Sigma$  states of  $\text{Ca}^{35}\text{Cl}$ .

	Optical <sup>b</sup> $B^2\Sigma(v')-X^2\Sigma(v'')$	Microwave <sup>c</sup> $X^2\Sigma(v'')$	Merge 1 <sup>d</sup>	OODR <sup>e</sup> $E^2\Sigma(v^*)-B^2\Sigma(v')$	Merge 2 <sup>f</sup>
	(0, 0)	$v'' = 0$		(0, 0)	
$T_0'$	16 855.1403 (20)		16 855.1426 (37)		16 855.1432 (25)
$B_0''$	0.151532 (82)	0.1518333 (36)	0.1518332 (23)		0.1518331 (28)
$\gamma_0'$	0.0071 (38)	0.001364 (90)	0.001363 (55)		0.001365 (72)
$B_0'$	0.153937 (86)		0.1542559 (52)	0.154208 (85)	0.1542525 (43)
$\gamma_0'$	-0.0592 (40)		-0.065243 (23)	-0.0659 (88)	-0.06525 (17)
$T_0^*$				17 434.8414 (68)	17 434.8364 (69)
$B_0^*$				0.162934 (85)	0.162979 (10)
$\gamma_0^*$				0.0039 (86)	0.00467 (37)
	(0, 0)	$v'' = 0$		(1, 0)	
$T_0'$	16 855.1403 (20)		16 855.1426 (37)		16 855.1433 (26)
$B_0''$	0.151532 (82)	0.1518333 (36)	0.1518332 (23)		0.1518331 (29)
$\gamma_0'$	0.0071 (38)	0.001364 (90)	0.001363 (55)		0.001364 (72)
$B_0'$	0.153937 (86)		0.1542559 (52)	0.154197 (84)	0.1542525 (44)
$\gamma_0'$	-0.0592 (39)		-0.065243 (23)	-0.0693 (79)	-0.06525 (17)
$T_1^*$				17 845.1993 (57)	17 845.1954 (61)
$B_1^*$				0.162057 (83)	0.162113 (10)
$\gamma_1^*$				0.0000 (78)	0.00400 (46)
	(1, 1)	$v'' = 1$		(2, 1)	
$T_1'$	16 851.8255 (22)		16 851.8262 (39)		16 851.8262 (26)
$B_1''$	0.151114 (53)	0.1510333 (31)	0.1510332 (17)		0.1510334 (23)
$\gamma_1'$	-0.0013 (32)	0.001342 (78)	0.001342 (45)		0.001340 (58)
$B_1'$	0.153453 (57)		0.1533671 (71)	0.153372 (85)	0.1533673 (52)
$\gamma_1'$	-0.0682 (32)		-0.065550 (28)	-0.0675 (88)	-0.06513 (19)
$T_2^*$				17 887.9588 (72)	17 887.9587 (72)
$B_2^*$				0.161253 (86)	0.161248 (10)
$\gamma_2^*$				0.0026 (87)	0.00499 (38)

<sup>a</sup>The double primed constants (") refer to the  $X^2\Sigma$  state, the single prime (') refers to the  $B^2\Sigma$  state and the asterisk (\*) refers to the  $E^2\Sigma$  state. In all cases the centrifugal distortion constants,  $D_e$ , were held fixed at  $4B_e^3/\omega_e^2$ . Numbers in parentheses refer to 95% confidence limits in the last digit.

<sup>b</sup>Constants derived from the  $B^2\Sigma-X^2\Sigma$ , ( $v'$ ,  $v''$ ) excitation spectra described in Ref. 2.

<sup>c</sup>Constants derived from the microwave spectrum of the  $X^2\Sigma$ ,  $v''$  state described in Ref. 3.

<sup>d</sup>Constants obtained from a combined fit of constants from (b) and (c).

<sup>e</sup>Constants from the present work on the excitation spectrum of the  $E^2\Sigma-B^2\Sigma(v^*, v')$  system.

<sup>f</sup>Final results from merging (b), (c) and (e).

precision of the ground state constants is projected into the  $B^2\Sigma$  and  $E^2\Sigma$  state values.

Albritton *et al.*<sup>14</sup> have detailed this correlated least squares approach to the combined fitting of spectroscopic data. First, separate least squares fits to the data from different analyses are performed. Then, provided certain criteria are fulfilled, the parameters and the covariance-variance matrices are combined to obtain the unique set of minimum variance linear unbiased (MVLU) parameters for all states. In the present case, the superior precision of the microwave measurements

in the  $X$  state is projected into both the  $E$ - and  $B$ -state constants by merging the results of the MODR,<sup>3</sup>  $B-X$  optical analysis,<sup>2</sup> the OODR excitation spectrum.

One important criterion for this second step is that the constants in common, derived from the first step, should agree within a reasonable error limit, say 95% confidence limits. Failure of this condition may be an indication of systematic errors in the data or model equations and the estimates of the "true" values of the parameters lose credibility. Of course these requirements of parameter consistency are particularly strin-

TABLE II. Equilibrium spectroscopic constants for the  $E^2\Sigma$  state.

$T_e$	34 268.17 (98) $\text{cm}^{-1}$
$\omega_e$	413.7 (16) $\text{cm}^{-1}$
$\omega_e x_e$	1.67 (82) $\text{cm}^{-1}$
$B_e$	0.163412 (17) $\text{cm}^{-1}$
$\alpha_e$	$8.66 (10) \times 10^{-4} \text{ cm}^{-1}$

gent in merging of data from three independent sources. Firstly, the  $X$ -state constants are common to both the  $B$ - $X$  optical analysis<sup>2</sup> and MODR study<sup>3</sup> while the  $B$ -state constants are common to both the OODR and  $B$ - $X$  analyses. Any systematic error in the  $B$ - $X$  analysis will thus be revealed twice.

Columns 1 and 2 of Table I provide an example of a minor discrepancy in the  $B_0''$  value determined from the  $B$ - $X$  analysis<sup>2</sup> and from the microwave measurements. Not surprisingly, the  $B_0'$  values from the OODR and  $B$ - $X$  analyses are also in slight discord. In contrast, the values of  $B_1''$  and  $B_1'$  are in satisfactory agreement. The slight difference in constants is attributed to the asymmetry of the  $B$ - $X$  (0,0) line position data about the band origin; the measured lines are predominantly  $P$  branches with very few  $R$  branches being assigned.<sup>2</sup> Conversely, the (1,1) band contains more equal numbers of data from  $P$  and  $R$  branches. As a result, the  $B_0$  values are very sensitive to minute systematic errors in the data or model equations while the effect on  $B_1$  is much less pronounced. For example, a 10% variation in the (frozen) centrifugal distortion constant changes  $B_0''$  sufficiently to bring it into accord with the microwave data, while  $B_1'$  is scarcely affected. Similarly,  $B_0'$  is in better agreement with the OODR determination. Fortunately however, the difference in the constants,  $B' - B''$ , which is the important quantity that is merged with the precise microwave data, is much less sensitive to any slight systematic error. Thus, merging the optical and microwave data results in no significant inaccuracy in the derived constants. A further indication of the validity of merging these two sets of constants is the improved agreement of the resulting  $B_0'$  value with that of the OODR work.

The results of all the least squares fits are contained in Table I. Merge 2 represents the optimum set of parameters for the  $X$ ,  $B$  and  $E$  states from all the measured data.

The (0,0), (1,0), and (2,1) band origins of the  $E$ - $B$  system were used to determine  $T_e$  and vibrational constants for the  $E$ -state using the previously obtained constants for the  $B$  state.<sup>2</sup> These values are listed in Table II.

The rather large error limits are due to the uncertainties in vibrational constants from the  $B$ -state being propagated through the calculation.

#### IV. DISCUSSION

Few high lying electronic states have been previously studied by laser excitation spectroscopy. In general,

access to states beyond the present tuning range of dye lasers occurs via metastable states produced in chemical reactions or electrical discharges.<sup>15,16</sup> However, the OODR technique can be successfully applied to short-lived intermediate states since the first laser adequately populates such strong transitions. Furthermore, the state selectivity of the first laser dramatically simplifies electronic band systems compared with those obtained from Boltzmann equilibrium metastable states. Both of these aspects of OODR are clearly evident in the present study of the  $E^2\Sigma$ - $B^2\Sigma$  system of  $\text{CaCl}$ . First, although the  $B$ -state has a radiative lifetime of only 38.2 nsec,<sup>7</sup> the laser induced steady state population is sufficiently high to pose no difficulty to detection of a subsequent laser excitation spectrum. And second, the excitation spectrum shown in Fig. 3 is uncomplicated by overlapping spin doubled branches, vibrational sequences, other band systems, and additional isotopic species. The subsequent rotational analysis is thus trivial compared with the labor usually associated with a conventional analysis.

The  $E$ -state constants call for little comment. The analysis confirms the identification as a  $^2\Sigma$  state and the vibrational constants are in accord with previous reports.<sup>4,5</sup> Moreover, the value of  $\omega_e x_e$  is in excellent agreement with that obtained from the Pekeris relation<sup>17</sup> using the derived values of  $B_e$ ,  $\omega_e$ , and  $\alpha_e$ .

The 7% decrease in the  $E$ -state bond length compared with the  $X$ -state value is probably a simple indication of the nonbonding  $4s\sigma(X^2\Sigma)$  electron becoming more bonding in nature upon excitation. The small value of the spin rotation constant may indicate that the  $E$  state is also primarily an  $s\sigma$  configuration. Furthermore, the close similarity of the energies of the  $E$  states of the homologous series  $\text{CaF}$ ,  $\text{CaCl}$  and  $\text{CaBr}$ <sup>18</sup> indicates that the energy is essentially independent of the halide and is more characteristic of the metal atom. Thus, we tentatively propose the  $E^2\Sigma$  state is primarily associated with the electron in the  $5s\sigma$  orbital located on the metal atom.

Additional experiments on the radiative lifetime of the  $E^2\Sigma$  state, and the relative transition moments of the  $E$ - $A$ ,  $E$ - $B$ , and  $E$ - $X$  systems are at present being undertaken with the aim of a more thorough characterization of the  $E$ -state.

#### ACKNOWLEDGMENTS

We acknowledge the loan of the CMX-4 from the Quantum Institute. Work supported by the National Science Foundation under Grant NSF-MPS-72-04978 and the Air Force Office of Scientific Research under Grant AFOSR-73-2565.

<sup>1</sup>R. W. Field, G. A. Capelle, and M. A. Revelli, *J. Chem. Phys.* **63**, 3228 (1975).

<sup>2</sup>P. J. Domaille, T. C. Steimle, N. B. Wong, and D. O. Harris, *J. Mol. Spectrosc.* **65**, 354 (1977).

<sup>3</sup>P. J. Domaille, T. C. Steimle, and D. O. Harris, *J. Mol. Spectrosc.* **66**, 503 (1977).

- <sup>4</sup>L. K. Khanna and V. S. Dubey, *Indian J. Pure Appl. Phys.* **11**, 510 (1973).
- <sup>5</sup>R. E. Herrington, thesis, University of California, Berkeley, 1942.
- <sup>6</sup>Fluorol 555 is the name given by the manufacturer, Exciton Chemical Co., Dayton, OH for the dye previously described as Fluorol 7GA by M. Lambropoulos, *Opt. Commun.* **15**, 35 (1975).
- <sup>7</sup>P. J. Dagdigian, H. W. Cruse, and R. N. Zare, *J. Chem. Phys.* **60**, 2330 (1974).
- <sup>8</sup>G. Herzberg, *Spectra of Diatomic Molecules* (Van Nostrand, Princeton, 1950).
- <sup>9</sup>J. I. Steinfeld, *Int. Rev. Sci. Phys. Chem.* **9**, 247 (1972).
- <sup>10</sup>T. Oka, *J. Chem. Phys.* **48**, 3135 (1968).
- <sup>11</sup>S. Gerstenkorn and P. Luc, "Atlas du Spectre d'Absorption de la Molécule d'Iode," Laboratoire Aime-Cotton, CNRS II 91405, Orsay, France.
- <sup>12</sup>See, for example, H. Walther in *Topics in Applied Physics, Laser Spectroscopy of Atoms and Molecules* (Springer, New York, 1976), Vol. 2.
- <sup>13</sup>R. N. Zare, A. L. Schmeltekopf, W. J. Harrop, and D. L. Albritton, *J. Mol. Spectrosc.* **46**, 37 (1973).
- <sup>14</sup>D. L. Albritton, A. L. Schmeltekopf, and R. N. Zare in *Molecular Spectroscopy: Modern Research*, edited by K. Narahari Rao (Academic, New York, 1976), Vol. II.
- <sup>15</sup>R. A. Gottscho and R. W. Field, Paper MF1, 32nd Symposium on Molecular Spectroscopy, Columbus, Ohio, June, 1977.
- <sup>16</sup>J. M. Lisy and W. Klemperer, Paper RG11, 32nd Symposium on Molecular Spectroscopy, Columbus, Ohio, June, 1977.
- <sup>17</sup>C. L. Pekeris, *Phys. Rev.* **45**, 98 (1934).
- <sup>18</sup>See *Spectroscopic Data Relative to Diatomic Molecules*, edited by B. Rosen (Pergamon, Oxford, 1970).



# Rotational Analysis of the $B^2\Sigma^+-X^2\Sigma^+$ System of SrF Using a cw Tunable Dye Laser<sup>1</sup>

TIMOTHY C. STEIMLE, PETER J. DOMAILLE, AND DAVID O. HARRIS

*Quantum Institute and Chemistry Department, University of California,  
Santa Barbara, California 93106*

A rotational analysis of the (0, 0), (1, 1), and (2, 2) bands of the  $B^2\Sigma^+-X^2\Sigma^+$  system of SrF at 580 nm has been performed using single-mode cw dye laser excitation spectroscopy. Spectroscopic constants ( $\text{cm}^{-1}$ ) obtained from a weighted least-squares fit of the data are given below. Numbers in parentheses refer to 95% confidence limits in the last digit.

	$X^2\Sigma^+$	$B^2\Sigma^+$
$T_e$	0	17267.42 (1)
$\omega_e$	502.4 (7)	495.8 (7)
$\omega_e x_e$	2.27 (21)	2.34 (21)
$B_e$	0.25075 (9)	0.24961 (9)
$D_e$	$2.50 (1) \times 10^{-7}$	$2.53 (1) \times 10^{-7}$
$\alpha_e$	0.00174 (9)	0.00175 (9)
$\gamma$ (spin-rotation)	0.004 (6)	-0.134 (6)

Franck-Condon factors were calculated from RKR potentials constructed from our spectroscopic data and compared with those derived from line intensity measurements. Discrepancies are attributed to the approximate nature of the line intensity expressions used. Anomalies in the rotational branch intensities provide evidence for the perturbed nature of the  $B^2\Sigma$  state by the close-lying  $A^2\Pi$  state.

## I. INTRODUCTION

In a continuing study of alkaline earth monohalides a rotational analysis of the  $B^2\Sigma^+-X^2\Pi^-$  system of SrF has been performed. In general, alkaline earth halides are observed to have complex spectra arising from electronic transitions in which the electron promotion is primarily from an  $ns\sigma$  ( $X^2\Sigma^+$ ) orbital to an  $np\pi$  ( $A^2\Pi$ ) or an  $np\sigma$  ( $B^2\Sigma^-$ ) orbital on the metal atom. The short lifetime ( $I$ ) is indicative of the fact that these transitions are essentially atomic in nature. Consequently, the electronic potential that the molecule experiences is very similar in all of these low-lying states and the molecular constants are relatively unchanged. The resulting band systems consist then of thoroughly overlapped sequences with  $\Delta v = 0$  being by far the most intense.

Single-mode cw dye laser excitation spectroscopy has been shown to be a powerful

<sup>1</sup> This research was supported by the National Science Foundation under Grant NSF-75-23621 and the Air Force Office of Scientific Research under Grant AFOSR-73-2565.

THIS PAGE IS BEST QUALITY PRACTICABLE  
FROM COPY FURNISHED TO DDC

tool in the analysis of complex spectra (2, 3). An excitation spectrum is a record of the total unresolved photoluminescence intensity as the laser frequency is swept. As such, it constitutes essentially the same information as a Doppler width limited absorption spectrum but with much increased sensitivity. In addition, each line of an excitation spectrum may be independently and unambiguously assigned by recording the resolved photoluminescence. For further discussion of the general technique see Refs. (2, 3).

## II. EXPERIMENTAL DETAILS

The production of  $\text{SrF}$  was accomplished in a fashion similar to that of other work carried out in this laboratory on alkaline earth oxides and halides (2, 4). Strontium vapor, produced in a heated alumina crucible, is entrained in an argon carrier gas. An oxidant,  $\text{SF}_6$ , is injected above the crucible producing visible reddish chemiluminescence. Figure 1 shows a trace of a portion of the spectrum from 575 to 665 nm. The  $\Delta v = 0$  sequences of both spin-orbit components of the  $A-X$  transition are apparent at 650 and 660 nm along with the  $\Delta v = 0$  sequence of the  $B-X$  system at 580 nm. Only the latter system was rotationally analyzed, because the  $A-X$  system is beyond the present tuning range of the dye laser.

A Spectra-Physics Model 580 cw dye laser operating single mode (bandwidth 20 MHz) was used for all excitation spectra. A small portion of the laser output was directed to a 3-GHz FSR spectrum analyzer, while the main beam was mechanically chopped at about 4 kHz and directed into the reaction cell. The dye laser was not scanned continuously but rather in 500-MHz steps corresponding to the cavity mode spacing. The Doppler width of lines at the operating temperature,  $\sim 650$  K, was between 900 and 1200 MHz and therefore no spectral information was lost in the excitation spectrum. A typical scan is shown in Fig. 2. For precise line position measurements a small portion of the laser beam was directed to a cell containing  $\text{I}_2$  vapor to simultaneously record

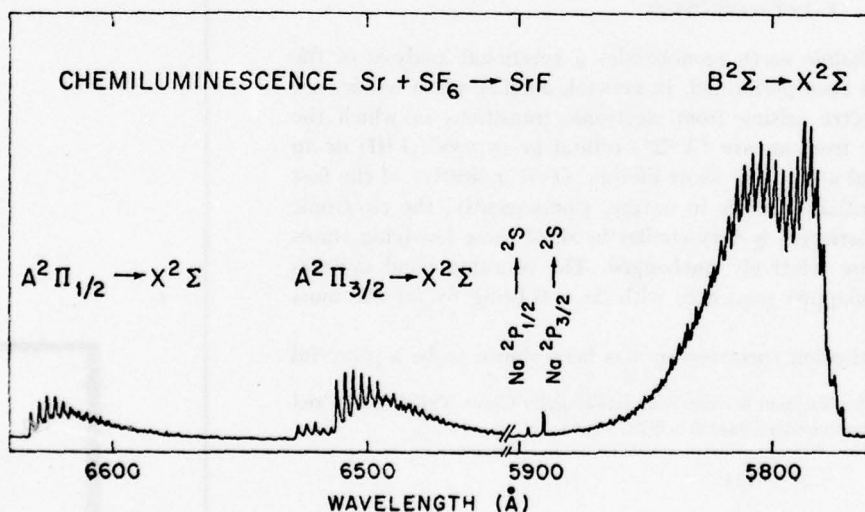


FIGURE 1

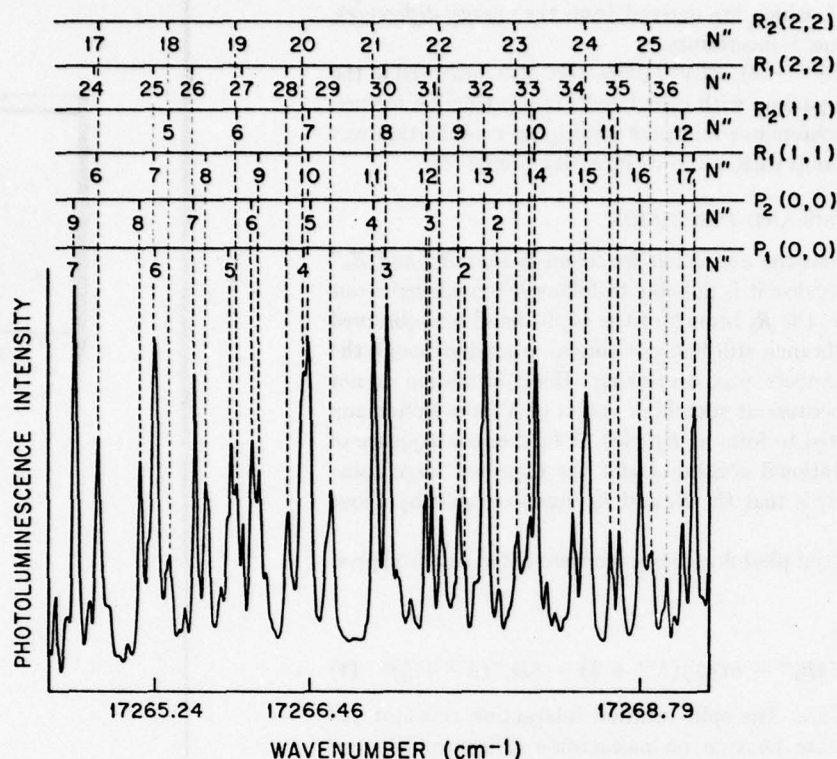


FIGURE 2

excitation spectra of both samples on a dual trace recorder. Absolute line positions of  $I_2$  are known to  $\pm 0.004 \text{ cm}^{-1}$  from the very recent interferometric measurements of Gerstenkorn and Luc (5).

After completing a scan the laser was set to a particular feature in the excitation spectrum and the resolved photoluminescence spectrum measured through a 1-m monochromator having a band pass of about 0.04 nm. Measurement of the  $P$ - $R$  spacings in the photoluminescence spectrum easily establishes the  $J$  numbering (2, 3). The separations of the  $P$ - $R$  doublets in the photoluminescence could be measured to  $\pm 0.2 \text{ cm}^{-1}$  whereas the line positions in the excitation spectrum could be measured to about  $0.02 \text{ cm}^{-1}$  with respect to the superimposed  $I_2$  spectrum. The laser was then tuned to the next line in the excitation spectrum and the process repeated. Every line in the excitation spectrum was assigned by this method until a sufficient number were obtained to be free from ambiguity; pattern recognition was then used to extrapolate further branch numbering.

Ground-state vibrational constants were obtained by measuring the positions of a  $P_1(29)$ ,  $R_1(27)$  pair in the (1, 0), (1, 1), and (1, 2) bands relative to standard Ne lines. The position of the standard Ne lamp was not changed between measurements so that alignment errors, which can produce about  $\pm 0.5 \text{ cm}^{-1}$  uncertainty in the absolute energy,



are cancelled. Values of  $\omega_e''$  and  $\omega_e x_e''$ , which are derived from the energy differences, will thus have absorbed less than  $0.5 \text{ cm}^{-1}$  uncertainty.

The relative intensities of several  $P(N'' + 2)$ ,  $R(N'')$  pairs were also measured in the (1, 0), (1, 1), and (1, 2) bands for comparison with calculated Franck-Condon factors. The wavelength response of the monochromator and photomultiplier combination was calibrated using a standard tungsten lamp with a known intensity profile (6).

### III. ANALYSIS AND DISCUSSION

One immediate feature apparent from the excitation spectrum is that  $B_v'$  and  $B_v''$  are very similar but that  $B_v' < B_v''$  because it is possible to follow  $R$ -branch series out to very high values of  $N$ . For example, the  $R_2$  branch of the (0, 0) band was observed to extend to  $R_2(132)$ . At this  $N''$  the branch still had not turned around although the spacing between adjacent branch members was decreasing. Head formation is not particularly distinct in the spectrum because at such high values of  $N''$  the Boltzmann population is low. The head is calculated to form at  $R_2(145)$ . A further consequence of this small difference between the rotational constants and the expected large spin-rotation constant in the  $B^2\Sigma^+$  state (8) is that the  $R_1$  and  $R_2$  heads are split by about  $19 \text{ cm}^{-1}$ .

The  $P$ - $R$  separations from the resolved photoluminescence were fitted to the expression (7):

$$\begin{aligned} \Delta_2 F(N'') &= F(N'' + 1) - F(N'' - 1) \\ &= (4B_v'' - 6D_v'')(N'' + \tfrac{1}{2}) - 8D_v''(N'' + \tfrac{1}{2})^2 \quad (1) \end{aligned}$$

using a weighted least-squares procedure. The spin-rotation interaction constant  $\gamma_v''$  was assumed small for the  $X^2\Sigma^+$  state because no measurable difference between  $P_1$ - $R_1$  and  $P_2$ - $R_2$  separations was observed; this constant was thus neglected in the fit. The accuracy of the fit and comparison of the  $B_0''$  with the previous value reported by Barrow and Beale (9) confirms the rotational assignment. The values of the  $B_v''$  and their associated uncertainties were also used as initial estimates in fitting the excitation spectra data. The data are not sufficiently precise to derive accurate values for  $D_v''$  although the range certainly encompasses the value obtained from the Kratzer relation.

Line positions in the excitation spectrum were fitted to the standard expressions (7)

$$R_1(N) = \nu_0 + F_1'(N + 1) - F_1''(N), \quad (2)$$

$$R_2(N) = \nu_0 + F_2'(N + 1) - F_2''(N), \quad (3)$$

$$P_1(N) = \nu_0 + F_1'(N - 1) - F_1''(N), \quad (4)$$

$$P_2(N) = \nu_0 + F_2'(N - 1) - F_2''(N), \quad (5)$$

where

$$F_1(N) = B_v N(N + 1) - D_v N^2(N + 1)^2 + \gamma_v N/2 \quad (6)$$

and

$$F_2(N) = B_v N(N + 1) - D_v N^2(N + 1)^2 - \gamma_v(N + 1)/2 \quad (7)$$

by a weighted least-squares procedure. The line positions and their assignments used in the fit are collected in Table I. Eight significant figures are retained in the quoted line

TABLE I  
Measured and Calculated Line Positions ( $\text{cm}^{-1}$ ) in the Excitation Spectra of SrF

Line	Frequency <sup>a</sup>	$\Delta v$ <sup>b</sup>	Line	Frequency	$\Delta v$	Line	Frequency	$\Delta v$
(0,0) band								
P <sub>2</sub> (2)	17263.042(20)	-0.005	P <sub>2</sub> (17)	17256.486(20)	-0.003	R <sub>1</sub> (27)	17275.200(20)	-0.026
(3)	62.460(32)	-0.014	(18)	55.989(28)	-0.031	(28)	75.576(20)	-0.012
(4)	61.895(30)	-0.003	(19)	55.538(20)	-0.011	(29)	75.941(20)	-0.006
(5)	61.327(20)	0.006	(20)	55.070(22)	-0.006	(30)	76.308(20)	0.004
(6)	60.740(35)	-0.001	(21)	54.584(24)	-0.017	(31)	76.648(30)	-0.010
(7)	60.146(27)	-0.012	(22)	54.120(20)	-0.003	(32)	77.001(20)	-0.008
(8)	59.576(20)	0.002	(23)	53.629(20)	-0.014	(33)	77.372(24)	0.013
(9)	58.980(20)	0.002	(24)	53.151(20)	-0.010	(34)	77.694(20)	-0.011
(10)	58.400(20)	0.002	(25)	52.684(26)	0.006			
(11)	57.838(20)	0.031	(26)	52.192(28)	0.001	R <sub>2</sub> (1)	17265.314(20)	-0.003
(12)	57.202(24)	-0.011	(27)	51.709(24)	0.006	(3)	66.436(20)	-0.002
(13)	56.601(28)	-0.017	(28)	51.222(26)	0.010	(4)	67.010(20)	0.014
(14)	55.989(20)	-0.031	(29)	50.739(20)	0.020	(5)	67.553(20)	0.003
(15)	55.408(20)	0.011	(30)	50.230(20)	0.006	(6)	68.088(20)	-0.014
(16)	54.820(20)	0.002	(31)	49.716(20)	-0.010	(7)	68.652(20)	-0.001
(17)	54.193(20)	-0.020	(32)	49.248(20)	0.020	(8)	69.201(20)	0.001
(18)	53.599(20)	-0.007	(33)	48.723(20)	-0.003	(9)	69.782(20)	0.036
(19)	53.006(20)	0.008	(34)	48.236(22)	0.013	(10)	70.305(33)	0.016
(20)	52.378(20)	-0.008				(11)	70.867(28)	0.037
(21)	51.782(20)	0.009	R <sub>1</sub> (0)	17264.564(20)	0.016	(12)	71.373(20)	0.005
(22)	51.149(23)	-0.008	(1)	64.975(20)	0.001	(14)	72.434(20)	-0.003
(23)	50.516(22)	-0.023	(2)	65.407(20)	0.009	(15)	72.940(27)	-0.028
(24)	49.935(20)	0.015	(3)	65.852(20)	0.032	(16)	73.497(20)	0.000
(25)	49.287(20)	-0.011	(4)	66.234(26)	-0.005	(17)	74.025(20)	0.001
(26)	48.670(20)	-0.003	(5)	66.653(20)	-0.003	(18)	74.545(33)	-0.003
(27)	48.051(20)	0.003	(6)	67.056(20)	-0.014	(19)	75.064(20)	-0.005
(28)	47.401(20)	-0.018	(7)	67.491(20)	0.008	(20)	75.576(27)	-0.012
(29)	46.803(20)	0.015	(8)	67.893(20)	0.000	(21)	76.107(20)	0.002
(30)	46.188(20)	0.032	(9)	68.302(26)	0.002	(22)	76.612(37)	-0.007
(31)	45.528(30)	0.007	(10)	68.699(20)	-0.006	(23)	77.115(20)	-0.016
			(11)	69.096(31)	-0.012	(24)	77.631(20)	-0.009
P <sub>2</sub> (2)	17263.265(20)	0.009	(12)	69.543(20)	0.034	(25)	78.142(20)	-0.005
(3)	62.803(20)	-0.017	(13)	69.911(20)	0.004	(26)	78.653(20)	0.001
(4)	62.354(20)	-0.028	(14)	70.305(28)	0.002	(27)	79.139(20)	-0.014
(5)	61.942(20)	-0.001	(15)	70.678(20)	-0.017	(28)	79.656(20)	0.003
(6)	61.499(20)	-0.002	(16)	71.097(20)	0.010	(29)	80.186(20)	0.035
(7)	61.066(20)	0.009	(18)	71.839(32)	-0.022	(30)	80.635(20)	-0.009
(8)	60.605(20)	-0.005	(19)	72.245(20)	0.000	(31)	81.149(20)	0.012
(9)	60.146(20)	-0.015	(20)	72.628(20)	0.001	(32)	81.658(20)	0.032
(10)	59.720(20)	0.010	(21)	73.044(27)	0.038	(33)	82.109(20)	-0.004
(11)	59.259(20)	0.003	(22)	73.381(20)	-0.001	(34)	82.594(20)	-0.003
(12)	58.816(20)	0.015	(23)	73.773(20)	0.017	(35)	83.071(20)	-0.008
(13)	58.354(20)	0.011	(24)	74.136(30)	0.009	(36)	83.539(20)	-0.019
(14)	57.887(20)	0.004	(25)	74.545(37)	0.049	(37)	84.036(20)	0.001
(15)	57.421(20)	0.000	(26)	74.858(20)	-0.004	(38)	84.512(20)	0.003
(16)	56.919(20)	-0.037				(39)	84.964(20)	-0.016
						(40)	85.924(20)	0.008

<sup>a</sup>The numbers in parentheses represent a one standard deviation estimate of the measured line position.

<sup>b</sup>The value  $\Delta v$  represents the difference between observed and calculated line position.

frequencies although the measurement uncertainty is in the seventh figure; this is done simply to enable any further workers who may desire to treat the data using a different model to derive constants without encountering any round-off errors. Similarly, because of the sensitivity of parameters to uncertainties in line positions, particularly at low  $N$  values, the uncertainty in the last digit is quoted in parentheses. Measurement uncertainties were estimated as described previously (2). The values of the  $D_v$ 's, as determined by the Kratzer relation, were held as fixed parameters. Because of the large correlation coefficients between the same parameters in both states ( $B_v'$ ,  $B_v''$  and  $\gamma_v'$ ,  $\gamma_v''$ ) the diagnostic least-squares procedure described by Curl (10) proved necessary to

TABLE I—Continued

Line	Frequency <sup>a</sup>	$\Delta v^b$	Line	Frequency	$\Delta v$	Line	Frequency	$\Delta v$
(1,1 band)								
P <sub>1</sub> (3)	17255.779 (38)	0.010	P <sub>2</sub> (20)	17248.424 (20)	-0.001	R <sub>1</sub> (27)	17268.413 (20)	0.002
(4)	55.206 (20)	-0.038	(21)	47.952 (20)	0.000	(28)	68.733 (25)	-0.034
(5)	54.584 (33)	0.009	(22)	47.500 (20)	0.022	(29)	69.096 (31)	-0.025
(6)	54.067 (20)	0.021	(23)	46.979 (20)	-0.021	(30)	69.484 (20)	0.011
(7)	53.460 (26)	-0.007	(24)	46.519 (20)	-0.001	(31)	69.811 (24)	-0.011
(8)	52.896 (20)	0.010	(25)	46.046 (20)	0.007	(34)	70.867 (28)	0.014
(9)	52.322 (28)	0.020	(26)	45.528 (20)	-0.026	(50)	75.941 (23)	0.018
(10)	51.709 (30)	-0.007				(51)	76.212 (30)	-0.003
(11)	51.122 (20)	-0.006	R <sub>1</sub> (1)	17258.270 (50)	0.014	(55)	77.372 (27)	0.020
(12)	50.516 (30)	-0.021	(2)	58.672 (30)	-0.004			
(13)	49.935 (20)	-0.010	(3)	59.098 (20)	0.003	R <sub>2</sub> (3)	17259.720 (43)	0.010
(14)	49.338 (40)	-0.012	(4)	59.526 (36)	0.015	(4)	60.295 (30)	0.032
(15)	48.723 (40)	-0.030	(5)	59.936 (20)	0.012	(5)	60.853 (36)	0.038
(16)	48.150 (20)	-0.004	(6)	60.319 (30)	-0.016	(6)	61.359 (20)	-0.004
(17)	47.541 (40)	-0.011	(7)	60.740 (30)	-0.004	(7)	61.942 (27)	0.031
(18)	46.950 (20)	0.021	(8)	61.146 (33)	-0.004	(8)	62.460 (24)	0.005
(19)	46.363 (20)	0.001	(9)	61.601 (20)	0.046	(9)	62.998 (20)	0.001
(20)	45.763 (20)	0.029	(10)	61.942 (24)	-0.014	(10)	63.532 (20)	-0.004
(21)	45.093 (20)	-0.030	(11)	62.354 (20)	-0.002	(11)	64.067 (20)	-0.006
P <sub>2</sub> (3)	17256.118 (35)	0.000	(14)	63.532 (20)	-0.007	(12)	64.614 (20)	0.006
(4)	55.667 (30)	-0.017	(15)	63.930 (25)	0.001	(14)	65.676 (20)	0.006
(5)	55.207 (20)	-0.040	(16)	64.302 (20)	-0.014	(15)	66.193 (20)	-0.004
(6)	54.820 (30)	-0.006	(17)	64.692 (20)	-0.008	(16)	66.722 (20)	0.000
(7)	54.354 (20)	-0.010	(18)	65.080 (20)	-0.003	(18)	67.788 (20)	0.023
(8)	53.943 (22)	0.019	(19)	65.452 (30)	-0.011	(19)	68.302 (27)	0.019
(9)	53.460 (26)	-0.018	(20)	65.852 (30)	0.011	(20)	68.796 (20)	-0.001
(11)	52.600 (20)	0.020	(21)	66.234 (30)	0.019	(21)	69.337 (20)	0.026
(12)	52.099 (20)	-0.028	(22)	66.582 (20)	-0.005	(22)	69.811 (30)	-0.007
(14)	51.222 (33)	0.007	(23)	66.928 (31)	-0.029	(23)	70.305 (24)	-0.022
(16)	50.306 (20)	0.012	(24)	67.327 (20)	0.002	(24)	70.807 (25)	-0.025
(17)	49.853 (20)	0.023	(25)	67.675 (30)	-0.014	(35)	76.212 (28)	-0.002
			(26)	68.056 (20)	0.005	(36)	76.648 (30)	-0.040
						(37)	77.694 (28)	0.005
(2,2 Band)								
P <sub>1</sub> (5)	17247.812 (20)	0.025	R <sub>1</sub> (18)	17258.152 (20)	0.008	R <sub>2</sub> (5)	17253.943 (33)	0.002
(7)	46.665 (20)	0.027	(19)	58.526 (20)	0.007	(6)	54.502 (20)	0.016
(8)	46.046 (20)	-0.015	(20)	58.887 (20)	-0.004	(7)	54.990 (20)	-0.038
(10)	46.188 (20)	-0.005	(21)	59.259 (35)	-0.002	(8)	55.538 (20)	-0.031
P <sub>2</sub> (7)	17247.541 (20)	-0.002	(22)	59.641 (20)	0.013	(9)	56.118 (28)	0.011
(8)	47.113 (20)	0.009	(23)	60.008 (20)	0.015	(11)	57.163 (20)	-0.013
(9)	46.665 (20)	0.003	(24)	60.319 (32)	-0.036	(12)	57.701 (20)	-0.005
(10)	46.188 (20)	-0.029	(25)	60.740 (43)	0.026	(13)	58.270 (35)	0.035
(11)	45.763 (20)	-0.008	(26)	60.066 (26)	-0.005	(16)	59.799 (20)	-0.006
(12)	45.330 (20)	0.007	(27)	61.422 (20)	-0.003	(17)	60.319 (20)	-0.004
R <sub>1</sub> (3)	17252.322 (33)	0.065	(28)	61.768 (20)	-0.009	(18)	60.853 (30)	0.014
(4)	52.684 (30)	0.048	(29)	62.120 (20)	-0.005	(19)	61.359 (30)	0.006
(5)	53.006 (30)	-0.039	(31)	62.803 (20)	-0.012	(21)	62.354 (22)	-0.017
(6)	53.460 (20)	0.008	(32)	63.160 (20)	0.003	(22)	62.882 (20)	0.004
(7)	53.851 (33)	-0.005	(33)	63.483 (20)	-0.011	(23)	63.377 (20)	-0.003
(8)	54.286 (23)	0.027	(34)	63.832 (20)	0.002	(24)	63.930 (25)	0.049
(10)	55.070 (33)	0.015	(35)	64.170 (20)	0.007	(25)	64.388 (20)	0.009
(11)	55.408 (20)	-0.019	(36)	64.504 (20)	0.012	(26)	64.877 (20)	0.002
(12)	55.826 (20)	-0.016	(37)	64.820 (20)	0.001	(28)	65.852 (30)	-0.005
(13)	56.225 (20)	-0.007	(39)	65.452 (33)	-0.012	(31)	67.327 (37)	0.015
(14)	56.601 (28)	-0.018	(45)	67.327 (22)	-0.004	(32)	67.788 (20)	-0.002
			R <sub>2</sub> (4)	17253.387 (20)	-0.006	(34)	68.733 (28)	-0.007

remove the numerical difficulties of the near singularity in the product  $(X, \bar{X})$  matrix.  $X$  is the Jacobian matrix (11). Initial estimates of the parameters and their associated uncertainties were obtained as follows.  $B_v''$  was obtained from the fit to the  $P$ - $R$  separation data.  $B_v'$  was estimated from the  $N$  value at the  $R_2$  head (2) in conjunction with the value of  $B_v''$ . The  $B$  state spin-rotation constant  $\gamma_v'$  was estimated on the basis of the pure precession unique perturber interaction (8, 12) between the  $A^2\Pi$  and  $B^2\Sigma^+$  states while  $\gamma_v''$  was assumed small and set equal to zero. In all cases our data better determine the parameters than the initial estimates; the diagnostic method of constraining poorly determined parameters proved unnecessary.



TABLE II  
Spectroscopic Constants ( $\text{cm}^{-1}$ )<sup>a</sup> of  $^{87}\text{SrI}^*$

	$X^2\Sigma^+$	P-R Data <sup>b</sup>	$B^2\Sigma^+$	$R(XB)^c$	$\Delta(XB)^d$
$B_0$	0.24985(5)	0.2517(20)	0.24870(4)	0.995	-0.001146(5)
$B_1$	0.24819(8)	0.2488(16)	0.24704(8)	0.998	-0.001153(6)
$B_2$	0.24626(19)	0.2477(23)	0.24509(18)	0.999	-0.001170(12)
$\gamma_2$	0.0018(37)		-0.1361(37)	0.999	-0.13786(18)
$\gamma_1$	0.0048(30)		-0.1329(29)	0.996	-0.13777(27)
$\gamma_2$	0.0049(30)		-0.1336(29)	0.995	-0.13848(31)
$\hat{\alpha}_e$	0.25075(9)		0.24961(9)		-0.001139(8)
$\alpha_e$	0.00174(9)		0.00175(8)		-0.000011(7)
$\alpha_e$	0.00151(7)	(Pekeris)	0.00155(7)		
$D_e$	$2.50(1) \times 10^{-7}$	(Kratzer)	$2.53(1) \times 10^{-7}$		
$\omega_e^e$	502.4(7)		495.8(7)		-6.58(1)
$\omega_e x_e^e$	2.27(21)		2.34(21)		0.069(3)
$T_e$	0		17267.42(1)		

<sup>a</sup> Uncertainties in parentheses represent 95% confidence limits in the last digit.

<sup>b</sup> From fit to measured PR separations in the photoluminescence spectra.

<sup>c</sup> Correlation coefficient between like parameters in the X and B states.

<sup>d</sup>  $\Delta(XB)$  is the difference, (B-X), between constants for the two states.

<sup>e</sup> Uncertainties in vibrational constants are estimated assuming the measured differences between lines in the (1,2), (1,1) and (1,0) bands is  $\pm 0.3 \text{ cm}^{-1}$ .

First column row 7 should read  $B_e$ . Row ten columns two and four should read  $\times 10^{-7}$ .

The square root of the variance of the fits to the (0, 0), (1, 1), and (2, 2) bands were 0.015, 0.018, and  $0.020 \text{ cm}^{-1}$ , respectively. The constants derived from the fit are collected in Table II. For comparison, the  $B_v''$  values obtained from the P-R separation included. The excellent agreement of the  $B_v''$  values from the two methods fully confirms the rotational assignment and supports the method of data treatment. Having obtained three values of  $B_v$  it is possible to determine  $B_e$  and  $\alpha_e$  for both states. These values are also collected in Table II along with the  $\alpha_e$  obtained from the Pekeris relation (13).

Our rotational analysis also determines values of the energy differences between the (0, 0), (1, 1), and (2, 2) vibrational band origins which in turn give precise values of the differences in vibrational constants ( $\omega_e' - \omega_e''$ ) and ( $\omega_e x_e' - \omega_e x_e''$ ) by standard formulae (7). These accurate differences indicated a deviation from hitherto accepted values of vibrational constants in the  $X^2\Sigma^+$  (14, 15) and  $B^2\Sigma^+$  states (16). The resolved photoluminescence measurements of the  $P_1(29)$  and  $R_1(27)$  line positions in the (1, 2), (1, 1), and (1, 0) bands, after being corrected for rotational energy contributions, yield values of  $\omega_e''$  and  $\omega_e x_e''$ . These values, and the above differences in turn give  $\omega_e'$  and  $\omega_e x_e'$ . These vibrational constants are also collected in Table II and, being derived from

band origin rather than from bandhead data, are superior to previous determinations.

In recent years it has become apparent that there are good reasons for not using such simplistic expressions as Eqs. (6) and (7) for the energy eigenvalues. Rather, we should construct the complete Hamiltonian matrix for both states, diagonalize them and, with initial estimates of the various parameters and consideration of selection rules, obtain the line positions. Such a procedure, along with an extensive discussion of its advantages, has been presented by Zare and co-workers (12). In particular, the energy expressions in Eqs. (6) and (7), when applied to an excited electronic  $^2\Sigma^+$  state with a close-lying  $^2\Pi$  state, lose the original meaning of particular parameters. For example, the rotational constant  $B_v$  is based on a quantum mechanical average over the vibrational state of the inverse square of the internuclear distance,  $\langle 1/r^2 \rangle$ . However, in addition to  $B'$ , which has an  $N(N+1)$  energy dependence, an additional term,  $q$ , due to magnetic interactions with the  $^2\Pi$  state, arises. Because of the same  $N$  dependence in the eigenvalues the strictly mechanical  $B_v$  is contaminated with a magnetic contribution. The original work on calculating the matrix elements of this more complete Hamiltonian was performed by Van Vleck (8) and put into a more convenient form by Mulliken and Christy (17). In considering the interaction between the electronic block of the  $B^2\Sigma^+$  state with a close-lying  $A^2\Pi$  state, three terms,  $o$ ,  $p$ , and the previously mentioned  $q$ , need to be included in the energy matrix for the  $B^2\Sigma$  state. The  $N$  dependence of the  $q$  term is the same as that of  $B_v$ , the  $N$  dependence of the  $p$  term is the same as the phenomenological constant  $\gamma$  while  $o$  has no  $N$  dependence and thus contributes to  $T_e$ . It should be noted that even in the absence of this electronic perturbation the eigenvalues of individual electronic blocks have terms of the form  $+\gamma N/2$  and  $-\gamma(N+1)/2$ , but in an excited state this effect is normally outweighed by the interactions with other electronic blocks. In the case where the  $^2\Sigma$  and  $^2\Pi$  states can be described as arising from the same atomic configuration, where  $L$  is considered to be a good quantum number, then  $o$ ,  $p$ , and  $q$  reduce to simple expressions. This is the case of a pure precession-unique perturber (12) interaction and should be rather good for alkaline earth halides because the electronic transition is essentially atomic  $ns \rightarrow np$  in nature with the  $A^2\Pi$  and  $B^2\Sigma$  states derived from the  $L=1$  projections onto the internuclear axis. Note also that the  $E_\Sigma - E_\Pi$  separation is sufficiently large that the anomalies encountered in spin-splitting constants in alkaline earth hydrides are not expected in the halides. An extended treatment such as that given by Veseth (18) is then unnecessary. The pure precession estimate of  $p$  which is assumed to be the dominant contributor to  $\gamma'$  is given by

$$p = 4A_\Pi B_v (E_\Sigma - E_\Pi) = 0.134 \text{ cm}^{-1}, \quad (8)$$

where  $A$  is the spin-orbit coupling constant in the  $A^2\Pi$  state. This value is in excellent agreement with the experimental parameter  $\gamma' = -p = -0.134 \text{ cm}^{-1}$  which further suggests that the contribution of  $q \approx (B_v p / A_\Pi)$  to the experimental rotational constant can be estimated. This correction of  $q = 0.00012 \text{ cm}^{-1}$  to the experimental  $B'$  to obtain an uncontaminated rotational constant is small but it may have particularly noticeable effects. Franck-Condon (FC) factors, which are sensitive functions of the change in rotational constants between the two states, are one such aspect.

In an attempt to further verify the magnetic contamination of  $B'$ , experimental FC factors were determined from the resolved laser-induced photoluminescence intensities and compared with calculated values based on an RKR potential (19). Calculations were

performed with  $B_v' = 0.24961 \text{ cm}^{-1}$  and, after correction for  $q$ ,  $B_v' = 0.24949 \text{ cm}^{-1}$ . The effects are small, namely an increase of about 10% in the off diagonal FC factors which are about 0.005, but this distinction should be measurable using laser-induced photoluminescence.

When a particular  $(v', J')$  level is excited the emission intensity is given approximately by the expression (20)

$$I_{v'v''} = K N_{v'J'} \nu_{v'v''}^4 |R_{v'v''}|^2 S_{v'v''} S_{J'J''}. \quad (9)$$

Single-line laser excitation produces several simplifications. First,  $N_{v'J'}$ , the number of (modulated) molecules in the upper state, is constant because it is populated only by the chopped laser and only these molecules are detected in the ac photoluminescence. Second, the rotational line strength contribution  $S_{J'J''}$  to all  $(v', v'')$  bands measured should be the same because only the same  $J$  values are measured. Consequently, the relative FC factors can be simply expressed as

$$S_{v'v''_1}/S_{v'v''_2} = I_{v'v''_1\nu_{v'v''_2}^4}/I_{v'v''_2\nu_{v'v''_1}^4}. \quad (10)$$

Experimental FC factors are then obtained from measurement of relative intensities of the same rotational lines in the (1, 0), (1, 1), and (1, 2) bands while pumping a particular rotational coincidence in the (1, 1) band. All  $|\Delta v| \geq 2$  transitions are neglected because of vanishingly small intensity. The expected photoluminescence spectrum consists then of three sets ( $\Delta v = 0, \pm 1$ ) of  $P$ - $R$  doublets with  $\Delta v = 0$  about 200 times more intense than  $\Delta v = \pm 1$ . Furthermore, the relative intensities of the  $P$  and  $R$  lines should be constant for the three pairs.

Unfortunately, the above simple expectations are not verified experimentally. The relative intensities of the  $P$  and  $R$  branches vary by almost a factor of two between the (1, 0) and (1, 2) bands and simple Hönl-London formulae (7) do not apply. In addition, it is observed that  $I(P_1) < I(R_1)$  and  $I(P_2) > I(R_2)$ ; that is, the relative line strengths of  $P$  and  $R$  branches reverse in the different spin manifolds. As an illustration, Table III lists some typical experimental measurements of relative intensities for different vibrational bands in both spin manifolds. A similar observation of "anomalous" branch intensities has been noted in several vibrational bands of the  $B^2\Sigma^- - X^2\Sigma^+$  system of  $\text{HgH}$  (21). Kopp and Hougen (22) have developed formulas for the branch intensities of  $\Delta\Omega = 0, \pm 1$  transitions in mixed (case  $(a')$ )  $\Omega = \frac{1}{2}$  states which explains such variations in terms of the relative values of the parameters  $\mu_{11}$  and  $\mu_{\perp}$ .  $\mu_{11} = 0, \mu_{\perp} = 1$  corresponds to a pure case (a)  $\Delta\Omega = \pm 1$  transition while  $\mu_{\perp} = 0, \mu_{11} = 1$  refers to a pure case (b)  $\Delta\Omega = 0$  transition. Intermediate values refer to differing extents of case  $(a')$  coupling. The explanation of the different branch intensities in different vibrational band systems must be considered as arising from of the  $B^2\Sigma - A^2\Pi$  interaction and its vibrational dependence. Different vibrational bands must be considered as arising from different degrees of intermediate case  $(a')$  coupling as a result of the vibrational dependence of the  $B^2\Sigma - A^2\Pi$  mixing. Experimentally, the largest variation from a pure case (b)  $^2\Sigma$  state occurs in the (1, 2) band where  $\mu_{11}, \mu_{\perp} \sim 8$ . However, in spite of the large variation in relative rotational line strengths the sum of the line strengths varies only slightly with such coupling because of the near cancellation of the cross terms  $\mu_{\perp}\mu_{11}$  in the summation. For example, for  $J = 20.5$  and  $\mu_{\perp} = 0.1\mu_{11}$ , the sum of the intensities  $P_1(21.5) + P_{12}(20.5)$



TABLE III

Comparison of Relative Intensities<sup>1,2</sup> of Several Rotational Lines in the  $(1, v')$  Bands of  $\text{SrF}$ 

Line	VIBRATIONAL BAND		
	(1,2)	(1,1)	(1,0)
$P_1(24)$	0.0047	0.988	0.0069
$R_1(27)$	0.0071	0.987	0.0061
$P_1(18)$	0.0040	0.989	0.0065
$R_1(16)$	0.0065	0.987	0.0059
$P_2(16)$	0.0052	0.989	0.0060
$R_2(14)$	0.0033	0.991	0.0061
$P_2(20)$	0.0061	0.988	0.0055
$R_2(18)$	0.0038	0.991	0.0054

<sup>1</sup>The estimated uncertainty is 10% in the (1,0) and (1,2) bands with the (1,1) band known to better than 1% accuracy.

<sup>2</sup>Specifically, the values listed above are  $(1/v_{v',v''}^4) / \sum_{v''} (I/v_{v',v''}^4)$ , where  $I$  is the measured intensity corrected for instrument response.

$+R_1(19.5)$  is only 2% larger than a pure case (b),  $\mu_1 = 0$ , sum. In contrast, the relative intensities of  $P_1(21.5) + P_{Q_{12}}(20.5)$  and  $R_1(19.5)$  varies by almost a factor of 2.

With the above realizations that the true meaning of FC factors has been clouded somewhat by several assumptions, the experimental intensity sums were used to derive the FC factors collected in Table IV. Agreement of experimental and calculated values

TABLE IV

Comparison of Experimental and Calculated Franck-Condon Factors

$(v', v'')$	$S_{v', v''}$		
	<u>Experimental<sup>1</sup></u>	<u>Calculated<sup>2</sup></u>	
		$B'_e = B'_e(\text{experimental})$	$B'_e = B'_e(\text{experimental}) - q_L$
	(I)	(II)	(III)
(1,0)	0.0061	0.0027	0.0032
(1,1)	0.9885	0.9918	0.9907
(1,2)	0.0054	0.0055	0.0061

<sup>1</sup>The estimated uncertainty in  $\Delta v = \pm 1$  factors is 10% with  $\Delta v = 0$  known to better than 1%.

<sup>2</sup>Parameters are as defined in the text;  $q_L$  is the extent of magnetic contamination of the rotational constant. Based on a unique perturber estimate (12)  $q_L = 0.00012 \text{ cm}^{-1}$ .

for the (1, 1) and (1, 2) bands is within experimental error but the measured value for (1, 0) is too large by a factor of 2. This discrepancy far exceeds the calculated 10% change which results from using a realistic  $B_e'$  value. Hence the correction of  $B'$  for magnetic contributions from the  $A^2\Pi$  state is insignificant when compared with other causes of discrepancies between observed and calculated FC factors. The reason for these differences lies in the extraction of experimental FC factors using Eqs. (9) and (10). Implicit in these expressions are several assumptions concerning the separability of the electronic, vibrational, and rotational motions. For example, the slow variation of the electronic transition moment with internuclear distance is assumed, thus allowing a separation into a product of an electronic term and an FC factor,  $|R_{e'e''}|^2 S_{v'v''}$ . Perhaps, in view of the presently unknown  $A^2\Pi$  state constants and incomplete perturbation analysis, it is best to treat the intensity measurements as raw data and not to attempt to extract meaningful FC factors.

Finally, it should be mentioned that Microwave-Optical-Double-Resonance (MODR) measurements (23, 24) have been made derive more accurate values of ground-state constants. The precision exemplified in microwave measurements is thus projected into constants for both states because of the high degree of correlation in the optical data.

#### ACKNOWLEDGMENTS

We warmly acknowledge discussion of the computational methods with Brian G. Wicke and the use of his computer programs.

RECEIVED: May 16, 1977

#### REFERENCES

1. P. J. DAGDIGIAN, H. W. CRUSE, AND R. N. ZARE, *J. Chem. Phys.* **60**, 2330 (1974).
2. P. J. DOMAILLE, T. C. STEIMLE, NING-BEW WONG, AND D. O. HARRIS, *J. Mol. Spectrosc.* **65**, 354 (1977).
3. R. W. FIELD, D. O. HARRIS, AND T. TANAKA, *J. Mol. Spectrosc.* **57**, 107 (1975).
4. J. W. WEST, R. S. BRADFORD, JR., J. D. EVERSOLE, AND C. R. JONES, *Rev. Sci. Instrum.* **46**, 164 (1975).
5. S. GERSTENKORN AND P. LUC, "Atlas du Spectre d'Absorption de la Molecule d'Iode Partie I." Laboratoire Aime-Cotton CNRSII 91405 Orsay, France, private communication.
6. R. STAIR, W. E. SCHWEIDER, AND J. K. JACKSON, *Appl. Opt.* **2**, 1151 (1963).
7. G. HERZBERG, "Spectra of Diatomic Molecules," Van Nostrand, Princeton, N. J., 1950.
8. J. H. VAN VLECK, *Phys. Rev.* **33**, 467 (1929).
9. R. F. BARROW AND J. R. BEALE, *Chem. Comm.* **12**, 606 (1967).
10. R. F. CURL, JR., *J. Comput. Phys.* **6**, 367 (1970).
11. D. L. ALBRITTON, A. L. SCHMELTEKOPF, AND R. N. ZARE, in "Molecular Spectroscopy: Modern Research" (K. Narahari Rao and C. Weldon Mathews, Eds.), Vol. II, Academic Press, New York, 1976.
12. R. N. ZARE, A. L. SCHMELTEKOPF, W. J. HARROP, AND D. L. ALBRITTON, *J. Mol. Spectrosc.* **46**, 37 (1973).
13. C. L. PEKERIS, *Phys. Rev.* **45**, 98 (1934).
14. M. M. NOVIKOV AND L. V. GURICH, *Opt. Spectrosc.* **22**, 395 (1967).
15. C. A. FOWLER, JR., *Phys. Rev.* **59**, 645 (1941).
16. R. C. JOHNSON, *Proc. Roy. Soc. Ser. A* **122**, 161 (1929).
17. R. S. MULLIKEN AND A. CHRISTY, *Phys. Rev.* **38**, 87 (1931).
18. L. VESETH, *Mol. Phys.* **20**, 1057 (1971).

19. R. RYDBERG, *Z. Phys.* **73**, 376 (1931); **80**, 514 (1933); O. KLEIN, *Z. Phys.* **76**, 226 (1932);  
A. L. G. REES, *Proc. Phys. Soc.* **59**, 998 (1947).
20. A. SCHADEE, *J. Quant. Spectrosc. Radiat. Transfer* **7**, 169 (1967).
21. R. RYDBERG, *Z. Phys.* **73**, 74 (1931).
22. I. KOPP AND J. T. HOUGEN, *Canad. J. Phys.* **45**, 2581 (1967).
23. P. J. DOMAILLE, T. C. STEIMLE, AND D. O. HARRIS, *J. Mol. Spectrosc.* **68**, 146 (1977).
24. R. W. FIELD, R. S. BRADFORD, D. O. HARRIS, AND H. P. BROIDA, *J. Chem. Phys.* **56**, 4712 (1972).



## The Rotational Spectrum of the $X^2\Sigma^+$ State of the SrF Radical Using Laser Microwave Optical Double Resonance<sup>1</sup>

PETER J. DOMAILLE, TIMOTHY C. STEIMLE, AND DAVID O. HARRIS

*Quantum Institute, Department of Chemistry, University of California,  
Santa Barbara, California 93106*

The pure rotational spectrum of the  $X^2\Sigma^+$  state of the gaseous SrF radical has been measured using microwave optical double resonance (MODR) techniques. The analysis fully confirms the recent dye laser excitation spectrum and rotational assignment of the  $B^2\Sigma^+-X^2\Sigma^+$  system. Transitions were measured in both the  $v'' = 0$  and  $v'' = 1$  states to give values of  $B_v'' = 0.250533 \text{ cm}^{-1}$ ,  $\alpha_v'' = 1.546 \times 10^{-3} \text{ cm}^{-1}$  and  $\gamma''$  (spin-rotation)  $= 2.49 \times 10^{-3} \text{ cm}^{-1}$ . General qualitative features of MODR in  $^2\Sigma^+$  states are treated and suggested improvements for obtaining experimental hyperfine constants are discussed. The more precise ground state constants are merged with the  $B-X$  optical analysis to obtain a more accurate set of constants for both states.

### INTRODUCTION

Rotational spectroscopy of  $^2\Sigma$  state molecules has occupied an intriguing position in conventional microwave methods in that only in the past 2 years have spectra of ground state molecules been recorded and analyzed; Dixon and Woods (1, 2) have reported studies of the CN radical (1) and the  $\text{CO}^+$  ion (2). Earlier, Jefferts had also reported the radiofrequency spectrum of the  $\text{H}_2^+$  ion (3) although his technique has not had far-reaching usage and the method is certainly not conventional. Prior to the CN and  $\text{CO}^+$  studies, previous work of microwave accuracy was restricted to excited electronic states such as  $\text{OH}(A^2\Sigma^+)$  (4) and  $\text{CN}(B^2\Sigma^+)$  (5) in ingenious studies utilizing microwave optical double resonance (MODR). However, the "optical" source in both these experiments were rather restrictive; for OH, a chance coincidence of  $A^2\Sigma^+-X^2\Pi$  with a zinc atomic emission line (4) and for CN an even more amazing chemical pumping and accidental degeneracy between the  $A^2\Pi$  and  $B^2\Sigma$  states (5). These elegant experiments are thus restricted because the optical selection of the rotational states cannot be varied. The single-mode cw tunable dye laser as an optical source removes this restriction, at least for molecules which absorb in the currently accessible dye laser range.

Following the recent rotational analysis of the  $B^2\Sigma^+-X^2\Sigma^+$  system of the SrF radical utilizing single-mode dye laser excitation spectroscopy (6), it became apparent that an MODR study to obtain a ground state ( $X^2\Sigma^+$ ) rotational spectrum of this molecule

<sup>1</sup> This research was supported by the National Science Foundation under Grant NSF-MPS-72-04978 and the Air Force Office of Scientific Research under Grant USAFOSR-73-2565.

was possible. The prime requirement for such a study is simply an optical assignment which extends to sufficiently low rotational quantum numbers that rotational transitions are in a frequency region accessible with normal microwave methods. This requirement was certainly fulfilled in SrF and has allowed a study of several rotational transitions in both the  $v'' = 0$  and  $v'' = 1$  vibrational states. The information provided by such a study is essentially higher-precision spectroscopic constants, but perhaps more importantly, an unambiguous confirmation of the previous optical assignment (6). In addition, it is often possible to observe hyperfine effects which are normally masked by the Doppler width of lines in single-photon optical spectra.

We report here a microwave study of the  $X^2\Sigma^+$  state of SrF which obtains more precise values of the spectroscopic constants  $B_e$ ,  $\alpha_e$ , and  $\gamma$ (spin-rotation). Hyperfine constants were not derived in the present study because of insufficient sensitivity to detect  $\Delta F = 0$  lines and inadequate resolution to separate the pairs of  $\Delta F = 1$  transitions. Improvements in the experiment, discussed in the text, are designed to eliminate these problems and to allow a more thorough study of these finer effects.

## II. GENERAL CONSIDERATIONS OF MODR IN $^2\Sigma^+$ STATES

Several discussions of the generalized three-level scheme describing the features of MODR have been published previously (7, 8). Briefly, a rotational transition,  $J \rightarrow J+1$ , is detected as a change in laser-induced photoluminescence intensity when the laser is tuned to an optical transition which connects either  $J$  or  $J+1$  to an excited electronic state. If the laser does not significantly deplete the pumped level (weak optical pumping), the MODR signal is detected as a change in fluorescence intensity resulting from the Boltzmann inequality between rotational levels. For a typical rotational temperature of 600 K this change is only about 0.1–0.5%. Furthermore, if the laser connects with level  $J$ , the microwave resonance appears as a *decrease* in photoluminescence intensity as molecules are pumped from  $J \rightarrow J+1$ . Conversely, if the laser pumps from level  $J+1$  the MODR appears as an *increase* in photoluminescence intensity. However, in the experiments described below the microwave resonance was always detected as an *increase* of about 5–10% in the photoluminescence intensity when *either*  $J$  or  $J+1$  was optically pumped. The indication then is that strong optical pumping is occurring and the major contribution to the rotational population inequality is the depletion caused by the laser. It is noteworthy that zero MODR intensity may accidentally result when level  $J$  is pumped and the laser intensity is just large enough to cancel the Boltzmann inequality. When searching for a particular resonance, then, it is experimentally wise to optically pump from the upper of two rotational states such as to drive the population difference further from thermal equilibrium.

The MODR of  $^2\Sigma^+$  states has several minor differences from that of  $^1\Sigma$  states discussed previously in the study of BaO (7). Of particular interest is the number of different transitions observed in MODR compared to conventional single-photon microwave absorption experiments. The unpaired electron spin in  $^2\Sigma^+$  state molecules couples to the molecular rotation and produces a doubling of all rotational levels. As a result, a conventional microwave absorption spectrum consists of sets of three lines (corresponding to  $\Delta J = 0, \pm 1$ ) spaced at approximately  $2B$  ( $\Delta N = \pm 1$ ). The relevant connections for an  $N'' = 2 \rightarrow 3$  transition are shown in Fig. 1 by the solid line and dashed lines.

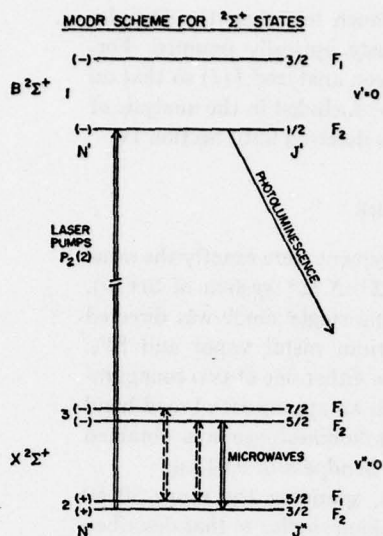


FIG. 1. Schematic of MODR in  $^2\Sigma^+$  states. Solid lines represent possible double-resonance transitions while the additional dashed lines show the two further transitions which would be observed in a conventional microwave spectrum. These dashed lines would also be observed in double resonance by optically pumping  $P_1(2)$ .

In practice, for an  $N \rightarrow N + 1$  transition, the line strengths of  $\Delta J = +1$  transitions increase with increasing  $J$  while for  $\Delta J = 0$  the intensity decreases rapidly with  $J$  (13). Thus, two lines of comparable intensity are expected, separated by  $\gamma$ , the spin doubling constant, and a weaker line displaced in frequency by  $-\gamma(N + 1)$  from the unsplit line center. However, in MODR the situation is altered somewhat because the laser selects one particular spin manifold. In SrF this selection is possible as a consequence of the much larger spin doubling in the  $B^2\Sigma^+$  electronic state caused by the close proximity of the  $A^2\Pi$  state (6, 9). Thus, the optical excitation spectrum shows clearly separated  $P_1$ ,  $P_2$ ,  $R_1$ , and  $R_2$  branches (6). If the laser pumps from the lower of two rotational levels in the  $F_2$  ( $J'' = N'' - \frac{1}{2}$ ) spin manifold, by either pumping a  $P_2(N'')$  or  $R_2(N'')$  coincidence, only one microwave transition is observed, as shown by the solid line in Fig. 1. In contrast, optical pumping of the  $F_1$  manifold will produce two MODR transitions, as shown by the dashed lines in Fig. 1, if the sensitivity is sufficient to observe the  $Q$ -branch ( $\Delta J = 0$ ) lines. For optical connections from the upper rotational level, the process is reversed; pumping  $F_2$  produces two lines while  $F_1$  produces only one resonance.

A further consequence of the unpaired electron spin is hyperfine effects from the electron spin-nuclear spin coupling.  $^{19}\text{F}$  has  $I = \frac{1}{2}$  such that nuclear quadrupole interactions are not expected. However, Fermi contact and spin dipolar interactions (10) are possible. As mentioned earlier, attempts to obtain hyperfine constants were thwarted because  $\Delta F = \pm 1$  transitions could not be resolved and the weaker  $\Delta F = 0$  transitions, which are split further apart, were not detectable. Hyperfine structure in MODR should be identical to that observed with conventional microwave methods because



these small effects cause line splittings which are very much less than the Doppler width and therefore all hyperfine levels are simultaneously optically pumped. Fortunately, the matrix isolation ESR spectrum of SrF has been analyzed (11) so that an approximate treatment of these unobserved effects could be included in the analysis of the microwave spectrum. Further discussion of this point is deferred until Section IV.

### III. EXPERIMENTAL PROCEDURE

The production of the SrF radical and the optical arrangement were exactly the same as those described in the rotational analysis of the  $B^2\Sigma^+-X^2\Sigma^+$  system of SrF(6). Namely, a Spectra-Physics Model 580 dye laser operating single mode was directed vertically into a flowing reaction cell containing strontium metal vapor and SF<sub>6</sub>. Photoluminescence was viewed perpendicular to the laser in either one of two configurations; excitation spectra were detected by viewing through an appropriate broad-band (20-nm) interference filter while spectrally resolved photoluminescence was obtained through a 1-m McPherson monochromator with a typical bandpass of 0.04 nm.

Microwaves from various phase-locked OKI klystrons, spanning the range 30–60 GHz, were directed into the cell via a horn radiator in a fashion similar to that described earlier in studies of BaO (7). Microwave frequency measurements were made in a standard manner by mixing the source klystron output with a phase-locked Varian X-13 klystron and locking to a 60-MHz IF. The source klystron was swept by applying a voltage ramp to the reflector of the X-13 and maintaining a phase lock. Typically the X-13 was scanned over about 4–5 MHz while the source klystron covered 15–30 MHz.

In all cases the MODR signal was detected as a change in the rotationally resolved photoluminescence intensity. Several advantages in signal-to-noise ratio are gained by monitoring changes in intensity of a particular rotational transition. The major contributions to noise in our spectra are from dye laser intensity and spatial fluctuations and from flame instabilities in the Sr + SF<sub>6</sub> reaction. Naturally, a decreased spectral bandwidth minimizes chemiluminescent flame intensity excursions. In addition, the optical spectrum is sufficiently dense that often more than one coincidence occurs during pumping of the desired transition. Resolved photoluminescence thus eliminates unwanted coincidences, which do not produce any MODR signal, and hence minimizes the troublesome photoluminescence noise contribution from laser amplitude fluctuations. In practice, resolved means tuning the monochromator to the member of the *PR* doublet which the laser is not pumping. The resolution becomes easier for increasing values of *J* because the *PR* spacing is greater and hence wider slits can be tolerated. Thus, better signal-to-noise ratios are obtained with higher-*J* transitions. Line strengths of both the optical and microwave transitions also increase approximately linearly with *J* so it is desirable to measure higher-*J* transitions.

It is also advantageous to optically pump *R*-branch coincidences rather than *P* branches because the  $R(N'')-P(N''+2)$  separation is larger than  $P(N'')-R(N''-2)$ . Three special *P*-branch coincidences,  $P_1(1)$ ,  $P_2(2)$ , and  $P_2(1)$ , should also be avoided because their corresponding *R* partners do not exist! Even with these considerations the S/N was only between 1 and 10 with a typical integration time of 3 sec.

TABLE I  
Measured Transition Frequencies in the Rotational Spectrum of the Ground  $X^2\Sigma^+$  state of SrF

TRANSITION (a)		MICROWAVE FREQUENCY (MHz)	LASER COINCIDENCE (cm <sup>-1</sup> ) <sup>(b)</sup>
v = 0	2, 3/2> -  1, 1/2>	29916.3(3.0)	R <sub>2</sub> (1), 17,265.31
v = 0	2, 5/2> -  1, 3/2>	29986.2(1.4)	R <sub>1</sub> (1), 17,264.98
v = 0	3, 5/2> -  2, 3/2>	44889.1(2.6)	P <sub>2</sub> (3), 17,262.80; R <sub>2</sub> (3), 17266.44
v = 0	3, 7/2> -  2, 5/2>	44961.3(2.7)	R <sub>1</sub> (2), 17,265.41; P <sub>1</sub> (2), 17263.04
v = 0	4, 7/2> -  3, 5/2>	59862.0(2.5)	R <sub>2</sub> (3), 17,266.44; R <sub>2</sub> (4), 17267.01
v = 0	4, 9/2> -  3, 7/2>	59935.5(1.3)	R <sub>1</sub> (3), 17,265.85
v = 1	3, 7/2> -  2, 5/2>	44684.6(5.3)	R <sub>1</sub> (3), 17,259.10
v = 1	4, 7/2> -  3, 5/2>	59491.8(3.0)	R <sub>2</sub> (3), 17,259.72; R <sub>2</sub> (4), 17260.30
v = 1	4, 9/2> -  3, 7/2>	59564.2(4.1)	R <sub>1</sub> (3), 17,259.10; R <sub>1</sub> (4), 17259.53

(a) Microwave transitions are listed as  $|N', J'\rangle - |N'', J''\rangle$ . There are, in fact, two unresolved hyperfine transitions under each, namely,

$$|N', J', F' = J' + 1/2\rangle - |N'', J'', F'' = J'' + 1/2\rangle \text{ and}$$

$$|N', J', F' = J' - 1/2\rangle - |N'', J'', F'' = J'' - 1/2\rangle.$$

(b) Laser coincidences are labelled in Hund's case(b) notation as  $R_1(N'')$ ,  $R_2(N'')$ , etc.

(c) Uncertainties in line positions are listed in parentheses. The numbers represent 95% confidence limits of the mean of several measurements.

## IV. ANALYSIS AND DISCUSSION

## A. General Considerations

The measured microwave transition frequencies and the laser coincidences used in observing the lines are collected in Table I. Only  $|\Delta N| = 1$ ,  $|\Delta J| = 1$  transitions were observed because the Q-branch,  $\Delta J = 0$ , lines were too weak. Line position measurements are less precise than in conventional microwave spectroscopy of stable molecules because of the lower S/N and because the linewidths are typically 15–20-MHz FWHM. Ninety-five percent confidence limits of the frequency measurements are contained in parentheses in Table I. This number represents the standard deviation of the mean of  $N$  measurements scaled by Student's  $t$  factor for  $(N - 1)$  degrees of freedom.

Several reasons for the broad lines exist. First, a transition denoted by  $|N', J'\rangle - |N'', J''\rangle$  in fact consists of two overlapped hyperfine transitions with  $F' = J' \pm \frac{1}{2}$  and  $F'' = J'' \pm \frac{1}{2}$ , second, stray magnetic fields from the tungsten basket heater and the earth's field can cause a large Zeeman splitting because of the unpaired electron spin, and finally, the large expected dipole moment and the high microwave power necessary to observe MODR may result in broadening. These effects are considered in more detail below.

Knight *et al.* (11) have previously analyzed the ESR spectra of matrix-isolated MgF, CaF, SrF, and BaF and have obtained <sup>19</sup>F hyperfine constants. The experimental values of  $A_{11}$  and  $A_1$  are related to the rotating molecule hyperfine constants,  $b_r$  and  $c_r$ , of Frosch and Foley (12), by the expressions

$$A_{iso} = (A_{11} + 2A_1)/3 = (8\pi/3)g_e\beta_e g_n\beta_n |\psi(0)|^2 = b_r + (c_r/3) \quad (1)$$

and

$$A_{dip} = (A_{11} - A_1)/3 = g_e\beta_e g_n\beta_n \langle (3 \cos^2\chi - 1)/2r^3 \rangle = c_r/3. \quad (2)$$

Using the experimental ESR values of  $A_{iso} = 105$  MHz and  $A_{dip} = 10$  MHz, it is then possible to calculate the hyperfine contributions to the rotational energy to examine their effect on the transition frequencies. The rotating molecule problem is conveniently formulated in a Hund's case  $b_{\beta J}$  basis set,  $|F I J S N A M_F\rangle$  (12, 1). Matrix elements of the Fermi contact,  $(b_r + c_r/3)\mathbf{I} \cdot \mathbf{S}$ , and spin dipolar,  $(c_r/3)6^{\frac{1}{2}}V_0^{(2)}(\mathbf{I}, \mathbf{S})$ , interactions in a case  $b_{\beta J}$  basis have been given by Dixon and Woods (1). Contributions due to the nuclear spin-rotation  $C_I N \cdot \mathbf{I}$  were neglected. Diagonalization of the Hamiltonian shows that, for the lines measured, two hyperfine transitions occur within about 1–2 MHz of each other. This overlap certainly constitutes an apparent line-broadening mechanism. Furthermore, the two hyperfine transitions are not symmetrically displaced from the unsplit line center. Although in most cases the discrepancy is less than the experimental line position uncertainty, the measured line positions have been corrected for this shift by assuming that both hyperfine transitions are of comparable intensity and their mean frequency is the unresolved line center. The difference between the mean frequency and the unperturbed line center was then applied as a correction to the measured line position. Table II lists the corrected frequencies and their least-squares-fitted values. The standard deviation of the fit improved by a factor of 2 with this correction. Justifiably the line position which had the most effect was the  $N = 1 \rightarrow 2$ ,  $J = \frac{1}{2} \rightarrow \frac{3}{2}$ , where the correction applied was the largest (–4.1 MHz) and lay outside the estimated experimental uncertainty. Figure 2 shows schematically a typical example



TABLE II

Experimental Line Positions of SrF Corrected for Hyperfine Effects and Comparison with Least-Squares-Fitted Value

TRANSITION	CORRECTED POSITION (MHz)	CALCULATED (MHz)
$v = 0 \quad  2, 3/2\rangle -  1, 1/2\rangle$	29912.2	29912.9
$v = 0 \quad  2, 5/2\rangle -  1, 3/2\rangle$	29988.0	29987.5
$v = 0 \quad  3, 5/2\rangle -  2, 3/2\rangle$	44888.8	44887.5
$v = 0 \quad  3, 7/2\rangle -  2, 5/2\rangle$	44962.2	44962.2
$v = 0 \quad  4, 7/2\rangle -  3, 5/2\rangle$	59861.3	59861.0
$v = 0 \quad  4, 9/2\rangle -  3, 7/2\rangle$	59936.0	59936.3
$v = 1 \quad  3, 7/2\rangle -  2, 5/2\rangle$	44685.5	44684.0
$v = 1 \quad  4, 7/2\rangle -  3, 5/2\rangle$	59491.2	59491.1
$v = 1 \quad  4, 9/2\rangle -  3, 7/2\rangle$	59564.7	59565.5

of the magnitude of these effects and more clearly indicates the coupling scheme. It is clear that observation of  $\Delta F = 0$  transitions for these higher- $N$  transitions is necessary to obtain experimental values of the hyperfine constants.

It is difficult to assess the exact magnitude of the stray magnetic fields present under operating conditions in the reaction zone. However, no attempt was made to cancel the effects of the earth's field so that fields of the order of 0.5–1 G are not unreasonable. In molecules with unbalanced spin angular momentum, fields of this magnitude cause Zeeman splittings of several megahertz but fortunately the splittings are symmetrical

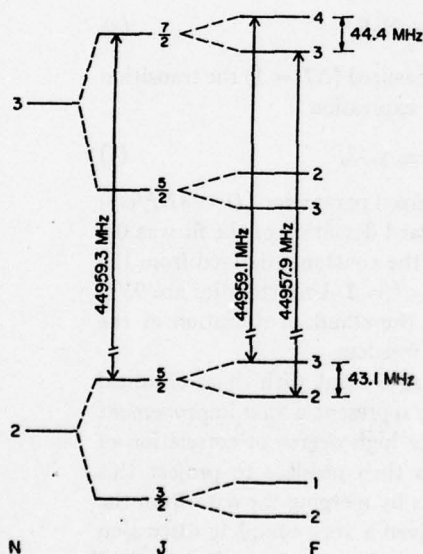


FIG. 2. Schematic diagram of hyperfine splitting in the  $X^2\Sigma^+$  state of SrF. The reason for the unresolved structure is apparent in the similar magnitudes of the splitting for different  $J$  states.

about the zero-field line position and do not affect the measured frequency. However, the magnetic fields can certainly contribute to line broadening.

Microwave power saturation can provide another mode of line broadening. Experimental attempts to determine the magnitude of this contribution failed because of the rapid decrease in signal intensity with decreasing microwave power. Quantitative experimental treatment of this effect requires much better initial signal-to-noise ratios to enable larger decreases of microwave power without complete loss of MODR signal.

Experimental apparatus is at present under construction to alleviate the problems of broad lines and low sensitivity discussed above. Briefly, a heat pipe oven (14, 15), which produces a homogeneous vapor distribution, is to be used for production of SrF from Sr metal and a trace of  $SF_6$ . Not only does this method provide a more uniform concentration distribution than a flame, but also symmetric placement of the heating elements in a four-way crossed heat pipe oven will minimize the heater magnetic fields. The arrangement is also conducive to placement of external Helmholtz coils to cancel the earth's field. In addition the microwaves can be introduced and the experiment performed inside the waveguide by contradicting the laser and microwaves collinearly and viewing the photoluminescence through a small slot milled in the waveguide wall (18). The anticipated improvement in resolution and sensitivity will allow measurement of weaker  $\Delta J = 0$  transitions, and further, extraction of experimental hyperfine parameters.

#### B. Data Treatment

The corrected transition frequencies listed in Table II were fitted to the standard model Hamiltonian for ground state  $^2\Sigma^+$  molecules (1, 16), namely,

$$\mathcal{H} = [B_v - N(N+1)D]N^2 - \gamma_v N \cdot S, \quad (3)$$

using a weighted least-squares procedure. For the lines measured ( $\Delta J = 1$ ) the transition frequencies for  $N \rightarrow N+1$  are given by the one simple expression

$$\nu = 2B_v(N+1) - 4D(N+1)^3 \pm \gamma_v/2, \quad (4)$$

where the  $\pm$  sign refers to  $J = N \pm S$ .  $D$  was held as a fixed parameter ( $D = 4B_v^2/\omega_e^2$ ) and the lines were used to fit  $B_v$  and  $\gamma_v$  only. The standard deviation of the fit was 0.8 MHz for  $v = 0$  and 1.7 MHz for  $v = 1$ . Table III lists the constants derived from the fit to the six measured lines in  $v'' = 0$  and three lines in  $v'' = 1$ . Uncertainties are 95% confidence limits in the last digit obtained by scaling the standard deviation of the parameters by Student's  $t$  factor for  $(n-2)$  degrees of freedom.

Not only are the constants from the fit in excellent agreement with those obtained from the  $B^2\Sigma^+ - X^2\Sigma^+$  optical analysis (6), but they also represent a vast improvement in accuracy. Because of this improved accuracy and the high degree of correlation of constants derived from the optical spectrum (6), it is then possible to project this improved accuracy into the excited state  $B^2\Sigma^+$  constants by merging the data from the two experiments. Albritton and co-workers (17) have given a very complete discussion of the significance and formalism of combining data and their recommended method has been followed. Briefly, this procedure uses two sets of spectroscopic constants and corresponding covariance-variance matrices, obtained from independent least-squares

TABLE III

Ground-State ( $X^2\Sigma^+$ ) Constants (MHz) of SrF Derived from a Least-Squares fit of Measured Microwave Frequencies <sup>a</sup>

$B_0''$	= 7487.61(13) MHz
$B_1$	= 7441.3(12) MHz
$\gamma_0''$	= 74.7(17) MHz
$\gamma_1''$	= 74(18) MHz
$D_1''$	= $D_0''$ (fixed) = 0.00743 MHz

<sup>a</sup> Uncertainties represent 95% confidence limits of the last digit.

fits of optical and microwave transition frequencies, as input data for a final merged fit. The spectroscopic constants  $\nu_0$ ,  $B_0'$ ,  $B_0''$ ,  $\gamma_0'$ , and  $\gamma_0''$  obtained from the fit to the optical transition frequencies were combined with the  $B_0''$  and  $\gamma_0''$  from the microwave data to obtain the final set of the five common constants. The values of these constants and subsequently derived equilibrium values are collected in Table IV. Uncertainties represent 95% confidence limits in the last digit. The estimated variance-covariance matrix used in the final correlated, weighted fit was obtained from a composition of the variance-covariance matrices from both the optical and microwave fits. Table IV clearly demonstrates the improvement in accuracy of excited state constants over those obtained from optical data alone ( $\sigma$ ) as a result of the high degree of correlation between parameters. A word of caution concerning the interpretation of the  $B$  value in the  $B^2\Sigma^+$  state is necessary. Our model defines  $B$  as the coefficient of  $N(N+1)$ . It certainly does not represent  $\langle 1/r^2 \rangle$ , to the degree of accuracy indicated in this constant because of the inescapable contamination of the rotational constant by magnetic contributions

TABLE IV

Spectroscopic Constants ( $\text{cm}^{-1}$ ) for the  $X^2\Sigma^+$  and  $B^2\Sigma^+$  States of SrF Derived from a Merged Fit of Microwave and Optical Excitation Spectra Data

	$X^2\Sigma^+$	$B^2\Sigma^+$	
$B_0$	0.249760(3)	0.248617(5)	
$B_1$	0.248214(6)	0.247060(8)	
$B_e$	0.250533(5)	0.249396(9)	
$\alpha_e$	$1.546(7) \times 10^{-3}$	$1.557(9) \times 10^{-3}$	
$D_e$	$2.49(1) \times 10^{-7}$	$2.52(1) \times 10^{-7}$	
$\gamma_0$ (spin-rotation)	0.00249(4)	-0.13537(18)	$= -\underline{p}_x$
$\gamma_1$ (spin-rotation)	0.00248(9)	-0.13528(27)	$= -\underline{p}_x$
$g_x$		0.00012	



from the nearby  $A^2\Pi_r$  state. An estimate of this contribution,  $q_z$ , for two states in pure precession ( $\delta$ ), is also contained in Table IV and this value should be subtracted from  $B$  to obtain a more realistic value of  $\langle 1/r^2 \rangle_v$ .

RECEIVED: May 16, 1977

#### REFERENCES

1. T. A. DIXON AND R. C. WOODS, *J. Chem. Phys.*, in press.
2. T. A. DIXON AND R. C. WOODS, *Phys. Rev. Lett.* 34, 61 (1975).
3. K. B. JEFFERTS, *Phys. Rev. Lett.* 23, 1476 (1969).
4. K. R. GERMAN AND R. N. ZARE, *Phys. Rev. Lett.* 23, 1207 (1969).
5. K. M. EVENSON, J. L. DUNN, AND H. P. BROIDA, *Phys. Rev.* 136, 1566 (1964); K. M. EVENSON, *Phys. Rev.* 178, 1 (1969); D. W. PRATT AND H. P. BROIDA, *J. Chem. Phys.* 50, 2181 (1969).
6. T. C. STEIMLE, P. J. DOMAILLE, AND D. O. HARRIS, *J. Mol. Spectrosc.* 68, §§§ (1977).
7. R. W. FIELD, A. D. ENGLISH, T. TANAKA, D. O. HARRIS, AND D. A. JENNINGS, *J. Chem. Phys.* 59, 2191 (1973).
8. R. F. WORMSBECHER, D. O. HARRIS, AND B. G. WICKE, *J. Mol. Spectrosc.* 64, 86 (1977).
9. R. N. ZARE, A. L. SCHMELTEKOPF, W. J. HARROP, AND D. L. ALBRITTON, *J. Mol. Spectrosc.* 46, 37 (1973).
10. T. M. DUNN, in "Molecular Spectroscopy: Modern Research" (K. Narahari Rao and K. W. Matthews, Eds.), Vol. I, p. 231, Academic Press, New York, 1972.
11. L. B. KNIGHT, JR., W. C. EASLEY, W. WELTNER, JR., AND M. WILSON, *J. Chem. Phys.* 54, 322 (1971).
12. R. A. FROSCHE AND H. M. FOLEY, *Phys. Rev.* 88, 1337 (1952).
13. G. HERZBERG, "Spectra of Diatomic Molecules," Van Nostrand, Princeton, N. J., 1950.
14. G. GERBER, K. SAKURAI, AND H. P. BROIDA, *J. Chem. Phys.* 64, 3410 (1976).
15. C. R. VIDAL AND J. COOPER, *J. Appl. Phys.* 40, 3370 (1969).
16. W. GORDY AND R. L. COOK, "Microwave Molecular Spectra," Interscience, 1970.
17. D. L. ALBRITTON, A. L. SCHMELTEKOPF, AND R. N. ZARE, in "Molecular Spectroscopy: Modern Research" (K. Narahari Rao and K. W. Matthews, Eds.), Vol. II, Academic Press, New York, 1976.
18. T. TANAKA, R. W. FIELD, AND D. O. HARRIS, *J. Chem. Phys.* 61, 3401 (1974).

AD-A065 291

CALIFORNIA UNIV SANTA BARBARA DEPT OF CHEMISTRY F/G 7/2  
PHOTOLUMINESCENCE SPECTROSCOPY WITH A CW DYE LASER. A STUDY OF --ETC(U)  
1977 D O HARRIS AFOSR-73-2565

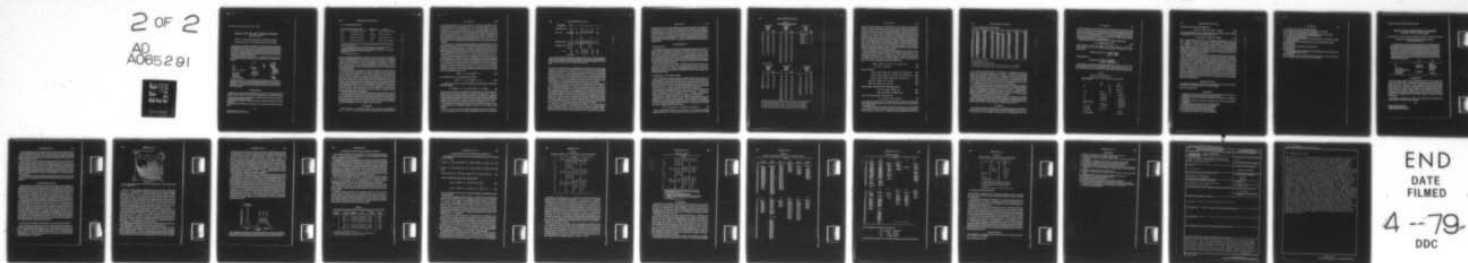
UNCLASSIFIED

AFOSR-TR-79-0101

NL

2 OF 2

AD  
A065291



END  
DATE  
FILMED

4 --79  
DDC



MICROCOPY RESOLUTION TEST CHART  
NATIONAL BUREAU OF STANDARDS-1963-A



## Continuous Wave Dye Laser Excitation Spectroscopy CaF $A^2\Pi-X^2\Sigma^+$

ROBERT W. FIELD,<sup>2</sup> DAVID O. HARRIS, AND TAKEHIKO TANAKA<sup>3</sup>

Quantum Institute, University of California, Santa Barbara, California 93106

Excitation spectra for the CaF  $A^2\Pi-X^2\Sigma(0,0)$ ,  $(1,1)$ , and  $(1,0)$  bands have been observed and assigned. The rotational analysis of the CaF  $A-X$  and  $B-X$  bands by B. S. Mohanty and K. N. Upadhyaya [*Ind. J. Pure Appl. Phys.* 5, 523 (1967)] is shown to be incorrect. Because it is possible to make independent rotational assignments of each line in an excitation spectrum by observing frequency differences and relative intensities in photoluminescence spectra, tunable laser excitation spectroscopy promises less ambiguity than traditional techniques for assignment of dense, badly overlapped spectra.

The following spectroscopic constants (in  $\text{cm}^{-1}$ ) are obtained for the CaF  $A^2\Pi$  and  $X^2\Sigma$  states. Numbers in parentheses correspond to three standard deviations uncertainty in the last digit.

	$X^2\Sigma$	$A^2\Pi$
$\nu_{00}$	0	$^2\Pi_1$ 16493.1(6) $^2\Pi_1$ 16565.6(6) $^2\Pi_1$ 586.8(9)
$\Delta G(\frac{1}{2})$	581.1(9)	
$B_0$	0.3385(11)	0.3436(12)
$B_0(\Omega = \frac{1}{2}) - B_0(\Omega = \frac{3}{2})$	—	0.00312(21)
$\alpha$	0.00255(48)	0.00283(45)
$D(\text{estimated})$	$4.44 \times 10^{-7}$	$4.55 \times 10^{-7}$
$\gamma(\text{spin-spin})$	$ \gamma  < 3 \times 10^{-3}$	—
$A_0(\text{spin-orbit})$	—	73.4(9)
$\rho(\text{lambda doubling})$	—	-0.045(4)

The origin of the  $A^2\Pi_1-X^2\Sigma(1,1)$  subband is measured  $5.54(15) \text{ cm}^{-1}$  to the blue of the corresponding  $(0,0)$  subband origin. The  $(0,0)$  band  $Q_2$  head is observed to form at  $J = 26 \pm 0.5$ . The difference of  $A^2\Pi_1$  and  $A^2\Pi_1$  effective rotational constants is  $2B^2/A$ . The  $A^2\Pi$  lambda doubling constant  $\rho$  agrees well with the pure precession estimate of the interaction between the  $A^2\Pi$  and  $B^2\Sigma$  states.

### I. INTRODUCTION

Tunable laser excitation spectroscopy has been shown to be a powerful tool for the analysis of complex electronic spectra. An excitation spectrum is a record of the intensity

<sup>1</sup> This research was supported by AFOSR Grant No. AFOSR-73-2565, Army Grant No. DA-ARO-D-31-124-73-G174, and NSF Grant GP-35672X.

<sup>2</sup> Present address: Department of Chemistry, Massachusetts Institute of Technology, Cambridge, Mass. 02139.

<sup>3</sup> Visiting Scientist from Department of Chemistry, Faculty of Science, Kyushu University, Fukuoka, Japan.

TABLE I -  $^2\Pi - ^2\Sigma^+$  Photoluminescence Lines

$^2\Pi$ Level Excited <sup>a,b</sup>	Photoluminescence Lines <sup>c</sup>	R-P Separation	Q Position
$F_{1c}(J')$	$R_1(J'-1), Q_{12}(J'), P_1(J'+1)$	$4J'b''$	$Q_{12}(J') - P_1(J'+1) = (J'+1)\gamma''$
$F_{1d}(J')$	$R_{12}(J'-1), Q_1(J'), P_{12}(J'+1)$	$(4J'+4)b''$	$R_{12}(J'-1) - Q_1(J') = J'\gamma''$
$F_{2c}(J')$	$R_2(J'-1), Q_{21}(J'), P_2(J'+1)$	$(4J'+4)b''$	$R_2(J'-1) - Q_{21}(J') = J'\gamma''$
$F_{2d}(J')$	$R_{21}(J'-1), Q_2(J'), P_{21}(J'+1)$	$4J'b''$	$Q_2(J') - P_{21}(J'+1) = (J'+1)\gamma''$

<sup>a</sup>  $F_1$  means  $N' = J' - \frac{1}{2}$ ,  $F_2$  means  $N' = J' + \frac{1}{2}$ . For a regular (inverted) case 'a'  $^2\Pi$  state,  $F_1$  levels are  $^2\Pi_{\frac{1}{2}}$  ( $^2\Sigma_{\frac{1}{2}}^+$ ) and  $F_2$  are  $^2\Pi_{\frac{3}{2}}$  ( $^2\Sigma_{\frac{3}{2}}^+$ ).

<sup>b</sup> c, d are rotation independent parity labels for  $^2\Pi$  lambda doublets. 'c' levels have the same total parity as  $^2\Sigma^+$  levels with the same value of J and N; 'd' levels have opposite parity.

<sup>c</sup> Transitions are designated by specifying the J-value for the lower electronic state,  $J''$ , in parentheses following the branch designation.  $R(J'-1)$  means  $J'' = J' - 1$ .

<sup>d</sup> Absent if  $J' = \frac{1}{2}$ .

<sup>e</sup>  $\gamma''$  is the  $^2\Sigma^+$  spin-rotation constant.

of laser excited photoluminescence obtained as the laser excitation wavelength is swept (*I*). Although information contained in an excitation spectrum is often equivalent to that in an absorption spectrum, excitation spectroscopy can be superior in sensitivity, resolution, and, most important, freedom from ambiguity in line assignment. Each line in an excitation spectrum may be assigned independently of all other lines on examination of photoluminescence excited while the laser remains tuned to coincide with the desired excitation line.

CaF  $A^2\Pi-X^2\Sigma$  bands were selected for study as an application of excitation spectroscopy to a band system considerably more complex and dense than BaO  $A^1\Sigma-X^1\Sigma$  (2) yet much simpler than NO<sub>2</sub>  $^2B_2-^2A_1$  (3). Rotational analyses have been completed for very few electronic transitions of alkaline earth monohalides (4-13) because their spectra are dense and extensive overlapping of vibrational sequence bands ( $\Delta v = \text{const}$ ) occurs. Even when spectral resolution is adequate to resolve individual rotational lines, the vast number of interleaved branches and bands makes the task of pattern recognition and line assignment by traditional combination-difference relations formidable. Portions of the CaF  $A^2\Pi-X^2\Sigma$  (0, 0), (1, 1), and (1, 0) bands are assigned by a procedure, described in Section II, which takes advantage of the tunability and monochromaticity of a cw dye laser as well as the ability to measure frequency separations between members of photoluminescence progressions.

A rotational analysis of the CaF  $A^2\Pi-X^2\Sigma$  (0, 0) band has been previously reported (11). We expected to be guided by that analysis, but soon found it to be entirely incorrect. Further, since two previously reported analyses of CaF  $B^2\Sigma-X^2\Sigma$  bands (11, 14) are based upon erroneous values of  $X^2\Sigma$  rotational constants, they too must be spurious. Rotational reanalysis of the CaF  $B-X$  bands by cw dye laser excitation spectroscopy must await availability of cw lasers tunable in the 529 nm region.

## II. DISCUSSION

$A^2\Pi-X^2\Sigma^+$  band has 12 rotational branches. Three branches, corresponding to  $J''-J''' = +1, 0, -1$  transitions (*R*, *Q*, *P* branches, respectively), originate from each

of four classes of  $^2\Pi$  levels:  $F_{1c}$ ,  $F_{1d}$ ,  $F_{2c}$ , and  $F_{2d}$ . 'c' and 'd' are parity labels with 'c' levels of  $^2\Pi$  having the same total parity as  $^2\Sigma^+$  levels with identical values of  $J$  and  $N$ .  $F_1$  levels have  $N' = J' - \frac{1}{2}$ ;  $F_2$  levels have  $N' = J' + \frac{1}{2}$ . Branch labels for the three transitions associated with each  $^2\Pi$  fine structure level are shown in Table I. In column 3 of Table I is the separation of  $R$ - and  $P$ -branch lines which originate from the same  $^2\Pi$  fine structure level. The  $R(J' - 1)$  line necessarily lies at shorter wavelength than  $P(J' + 1)$ .  $Q(J')$  lines are not generally located midway between  $R(J' - 1)$  and  $P(J' + 1)$  lines; instead they are nearly coincident with either the  $R(J' - 1)$  or  $P(J' + 1)$  line as indicated in column 4. The degree of coincidence depends on the spin-rotation constant,  $\gamma''$ , and  $J'$ .

In order to make a complete rotational assignment of a line belonging to a  $^2\Pi-^2\Sigma^+$  band, it is sufficient to know with which  $^2\Pi$  fine structure level the line is associated, and whether it is a member of an  $R$ ,  $Q$ , or  $P$  branch. If it is possible to examine the photoluminescence spectrum which results when the line in question is optically pumped, two of the four possible classes of  $^2\Pi$  fine structure levels may be ruled out, one or two of the three possible branches may be ruled out, and  $J'$  may be determined if  $B''$  is known.

The  $^2\Pi-^2\Sigma^+$  photoluminescence spectrum will consist of groups of three lines or of two lines if the  $Q$  line is not resolved from an  $R$  or  $P$  line because  $\gamma''$  is small. Each group of lines corresponds to a transition to a different vibrational level of the  $^2\Sigma^+$  state. In general  $\gamma'' \ll B''$ , thus the  $Q$  line will be nearer the long wavelength line if the  $^2\Pi$  level is  $F_{1c}$  or  $F_{2d}$  or nearer the short wavelength line if  $F_{1d}$  or  $F_{2c}$  (see Table I). If the optically pumped line is one of the long  $\lambda$  members of a group, then it is  $P$  or  $Q$ , if it is one of the short  $\lambda$  members, it is  $R$  or  $Q$ . If it is the isolated member of a group of three lines (or the weak member of a group of two), then it does not belong to a  $Q$  branch. If the  $^2\Pi$  level belongs to  $F_{1c}$  or  $F_{2d}$  (doublet at long  $\lambda$ ), then

$$[R(J' - 1) - P(J' + 1)]/4B'' = J'; \quad (1a)$$

but if it belongs to  $F_{1d}$  or  $F_{2c}$  (doublet at short  $\lambda$ ), then

$$[R(J' - 1) - P(J' + 1)]/4B'' = J' + 1. \quad (1b)$$

An approximate value of  $B''$  may be obtained from  $R$ - $P$  separations of consecutive lines of any branch

$$B'' = \frac{1}{4}[[R(J' - 1) - P(J' + 1)] - [R(J' - 2) - P(J')]]. \quad (2)$$

Consecutive lines in a branch are recognizable in the following ways. Photoluminescence excited via such lines will have similar total intensity and similar  $R$ ,  $Q$ ,  $P$  patterns. Consecutive lines correspond to the smallest possible nonzero change in  $R$ - $P$  separation. Even if two lines belong to different branches of the same vibrational band, the difference in associated  $R$ - $P$  separations can only be an integral number of  $4B''$  units. Lines belonging to the same branch are related by constant second differences,  $2(B' - B'')$ .

Two ambiguities in line assignment remain. The first is related to the sign of  $A'$ , the  $^2\Pi$  spin-orbit constant. The second is related to the sign of  $\gamma''$ , the  $^2\Sigma^+$  spin-rotation constant.

The  $R$ ,  $Q$ ,  $P$  pattern determines whether the optically pumped  $^2\Pi$  level belongs to  $F_{1d}$  or  $F_{2c}$  as opposed to  $F_{1c}$  or  $F_{2d}$ . Lack of knowledge of the sign of  $A'$  means that,



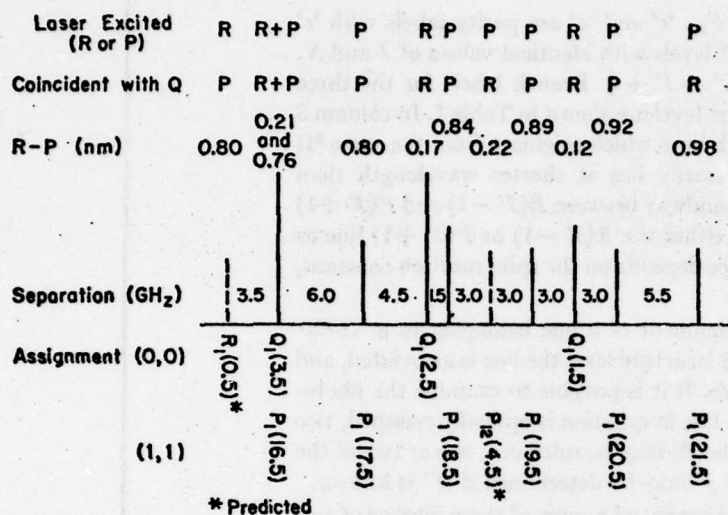


FIG. 1. Section of CaF excitation spectrum near 606 nm. Each feature in the excitation spectrum is indicated by a line. Length of line indicates relative intensity. Two predicted but not observed lines are included to provide examples of all four possible combinations of laser excitation (long or short  $\lambda$  component) and photoluminescence pattern (intense line at long or short  $\lambda$ ).

even if one knows whether the level excited belongs to the higher or lower energy  $^3\Pi$  spin component, one does not know whether an  $F_1$  or  $F_2$  level is involved. It is not possible to determine the sign of  $A'$  until many lines of several branches have been partially assigned. The sign of  $A'$  is determined by finding the  $P$  branch that starts with a  $P(3)$  line, the  $Q$  branch that starts with a  $Q(3)$  line, or by detailed examination of the lambda doubling in the  $^3\Pi$  state. If it is possible to find a branch, the first member of which terminates in a  $J' = \frac{1}{2}$  level, that branch is associated with  $^3\Pi_1$ . If that branch is associated with the lower energy  $^3\Pi$  spin component, then the  $^3\Pi$  state is regular.

The ambiguity related to the sign of  $\gamma''$  may be resolved by determining which of the two closely spaced components of a resolved  $R$ ,  $Q$ ,  $P$  triplet is the  $Q$  line. Whenever  $\gamma'' > 0$ , a  $Q(J')$  line belonging to any of the four possible  $Q$  branches will fall between  $R(J' - 1)$  and  $P(J' + 1)$  lines. If  $\gamma'' < 0$ , the  $Q$  line will fall outside the  $R$  and  $P$  lines. If examples of photoluminescence triplets arising from all four classes of  $^3\Pi$  fine structure components are obtained, regardless of the  $^3\Pi$  coupling case, in at least two of the four cases the  $Q$  line will have more than twice the intensity of the neighboring  $R$  or  $P$  line, which in turn will have intensity comparable to the isolated member of the photoluminescence triplet (15). Thus if a triplet is observed where one line has more than twice the intensity of either of the other two, then if the intense line lies between the other two lines,  $\gamma'' > 0$  and  $Q$  lines will always lie between  $R$  and  $P$  lines.

In summary, the analysis of a band proceeds as follows. A map of the excitation spectra is constructed similar to the example in Fig. 1. Information recorded includes: frequency differences between adjacent excitation lines,  $R$ - $P$  separations in photoluminescence spectra obtained for each excitation line, an indication of which member

of the photoluminescence triplet coincides with the excitation line, and the position of the  $Q$  line relative to the  $R$  and  $P$  lines. This information is sufficient to sort lines into 12 different branches, to establish  $J'$  for each line, to obtain  $B''$  from  $R$ - $P$  separation of consecutive lines of the same branch, to determine  $\gamma''$ , and to label each branch as  $R$ ,  $Q$ , or  $P$ . When  $J' = \frac{1}{2}$  lines are located the final branch labels and the sign of  $A$  are unambiguously determined. Finding  $J' = \frac{1}{2}$  lines by photoluminescence spectroscopy is much easier than locating them in a necessarily crowded region of an absorption or emission band.

### III. EXPERIMENTAL

#### A. Production of CaF

The experimental arrangement used for observing photoluminescence and excitation spectra of CaF was similar to that employed in experiments with BaO (2). Dye laser light entered the photoluminescence region from the top through a Brewster angle window and a 3 mm aperture. Calcium metal was vaporized from an alumina crucible in a tungsten basket heater. Calcium vapor was entrained in argon and carried into the photoluminescence region where it reacted with  $SF_6$ . Photoluminescence was monitored simultaneously through a  $\frac{1}{2}$  meter double monochromator and through a 20 nm FWHM interference filter centered at 600 nm.

The calcium oven operated near 900 °K with 220 W power input. Five hours of continuous oven operation was typical with a 2 g initial charge of calcium. Argon carrier gas flow rate was 2 cm<sup>3</sup> sec<sup>-1</sup>. Pressure in the photoluminescence chamber was 0.5 Torr. Under these conditions a weak, diffuse, red chemiluminescent glow was observed in the photoluminescence region.

#### B. Photoluminescence and Excitation Spectra

The cw, rhodamine 6-G dye laser, frequency stabilized and fine tuned by two intracavity etalons, has been described elsewhere (2). The wavelength range, 570–615 nm, over which the dye laser could be tuned continuously with spectral bandwidth less than 0.001 cm<sup>-1</sup> and power greater than 10 mW permitted excitation of CaF  $A^2\Pi-X^2\Sigma$  bands which belong to  $v_A'-v_X'' = 0$  and  $+1$  sequences (16). Photoluminescence was observable only in  $\Delta v = +1, 0, -1$  sequences near 585, 605, and 625 nm, respectively.

Photoluminescence progressions excited by the dye laser consisted of three pairs of lines, except when a  $v_A' = 0$  level was excited, in which case the  $\Delta v = +1$  doublet near 585 nm was necessarily absent. The absence of a  $\Delta v = +1$  doublet enabled features excited in the  $\Delta v = 0$  region (near 605 nm) to be assigned to the (0, 0) band.

The observation of pairs of lines rather than triplets in photoluminescence spectra implies that  $\gamma''$  is very small. An upper limit for  $\gamma''$  was obtained from examination of the feature in the excitation spectra assigned as  $P_1(22.5) + Q_{12}(21.5)$ . As the dye laser was tuned with spectral bandwidth less than 0.001 cm<sup>-1</sup> through this feature in 0.003 cm<sup>-1</sup> steps, no splitting could be detected, thus

$$|\gamma''| < \Delta\nu_{\text{Doppler}}/(N+1) = 0.06/23 < 3 \times 10^{-3} \text{ cm}^{-1}. \quad (3)$$

The fact that  $Q$ -branch lines always coincide with an  $R$ - or  $P$ -branch line simplified assignment of the CaF  $A$ - $X$  excitation spectrum. Figure 1 shows a portion of a typical

TABLE II  
Observed Spacings between Adjacent Lines

(0-0) Band ( $\Delta v = \frac{1}{2}$ )			(0-0) Band ( $\Delta v = \frac{1}{2}$ )			(0-0) Band ( $\Delta v = \frac{1}{2}$ )		
<u>G<sub>1</sub> Branch</u>			<u>F<sub>1</sub> Branch</u>			<u>Other</u>		
J"	GHz	Obs-calc	J"	GHz	Obs-calc	Label	GHz	Obs-calc
15.5	13.0	0.3	2.5	9.0	0.1	G <sub>1</sub> (1.5)-		
15.5	12.5	0.0	3.5	9.0	0.3	P <sub>1</sub> (2.5)	37.0	-0.7
14.5	12.0	-0.3	4.5	8.5	0.0	G <sub>1</sub> (1.5)-	3.0	0.2
13.5	12.0	-0.1	5.5	8.5	0.2	G <sub>1</sub> (6.5)		
12.5	12.0	0.1	6.5	8.5	0.2	F <sub>12</sub> (3.4)-	0.0	-0.2
11.5	12.3	0.6	7.5	8.0	0.1	F <sub>1</sub> (14.5)		
10.5	11.5	0.0	8.5	8.0	0.3	P <sub>1</sub> (20.5)-	867.9	-0.6
9.5	11.0	-0.3	9.5	8.0	0.5	P <sub>1</sub> (22.5)		
8.5	12.0	0.9	10.5	7.0	-0.3			
7.5	11.0	0.1	11.5	7.0	-0.1			
6.5	11.0	0.3	12.5	7.0	0.1			
5.5	11.0	0.5	13.5	6.8	0.1			
4.5	10.5	0.2	14.5	6.5	0.0			
3.5	10.5	0.4	15.5	6.5	0.2			
2.5	10.5	0.6	16.5	6.5	0.4			
1.5			17.5	6.0	0.1			
			18.5	6.5	0.8			
			19.5	5.5	0.0			
			20.5	5.5	0.2			
			21.5	5.0	-0.1			
			22.5 <sup>a</sup>					

TABLE II (continued)

(0-0) Band ( $\Delta v = \frac{1}{2}$ )			(1-1) Band ( $\Delta v = \frac{1}{2}$ )			(1-0) Band ( $\Delta v = \frac{1}{2}$ )		
<u>G<sub>2</sub> Branch</u>			<u>F<sub>1</sub> Branch</u>			<u>F<sub>1</sub> Branch</u>		
J"	GHz	Obs-calc	J"	GHz	Obs-calc	J"	GHz	Obs-calc
3.5	8.0	-0.4	4.5	9.3	0.8	2.5	9.0	-0.4
4.5	8.0	0.0	5.5	8.5	0.1	3.5	9.0	-0.3
5.5	7.7	0.1	6.5	8.5	0.3	4.5	9.0	-0.3
6.5	7.3	0.1	7.5	7.7	-0.3	5.5	9.2	-0.1
7.5	7.0	0.2	8.5	7.7	-0.1	6.5	9.3	0.1
8.5	13.0	0.5	9.5	7.0	-0.6	7.5	9.4	0.2
10.5	5.7	0.0	10.5	8.0	0.6	8.5	9.3	0.1
11.5	5.5	0.2	11.5	7.0	-0.3	9.5	9.3	0.2
12.5	32.8	-0.4	12.5	7.0	-0.1	10.5	9.0	-0.1
25.5 <sup>b</sup>	head	-0.2	13.5	7.0	0.1	11.5	9.2	0.1
27.5 <sup>b</sup>			14.5	6.5	-0.2	12.5	9.0	-0.1
			15.5	7.5	1.0	13.5	9.0	0.0
			16.5 <sup>c</sup>	6.0	-0.3	14.5	9.0	0.0
			17.5	6.0	-0.1	15.5 <sup>d</sup>	9.0	0.0
			18.5	6.0	0.0			
			19.5	6.0	0.2			
			20.5	5.5	-0.1			
			21.5	5.0	-0.4			
			22.5					

<sup>a</sup>The F<sub>1</sub>(22.5) line was observed 0.112 ± 0.02 nm to the blue of the He line at  $\lambda_{\text{air}} = 605.4536$  nm.

<sup>b</sup>The G<sub>2</sub> bandhead was observed 0.698 ± 0.02 nm to the red of the He line at  $\lambda_{\text{air}} = 602.9997$  nm.

<sup>c</sup>The F<sub>1</sub>(16.5) line was observed 0.358 ± 0.02 nm to the blue of the He line at  $\lambda_{\text{air}} = 605.4536$  nm.

<sup>d</sup>The F<sub>1</sub>(16.5) line was observed 0.244 ± 0.02 nm to the red of the He line at  $\lambda_{\text{air}} = 585.2488$  nm.



annotated excitation spectrum.  $R$ - $P$  separations in  $\Delta v = 0$  bands were measured to  $\pm 0.01$  nm using a monochromator with spectral slitwidth of 0.05 nm. Separation of successive lines in the excitation spectrum were measured to  $\pm 0.5$  GHz ( $\pm 0.01$  cm $^{-1}$ ) using an optical spectrum analyzer with 3.0 GHz free spectral range. Whether the laser excited an  $R$ - or  $P$ -branch line was established by noting whether the laser frequency coincided with the short or long  $\lambda$  component of a photoluminescence doublet. The  $Q$ -branch line coincided with the more intense doublet component. The above observations are sufficient to assign the features shown in Fig. 1. The branch designations of Fig. 1 are trial assignments, made by assuming that the lower energy  $A^2\Pi$  spin substate is  $^2\Pi_1$  and by noting whether the line excited belongs to a branch associated with the higher or lower energy  $^2\Pi$  substate. These trial branch designations were subsequently verified by locating the  $Q_1(0.5)$  line, thereby proving that the lower energy  $^2\Pi$  substate is in fact  $^2\Pi_1$  and that the CaF  $A^2\Pi$  state is regular.

Frequency differences measured between lines belonging to CaF  $A^2\Pi-X^2\Sigma$  (0, 0), (1, 1), and (1, 0) bands are listed in Table II. All of these frequency differences were simultaneously least-squares fitted to obtain  $B_v''$ ,  $\alpha''$ ,  $B_v'(\Omega = \frac{1}{2})$ ,  $B_v'(\Omega = \frac{3}{2})$ ,  $\alpha'$ , and the lambda doubling constant  $p$ . Centrifugal distortion constants calculated from  $D = 4B_v^3/\omega_e^2$  (17) were included as fixed parameters and it was assumed that  $\alpha'(\Omega = \frac{1}{2}) = \alpha'(\Omega = \frac{3}{2})$ . Energy expressions used were, for  $^2\Sigma$

$$F_1(N) = F_2(N) = B_v''N(N+1) - D''N^2(N+1)^2, \quad (4)$$

$$B_v'' = B_v'' - \alpha''(v + \frac{1}{2}), \quad (5)$$

and for  $^2\Pi$  (19, 20)

$$F_{1c}(J) = B_v'(\Omega = \frac{1}{2})J(J+1) - D'J^2(J+1)^2 - p/2(J + \frac{1}{2}), \quad (6a)$$

$$F_{1d}(J) = B_v'(\Omega = \frac{1}{2})J(J+1) - D'J^2(J+1)^2 + p/2(J + \frac{1}{2}), \quad (6b)$$

$$F_{2c}(J) = F_{2d}(J) = B_v'(\Omega = \frac{3}{2})J(J+1) - D'J^2(J+1)^2, \quad (6c)$$

$$B_v'(\Omega = \frac{1}{2}) = B_v'(\Omega = \frac{3}{2}) - \alpha'(v + \frac{1}{2}), \quad (7a)$$

$$B_v'(\Omega = \frac{3}{2}) = B_v'(\Omega = \frac{3}{2}) - \alpha'(v + \frac{1}{2}). \quad (7b)$$

Subband origins, defined consistent with Herzberg (21) are

$$\nu_0(\Omega = \frac{1}{2}) = Q_1(\frac{1}{2}) - \frac{3}{4}B_v'(\Omega = \frac{1}{2}), \quad (8a)$$

$$\nu_0(\Omega = \frac{3}{2}) = R_{21}(\frac{1}{2}) - 15/4B_v'(\Omega = \frac{3}{2}), \quad (8b)$$

and the spin-orbit splitting of a  $^2\Pi$  state is (22)

$$A = \nu_0(\Omega = \frac{3}{2}) - \nu_0(\Omega = \frac{1}{2}) + 2B. \quad (9)$$

Band origins were obtained from extrapolated positions of  $Q_1(\frac{1}{2})$  or  $R_{21}(\frac{1}{2})$  lines and wavelengths of specific features of the excitation spectrum measured relative to standard Ne atomic lines (23).

Wavelengths of several features of the excitation spectra were measured. Uncertainties given are estimates of three standard deviations. In the (0, 0) band the  $P_1(22.5)$  line is  $0.112 \pm 0.02$  nm to the blue of  $\lambda_{\text{air}} = 606.4536$  nm; the  $Q_2$  bandhead observed to form

TABLE III - CaF A<sup>2</sup>Π-X<sup>2</sup>Σ (0,0) Band Calculated Spectrum

J''	P <sub>1</sub> (J)+Q <sub>12</sub> (J-1)	Q <sub>1</sub> (J)+P <sub>12</sub> (J-1)	R <sub>1</sub> (J)	P <sub>12</sub> (J)	P <sub>2</sub> (J)	Q <sub>2</sub> (J)+P <sub>21</sub> (J+1)	P <sub>2</sub> (J)+Q <sub>21</sub> (J+1)	R <sub>21</sub> (J)
0.5	-	10953.33 <sup>a,b</sup>	10994.42	-	-	10954.26	10965.21	10966.89
1.5	10922.70	93.62	95.47 <sup>b</sup>	1091.31	-	64.56	65.98	67.95
2.5	92.40 <sup>c</sup>	23.95	95.53	90.28	10562.84	64.21 <sup>b</sup>	65.97	68.92
3.5	92.10 <sup>c</sup>	24.33	97.60	89.21 <sup>b</sup>	61.86	64.21 <sup>b</sup>	67.36	70.06
4.5	91.81 <sup>b</sup>	24.67	98.67	88.26	60.90	63.92 <sup>b</sup>	67.77	71.14
5.5	91.52 <sup>b</sup>	25.06	99.74	87.25	59.94	63.72 <sup>b</sup>	68.19	72.24
6.5	91.25 <sup>b</sup>	25.38	100.83	86.26	59.00	63.47 <sup>b</sup>	68.62	73.35
7.5	90.98 <sup>b</sup>	25.74	101.92	85.26	58.07	63.23 <sup>b</sup>	69.07	74.47
8.5	90.71 <sup>b</sup>	26.12	103.02	84.28	57.16	63.00 <sup>b</sup>	69.53	75.60
9.5	90.45 <sup>b</sup>	26.43	104.12	83.30	56.26	62.78 <sup>b</sup>	70.00	76.75
10.5	90.20 <sup>b</sup>	26.86	105.23	82.33	55.37	62.58 <sup>b</sup>	70.49	77.91
11.5	89.96 <sup>b</sup>	27.27	106.34	81.37	54.49	62.40 <sup>b</sup>	70.99	79.08
12.5	89.72 <sup>b</sup>	27.67	107.47	80.41	53.63	62.22 <sup>b</sup>	71.50	80.26
13.5	89.49 <sup>b</sup>	28.07	108.60	79.46	52.78	62.06	72.02	81.46
14.5	89.26 <sup>b</sup>	28.48	109.73	78.52	51.95	61.91	72.56	82.67
15.5	89.05 <sup>b</sup>	28.90	110.87	77.58	51.12	61.77	73.11	83.89
16.5	88.84 <sup>b</sup>	29.32	112.02	76.66	50.31	61.65	73.67	85.13
17.5	88.64 <sup>b</sup>	29.75	113.18	75.73	49.52	61.54	74.24	86.38
18.5	88.45 <sup>b</sup>	10953.19	114.34	74.82	48.73	61.44	74.83	87.64
19.5	88.26 <sup>b</sup>	0.63	115.51	73.91	47.96	61.35	75.43	88.91
20.5	88.08 <sup>b</sup>	01.08	116.68	73.01	47.20	61.28	76.04	90.19
21.5	87.89 <sup>b,c</sup>	01.54	117.85	72.11	46.46	61.22	76.67	91.49
22.5	87.71 <sup>b,c</sup>	02.00	119.05	71.22	45.73	61.18	77.31	92.80
23.5	87.55 <sup>b</sup>	02.47	120.24	70.34	45.01	61.14	77.96	94.12
24.5	87.39 <sup>b</sup>	02.95	121.44	69.47	44.31	61.12 <sup>b,d</sup>	78.62	95.46
25.5	87.24 <sup>b</sup>	03.43	122.64	68.60	43.62	61.116 <sup>b,d</sup>	79.30	96.81
26.5	87.09 <sup>b</sup>	03.92	123.85	67.74	42.94	61.122 <sup>b,d</sup>	79.99	98.17

<sup>a</sup> R<sub>12</sub> (-0.5) line does not exist.

<sup>b</sup> Observed and assigned in excitation spectrum.

<sup>c</sup> The P<sub>1</sub>(22.5) line is observed 0.112 ± 0.02 nm to the blue of the He line at λ<sub>air</sub> = 606.4536 nm.

<sup>d</sup> The Q<sub>2</sub> bandhead is observed 0.638 ± 0.02 nm to the red of the He line at λ<sub>air</sub> = 602.9997 nm.

at J'' = 26 ± 0.5 is 0.658 ± 0.02 nm to the red of λ<sub>air</sub> = 602.9997 nm. Also in the (0,0) band, the frequency separation of the R<sub>1</sub>(20.5) - P<sub>1</sub>(22.5) photoluminescence doublet was measured to be 28.95 ± 0.21 cm<sup>-1</sup> while the dye laser excited P<sub>1</sub>(22.5). The quoted uncertainty is three times the rms deviation of six measurements. When the dye laser excited the P<sub>1</sub>(16.5) line of the (1,0) band, the wavelengths of the P<sub>1</sub>(16.5) lines in the (1,0) and (1,1) bands were observed respectively 0.244 ± 0.02 nm red of λ<sub>air</sub> = 585.2488 nm and 0.358 ± 0.02 nm blue of λ<sub>air</sub> = 606.4536 nm.

The rotational quantum number at the (0,0) Q<sub>2</sub> head was determined by tuning the laser into the region of the head from the long λ side until the onset of photoluminescence. The observed separation between Q<sub>2</sub>(J) + P<sub>21</sub>(J+1) and R<sub>21</sub>(J-1) photoluminescence lines corresponded to simultaneous excitation of Q<sub>2</sub>(25.5) and Q<sub>2</sub>(26.5) but not Q<sub>2</sub>(24.5) or Q<sub>2</sub>(27.5). The calculated line positions for the CaF A-X (0,0) band, listed in Table III, show that the Q<sub>2</sub> head in fact forms at Q<sub>2</sub>(25.5).

In the course of recording the excitation spectrum in the Δv = 0 region, lines belonging to both (0,0) and (1,1) bands were recorded and assigned. Combining measured separations of lines belonging to (0,0) and (1,1) bands with fitted rotational constants, the separation of the A<sup>2</sup>Π<sub>1</sub> - X<sup>2</sup>Σ (0,0) and (1,1) origins is 5.54 ± 0.15 cm<sup>-1</sup>.

#### IV. RESULTS

The raw data from the excitation spectrum are interferometrically measured relative line positions, several lines measured with a scanning monochromator relative to Ne standard lines, and one carefully measured (with a monochromator) R(J-1)

—  $P(J+1)$  interval. All other measured  $R-P$  separations were used only to assign lines and were not used in least-squares fitting to obtain spectroscopic constants. The constants thus obtained are listed in Table IV. Table III lists calculated frequencies for lines of the  $A-X$  (0,0) band through  $J'' = 26.5$ . Features assigned in the excitation spectrum are indicated in Table III. Table III is included to enable future comparison with photographic absorption or emission spectra.

Constants for the CaF  $A^2\Pi$  and  $X^2\Sigma^+$  states satisfy Pekeris' relation (24)

$$\alpha = (6/\omega_e)[(B_e^2\omega_e x_e)^2 - B_e^2]. \quad (10)$$

Using vibrational constants from Rosen (16) ( $X^2\Sigma \omega_e = 587.4$ ,  $\omega_e x_e = 2.84$   $\text{cm}^{-1}$ ;  $A^2\Pi \omega_e = 592.6$ ,  $\omega_e x_e = 3.27$   $\text{cm}^{-1}$  which are the average of constants for the  $^2\Pi_1$  and  $^2\Pi_2$  states,

$$\begin{aligned} \text{calculated values of } \alpha \text{ are: } \alpha(X^2\Sigma) &= 0.0022, \\ \alpha(A^2\Pi) &= 0.0025, \end{aligned}$$

which compare with

$$\begin{aligned} \text{observed values: } \alpha(X^2\Sigma) &= 0.00255(48), \\ \alpha(A^2\Pi) &= 0.00283(45) \text{ cm}^{-1}. \end{aligned}$$

The  $A^2\Pi$  state is a particularly well-behaved regular  $^2\Pi$  state. Since  $A/B = 214$ ,  $A^2\Pi$  is near the Hund's case 'a' limit, and energy formulas are particularly simple for  $J' < 30$  (20). The effective rotational constants  $B(\Omega = \frac{1}{2})$  and  $B(\Omega = \frac{3}{2})$  differ by 0.00312 (21)

TABLE IV  
Constants for CaF  $X^2\Sigma$  and  $A^2\Pi$  in  $\text{cm}^{-1}$

(Numbers in parentheses correspond to three standard deviations uncertainty in the last digit)

	$X^2\Sigma$		$A^2\Pi$
$\nu_{00}$	0.0	$^2\Pi_{1/2}$	16493.1 (6)
		$^2\Pi_{3/2}$	16565.6 (6)
$\Delta G(\tilde{v})$	581.1 (9)	$^2\Pi_{1/2}$	586.8 (9)
$B_0$	0.3373 (11)		0.3422 (11)
$B_1$	0.3347 (12)		0.3393 (13)
$B_e$	0.3385 (11)		0.3436 (12)
$B_e(2-3/2) - B_e(\Omega=1/2)$	-		0.00312 (21)
$\alpha$	0.00255 (48)		0.00283 (45)
$\gamma(\text{estimated})$	$4.44 \times 10^{-7}$		$4.55 \times 10^{-7}$
$\gamma(\text{spin-spin})$	$ \gamma  < 3 \times 10^{-9}$		-
$A_0(\text{spin-orbit})$	-		73.4 (9)
$\lambda(\text{lambda doubling})$	-		-0.045 (4)



compared with the expected (19) difference of

$$B(\Omega = \frac{3}{2}) - B(\Omega = \frac{1}{2}) = 2B^2/A = 0.00321. \quad (11)$$

The lambda doubling constant  $p$  agrees with the pure precession estimate (20, 25), assuming interaction only with the nearby  $B^2\Sigma^+$  state.

$$p = 2A_{\Pi}B_{\Pi}l(l+1)/E(A^2\Pi) - E(B^2\Sigma). \quad (12)$$

If  $l = 1$  (the unfilled  $\pi$  orbital is a  $p\pi$  orbital located predominantly on Ca) and  $E(A) - E(B) = -2337 \text{ cm}^{-1}$  (16), then  $p = -0.0431$  compared to the observed value  $p = -0.045(4) \text{ cm}^{-1}$ . If the second lambda doubling constant  $q$  is related to  $p$  (20, 25) by  $q = pB_{\Pi}/A_{\Pi} \sim 2 \times 10^{-4}$ , then  $q$  would have been too small to measurably affect excitation spectra associated with either  $\Pi_1$  or  $\Pi_2$  below  $J' = 20.5$ . Using Mulliken and Christy's (20, 25) formulas for  $\Lambda$  doubling in an intermediate case 'a-b'  $^2\Pi$  state and assuming  $q = p(B/A)$ , the lambda doubling in  $^2\Pi_1$  at  $J = 20.5$  is less than  $0.03 \text{ cm}^{-1}$ , but in  $^2\Pi_2$  it is calculated to be  $0.94 \text{ cm}^{-1}$ .

The  $\Lambda$  doubling and spin-orbit constants for the CaF  $A^2\Pi$  state are well behaved as they are for BaF (13). The  $^2\Sigma^+$  ground state configuration of the alkaline earth halides is  $z\sigma^2 y\sigma^2 w\pi^4 x\sigma$  where the  $x\sigma$  orbital is primarily a metal  $ns$  orbital. The lowest  $^2\Pi$  state is expected to have a configuration which is predominantly  $z\sigma^2 y\sigma^2 w\pi^4 v\pi$  ( $v\pi$  = metal  $np\pi$ ) giving rise to a regular  $^2\Pi$  state. The configuration  $z\sigma^2 y\sigma^2 w\pi^3 x\sigma^2$  would lead to an inverted  $^2\Pi$  state. In the lowest  $^2\Pi$  state of BeF, the  $\Lambda$  doubling constant  $p$  is positive which would normally imply an inverted state, but this is interpreted as being due to a small  $\text{Be}^+$  atomic spin-orbit constant combined with configuration interaction which mixes in a small amount of the  $z\sigma^2 y\sigma^2 w\pi^3 x\sigma^2$  configuration with the predominant  $z\sigma^2 y\sigma^2 w\pi^4 v\pi$  configuration (26). Similar configuration interaction would be expected in CaF; however, the atomic spin-orbit constant for  $\text{Ca}^+$  is far larger than for  $\text{Be}^+$  so that despite the configuration mixing the  $A^2\Pi$  state for CaF is expected to remain regular in accordance with experiment.

#### ACKNOWLEDGMENTS

We would like to thank Professor H. P. Broida for his continued interest in this work. We would also like to express our appreciation to Professor H. W. Lewis for his support.

RECEIVED: August 19, 1974

#### REFERENCES

1. A. SCHULTZ, H. W. CRUSE, AND R. N. ZARE, *J. Chem. Phys.* **57**, 1354 (1972); H. W. CRUSE, P. J. DAGDIGIAN, AND R. N. ZARE, *Farad. Disc. Chem. Soc.* **55**, 277 (1973).
2. R. W. FIELD, A. D. ENGLISH, T. TANAKA, D. O. HARRIS, AND D. A. JENNINGS, *J. Chem. Phys.* **59**, 2191 (1973).
3. T. TANAKA, A. D. ENGLISH, R. W. FIELD, D. A. JENNINGS, AND D. O. HARRIS, *J. Chem. Phys.* **59**, 3217 (1973).
4. R. COLIN, M. CARLEER, AND F. PREVOT, *Can. J. Phys.* **50**, 171 (1972).
5. T. E. H. WALKER AND R. F. BARROW, *J. Phys. B* **2**, 102 (1969).
6. M. M. PATEL AND P. D. PATEL, *Proc. Phys. Soc.* **2**, 515 (1969).
7. E. MORGAN AND R. F. BARROW, *Nature* **192**, 1182 (1961).
8. M. M. PATEL AND P. D. PATEL, *Ind. J. Phys.* **42**, 254 (1968).
9. R. F. BARROW AND J. R. BEALE, *Proc. Phys. Soc.* **91**, 483 (1967).

10. E. MORGAN AND R. F. BARROW, *Nature* 185, 754 (1960).
11. B. S. MOHANTY AND K. N. UPADHYA, *Ind. J. Pure Appl. Phys.* 5, 523 (1967).
12. R. F. BARROW AND J. R. BEALE, *Chem. Comm.* 606 (1967).
13. R. F. BARROW, M. W. BASTIN, AND B. LONGBOROUGH, *Proc. Phys. Soc.* 92, 518 (1967).
14. D. P. NANDA, B. S. MOHANTY, *Curr. Sci. (India)* 39, 300 (1970).
15. L. T. EARLS, *Phys. Rev.* 48, 423 (1935).
16. B. ROSEN, "Spectroscopic Data Relative to Diatomic Molecules," p. 108, Pergamon Press, Elmsford, New York, 1970.
17. G. HERZBERG, "Spectra of Diatomic Molecules," p. 103, Van Nostrand, New York, 1950.
18. Ref. (17), p. 222.
19. Ref. (17), p. 233.
20. R. S. MULLIKEN AND A. CHRISTY, *Phys. Rev.* 38, 87 (1931)..
21. Ref. (17), p. 261.
22. Ref. (17), p. 232.
23. H. M. CROSSWHITE AND G. H. DIEKE, "Amer. Inst. Physics Handbook," 2nd ed., (Dwight E. Gray, Ed.), McGraw-Hill, New York, 1963.
24. Ref. (17), p. 108.
25. R. K. HINKLEY, J. A. HALL, T. E. H. WALKER, AND W. G. RICHARDS, *J. Phys. B* 5, 204 (1972).
26. T. E. H. WALKER AND W. G. RICHARDS, *J. Phys. B* 3, 271 (1970).

# Microwave Optical Double Resonance and Reanalysis of the CaF $A^2\Pi-X^2\Sigma$ Band System<sup>1</sup>

JUN NAKAGAWA, PETER J. DOMAILLE, TIMOTHY C. STEIMLE, AND DAVID O. HARRIS

*Department of Chemistry and Quantum Institute, University of California  
Santa Barbara, California 93106*

A laser excitation spectrum of the (0,0) and (1,1) bands of the CaF  $A^2\Pi-X^2\Sigma$  system has been recorded and all 12 rotational branches assigned on the basis of laser induced fluorescence measurements. Microwave optical double resonance (MODR) measurements were also made on several low- $J$  transitions to obtain precise spectroscopic constants of the  $X^2\Sigma$  state. The present set of molecular constants for both the  $A^2\Pi$  and  $X^2\Sigma$  states represent a vast improvement in precision over previously reported values because of the larger number of line position measurements and the use of a more reasonable Hamiltonian. The excellent agreement between the rotational constants derived from the optical and microwave measurements fully validates the assignments. Important derived constants are listed below (in  $\text{cm}^{-1}$ ) with 95% confidence limits in parentheses.

	$X^2\Sigma$	$A^2\Pi$
$T_e$	0	16526.8
$B_e$	0.343704 (23)	0.348744 (27)
$\alpha_e$	0.002436 (21)	0.002529 (26)
$A$ (spin-orbit)		71.475 (14)
$\alpha(A)$ (vibration-spin-orbit)		0.027 (12)
$\gamma$ (spin-rotation)	0.00131 (46)	
$p$ (A-doubling)		-0.0438 (3)

## I. INTRODUCTION

Microwave optical double resonance (MODR) spectroscopy has previously been shown to be a useful tool for the assignment of optical spectra, and in obtaining more precise spectroscopic constants (1-5). If the frequencies of ground state rotational transitions are known, it is possible to identify electronic transitions which are optically connected with the rotational levels. Conversely, if the rotational analysis of an electronic band system extends to sufficiently low  $J$  values, MODR can be applied to unambiguously verify the optical assignment (4). Moreover, more accurate spectroscopic constants can be obtained because of the superior precision of microwave frequency measurements.

<sup>1</sup>This research was supported by the AFOSR and the National Science Foundation, Grants AFOSR-73-2565 and NSF-MPS-72-04978, respectively.



In the present paper, the latter approach has been taken because the ground state rotational transition frequencies were not previously known. The excitation spectrum of the  $A^2\Pi-X^2\Sigma^+$  band system of CaF has been rotationally assigned and MODR applied to obtain more precise rotational and spin-rotation interaction constants of the  $X^2\Sigma^+$  ground electronic state.

The A-X band system was recently optically analyzed by Field *et al.* (6). However, the spectroscopic constants obtained were relatively inaccurate, because of the low precision of the line position measurements. Frequency spacings were measured using an optical spectrum analyzer with a nominal 3.0 GHz free spectral range (FSR) and absolute frequencies were made relative to standard neon atomic lines. It has subsequently been determined that the FSR of the spectrum analyzer is only known to within about 1 to 2% of its specified value and is thus inappropriate for accurate line position measurements (5).

The present paper extends the assignments to all 12 branches and also up to much higher  $J$  values thus giving greatly improved statistics in the extraction of spectroscopic constants.

## II. EXPERIMENTAL DETAILS

The excitation spectrum was measured using the same experimental arrangement as described previously (5). The frequencies of the optical transitions were calibrated by simultaneously recording an excitation spectrum of molecular iodine whose absolute frequencies are known to about  $0.004\text{ cm}^{-1}$  from recent interferometric data (7). The accuracy of the line positions of CaF is believed to be about  $0.02\text{ cm}^{-1}$ . The observed frequency regions, between  $16\,473$  and  $16\,508\text{ cm}^{-1}$  and between  $16\,546$  and  $16\,582\text{ cm}^{-1}$ , correspond to  $\Delta v = 0$  sequences of the  $A^2\Pi_1-X^2\Sigma$  and  $A^2\Pi_1-X^2\Sigma$  subbands, respectively.

The experimental set up for the MODR was described in Ref. (4). Microwave radiation of about 700 mW (41 GHz) and 200 mW (61 GHz) was generated by OKI 40 V12 and 60 V12 phase-locked klystrons and introduced into the cell via a horn radiator. The MODR signal was detected by observing increases of the photoluminescence intensity as a function of microwave frequency. The photoluminescence detected was not total undispersed photoluminescence but rather the other line which was not coincident with the laser frequency. For example, when the laser frequency was tuned to the  $R_{21}$  (2.5) transition, the photoluminescence corresponding to the  $Q_2$  (3.5) and  $P_{21}$  (4.5) lines was detected through a monochromator with a bandpass of about  $0.08\text{ nm}$ . The intensity of the photoluminescence increased 1 to 2% at microwave resonance when either the upper or lower rotational level was optically pumped, indicating the laser field is significantly depleting the ground state.

## III. SPECTRAL FEATURES AND ASSIGNMENT OF THE EXCITATION SPECTRA

There are 12 rotational branches in the  $A^2\Pi-X^2\Sigma$  band system. These branches are the  $P$ ,  $Q$ , and  $R$  branches which originate in one of four classes of  $^2\Pi$  levels,  $F_{1c}$ ,  $F_{1d}$ ,  $F_{2c}$ ,  $F_{2d}$ . Since the spin-orbit coupling constant of the CaF  $A^2\Pi$  state is moderately large ( $A \approx 72\text{ cm}^{-1}$ ), the 12 rotational branches divide into two subband systems corresponding to  $F_1$  and  $F_2$  levels. These are the  $^2\Pi_1$  and  $^2\Pi_2$  fine structure levels, respectively, because  $A$  is positive (6).

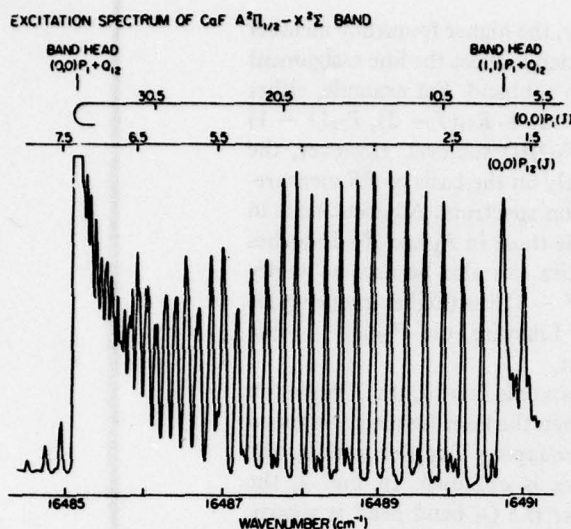


Fig. 1. A typical excitation spectrum of the CaF  $A^2\Pi_{1/2} - X^2\Sigma^+$  band. The  $P_1 + Q_{12}$  band heads of (0,0) and (1,1) bands are shown.

Not only were (0,0) vibrational transitions evident, but also the hot band series (1,1), (2,2), ... overlapped in these regions because of the small change in vibrational constants. The  $P_1(J) + Q_{12}(J - 1)$  branches formed heads at 16 485.1, 16 490.7, 16 495.9, and 16 500.7  $\text{cm}^{-1}$  for the (0,0), (1,1), (2,2), and (3,3) bands, respectively. Also the  $Q_2(J) + P_{21}(J + 1)$  branches formed heads at 16 560.2, 16 565.9, 16 571.2, and 16 576.1  $\text{cm}^{-1}$  for these same bands. These overlapping branches make the spectrum complicated, but the regular and strong series assigned to the  $R_1$  and  $R_2$  branches could readily be observed to higher frequency. Also, the  $P_{12}$  and  $P_2$  branches were fairly simple without overlapping of the other strong branches. In Fig. 1, the excitation spectrum near the  $^2\Pi_{1/2}$  (0,0) subband origin is shown with assignments of some series.

Because of the small value of the ground state spin-rotation constant the  $Q_{12}(J - 1)$  and  $P_1(J)$  branches are overlapped until higher  $J$  values. At  $J$  values greater than 27.5 the splitting into separated branches becomes apparent. On the other hand, the splitting of the  $Q_{21}(J)$  and  $R_2(J - 1)$  lines is not resolved although the maximum  $J$  value observed was also  $R_2$  (27.5). However, in spite of not being resolved, a broadening of these lines is apparent. Conversely, no apparent broadening nor splitting of the overlapped  $Q_2(J - 1)$ ,  $P_{21}(J)$  branches and the  $Q_1(J)$ ,  $R_{12}(J - 1)$  branches was observed. The explanation of this phenomenon is deferred until later.

Rotational analyses were performed on the (0,0) and (1,1) bands, because these two bands were sufficient to determine the spectroscopic constants of interest.

The assignments of the individual lines have been made on the basis of the  $P$ - $R$  separation measurements described in detail by Field *et al.* (6). Because the spin-rotation coupling constant  $\gamma''$  is small, the photoluminescence spectra are not resolved into  $P$ ,  $Q$ , and  $R$  branches, but only into  $P$  and  $R$  branches, the  $Q$  branch being coincident with one or the other (6). If the laser is coincident with the lower frequency component



then this line is a member of a *P* or *Q* branch. Conversely, the higher frequency member corresponding to an *R* or *Q* branch. This simple observation reduces the line assignment to a choice between one of two possibilities within each subband. For example, either an  $R_1(J-2)$ ,  $P_1(J) + Q_{12}(J-1)$  pair or else a  $Q_1(J-2) + R_{12}(J-3)$ ,  $P_{12}(J-1)$  pair would be observed in transitions involving the  $F_1(^2\Pi_1)$  sublevel. However, the distinction between these possibilities is not possible solely on the basis of *PR* measurements; the final choice is determined from the excitation spectrum. Adjacent lines in the  $P_{12}$  and  $R_1$  branches are separated by about  $3B$  while those in  $P_1$  and  $R_{12}$  branches are separated by about  $B$ . Photoluminescence intensities can also be used to verify the choice because, for a pure case (a) molecule, the  $R_1(J-2)$  line (higher frequency) is weaker than the sum of the  $P_1(J) + Q_{12}(J-1)$  pair. Likewise, the  $P_{12}(J-1)$  line (lower frequency) is weakest in the alternate assignment.

If the approximate rotational constant of the ground state is known, the  $J$  value can be calculated from the measured *P-R* separation (6). When the laser frequency is tuned to the band head, where several transitions have overlapping Doppler profiles, the photoluminescence spectrum of several coincident lines is obtained. In Fig. 2, the photoluminescence spectrum obtained by pumping near the  $Q_2$  band head is shown. The fact that the intensities of the  $R_{21}$  (23.5) and  $R_{21}$  (25.5) lines are stronger than that of  $R_{21}$  (24.5) shows  $Q_2$  (25.5) is closer to the head and the laser frequency is about  $0.01 \text{ cm}^{-1}$  bluer than the head. From this spectrum, the approximate ground state rotational constant,  $B''$ , can be determined since the frequency difference between adjacent lines is approximately equal to  $4B''$ . If a number of *P-R* separations are measured in photoluminescence spectra, and their  $J''$  values assigned, a more accurate value of  $B''$  can be obtained. However, this constant is only moderately precise because the inadequate resolving power and slight nonlinearity of the monochromator cause inaccuracies in line position measurements.

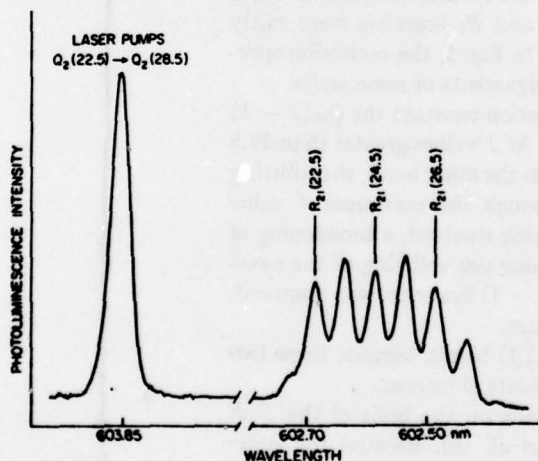


FIG. 2. Photoluminescence spectrum of CaF excited by a single mode cw dye laser tuned to  $Q_2$  head of (0,0) band. The fact that the intensities of  $R_{21}$  (23.5) and  $R_{21}$  (25.5) are stronger than  $R_{21}$  (24.5) shows  $Q_2$  (25.5) forms the head and the laser frequency is about  $0.01 \text{ cm}^{-1}$  to the blue of the head.



## IV. MICROWAVE OPTICAL DOUBLE RESONANCE SPECTRUM

Four rotational transitions of the ground  $X^2\Sigma^+$ ,  $v'' = 0$  state and three transitions of the  $v'' = 1$  state were measured. The measured microwave frequencies and the laser pumping transitions are listed in Table I.

The hyperfine structure of these transitions was not resolved, because the half-width of the MODR lines was about 20 MHz. There are several sources of line broadening, namely Zeeman splitting, pressure broadening, and microwave power saturation (4). Although the hyperfine constants could not be experimentally obtained, the frequencies of these low  $J$  transitions are significantly affected by the hyperfine interactions. Fortunately, the hyperfine constants  $A_1$  and  $A_{11}$  were available from the neon matrix isolation ESR data of Knight *et al.* (8) so an approximate treatment of these effects was possible. The observed frequencies were corrected for these contributions in order to derive realistic rotational and spin-rotation interaction constants.

The Fermi contact interaction constant,  $b_s + c_s/3$ , is related to the ESR constants as  $(b_s + c_s/3) = \frac{1}{3}(A_1 + 2A_{11})$  and to the tensor interaction constant  $c_s = (A_1 - A_{11})$  (9). Using  $(b_s + c_s/3) = 120$  MHz and  $c_s = 43$  MHz, along with approximate values of  $B''$ ,  $D''$  and  $\gamma''$ , the transition frequencies were calculated.

The difference between these values calculated with and without hyperfine contributions was applied as a correction to the measured transition frequencies. These corrected values are listed in Table I along with those calculated from constants derived from a least-squares fit.

It should be noted that the signs of the hyperfine constants  $A_1$  and  $A_{11}$  were not determined from the ESR data. Thus, the transition frequencies were calculated for the four possible cases of the signs of the hyperfine constants. Afterward, one of four cases was selected based on the observed spectrum; three of the choices produce hyperfine transitions which should have been resolved. For the preferred choice, the signs of the hyperfine constants were determined to be both positive.

TABLE I

Measured and Fitted Frequencies (MHz) in the MODR Spectrum of the  $X^2\Sigma^+$  State of CaF

Vibrational State	$A^2\Sigma^+ - X^2\Sigma^+$ Transition	Rotational Transition <sup>a)</sup>	Frequency		Least Squares
			Measured <sup>b)</sup>	Corrected <sup>c)</sup>	
$v''=0$	$Q_2(1.5)$	$ 2,1.5\rangle -  1,0.5\rangle$	41059.1(2.8)	41051.6	41050.1
	$R_{21}(2.5)$	$ 2,2.5\rangle -  1,1.5\rangle$	41085.4(1.1)	41089.7	41089.1
	$Q_3(2.5)$	$ 3,2.5\rangle -  2,1.5\rangle$	61586.3(4.2)	61583.0	61584.1
	$R_{21}(3.5)$	$ 3,3.5\rangle -  2,2.5\rangle$	61620.2(1.8)	61622.9	61623.1
$v''=1$	$R_{21}(2.5)$	$ 2,2.5\rangle -  1,1.5\rangle$	40792.5(3.0)	40796.7	40798.3
	$Q_3(2.5)$	$ 3,2.5\rangle -  2,1.5\rangle$	61148.3(4.3)	61145.2	61145.5
	$R_{21}(3.5)$	$ 3,3.5\rangle -  2,2.5\rangle$	61185.0(3.5)	61187.5	61186.3

a) Transitions are labelled as  $|N',J'\rangle - |N'',J''\rangle$ .

b) Numbers in parentheses represent two standard deviations of several measurements.

c) Corrected for contributions from hyperfine effects. See text.

## V. DETERMINATION OF THE SPECTROSCOPIC CONSTANTS

The energy levels of  $^2\Pi$  states are given by the following formulas (11, 12) for a good case (a) molecule:

$$F_{1c}(J) = T_0 - \frac{A_0}{2} + B'_0(\Omega = \frac{1}{2})J(J+1) - D'_0(\Omega = \frac{1}{2})J^2(J+1)^2 - \frac{p_0}{2}(J + \frac{1}{2}), \quad (1a)$$

$$F_{1d}(J) = T_0 - \frac{A_0}{2} + B'_0(\Omega = \frac{1}{2})J(J+1) - D'_0(\Omega = \frac{1}{2})J^2(J+1)^2 + \frac{p_0}{2}(J + \frac{1}{2}), \quad (1b)$$

and

$$F_{2c}(J) = F_{2d}(J) = T_0 + \frac{A_0}{2} + B'_0(\Omega = \frac{3}{2})J(J+1) - D'_0(\Omega = \frac{3}{2})J^2(J+1)^2 \quad (1c)$$

and for a case (b)  $^2\Sigma$  state, the energy levels are given by:

$$F_1(N) = B''_0 N(N+1) - D''_0 N^2(N+1)^2 + \frac{\gamma''_0}{2} N \quad (2a)$$

$$F_2(N) = B''_0 N(N+1) - D''_0 N^2(N+1)^2 - \frac{\gamma''_0}{2} (N+1), \quad (2b)$$

where the symbols have their usual spectroscopic meanings and hyperfine interaction terms are neglected.

The ground state constants, listed in column 1 of Table II, were calculated from fitting the corrected MODR frequencies mentioned in the last section to the expressions (2a) and (b). In this analysis, the centrifugal distortion constant was fixed at  $D_0 = 4B_0^2/\omega_0^2$  on the assumption of a Morse potential function. The numbers in parentheses represent 95% confidence limits obtained by scaling the standard error by Student's  $t$  factor. The uncertainties are rather large by microwave spectroscopy standards due to small number of observed transitions and the rapid increase of the  $t$  factor with decreased degrees of freedom. The  $t$  factor of 200 degrees of freedom for 95% confidence limit is 1.97 whereas that of 1 degree of freedom, which is the case for the MODR of the  $v'' = 1$  state, is 12.7.

The spectroscopic constants derived from the optical data were obtained by two methods: the first of which was a linear least-squares fit to pure case (a) formulas while the other was a more rigorous nonlinear least-squares fit which determined the parameters using a more complete Hamiltonian matrix based on case (a) basis functions (10).

Column 2 of Table II shows the constants derived from linear least-squares fits to our optical data for the (0,0) and (1,1) bands, respectively. In these fits, the spin-rotation constants  $\gamma''_0$  and  $\gamma''_1$  were held fixed at the values obtained from the MODR data, because the splittings due to  $\gamma''$  were only observed for a few optical transitions. The centrifugal distortion constants were determined as fitted parameters.

Column 3 contains the results of the nonlinear "direct approach" method of obtaining spectroscopic constants as discussed by Zare and co-workers (10). In the present case, the  $A^2\Pi$  eigenvalues were determined from a Hamiltonian matrix which included the off-diagonal contributions. In these calculations,  $\gamma''$  was fixed to the value obtained

TABLE II  
Spectroscopic Constants ( $\text{cm}^{-1}$ ) of CaF derived from the  $A^2\Pi-X^2\Sigma$  Band System<sup>a,b</sup>

MODR	(0,0) Band		
	linear	non-linear	combined
$T_0$	16528.835 (4)	16529.671 (5)	16529.671 (5)
$A_0$	71.923 (7)	71.486 (9)	71.488 (9)
$B^*_{1/2}$	0.34597 (18)		
$B^*_{3/2}$	0.34907 (18)		
$B^*_0$		0.34736 (13)	0.347479 (17)
$B^*_0$	0.342488 (19)	0.34259 (17)	0.34237 (13)
$B^*_0$		0.34237 (13)	0.342486 (15)
$D^*_0$		-0.0417 (5)	-0.0435 (4)
$D^*_{1/2}$		-0.0435 (4)	-0.0435 (4)
$D^*_{3/2}$		$8.6 \times 10^{-7}$ (17)	
$D^*_0$		$8.5 \times 10^{-7}$ (17)	
$D^*_0$		$3.5 \times 10^{-7}$ (13)	$4.4 \times 10^{-7}$ (9)
$D^*_0$	$4.66 \times 10^{-7}$	$8.2 \times 10^{-7}$ (16)	$3.6 \times 10^{-7}$ (13)
$D^*_0$		$3.6 \times 10^{-7}$ (13)	$4.5 \times 10^{-7}$ (9)
$\gamma^*_0$	$1.30 \times 10^{-3}$ (20)	$1.30 \times 10^{-3}$	$1.30 \times 10^{-3}$
$q^*_0$		$-2.05 \times 10^{-4}$	$-2.05 \times 10^{-4}$
$o^*_0$		-1.120	-1.118
$N^{(c)}$	4	283	287

from MODR, the A-doubling constant,  $q$ , was fixed to the calculated value of  $p_0(B_0/A_0)$  and the constant  $o$ , was internally calculated from  $o_0 = (1/8)(A_0/B_0)p_0$ . The standard deviations of the fits to the (0,0) and (1,1) bands were 0.015 and 0.013  $\text{cm}^{-1}$ , respectively.

The microwave and optical data were simultaneously fitted (16) to obtain the constants listed in Column 4. In these calculations, the weight of the microwave data was  $4 \times 10^4$  times greater than that of the optical data because the uncertainties in the microwave transition frequencies were approximately 200 times smaller than those of the optical measurements. The ground state spin-rotation constant,  $\gamma''$ , was fixed to the MODR value. Inclusion of this parameter as a variable in a simultaneous fit was deemed unwise since only a few resolved optical transitions determine this parameter at all, and these few data points are outweighed by the large number which artificially ascribe  $\gamma'' = 0$  because the branch splitting is not observed. The observed line positions and the differences between observed and calculated frequencies, based on the constants in Column 4, are collected in Table III.

Last, Table IV has been composed to collect the equilibrium constants for both states. Vibrational constants were taken from the compilation of Rosen (15) with the choice of his values for the  $^2\Pi_1$  state, because of the better agreement with the present (0,0) and (1,1) band origin differences. The value of  $T_0$  absorbs errors in the vibrational constants and hence is listed without confidence limits. The symbol  $\alpha(A)$  refers to the vibrational dependence of the spin-orbit constant. Parameters listed without an equilibrium subscript are the weighted average of  $v = 0$  and  $v = 1$  values.



TABLE II—Continued

(2,1) Band				
$T_1$		16534.473(3)	16535.316(5)	16535.316(5)
$A_1$		71.979(6)	71.513(8)	71.512(4)
$B'_{1/2}$		0.34327(19)		
$B'_{3/2}$		0.34633(18)		
$B'_1$			0.34470(16)	0.344950(20)
$B''_1$	0.34005(9)	0.33997(18)	0.33980(16)	0.340050(14)
$D'_1$		-0.0438(3)	-0.0440(3)	-0.0440(3)
$D'_{1/2}$		$3.1 \times 10^{-7}$ (23)		
$D'_{3/2}$		$2.6 \times 10^{-7}$ (22)		
$D'_1$			$6.0 \times 10^{-8}$ (187)	$3.0 \times 10^{-7}$ (10)
$D''_1$	$4.56 \times 10^{-7}$	$2.7 \times 10^{-7}$ (21)	$8.0 \times 10^{-8}$ (184)	$3.2 \times 10^{-7}$ (10)
$\gamma''_1$	$1.36 \times 10^{-3}$ (99)	$1.36 \times 10^{-3}$	$1.36 \times 10^{-3}$	$1.36 \times 10^{-3}$
$q'_1$			$-2.10 \times 10^{-4}$	$-2.10 \times 10^{-4}$
$o'_1$			-1.142	-1.140
$n^{(c)}$	3	203	203	206

- a) Figures in parentheses represent 95% reliability intervals attached to the last significant figure. The figures which have no uncertainties stated are values which are fixed.
- b) The column headings have the following significance:
- (i) MODR: Values from the microwave measurements.
  - (ii) linear: from a linear least squares fit to the optical measurements.
  - (iii) non-linear: "direct approach" of Ref. 10 fit to the optical data.
  - (iv) combined: non-linear fit using the optical and microwave data simultaneously.
- c) Number of transitions used in the fit.

## VI. DISCUSSION

Although the basic conclusions of the earlier work (6) are not altered, the constants derived from the present analysis differ somewhat from those of the previous two studies (6, 14). Undoubtedly, the analysis of Mohanty and Upadhyaya (14) is incorrect. Also, although the assignment of Field *et al.* (6) appears sound, the derived constants are slightly in error because of inaccuracies in the line position measurements made with a 3.0-GHz FSR spectrum analyzer (5).

The excellent agreement of rotational constants obtained from the MODR fit and from direct optical measurements leave no doubt as to the validity of our assignment. However, the microwave data are of disappointingly low precision because of the poor signal-to-noise ratio, breadth of the rotational lines and paucity of measured lines. The anticipated large improvement in accuracy is not obtained. For the  $v'' = 0$  state only a sevenfold decrease in uncertainty of the rotational constant is realized, while for  $v'' = 1$  the precision of the MODR data and optical analysis are about the same. However, the microwave data do determine the sign and magnitude of  $\gamma''$  quite well, whereas the optical spectrum has only a few lines from which to determine this parameter. Additional measurement of more pure rotational lines at higher resolution is required to further improve the constants.

An interesting comparison of the results of the linear versus nonlinear fits is available by correcting the effective values obtained from the linear fit for magnetic contributions

TABLE III  
Observed and Calculated Frequencies in the CaF  $A^2\Pi-X^2\Sigma$  Band (in  $\text{cm}^{-1}$ )

(0,0) Band						
J	$P_1(J)$ Frequency $\Delta v$	$Q_1(J)$ Frequency $\Delta v$	$O_1(J)$ Frequency $\Delta v$	$R_1(J)$ Frequency $\Delta v$	$R_2(J)$ Frequency $\Delta v$	$P_2(J)$ Frequency $\Delta v$
0.5				16493.450 5		16491.071 11
1.5				93.775 -7		90.033 12
2.5				94.142 15		
3.5	16491.050 -5	16491.050 -10	93.775 -4	94.475 -3	97.451 19	
4.5	91.547 -10	91.267 -6	94.475 3	94.823 -13	98.532 16	
5.5	91.267 1	90.987 -2	94.823 -5	95.200 0		86.959 14
6.5	90.987 6	90.709 -4	95.200 8	95.567 -4	16500.711 5	85.938 5
7.5	90.709 6	90.439 -4	95.567 4	95.939 -11	01.012 2	84.944 16
8.5	90.439 7	90.162 3	95.939 0	96.330 -3	02.092 -29	83.936 8
9.5	90.162 15	89.924 2	96.330 9	96.722 -3	04.047 9	82.946 7
10.5	89.924 16	89.676 4	96.722 11	97.108 -15	05.173 11	81.947 -7
11.5	89.676 19	89.430 2	97.108 0		06.316 24	80.967 -10
12.5	89.430 18	89.190 7	97.509 -2		07.443 14	80.000 1
13.5	89.190 24	88.962 1	97.926 5		08.571 -1	79.057 14
14.5	88.962 20	88.737 -3	98.337 -1			78.075 -12
15.5	88.737 19	88.514 -7	98.753 -9			77.130 -7
16.5	88.514 14	88.302 -9	99.190 -2			76.216 20
17.5	88.302 14	88.103 -5	99.632 2			75.244 -14
18.5	88.103 20	87.905 -8	16500.072 -2			74.330 -2
19.5	87.905 19	87.711 -10	00.527 2			73.393 -19
20.5	87.711 16	87.526 -12	00.974 -9			
21.5	87.526 16	87.357 -5	01.443 -5			
22.5	87.357 24	87.190 -3	01.967 -13			
23.5	87.190 20	87.022 -8	02.385 -14			
24.5	87.022 24	86.869 -5	02.892 7			
25.5	86.869 27	86.722 -4	03.375 -3			
26.5	86.722 30	86.593 9	03.873 -5			
27.5	86.593 9	86.464 -6	04.372 -13			
28.5	86.464 0	86.339 -3	04.885 -14			
29.5	86.339 -1	86.203 2	05.406 -14			
30.5	86.203 6	86.091 4	05.930 -19			
31.5	86.091 10	85.970 -10	06.469 -16			
32.5		85.873 -8	06.995 -32			
33.5	85.841 3	85.773 -16	07.558 -20			
34.5	85.736 -8	85.690 -14	08.096 -39			
35.5		85.102 -24				
36.5		85.538 -17				
37.5		85.469 -22				
38.5		85.409 -26				
39.5		85.354 -53				
40.5		85.288 -55				

J	$P_2(J)$	$Q_2(J)$	$P_{21}(J)$	$R_2(J)$	$Q_{21}(J)$	$R_{21}(J)$
0.5		16564.059 -2		16565.433 2		16567.162 -11
1.5		63.745 -7		65.811 5		60.241 -4
2.5	16562.004 -3	63.430 -17	16564.059 1	66.591 -4	16565.433 4	60.351 21
3.5		63.142 -10	63.745 -2	66.999 -10	66.591 1	70.409 -19
4.5	60.043 12	62.896 -5	63.430 -11	67.410 -26	66.999 -2	71.541 4
5.5	59.964 1	62.641 -3	63.162 -3	67.824 -52	67.410 -19	72.653 -10
6.5	59.108 1	62.399 0	62.896 3	68.315 -13	67.824 -42	73.796 -3
7.5	57.163 -2	62.161 -7	62.641 7	68.782 -12	68.315 -2	74.957 9
8.5	56.234 -1	61.947 -2	62.399 11	69.256 -16	68.782 1	76.134 24
9.5	55.321 3	61.718 -6	62.161 6	69.745 -17	69.256 -2	77.287 2
10.5	54.410 -5	61.546 -5	61.947 11	70.245 -21	69.745 -2	78.474 1
11.5	53.524 0	61.365 -7	61.738 9	70.757 -25	70.245 -4	79.685 12
12.5	52.638 -8	61.204 -2		71.301 -10	70.757 -7	80.901 -6
13.5	51.705 3			71.832 -20	71.301 10	
14.5	50.827 -3			72.379 -27	71.832 2	
15.5	50.091 0	60.905 -7		72.954 -18	72.379 -5	
16.5	49.279 14	60.766 -19		73.554 -18	72.954 4	
17.5	48.462 10	60.603 13		74.132 -11	73.554 6	
18.5	47.650 -2	60.521 -48		74.729 -18	74.132 14	
19.5	46.870 4	60.465 -16		75.361 -3	74.729 8	
20.5		60.403 -3		75.976 -17	75.361 25	
21.5		60.343 -1		76.621 -13	75.976 12	
22.5				77.287 -1	76.621 17	
23.5				77.933 -21	77.287 31	
24.5				78.618 -15	77.933 12	
25.5				79.299 -25	78.618 20	
26.5				80.020 -6	79.299 11	
27.5					80.020 30	
28.5						
29.5						
30.5		60.343 27				
31.5		60.403 32				
32.5		60.465 26				
33.5		60.521 2				
34.5		60.609 36				
35.5		60.750 30				
36.5		60.862 23				
37.5		60.985 13				
38.5		61.140 23				
39.5		61.300 25				
40.5		61.467 21				
41.5		61.646 16				
42.5		61.847 20				
43.5		62.051 15				
44.5		62.262 24				
45.5		62.509 16				
46.5		62.794 13				
47.5		63.017 15				
48.5		63.287 12				
49.5		63.573 12				
50.5		63.905 5				
51.5		64.169 -2				
52.5		64.511 16				
53.5		64.824 -7				
54.5		65.171 -10				
		65.530 -13				

TABLE III—Continued

(1,1) Band					
$P_1(J)$	$Q_{12}(J)$	$Q_1(J)$	$R_{12}(J)$	$R_1(J)$	$P_{12}(J)$
0.5					
1.5	16498.097 14	16498.097 12			
2.5	97.785 11	97.783 7			
3.5		97.184 2	16499.386 6	16499.386 3	16499.684 4
4.5	97.184 8	96.883 -9	99.722 2	99.722 -3	
5.5	96.883 -2	96.623 12	16500.429 10	16500.429 2	92.602 -3
6.5	96.623 21		00.775 -4	01.149 -6	92.588 -5
7.5		96.066 -9	01.149 4	01.519 -10	90.587 -2
8.5	96.066 2	95.810 3	01.519 1		89.589 -7
9.5	95.810 15	95.567 15		16507.364 8	88.616 5
10.5	95.567 29	95.303 0	02.271 -12	02.678 -13	87.623 -9
11.5	95.303 16	95.057 -3	02.678 3		
12.5	95.057 14	94.823 -2	03.078 4	03.078 -13	
13.5	94.823 17	94.590 0	03.479 -1		84.748 9
14.5	94.590 20	94.363 -9			82.787 2
15.5	94.363 12	94.142 -14	04.315 3		82.850 10
16.5	94.142 0	93.937 -5	04.734 -4		81.903 0
17.5	93.937 15	93.730 -5			
18.5	93.730 20	93.538 -9	05.611 1		80.042 -6
19.5	93.538 18	93.351 -6	06.039 -17		79.131 0
20.5	93.351 22	93.171 -1	06.562 -7		78.216 -6
21.5	93.171 27	92.986 -11			77.307 -12
22.5	92.986 20	92.820 1			76.425 1
23.5	92.820 33	92.662 -2	07.902 -8		75.536 -10
24.5	92.662 31		08.371 -19		74.653 -2
25.5		92.333 -25			73.775 -7
26.5	92.333 11				72.919 3
27.5		92.071 -8			
28.5	92.045 4	91.948 -2			
29.5	91.912 2	91.799 -29			
30.5	91.771 -15	91.686 -27			
31.5	91.650 -20				
32.5		91.471 -32			
33.5	91.446 -11	91.377 -32			
34.5	91.347 -15				
$P_2(J)$	$Q_2(J)$	$P_{21}(J)$	$R_2(J)$	$Q_{21}(J)$	$R_{21}(J)$
0.5			16571.079 -10		16571.770 2
1.5			71.453 -9	16571.079 -8	72.807 -12
2.5	16567.684 -6	16569.428 6		71.453 -5	73.911 20
3.5		69.118 -9	72.247 2		74.957 -3
4.5	65.741 13	69.118 -3		72.247 8	
5.5	64.730 -7	68.545 -31	73.067 -10		77.142 -9
6.5	63.780 -28	68.545 -22	73.511 -2	73.067 -2	78.269 3
7.5	62.896 17	68.050 -17	73.964 3	73.511 8	
8.5	61.947 -8	68.050 -6	74.417 -5	73.964 14	80.536 3
9.5		67.608 -18	74.889 -6	74.417 8	81.635 -50
10.5		67.608 -4	75.361 -20	74.889 8	
11.5	59.239 -19	67.214 -14	75.869 -10	75.361 -4	
12.5	58.387 2	67.060 -6	76.383 -7	75.869 7	
13.5	57.533 9	66.867 -14	76.903 -10	76.383 11	
14.5	56.677 1	66.722 -4	77.426 -22	76.903 10	
15.5	55.846 5	66.581 6		77.426 -2	
16.5	55.044 25	66.462 -14	78.550 -7		
17.5	54.221 13	66.331 -9	79.125 -5	78.550 17	
18.5	53.410 7	66.233 -4		79.125 20	
19.5	52.638 12	66.140 -7	80.306 -7		
20.5	51.886 2	66.078 9		80.306 21	
21.5	51.124 29	66.015 6			
22.5	50.367 19	65.960 7			
23.5					
24.5	48.996 3				
25.5	48.190 6				
26.5	47.509 20				
27.5		Band head			
28.5					
29.5		65.960 11			
30.5		66.011 11			
31.5		66.070 15			
32.5		66.140 0			
33.5		66.233 4			
34.5		66.331 0			
35.5		66.442 -2			
36.5		66.561 18			
37.5		66.722 9			
38.5		66.867 1			
39.5		67.040 8			
40.5		67.214 3			
41.5					
42.5		67.608 2			
43.5					
44.5		68.050 6			

a)  $\Delta v = (\text{Obs.} - \text{Calc.}) \times 1000 \text{ cm}^{-1}$ 

(10). For example, the results for the (0,0) fits are

$$T_0 = 16\,529.650 \quad (16\,529.671)$$

$$A_0 = 71.503 \quad (71.486)$$

$$B_0 = 0.34752 \quad (0.34736)$$

where the first values refer to the corrected linear quantity from column 2 of Table II



TABLE IV  
Equilibrium Constants<sup>a,b</sup> (cm<sup>-1</sup>) for the X<sup>2</sup>Σ and A<sup>2</sup>Π State of CaF

	X <sup>2</sup> Σ	A <sup>2</sup> Π
T <sub>0</sub>	0	16526.8
ω <sub>e</sub>	587.4	593.4
ω <sub>e</sub> X <sub>e</sub>	2.84	3.11
B <sub>0</sub>	0.343704 (23)	0.348744 (27)
α <sub>e</sub>	0.002436 (21)	0.002529 (26)
A <sub>0</sub> (spin-orbit)		71.475 (14)
a (A) (°)		0.027 (12)
p (Λ-doubling)		-0.0438 (3)
γ (spin rotation)	0.00131 (46)	

a) Vibrational constants from the tables given by Rosen (15).

b) Non-subscripted parameters are the weighted average of v=0 and v=1.

c) The vibrational dependence of the spin-orbit coupling constant.

Note. Uncertainties are 95% confidence limits.

and the number in parentheses refer to directly fitted nonlinear values. As expected, the agreement is seen to be very good because the A<sup>2</sup>Π state is a good case (a) state with A/B ≈ 200.

As mentioned in Section III, the splittings due to γ'' could only be observed for high J transitions of the P<sub>1</sub>(J) + Q<sub>12</sub>(J - 1) branches and not for those of the Q<sub>2</sub>(J - 1) + P<sub>21</sub>(J) branches, in spite of the similar magnitudes. This is readily explained from consideration of the intensity factors.

Although the A<sup>2</sup>Π state of CaF is a good case (a) at low J, the state becomes intermediate between case (a) and (b) as J increases and pure case (a) intensity formulas (13) are no longer applicable. The intensities for an intermediate case (a)-case (b) molecule can be readily calculated from the transformation matrix which diagonalizes the <sup>2</sup>Π<sub>1</sub>, <sup>2</sup>Π<sub>1</sub> energy matrix and Mulliken's pure case (a) formulas (13). For a typical J = 35.5, the results of the calculation show (17) that the relative intensities (denoted by I(P<sub>1</sub>/Q<sub>12</sub>), etc.) are I(P<sub>1</sub>/Q<sub>12</sub>) = 0.95 and I(Q<sub>2</sub>/P<sub>21</sub>) = 4.1. In contrast, pure case (a) formulas predict I(P<sub>1</sub>/Q<sub>12</sub>) = 0.5 and I(Q<sub>2</sub>/P<sub>21</sub>) = 2.0. This situation means that, at J values where the magnitude of the splitting is resolvable, the P<sub>1</sub> and Q<sub>12</sub> branches appear with approximately equal intensity but the P<sub>21</sub> branch is masked by the Q<sub>2</sub> lines which appear about four times as intense. Hence, the splitting between the P<sub>1</sub> and Q<sub>12</sub> branches is easily observed but the P<sub>21</sub>, Q<sub>2</sub> splitting is not because the P<sub>21</sub> branch is buried among stronger lines.

#### ACKNOWLEDGMENT

One of the authors (J.N.) thanks the Yoshida Foundation of Science & Technology for financial support while this work was undertaken.

RECEIVED: September 22, 1977

## REFERENCES

1. T. TANAKA, R. W. FIELD, AND D. O. HARRIS, *J. Chem. Phys.* **61**, 3401 (1974).
2. T. TANAKA AND D. O. HARRIS, *J. Mol. Spectrosc.* **59**, 413 (1976).
3. R. W. FIELD, A. D. ENGLISH, T. TANAKA, D. O. HARRIS, AND D. A. JENNINGS, *J. Chem. Phys.* **59**, 2191 (1973).
4. P. J. DOMAILLE, T. C. STEIMLE, AND D. O. HARRIS, *J. Mol. Spectrosc.* **68**, 146 (1977).
5. P. J. DOMAILLE, T. C. STEIMLE, AND D. O. HARRIS, *J. Mol. Spectrosc.* **65**, 354 (1977).
6. R. W. FIELD, D. O. HARRIS, AND T. TANAKA, *J. Mol. Spectrosc.* **57**, 107 (1975).
7. S. GERSTENKORN AND P. LUC, Atlas du Spectre de la Molecule de l'Iode, private communication.
8. L. B. KNIGHT, JR., W. C. EASLEY, W. WELTNER, JR., AND M. WILSON, *J. Chem. Phys.* **54**, 322 (1971).
9. R. A. FROSCHE AND H. M. FOLEY, *Phys. Rev.* **88**, 1337 (1952).
10. R. N. ZARE, A. L. SCHMELTEKOPF, W. J. HARROP, AND D. L. ALBRITTON, *J. Mol. Spectrosc.* **46**, 37 (1973).
11. G. HERZBERG, "Spectra of Diatomic Molecules," Van Nostrand, New York, 1950.
12. R. S. MULLIKEN AND A. CHRISTY, *Phys. Rev.* **38**, 87 (1931).
13. R. S. MULLIKEN, *Rev. Mod. Phys.* **3**, 89 (1931).
14. B. S. MOHANTY AND K. N. UPADHYA, *Ind. J. Pure Appl. Phys.* **5**, 523 (1967).
15. B. ROSEN, "Selected Constants Relative to Diatomic Molecules," Pergamon, New York, 1970.
16. D. L. ALBRITTON, A. L. SCHMELTEKOPF, AND R. N. ZARE, in "Molecular Spectroscopy: Modern Research" (K. Narahari Rao, Ed.), Vol. II, Academic Press, New York, 1976.
17. L. T. EARLS, *Phys. Rev.* **48**, 423 (1935).

UNCLASSIFIED

SECURITY CLASSIFICATION OF THIS PAGE (When Data Entered)

REPORT DOCUMENTATION PAGE		READ INSTRUCTIONS BEFORE COMPLETING FORM
1. REPORT NUMBER <b>AFOSR-TR- 79-0101</b>	2. GOVT ACCESSION NO.	3. RECIPIENT'S CATALOG NUMBER
4. TITLE (and Subtitle) PHOTOLUMINESCENCE SPECTROSCOPY WITH A CW DYE LASER: A STUDY OF THE DIATOMIC ALKALINE EARTH METAL HALIDES AND OXIDES		5. TYPE OF REPORT & PERIOD COVERED Final
		6. PERFORMING ORG. REPORT NUMBER
7. AUTHOR(s)  D. O. Harris		8. CONTRACT OR GRANT NUMBER(s)  AFOSR-73-2565 <i>new</i>
9. PERFORMING ORGANIZATION NAME AND ADDRESS Department of Chemistry University of California Santa Barbara, California 93106		10. PROGRAM ELEMENT, PROJECT, TASK AREA & WORK UNIT NUMBERS  61102F 2303/B1
11. CONTROLLING OFFICE NAME AND ADDRESS  AF Office of Scientific Research/NC Bolling AFB, D.C. 20332		12. REPORT DATE 1977
		13. NUMBER OF PAGES 118
14. MONITORING AGENCY NAME & ADDRESS (if different from Controlling Office)		15. SECURITY CLASS: (of this report)  Unclassified
		15a. DECLASSIFICATION/DOWNGRADING SCHEDULE
16. DISTRIBUTION STATEMENT (of this Report)  Approved for public release; distribution unlimited.		
17. DISTRIBUTION STATEMENT (of this abstract entered in Block 20, if different from Report)		
18. SUPPLEMENTARY NOTES		
19. KEY WORDS (Continue on reverse side if necessary and identify by block number)		
20. ABSTRACT (Continue on reverse side if necessary and identify by block number) There has been considerable interest in efficient chemiluminescent reactions between metal atoms and suitable oxidants as candidates for chemically pumped laser systems. This prompted a detailed study of the nature and mechanism of the reaction of Barium with N <sub>2</sub> O, O <sub>2</sub> and NO <sub>2</sub> . Experiments were carried out in which single vibrational levels v', of the A singlet sigma state were pumped from adjacent ground state vibrational levels using a tunable cw dye laser. By monitoring the photoluminescence intensity originating from a pumped excited (Continued)		

DD FORM 1 JAN 73 1473

UNCLASSIFIED

SECURITY CLASSIFICATION OF THIS PAGE (When Data Entered)



20. ABSTRACT (Continued)

state level,  $v'$ , to a third ground state level it was possible to measure the relative populations of the two adjacent ground state vibrational levels. Using previously available data and our results suggest that a population inversion may exist between A singlet sigma ( $v'=1$ ) and X singlet sigma ( $v''=7$ ). A second area of interest was the details of the mechanism of the Ba + N<sub>2</sub>O reaction which leads to the observed high A-X chemiluminescence efficiency and why such a large proportion of the emitting molecules are in the A singlet sigma ( $v'=1$ ) state. It had been proposed that metastable BaO(a triplet pi) which cannot emit to the ground state serves as a reservoir state for the reaction. It had been further proposed that the BaO(a triplet pi) was initially formed via the reaction of Ba(triplet D) excited state atoms. We carried out a series of experiments in which total A singlet sigma - X singlet sigma chemiluminescent yield as a function of Ba(triplet D) concentration was monitored. An increase of Ba (triplet D) concentration by a factor of ten to a hundred had no significant effect on chemiluminescent yield. We recently completed our laser induced fluorescence study of MgO. As was expected a B singlet sigma - X singlet sigma P-R doublet is seen, but in addition transitions to a triplet pi<sub>0</sub> and a triplet pi<sub>1</sub> are also observed. Unallowed B singlet sigma - a triplet pi "extra" lines are made possible by specific perturbations between levels of the X singlet sigma and a triplet pi manifolds. Analysis of these perturbations using some sixty lines has resulted in an accurate determination of the molecular constants of the a triplet pi state. We have carried out an extensive program on the spectroscopy of the alkali metal halides. It has been possible to use tunable lasers to completely characterize several electronic states of several alkaline earth monohalides. Included are (1) a study of the B doublet sigma - X doublet sigma system of CaCl using tunable laser excitation spectroscopy; (2) an accurate determination of the ground state constants of CaCl using laser-microwave optical double resonance and (3) a rotational analysis of the E doublet sigma - B doublet sigma system of CaCl using optical-optical double resonance. Similar studies on SrF and CaF have also been carried out.